Dissertation zur Erlangung des Doktorgrades
der Fakultät für Chemie und Pharmazie
der Ludwig-Maximilians-Universität München

Drug delivery systems for pretubulysin-based combination chemotherapies

Ines Vera Viktoria Truebenbach
aus Marburg, Deutschland

2019

Erklärung

Diese Dissertation wurde im Sinne von § 7 der Promotionsordnung vom 28. November 2011 von Herrn Prof. Dr. Ernst Wagner betreut.

Eidesstattliche Versicherung

Diese Dissertation wurde eigenständig und ohne unerlaubte Hilfe erarbeitet.

München, 12.09.2019

.....

Ines Truebenbach

Dissertation eingereicht am 12.09.2019

1. Gutachter: Prof. Dr. Ernst Wagner

2. Gutachterin: Prof. Dr. Angelika Vollmar

Mündliche Prüfung am 29.10.2019

Meinem Vater

Table of contents

1 Introduction

1.1 Combination chemotherapy

Several studies have demonstrated the superiority of combination chemotherapy over monotherapy in cancer treatment. Two drugs with different intracellular targets can act additively or synergistically in their mechanisms of action.[1, 2] This can lead to an overall improvement in the therapeutic outcome. Additionally, due to the increased efficacy of the combination, lower doses can be administered and thus, overall systemic toxicity can be reduced.[3, 4] Furthermore, the risk for chemoresistance formation is lowered.[5] The first combination chemotherapy approach, referred to as POMP regimen, was successfully administered in 1965. It contained methotrexate (MTX), 6-mercaptopurine, vincristine and prednisone and resulted in long-term remission in children with acute lymphocytic leukemia. [6-8] This chapter gives a brief overview of the different therapeutic modalities used in combination in this thesis.

1.1.1 Pretubulysin

Given its central role in cell division, the microtubule system represents a major target for chemotherapeutic drugs. Microtubule targeting drugs can be assigned to two groups, the microtubule-stabilizing agents, e.g. taxanes, or microtubule-destabilizing agents, such as vinca alkaloids or colchicine. Drugs like the vinca alkaloids, paclitaxel and epothilone, exhibit highly effective anticancer properties and are widely used in the clinics. The complex chemical synthesis of these compounds, the resistances that frequently occur with Vinca alkaloids and their neurotoxicity necessitate the search for other microtubule binding drugs.[9-12]

The tubulysins, a group of microtubule- destabilizing agents, were first discovered by Sasse et al. in 2000 and are produced by myxobacteria. They are biosynthetically assembled by the hybrid polyketide synthase/non-ribosomal peptide synthetase and consist of the proteinogenic amino acid isoleucine (Ile), and three non-proteinogenic amino acids namely N-methyl pipecolic acid (Mep), tubuvaline (Tuv), and a chain extended analog of either phenylalanine or tyrosine called tubuphenylalanine (Tup) or tubutyrosine (Tut).[13] Tubulysins prevent tubulin polymerization by binding to the vinca

domain of ß-tubulin, which results in G2/M arrest. This ultimately leads to microtubule depletion and apoptosis of the treated cells. Importantly, the ability of the tubulysin family to suppress cancer cell growth exceeds that of other tubulin binding drugs, like epothilones, vinblastine and paclitaxel, by 20- to 100-fold. [11, 14, 15] The biosynthetic yields after fermentation and isolation, however, are low and the chemical synthesis of the tetrapeptide derivative is challenging.

Pretubulysin (PT) is a chemically accessible biosynthetic precursor of the tubulysins with similar biological properties.[10, 11, 16] It has been shown to have antitumoral[8, 10, 17,18] and antiangiogenic properties, vascular disrupting effects[19] as well as antimetastatic potential.[9] The chemical structures of the native Tubulysin A and PT are depicted in Scheme 1

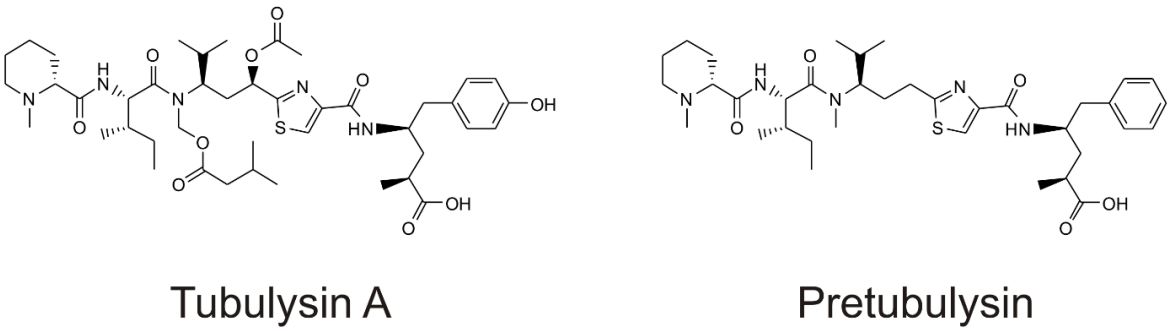

Scheme 1. Chemical structures of myxobacterial compounds tubuylsin A and pretubulysin.

1.1.2 Methotrexate

Antifolates were among the first chemotherapeutic drugs to be investigated for the cure of metastatic cancer. Methotrexate (MTX) represents one of the most prominent anti-folates and has already been used in early approaches of anticancer drug therapy.[7] Already in 1956, Li et al. reported that MTX produced complete responses in women suffering from choriocarcinoma.[20] A follow-up study 5 years later showed that many of these women had been cured.[21]

As a folate antagonist, MTX enters the cell via the reduced folate carrier (RFC) or the folate receptor (FR).[22, 23] MTX is mainly taken up by the RFC. Nevertheless, substantial influx can also occur via the FR even though the affinity of the FR to MTX is much lower than towards its native ligand FolA.[24] The FR is overexpressed in many epithelial

tumors and can therefore be used for targeted cancer therapy.[25, 26] Upon cell entry, MTX is polyglutamylated with up to five glutamate residues. In its active form it competitively inhibits the enzyme dihydrofolate reductase (DHFR) and by that the conversion of folic acid to dihydrofolic acid and tetrahydrofolic acid. These steps are crucial for thymidylate, purine as well as methionine and serine biosynthesis.[27, 28]

MTX is still widely used in cancer chemotherapy, e.g. as a modulator to increase the effectiveness of other drugs. Acquired resistance to MTX, however, represents a common problem of monotherapeutic approaches.[29-31] The four major mechanisms of MTX resistance are a decrease in cell uptake, a decrease in intracellular retention due to ineffective polyglutamylation, an increase in DHFR activity or a decrease in binding of MTX to the enzyme.[32] This hurdle can possibly be overcome by combining MTX with a second antitumoral agent. A beneficial combination effect of another tubulin-binding agent, vinblastine, and low-dose MTX was reported in a recent clinical study, highlighting the possible advantage of this type of drug combination.[33] In this work, the novel microtubule inhibitor PT was combined with MTX to elucidate possible combination benefits.

In addition to cancer chemotherapy, MTX is used in lower doses for the treatment of autoimmune diseases, like psoriasis, rheumatoid arthritis and Morbus Crohn.[34]

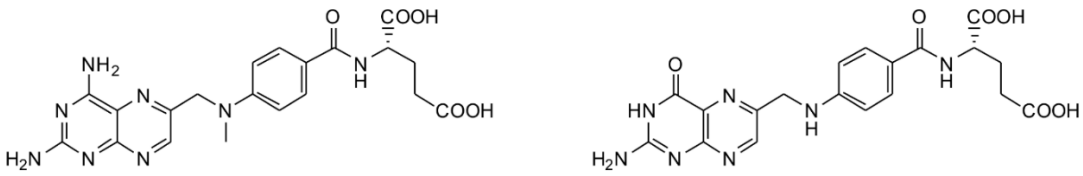

Scheme 2. Chemical structures of the antimetabolite methotrexate (MTX) and folic acid (FolA).

1.1.3 Eglin 5 siRNA

Small interfering RNA (siRNA) facilitates the specific silencing of genes involved in disease pathogenesis. Craig Mello first discovered Gene silencing by RNA interference (RNAi) in 1998 in C. elegans. By 2001, Elbashir et al. had reported on the basic principles of siRNA structure, RNAi mechanism and used synthetic siRNA for silencing.

Since then, selective gene silencing using synthetic siRNAs has been widely used for the study of gene function.[35, 36] Since siRNAs can theoretically be tailored to target any gene of interest, RNAi based gene silencing can be applied to a great number of human diseases.[35] The first RNAi based drug was approved by the FDA in 2018. Alnylam Pharmaceuticals developed Onpattro (patisiran) for the treatment of polyneuropathy caused by transthyretin amyloidosis. Several further therapeutic siRNAs are currently investigated in late stage clinical trials and expected to gain approval soon.[37] Designed siRNAs against targets promoting tumor survival, like Ran or Eg5, present an emerging class of therapeutics for tumor therapy. [38-41] The EG5 gene encodes a kinesin-5 subclass protein (KSP or Eg5) which is essential for the organization of the mitotic spindle apparatus. Gene knockdown therefore inhibits mitosis and induces cancer cell death.[42, 43]

However, the successful intracellular delivery of siRNA into the target cell presents a major challenge in the field of siRNA therapy. Naked siRNA has limited extracellular stability in biological fluids since it is rapidly degraded by nucleases. The half-life of naked siRNA in serum is usually less than one hour.[35] Additionally, its negative charge and its high molecular weight prevent the efficient cellular internalization.[38, 44, 45] Since siRNAs are taken up into the cell via endocytosis, sufficient release from the endosome is crucial for them to exert their effects.[46] To circumvent these issues siRNA can be incorporated into delivery systems, like liposomes, polymeric or inorganic nanoparticles.[47] Also, various polycations or cationic lipids were shown to successfully form polyplexes for efficient intracellular siRNA delivery *in vitro* and *in vivo.*[48-51] Onpattro uses cationic amino MC3 lipid nanoparticles (MC3: heptatriaconta-6,9,28,31-tetraen-19-yl 4-(dimethylamino)butanoate) for siRNA encapsulation.[37]

Even though the field of siRNA therapeutics holds great potential in cancer therapy, several studies have shown that downregulation of gene expression can only partially inhibit tumor progression. Cross-talk between oncogenic pathways and compensatory activation of signal transduction have been observed.[40] As a result, therapeutic siRNAs are often combined with chemotherapeutic drugs to increase the therapeutic efficacy.[52, 53]

In a previous study, we demonstrated an enhanced combined cytotoxicity of a cytotoxic siRNA, namely poly (I:C), and synthetic, polyglutamylated MTX ligands.[54] In this thesis, PT and siEG5 were co-incorporated into a polyplex.

1.2 Tumor targeted drug delivery systems

The major limitation of traditional anticancer drugs is their lack of selectivity and specificity. After systemic application, the cytotoxicity of these compounds is not confined to their target cell, namely a cancer cell, but also healthy tissue is destroyed. This limits their applicability in the clinics.[55] Nanoparticulate incorporation or conjugation to a targeting ligand or antibody facilitates the targeted delivery of the anticancer compound to the tumor site via passive and active targeting (Scheme 3) and could therefore help circumvent their narrow safety profile and facilitate their clinical use. Furthermore, nanosized drug delivery systems can improve the bioavailability of drugs. Most anticancer therapeutics are water-insoluble small molecules with low molecular weights. Nanoformulation can facilitate their solubilization and prevent their rapid excretion from systemic circulation.[56]

One major hurdle in combination therapy is the different pharmacokinetic behavior of two drugs after *in vivo* administration.[57] The interactions of two drugs with blood components, like albumin, determine their biological fate and distribution. Instability under physiological conditions, unspecific biodistribution and rapid clearance render many anticancer drugs unsuitable for clinical application. Nanoparticulate incorporation of drugs may enable the controlled and simultaneous delivery of two drugs at specific molar ratios, which achieve maximal synergy, to the tumor site and prolong their circulation time.[58-62] The first liposomal formulation which co-delivers a synergitstic molar ratio of daunorubicine and cytarabine was approved by the European Medicines Evaluation Agency (EMA) in 2018 for the treatment of therapy-related acute myeloid leukemia (t-AML) or AML with myelodysplasia-related changes.[63]

1.2.1 Passive tumor targeting

When nanosized delivery systems accumulate in the tumor via extravasation through the leaky tumor capillary fenestration they reach their target tissue by passive targeting. Moreover, due the absence of lymphatic system, the delivery systems are inefficiently

removed and thus, remain in the tumor tissue. This effect was discovered by Matsumara et al. and is termed enhanced permeability and retention (EPR) effect, It enables the tumor selective delivery of nanoparticles.[61, 64, 65] The clinical relevance of the EPR effect is controversially debated today. Firstly, the extent of passive targeting is highly dependent on tumor pathophysiology. The applicability of a tumor type for nanoparticulate drug delivery systems varies highly from one tumor cell type to the other.[66] Secondly, nanoparticles frequently show higher tumor accumulation relative to controls, but only a small fraction (5 %) of the overall administered dose is actually delivered to the target side, while a majority accumulates in the liver and spleen.[67] Nevertheless, several nanomedicine based drug delivery systems are routinely used in tumor therapy. Notably, Abraxane, albumin bound paclitaxel, has demonstrated superiority over paclitaxel and is approved for the treatment of breast, lung and pancreatic cancer.[68]

For a nanoparticle to reach its target side via the EPR effect, they need to circulate for a long period and evade recognition by the immune system and subsequent opsonization by the reticulo-endothelial system (RES). The biophysical properties of a delivery system can be optimized by covalent functionalization with shielding agents, like polyethylene glycol (PEG), to minimize the risk of unspecific interactions with biological components. Several studies have shown a > 100 % increase in tumor accumulation of nanoparticles following PEGylation.[67] One of the first nanomedicines approved by regulatory authorities, Doxil, is a PEGylated liposomal formulation of doxorubicine. In addition to a prolonged circulation time, it has been shown to display a lower cardiotoxicity than free doxorubicine.[64]

1.2.2 Active tumor targeting

After the delivery system has reached the tumor tissue by passive targeting, active tumor targeting enables the selective uptake of the delivery system into the target cell. Therefore, the nanocarrier surface is equipped with a targeting ligand which binds to the appropriate receptors overexpressed on the tumor cell. The ligand is chosen to bind a receptor which is selectively overexpressed by the target cell and not a healthy cell.[64]

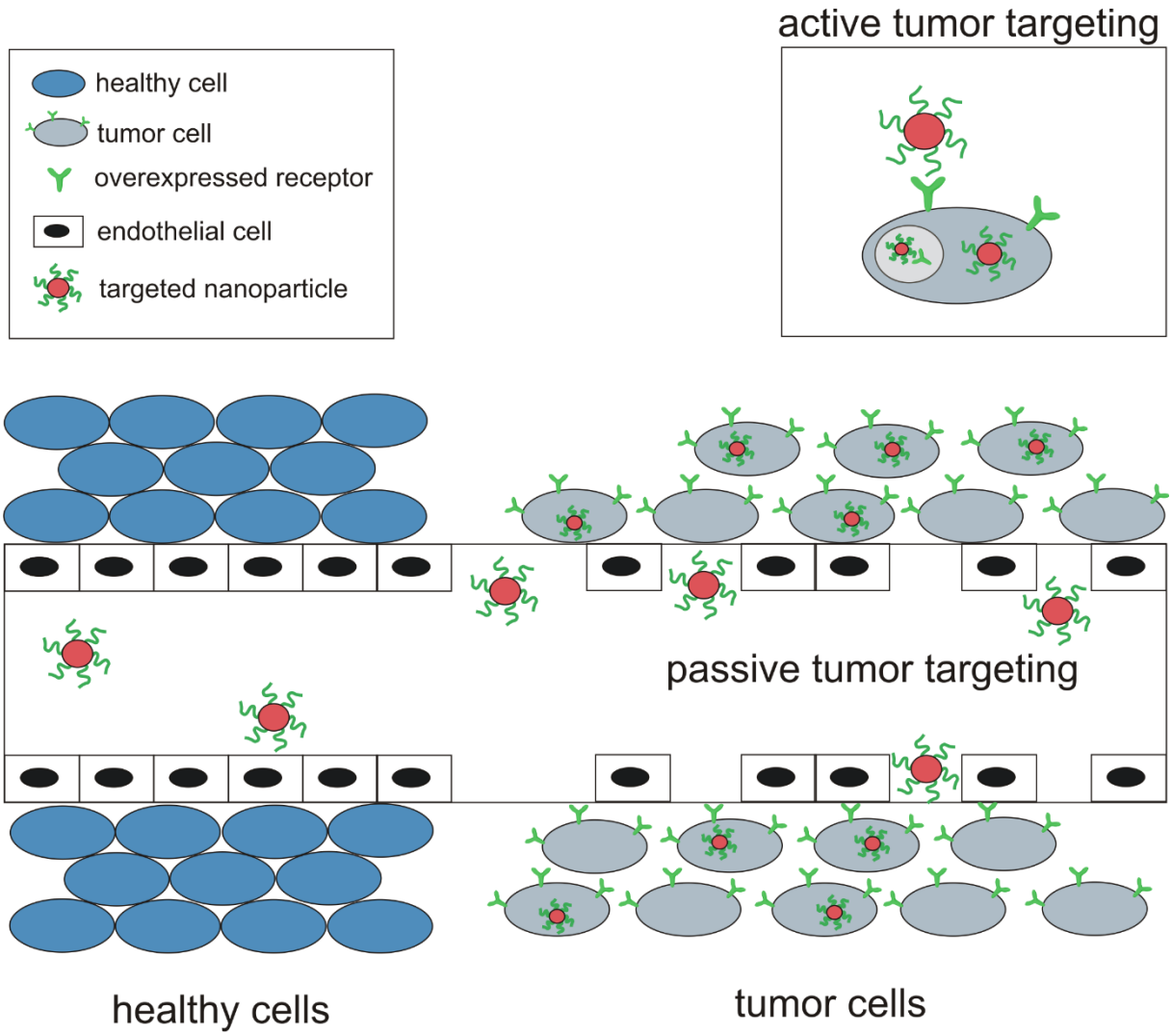

Scheme 3. Passive and active targeting of nanoparticulate delivery systems to tumor cells. Due to the leaky capillary fenestration, nanosized delivery systems can extravasate into the tumor tissue (passive tumor targeting). After reaching their target tissue, nanoparticles can be internalized into the cell through active tumor targeting.

1.2.2.1 FR targeting

The folic acid receptor (FR) is overexpressed on many tumor types.[23, 69] It offers a prominent approach to selectively target FR-positive cancer cells in targeted drug delivery approaches by binding folic acid (FolA) and FolA-derivatives with very high affinity.[70-76] The reduced folate carrier (RFC) constitutes another common transport protein involved in the membrane transport of folic acid metabolites. Therefore, FolA and MTX can serve as targeting ligands for tumor selective therapy [54, 70-78] and facilitate the transport of FolA- or MTX-derivatives into cancer cells. In contrast to FolA, MTX does not only possess ligand properties but, in its polyglutamylated form, shows increased inhibition of the enzyme dihydrofolate reductase (DHFR), which is vital in

the nucleotide biosynthesis pathway, evades efflux transport mechanisms and can induce cellular impairment.[7] Therefore, in FR selective drug delivery, MTX can serve both as targeting ligand and as an additional drug agent for combinatorial tumor therapy.[54, 74-79]

1.2.2.2 EGFR targeting

The epidermal growth factor receptor (EGFR), a protein-tyrosine kinase, is overexpressed on different cancer cell types. Its positive signaling causes increased proliferation, decreased apoptosis, enhanced tumor cell motility and angiogenesis. Therefore, the EGFR is considered an important target for receptor-mediated drug delivery. Its native ligand EGF has strong mitogenic and neoangiogenic activity and is therefore not a suitable targeting ligand.[80] The peptide GE11 has a high affinity to the EGFR, is not immunogenic and synthetically easily accessible and can therefore be considered an effective targeting ligand for EGFR directed nanoparticles.[81-84] Several studies have demonstrated the successful systemic delivery of GE11 coated nanoparticles to EGFR overexpressing tumors.[83-86]

1.3 Solid-phase derived carriers

Our lab developed a delivery platform facilitating the intracellular transport of different cargos, like siRNA, proteins and drugs.[87, 88] These oligoaminoamides (OAAs, also called oligomers or oligoamides) consist of natural α-amino acids, artificial amino acids and fatty acids and are sequentially assembled via solid-phase assisted peptide synthesis (SPS).[89] The sequence-defined nature of the synthesis route facilitates the manufacturing of tailored delivery vehicles and offers the option to incorporate multiple environment-responsive delivery functions. The artificial amino acid succinyl tetraethylenepentamine (Stp) for instance, facilitates the delivery of therapeutic cargo to the cytosol by causing endosomal escape via the proton sponge effect.[89, 90] Furthermore, the cationic nature of Stp enables the complex formation with negatively charged cargo, like nucleic acids or MTX. Various topological oligomer subclasses, like linear, 2-arm, 4-arm or T-shaped structures, have been developed.[89]

Together with their therapeutic payload, the oligomers form a delivery system with custom-made properties. In several studies, the oligomers were optimized towards

their respective payload e.g. nucleic acids, proteins or drugs.[48, 91, 92] This chapter outlines the different kinds of oligomers which were used in this thesis to co-deliver PT and MTX or PT and siEG5, respectively.

1.3.1 Small molecule drug conjugates

Small molecule drug conjugates (SMDCs) for the targeted delivery of potent drugs to the tumor site can be manufactured by the above-described SPS method. They typically consist of three domains (Scheme 4): the therapeutic payload, a targeting ligand and a linker. The linkers can on the one hand be cleavable bridges, which are stable during circulation, and release the cargo after it reaches its therapeutic destination, e.g. disulfide bonds. On the other hand, they can contain hydrophilic sequences, e.g. PEG spacers, which facilitate the solubility of the often hydrophobic anticancer compound.[55, 93] Prominent targeting ligands for SMDCs, which have previously been investigated in clinical studies, are folic acid (FolA) and the prostate-specific membrane antigen (PSMA). Endocyte has investigated several FR-targeted SMDCs, containing vinblastine, tubulysins and epothilones as payloads in clinical studies.[94] However, vintafolate, a FolA-conjugate of vinblastine, was evaluated in combination with PEGylated liposomal doxorubicin (PLD) for the therapy of FR positive platinum-resistant ovarian cancer (Proceed study) and in combination with docetaxel for non-small-cell lung cancer (NSCLC, Target study) and failed in the clinical studies phase III (Proceed) and phase II (Target).[95] Despite these negative results, five FR-targeted delivery systems are currently investigated in phase I, with one of them being an SMDC.[96]

Scheme 4. Schematic representation of SMDC.

1.3.2 Nanoparticulate drug delivery systems

The cationizable nature of the oligomers, which can be introduced by including Stp into the oligomer sequence, enables the formation of nanoparticles with oppositely charged cargo. Polyelectrolyte complexes (PECs) formed through cooperative electrostatic

interactions upon mixing of two oppositely charged molecules have already attracted a great deal of interest for drug delivery.[97, 98]

Several studies describe the favorable properties of the T-shape lipo-oligomer ***454*** and related cationizable lipo-OAAs as carriers in siRNA delivery.[49, 87, 91, 99, 100] The linear backbone of ***454*** contains four Stp units which facilitate nanoparticle formation with negatively charged siRNA. Upon cell uptake, protonation under acidifying endosomal conditions promote endosomal escape.[51] N- and C-terminal cysteines stabilize nanoparticle complexes due to their disulfide crosslinking potential.[87, 89] Additionally, ***454*** contains two oleic acid chains (OleA), and tyrosine tripeptide units which serve as further stabilizing domains of polyplexes.[91, 101]

Steinborn et al. have recently reported on the nanoparticle formation properties of cationic lipo-oligomer ***454*** with the negatively charged drug MTX and various polyglutamylated polyanionic MTX analogs, and applied it for siRNA and MTX co-delivery.[48] In this thesis, ***454*** and its analog ***1198*** were used to co-incorporate PT in nanosized delivery vehicles, based on electrostatic interactions with either MTX or siEG5.

1.4 Aim of the thesis

The combination of different therapeutic modalities has become the gold standard in cancer chemotherapy. By combining drugs, which address different intracellular targets, the therapeutic efficiency can be increased and the risk for resistance formation is reduced. The major problems of cancer chemotherapy are the lack of drug selectivity, unfavorable bioavailability, and the rapid clearance of the small molecules from the bloodstream. Targeted drug delivery systems aim at selectively delivering drugs to their target side, namely the tumor tissue, by passive and active targeting. Nanoparticulate combination therapy can unify different pharmacokinetic behavior of two drugs and facilitate a spatially and temporarily controlled delivery to the tumor site. In this thesis, two combination chemotherapies based on the novel microtubule binding drug PT and the established antifolate MTX or the therapeutic siRNA siEG5 were evaluated. The therapeutic combinations were co-incorporated into different delivery

systems. Their *in vivo* and *in vitro* properties were assessed in comparison to the free drugs.

The first chapter of the thesis focuses on the development of SMDCs as a co-delivery system which contains PT derivatives as a therapeutic payload, a hydrophilic spacer and the targeting moiety FolA or the antimetabolite MTX, which has targeting as well as cell killing properties. A set of FR targeted oligoamides with varied topology and different numbers of ligands was to be synthesized by SPS. The oligomers were designed to contain a cysteine for conjugation to thiol activated PT. Structure activity relationships were to be investigated regarding different demands of the SMDCs, such as DHFR inhibition, cellular uptake and effect of viability on FR-overexpressing KB cervix carcinoma and L1210 leukemia cells. After subsequent chemical conjugation of PT to the oligoamides, the SMDCs were to be screened for their intracellular delivery of PT. Structure activity relationship studies aimed at identifying an ideal SMDC with favorable combinatorial, antitumoral properties *in vitro*. Additionally, the most promising SMDC was to be evaluated in an intratumoral treatment study in comparison to unmodified PT.

Secondly, based on the beneficial effect of the conjugated PT-derivative and MTX in the SMDCs, the combination effect of the free drugs PT+MTX was assessed in different assays. Besides thorough investigations into the antitumoral effect of the combination PT+MTX, its effect on the cell cycle as well as cellular architecture, namely the tubulin and actin skeleton, had to be evaluated in comparison to both free drugs.

The aim of third chapter of the thesis was the development of nanosized drug delivery vehicles containing PT+MTX. Polyelectrolyte complexes were to be formed from the cationizable lipo-oligomer ***454*** and the anionic drug MTX; PT was to be co-incorporated. The biophysical nanoparticle characteristics, like size and drug incorporation, had to be determined. The stability of the PECs was to be evaluated in different media. Furthermore, cellular effects of the delivery system, like uptake, antitumoral efficiency and influence on the cell cycle had to be investigated. Finally, the effect of nanoparticulate incorporation of PT+MTX on tumor growth was assessed *in vivo* in subcutaneous L1210 tumors.

The final aim of the thesis was the co-delivery of PT and therapeutic siRNA. Polyplexes were formed from siEG5 and azide containing lipo-oligomer ***1198***. Payload incorporation of the dual delivery systems had to be determined. The polyplex surface was modified by click chemistry to introduce a PEG shielding agent (DBCO-PEG) or the EGFR targeting peptide GE11 (DBCO-PEG-GE11). The biological effects of the unmodified and functionalized nanoparticles were to be investigated. The ligand-mediated intracellular delivery of the siRNA had to be assessed in uptake experiments, GFP gene silencing as well EG5 specific mRNA downregulation experiments. Lastly, the antitumoral activity of the combination formulation had to be evaluated in comparison to the free drug PT and the siEG5 containing polyplex.

2 Materials and Methods

2.1 Materials

The solvents, reagents and buffers used for the experiments are summarized in Table 1, Table 2 and Table 3, together with their CAS numbers and sources of supply.

Solvent	CAS-No.	Supplier
Acetonitrile[1]	75-05-8	VWR Int. (Darmstadt, Germany)
Chloroform-d[2]	865-49-6	Euriso-Top (Saint-Aubin Cedex, France)
Deuterium oxide[2]	7789-20-0	Euriso-Top (Saint-Aubin Cedex, France)
Dichloromethane[3]	75-09-2	Bernd Kraft (Duisburg, Germany)
*N,N-D*imethylformamide[4]	68-12-2	Iris Biotech (Marktredewitz, Germany)
Dimethylsulfoxide[5]	67-68-5	Sigma-Aldrich (Munich, Germany)
n-Hexane[6]	110-54-3	Brenntag (Mülheim/Ruhr, Germany)
Methanol[3]	67-56-1	Fisher Scientific (Schwerte, Germany)
Methyl-*tert*-butyl ether[7]	1634-04-4	Brenntag (Mülheim/Ruhr, Germany)
N-Methyl-2-pyrrolidone[4]	872-50-4	Iris Biotech (Marktredewitz, Germany)
Water[8]	7732-18-5	In-house purification

Table 1. Solvents used for experimental procedures

[1] HPLC grade; [2] NMR grade (> 99.9 %); [3] analytical grade; [4] peptide grade; [5] BioReagent grade (> 99.9 %); [6] purissimum; [7] synthesis grade; [8] purified, deionized

Chemicals and Reagents	CAS-No.	Supplier
1-Hydroxybenzotriazole hydrate	123333-53-9	Sigma-Aldrich (Munich, Germany)
2-Chlorotritylchloride resin	42074-68-0	Iris Biotech (Marktredewitz, Germany)
4-[[(2,4-diamino-6-pteridinyl) methyl] methylamino] benzoic acid	19741-14-1	Niels Clauson-Kaas A/S (Farum, Denmark)
4′,6-Diamidin-2-phenylindol (DAPI)	50-63-5	Sigma-Aldrich (Munich, Germany)
Agarose NEEO Ultra	9012-36-6	Carl Roth (Karlsruhe, Germany)
Ammonia solution 25 %	1336-21-6	Carl Roth (Karlsruhe, Germany)
Boc-L-Cys(Trt)-OH	76880-29-0	Bachem (Bubendorf, Switzerland)
Boric acid	10043-35-3	Sigma-Aldrich (Munich, Germany)
Collagen	-	Biochrom (Berlin, Germany)
Coenzyme A	-	Sigma-Aldrich (Munich, Germany)
D-(+)-Glucose monohydrate	28718-90-3	Sigma-Aldrich (Munich, Germany)
D-luciferin sodium	-	Promega (Mannheim, Germany)
Dibenzocyclooctyne-acid	1353016-70-2	Sigma-Aldrich (Munich, Germany)
Dibenzocyclooctyne-NHS ester	1353016-71-3	Sigma-Aldrich (Munich, Germany)
DBU	14431-43-7	Merck Millipore (Darmstadt, Germany)
Dihydrofolate reductase (assay kit)	-	Sigma-Aldrich (Munich, Germany)
EDTA disodium salt dihydrate	156648-40-7	Iris Biotech (Marktredewitz, Germany)
Fmoc-L-Asn(Trt)-OH	132388-59-1	Iris Biotech (Marktredewitz, Germany)

Fmoc-L-Cys(Trt)-OH	103213-32-7	Iris Biotech (Marktredewitz, Germany)
Fmoc-L-Gln(Trt)-OH	132327-80-1	Iris Biotech (Marktredewitz, Germany)
Fmoc-L-Gly-OH	29022-11-5	Iris Biotech (Marktredewitz, Germany)
Fmoc-L-His(Trt)-OH	109425-51-6	Iris Biotech (Marktredewitz, Germany)
Fmoc-L-Ile-OH	71989-23-6	Iris Biotech (Marktredewitz, Germany)
Fmoc-L-Lys(Dde)-OH	204777-78-6	Iris Biotech (Marktredewitz, Germany)
Fmoc-L-Lys(Fmoc)-OH	78081-87-5	Iris Biotech (Marktredewitz, Germany)
Fmoc-L-Lys(N_3)-OH	159610-89-6	Iris Biotech (Marktredewitz, Germany)
Fmoc-L-Pro-OH	71989-31-6	Iris Biotech (Marktredewitz, Germany)
Fmoc-L-Thr-OH	73731-37-0	Iris Biotech (Marktredewitz, Germany)
Fmoc-L-Trp(Boc)-OH	43824-78-6	Iris Biotech (Marktredewitz, Germany)
Fmoc-L-Tyr(tBu)-OH	71989-38-3	Iris Biotech (Marktredewitz, Germany)
Fmoc-L-Val-OH	68858-20-8	Iris Biotech (Marktredewitz, Germany)
Fmoc-*N*-amido-dPEG12-acid	756526-01-9	Quanta Biodesign (Powell, Ohio, USA)
Fmoc-*N*-amido-dPEG24-acid	756526-01-9	Quanta Biodesign (Powell, Ohio, USA)
Fmoc-STODTA-OH	172089-14-4	Sigma-Aldrich (Munich, Germany)
Fmoc-Stp(Boc_3)-OH	-	In-house synthesis [89, 90]
Folic acid	59-30-3	Sigma-Aldrich (Munich, Germany)
GelRed	-	Biotium Inc. (Hayward, CA, USA)
HBTU	94790-37-1	Multisyntech (Witten, Germany)
Heparin sodium 5000 I.E/mL	9041-08-1	ratiopharm GmbH (Ulm,.Germany)
HEPES	7365-45-9	Biomol (Hamburg, Germany)
Hydrazine monohydrate	7803-57-8	Merck Millipore (Darmstadt, Germany)
Hydrochloric acid solution (1 M)	7647-01-0	Sigma-Aldrich (Munich, Germany)
Magnesium chloride hexahydrate	7791-18-6	AppliChem (Darmstadt, Germany)
MTT	298-93-1	Sigma-Aldrich (Munich, Germany)
MTX	59-05-2	Sigma-Aldrich (Munich, Germany)
N^{10}-Pteroic acid	37793-53-6	Sigma-Aldrich (Munich, Germany)
N,N-Diisopropylethylamine	7087-68-5	Iris Biotech (Marktredewitz, Germany)
Ninhydrin	485-47-2	Sigma-Aldrich (Munich, Germany)
Oleic acid	112-80-1	Sigma-Aldrich (Munich, Germany)
Paraformaldeyhde	30525-89-4	Sigma-Aldrich (Munich, Germany)
Phenol	108-95-2	Sigma-Aldrich (Munich, Germany)
Piperidine	110-89-4	Iris Biotech (Marktredewitz, Germany)
Potassium cyanide	151-50-8	Sigma-Aldrich (Munich, Germany)
Propidium Iodide (PI)	25535-16-4	Sigma-Aldrich (Munich, Germany)
PyBOP®	128625-52-5	Multisyntech GmbH (Witten, Germany)
Sephadex® G-10	9050-68-4	GE Healthcare (Freiburg, Germany)
Sodium citrate	6132-04-3	Sigma-Aldrich (Munich, Germany)
Sodium hydroxide (anhydrous)	1310-73-2	Sigma-Aldrich (Munich, Germany)
Triethylamine	121-44-8	Sigma-Aldrich (Munich, Germany)
Trifluoroacetic acid	76-05-1	Iris Biotech (Marktredewitz, Germany)
Triisopropylsilane	6485-79-6	Sigma-Aldrich (Munich, Germany)
Triton™ X-100	9002-93-1	Sigma-Aldrich (Munich, Germany)
Trizma® Base	77-86-1	Sigma-Aldrich (Munich, Germany)

Table 2. Chemicals and reagents used for experimental procedures

Buffer	Composition
10 mM HCl SEC solvent	693 mL water, 300 mL acetonitrile, 7 mL 1M HCl solution
HBG	20 mM HEPES, 5 % glucose, pH 7.4
LAR buffer	1 M glycylglycine, 100 mM MgCl2, 500 mM EDTA, DTT, ATP, coenzyme A)
Microtubule Stabilizing Buffer	80 mM PIPES pH 6.8, 1 mM $MgCl_2$, 5mM EGTA-K, and 0.5% Triton X-100
TBE buffer	89 mM Trizma® base, 89 mM boric acid, 2 mM EDTA-Na_2

Table 3. Buffers used for experimental procedures

2.1.1 Equipment for solid-phase synthesis

A Biotage Syro Wave (Biotage, Uppsala, Sweden) peptide synthesizer was used for synthesis supported with microwave irradiation. Disposable polypropylene (PP) syringe microreactors with the volume sizes 2 mL, 5 mL, and 10 mL were purchased from Multisyntech (Witten, Germany). It was conducted with polytetrafluoroethylene (PTFE) filters. The recommended size of the reactors was chosen according to the amount of resin. Microreactors with polyethylene filters (Multisyntech, Witten, Germany) were used for manual solid-phase synthesis. Reactions were carried out under steady shaking with an overhead shaker.

2.1.2 Nucleic acids

2.1.2.1 siRNA

All siRNAs and modified siRNA compounds used are presented in Table 4. They were synthesized by Roche Kulmbach GmbH (now Axolabs GmbH, Kulmbach, Germany).

siRNA	Target	Sequence
Cy5-siAHA1	AHA1	5’-(Cy5)(NHC6)GGAuGAAGuGGAGAuuAGudTsdT-3’ (sense) 5’-ACuAAUCUCcACUUcAUCCdTsdT-3’ (antisense)
Cy7-siAHA1	AHA1	5’-(Cy7)(NHC6)GGAuGAAGuGGAGAuuAGudTsdT-3’ (sense) 5’-ACuAAUCUCcACUUcAUCCdTsdT-3’ (antisense)
siCtrl	-	5’-AuGuAuuGGccuGuAuuAGdTsdT-3’ (sense) 5’-CuAAuAcAGGCcAAuAcAUdTsdT-3’(antisense)

siEG5	EG5/KSP	5'-ucGAGAAucuAAAcuAAcudTsdT-3' (sense) 5'-AGUuAGUUuAGAUUCUCGAdTsdT-3' (antisense)
siGFP	eGFP-Luc	5'-AuAucAuGGccGAcAAGcAdTsdT-3' (sense) 5'-UGCUUGUCGGCcAUGAuAUdTsdT-3' (antisense)

Table 4. Small letters: 2'-methoxy-RNA, s: phosphorothioate. All nucleic acids were synthesized by the Roche Kulmbach GmbH (now Axolabs GmbH, Kulmbach, Germany).

2.1.2.2 Cell culture

Cell culture media, antibiotics and fetal bovine serum (FBS) were purchased from Invitrogen (Karlsruhe, Germany), Sigma Aldrich (Munich, Germany) or Life Technologies (Carlsbad, USA). The individual media used for the different cell cultures are summarized in Table 5. All media were supplemented with 10 % FBS, 100 U/mL penicillin and 100 µg/mL streptomycin. Cell lines were cultured at 37 °C and 5 % CO_2 in an incubator with a relative humidity of 95 %.

Exponentially growing cells were detached from the culture flasks using Millipore water, supplemented with 0.05 % trypsin-EDTA (Invitrogen, Karlsruhe, Germany), and followed by resuspension in the required culture media. Cell suspensions were seeded at the desired density for each experiment. Luciferase cell culture lysis buffer and D-luciferin sodium salt were purchased from Promega (Mannheim, Germany).

Cell line	Description	Medium
KB	Human cervix carcinoma cells	DMEM, low glucose; RPMI-1640, folate free
KB-eGFP-Luc	Human cervix carcinoma cells	DMEM, low glucose; RPMI-1640, folate free
Huh7	Human hepatocellular carcinoma cells	DMEM, low glucose
L1210	Mouse lymphocytic leukemia cells	RPMI-1640, +/- folate

Table 5. Overview cell lines and culture media

2.2 Methods

2.2.1 Synthesis of oligomers and post-modification agents via solid phase synthesis (SPS)

2.2.1.1 Loading of a 2-chlorotrityl chloride resin with an Fmoc protected amino acid

The desired amount of 2-chlorotrityl chloride resin (1.6 mmol/g chloride loading) was weighed in a syringe reactor and swelled in dry DCM for 30 min. After swelling, the first Fmoc protected amino acid of the respective topology as well as a threefold molar excess of DIPEA were added to the resin and incubated for 1 h at room temperature (rt) (see Table 6 for the different topologies and molar amounts of respective amino acids).The reaction solvent was drained and the resin was incubated with DCM/MeOH/DIPEA (80/15/5) for at least 30 min at rt to cap residual reactive functions on the resin. After the removal of the mixture, the resin was washed with DMF (10 mL/g resin) and DCM (10 mL/g resin) 5 times each.

Topology	Amino acids	Molar amounts
linear	Fmoc-L-Cys(Trt)-OH	0.4 eg.
2-arm	Fmoc-L-Cys(Trt)-OH	0.4 eq.
4-arm	Fmoc-L-Cys(Trt)-OH	0.3 eq.
T-shape	Fmoc-L-Cys(Trt)-OH	0.3 eq.
PEGylation reagent	Fmoc-dPEG$_{24}$-OH	0.3 eq.
GE11-targeted PEGlyation agent	Fmoc-Ile-OH	0.4 eq.

Table 6. Molar amounts of amino acids used for different oligomer topologies

The resin loading was determined by quantification of released fluorenyl derivative after piperidine deprotection. About 50 mg of the resin were removed and dried *in vacuo* to determine the loading of the resin. Therefore, an exact amount of resin was treated with 1 mL deprotection solution (20 % piperidine in DMF) for 1 h. Afterwards, the solution was diluted, and absorption was measured at 301 nm. The resin loading was calculated according to the equation: resin load [mmol/g] = (A*1000)/(m [mg]*7800*df) with df as dilution factor.

The resin was treated four times with 20 % piperidine in DMF to remove the Fmoc protection group. Reaction progress was monitored by Kaiser test (cf. 2.2.2). Afterwards, the resin was washed with DMF and DCM and dried *in vacuo*.

2.2.1.2 General description of solid-phase synthesis procedure

The sequential synthesis on solid phase was carried out in defined steps of a synthesis cycle. Oligomers were either synthesized manually or automatically. General steps of the manual and automated synthesis procedure are shown in Table 7 and Table 8. Under manual synthesis conditions, the presence or absence of free amines was confirmed qualitatively by Kaiser test (cf. 2.2.2) after each coupling or deprotection step. In case of an ambiguous result (negative after deprotection or positive after coupling), the respective deprotection or coupling step was repeated. Since an automated synthetic procedure does not offer the possibility of an in-process Kaiser test, deprotection and coupling steps were extended. For amino acid coupling, the resin was incubated with a 4-fold excess of an Fmoc protected amino acid (Fmoc-AA) predefined by the oligomer sequence. During manual synthesis, activation of the carboxylic acid function was achieved with equimolar amounts of HOBt (1-Hydroxybenzotriazole), equimolar amounts of PyBOP (Benzotriazol-1-yl-oxytripyrrolidinophosphonium hexafluorophosphate) and a twofold molar excess of DIPEA. For automated synthesis, PyBOP was exchanged with HBTU (2-(1H-benzotriazole-1-yl)-1,1,3,3-tetramethyluronium hexafluorophosphate). Incubation times during a coupling cycle were 60 min at RT or 10 min at 60 °C (microwave irradiation). Fmoc-deprotection was accomplished by 4 × 10 min incubation with 20 % piperidine in DMF (10 mL g−1 resin).

Step	Description	Solvent	Volume	Time
1	Coupling	DCM/DMF 50/50	5 mL/g resin	60 min
2	Wash	DMF and DCM	10 mL/g resin	3 x 1 min each
3	Kaiser test	-	-	-
4	Fmoc deprotection	20 % piperidine/DMF	10 mL/g resin	4 x 10 min
5	Wash	DMF and DCM	10 mL/g resin	3 x 1 min each
6	Kaiser test	-	-	-

Table 7. General steps of a manually conducted synthesis cycle

Step	Description	Solvent	Volume	Time
1	Coupling	NMP/DMF	5 mL/g resin	12 min at 50 °C
2	Double-coupling	NMP/DMF	5 mL/g resin	12 min at 50 °C
3	Wash	DMF	8 mL/g resin	5 x 1 min
4	Fmoc deprotection	20 % piperidine/DMF	7 mL/g resin	4 x 10 min
5	Wash	DMF and DCM	10 mL/g resin	3 x 1 min each

Table 8. General steps of an automatically conducted synthesis cycle.

2.2.1.3 Synthesis of linear, 2-arm and 4-arm structures

Oligoamides were synthesized using a 2-chlorotrityl resin preloaded with the first C-terminal amino acid cysteine (C) of the respective topology as solid support. They were synthesized manually under standard Fmoc SPS conditions using syringe microreactors. Coupling steps were carried out using 4 eq. Fmoc-amino acid, 4 eq. HOBt, 4 eq. PyBOP and 8 eq. DIPEA in dichloromethane (DCM)–DMF 1 : 1 (10 mL g−1 resin) for 90 min. Equivalents were calculated relative to free resin-bound amines (1 eq.). Fmoc deprotection was accomplished by 4 × 10 min with 20 % piperidine in DMF (10 mL g−1 resin). A washing procedure comprising 3 × 1 min DMF, 3 × 1 min DCM incubation (10 mL g−1 resin) and a Kaiser test[102] were performed after each coupling and deprotection step. Symmetrical branching points were introduced using Fmoc-Lys(Fmoc)-OH. As (anti)folates are composed of a glutamate substructure and a pteroic acid derivative, the ligand structure was generated by a two-step procedure: Fmoc-Glu-OtBu was coupled, followed by Fmoc deprotection and subsequent coupling of N^{10}-(trifluoroacetyl) pteroic acid. The TFA protection group was removed by 4 x 30 min incubation with ammonia solution (25 %) - DMF 1 : 1 (10 mL g−1 resin). MTX was assembled analogously using the pteroic acid derivative 4-[[(2,4-diamino-6-pteridinyl)methyl]methylamino]benzoic acid.

Finally, all oligoamides were cleaved off the resin by incubation with TFA - TIS - H_2O - EDT 94 : 2.5 : 2.5 : 1 (10 mL g−1 resin) for 90 min. The cleavage solution was concentrated by flushing nitrogen and oligoamides were precipitated in 40 mL of pre-cooled MTBE–n-hexane 1 : 1. All oligoamides were purified by size exclusion chromatography using an Äkta purifier system (GE Healthcare Bio-Sciences AB, Uppsala, Sweden), a Sephadex G-10 column and water–acetonitrile 7 : 3 as solvent. All oligoamides were lyophilized. Oligoamide sequences were validated by mass

spectrometry and ^{1}H-NMR. Purity was evaluated via HPLC analysis (Silica C-18, ACN/H_2O gradient with 0.1 % TFA, 5 % ACN - 100 % ACN).

2.2.1.4 Synthesis of T-shapes 454 and 1198

The published lipo-oligomer ***454***[91] was modified by introducing the azide containing azidolysine at the N-terminal site of the peptide. ***1198***[100] was synthesized using a 2-chlorotrityl resin preloaded with the first C-terminal amino acid cysteine (C). The sequence C(Trt)-[Y(tBu)]$_3$-[Stp(Boc)$_3$]$_2$-K(Dde)-[Stp(Boc)$_3$]$_2$-[Y(tBu)]$_3$-C(Trt) was synthesized using a SyroWave^{TM}synthesizer (Biotage, Uppsala, Sweden). Coupling steps were carried out using 4 eq. Fmoc-amino acid, 4 eq. HOBt, 4 eq. HBTU, and 8 eq. DIPEA in NMP/DMF (5 mL g^{-1} resin) twice for 12 min at 50 °C. The Fmoc protection group was removed by 5 x 10 min incubation with 20% piperidine in DMF (7 mL g^{-1} resin). After every coupling or deprotection step, the resin was washed six times with DMF (6 x 1 min, 8 mL g^{-1} resin). All further synthesis steps were performed manually under standard Fmoc solid-phase peptide synthesis conditions using syringe microreactors. Coupling steps were carried out using 4 eq. Fmoc-amino acid, 4eq. HOBt, 4 eq. PyBOP, and 8 eq. DIPEA in DCM : DMF (1:1; 10 mL g^{-1} resin) for at least 60 min. Fmoc deprotection was accomplished by 4 × 10 min incubation with 20% piperidine in DMF (10 mL g^{-1} resin). The resin was washed with DMF (3 x 1 min, 10 mL g^{-1} resin) and DCM (3 x 1 min, 10 mL g^{-1} resin) after each coupling and deprotection step, followed by a Kaiser Test. Fmoc-Lys(N_3)-OH was coupled to the backbone and after the removal of the Fmoc protecting group, the N-terminal NH_2-group was protected with 10 eq. Boc anhydride and 10 eq. DIPEA in DCM/DMF. Dde-deprotection was accomplished using a hydrazine - DMF solution (3 x 5 min). Afterwards, the resin was washed with 5 x 1 min DMF 5 x 1 min 10% DIPEA/DMF and 3 x 1min DCM (10 mL g^{-1} resin). A symmetrical branching point was introduced using Fmoc-Lys(Fmoc)-OH. In the final coupling step oleic acid was coupled to yield lipo-oligomer ***1198***. The lipo-oligomer was cleaved off the resin using the optimized cleavage protocol for oleic acid containing structures, i.e., TFA cleavage condition with pre-cooling to avoid hydroxylation of the oleic acid double bonds.[103] Lipo-OAA ***1198*** was then purified by size exclusion chromatography (SEC) using a Äkta purifier system (GE Healthcare Bio-Sciences AB, Uppsala, Sweden), a Sephadex G-10 column (60 cm) and 10 mM hydrochloric acid solution : acetonitrile (7:3) as solvent. The lipo-oligomer ***1198*** was

lyophilized. The identity of the synthesized structures was confirmed by MALDI mass spectrometry.

Oligomer ***454*** was synthesized on a 2-chlorotrityl chloride resin preloaded with Fmoc-L-Cys(Trt)-OH. The backbone sequence C(Trt)-[Y(tBu)]$_3$-[Stp(Boc)$_3$]$_2$-K(Dde)-[Stp(Boc)$_3$]$_2$-[Y(tBu)]$_3$-C(Trt) was synthesized automatically. To introduce the hydrophobic domains, Dde removal was conducted with 2 % hydrazine in DMF (v/v) for 15 cycles lasting 3 min each. Finally, Fmoc-L-Lys(Fmoc)-OH was coupled to introduce a symmetrical branching prior to attaching oleic acids on both arms. The deprotected oligomer was obtained after cleavage, following the protocol for oleic acids.[103]

2.2.1.5 Synthesis of shielding agent DBCO-PEG

The DBCO-PEG shielding agent was synthesized by manual SPS. The 2-chlorotrityl resin was preloaded with Fmoc-dPEG$_{24}$-OH. After Fmoc deprotection (4 × 10 min with 20 % piperidine in DMF, 10 mL g^{-1} resin), DBCO was conjugated using 4 eq. DBCO-COOH, 4 eq. HOBt, 4 eq. HBTU and 8 eq. DIPEA in dichloromethane DCM–DMF 1 : 1 (10 mL g^{-1} resin) for 90 min. A washing procedure comprising 3 × 1 min DMF, 3 × 1 min DCM incubation (10 mL g−1 resin) and a Kaiser test were performed after each coupling and deprotection step. The structure was cleaved off the resin by incubation with TFA-TIS-H_2O - 95: 2.5: 2.5 (10 mL g−1 resin) for 90 min. DBCO-PEG was purified by SEC (see ***1198*** purification procedure).

2.2.1.6 Synthesis of DBCO-PEG-GE11 structures

For the synthesis of DBCO-PEG-GE11, a 2-chlorotrityl resin was preloaded with Fmoc-Ile-OH, the first C-terminal amino acid of the GE11 sequence. After deprotection, the GE11 sequence was completed via automated SPS. After the final automated deprotection step, Fmoc-dPEG$_{24}$-OH was coupled manually under the above described conditions. Finally, the sequence was cleaved off the resin by incubation with TFA - TIS - H_2O - 95 : 2.5 : 2.5 (10 mL g^{-1} resin) for 90 min followed by immediate precipitation in 40 mL of pre-cooled MTBE - n-hexane (1:1).

Next, DBCO-NHS was conjugated to the free N-terminus. The cleaved structure was dissolved in PBS, the pH was adjusted to 8 using 1 M NaOH. DBCO-NHS was dissolved in DMSO and added at 1 eq. to the free primary amine of the oligomer. After 1 h coupling time, the mixture was purified via preparative HPLC (LaPrep system, VWR International GmbH, Darmstadt, Germany) and a Waters SymmetryPrep C18 column (7µm, 19x150mm) with an ACN/H_2O gradient with 0.1% TFA (5 % ACN to 100 % ACN over 20 min). The targeting ligand conjugate was lyophilized, the successful coupling reaction was confirmed via MS.

2.2.2 Kaiser test[102]

Free amines of deprotected amino acids on the resin were determined qualitatively by Kaiser test. To that extent, a small sample of DCM washed resin was transferred into an Eppendorf reaction tube. One drop of 80 % phenol in EtOH (w/v), 5 % ninhydrin in EtOH (w/v) and 20 µM potassium cyanide (KCN) in pyridine (mixture of 1 mL aqueous 0.001 M KCN solution and 49 mL pyridine) each were added. The mixture was incubated at 99 °C for 4 min under steady shaking. The presence of free amines was indicated by a deep blue color.

2.2.3 Cleavage conditions

2.2.3.1 General cleavage conditions

Oligomers were cleaved off the resin by incubation with TFA - EDT - H_2O - TIS (94 : 2.5 : 2.5 : 1.0; 10 mL g−1 resin) for 90 min. The cleavage solution was concentrated by flushing nitrogen. Oligomers were precipitated in 50 mL of pre-cooled MTBE–n-hexane (1 : 1). All oligomers were purified by size exclusion chromatography (SEC) using an Äkta purifier system (GE Healthcare Bio-Sciences AB, Uppsala, Sweden), a Sephadex G-10 column and 10 mM hydrochloric acid solution - acetonitrile (7 : 3) as solvent. The relevant fractions were lyophilized, obtaining HCl salts of all oligomers.

2.2.3.2 Cleavage of oligomers containing oleic acid

Due to reactive double bonds in the structure the cleavage of oligomers containing oleic acid was optimized by Reinhard et al..[103] The resin was incubated with a mixture

of TFA - EDT - H2O - TIS (94 : 2.5 : 2.5 : 1.0; 10 mL g−1 resin, cooled to 4 °C prior to addition) for 30 min, followed by immediate precipitation in 50 mL of pre-cooled MTBE - n-hexane (1 : 1). The oligomers were purified by SEC as described above.

2.2.4 Synthesis of PT-H-SS-Py (2)

PT-H-SS-Py was synthesized by Dr. Jan Gorges (Organic Chemistry, Saarland University). Pretubulysin TFA salt (134 mg, 0.17 mmol, 1.0 eq.) was dissolved in 4 mL dry DCM. At room temperature 2-(pyridin-2-yldisulfanyl)ethyl hydrazinecarboxylate[104] (44 mg, 0.18 mmol, 1.05 eq.), HOBt (29 mg, 0.19 mmol, 1.1 eq.), *N*-methylmorpholine (42 mg, 0.41 mmol, 2.4 eq.) and *N*-(3-dimethylaminopropyl)-*N'*-ethylcarbodiimide hydrochloride (36 mg, 0.19 mmol, 1.1 eq.) were added. The reaction mixture was stirred at room temperature for 21 hours. Subsequently, 1 mL of saturated $NaHCO_3$ solution and 5 mL of DCM were added, the layers were separated, and the solvent of the organic phase was evaporated under reduced pressure. The crude product was purified by reversed-phase column chromatography (silica C-18, ACN/H_2O gradient, 0 % ACN → 35 % ACN). The product was isolated as a colourless amorphous solid (70 mg, 0.078 mmol, 46%). For analytical data (^{1}H-NMR, ^{13}C-NMR) see Appendix.

2.2.5 Synthesis of PT-O-SS-Py (3)

PT-O-SS-Py was synthesized by Dr. Jan Gorges (Organic Chemistry, Saarland University). Pretubulysin TFA salt (20 mg, 0.026 mmol, 1.0 eq.) was dissolved in 0.3 mL dry DCM and cooled with an ice bath. At 0 °C 2-(pyridin-2-yldisulfanyl)ethan-1-ol (6 mg, 0.032 mmol, 1.25 eq.), DMAP (*N,N*-dimethylpyridin-4-amine) (3 mg, 0.026 mmol, 1.0 eq.), and N-(3-dimethylaminopropyl)-*N*'-ethylcarbodiimide hydrochloride (5 mg, 0.028 mmol, 1.1 eq.) were added. The reaction mixture was stirred at room temperature for 20 hours. Subsequently, the solvent was evaporated under reduced pressure and the crude product was purified by column chromatography (silica DCM/MeOH, 10 % MeOH). The product was isolated as a colorless amorphous solid (18 mg, 0.019 mmol, 75 %). For analytical data (^{1}H-NMR, ^{13}C-NMR) see Appendix.

2.2.6 Synthesis of PT-H-oligomer conjugates

Oligoamides were dissolved in HBG and conjugated to the activated PT-hydrazide-molecule PT-H-SS-Py (2) by stoichiometric mixing of 10 µM solutions in HBG for *in situ* disulfide exchange. The mixture was incubated on a shaker for 1 hour. Incubation time of 1 hour was established to be sufficient for conjugation by photometric measurement of the released pyridine-2-thiol. Formation of oligoamide PT conjugates was demonstrated by HPLC analysis for the 2-arm E4-MTX-H-PT construct (Figure 7).

2.2.7 Fluorescein labeling of oligomers

For fluorescein-5-maleimide labeling, the sulfhydryl containing oligoamides, which are prone to disulfide formation, were reduced with TCEP reducing gel (Pierce™ Immobilized TCEP Disulfide Reducing Gel, Thermo Fisher Scientific). The reduction was conducted according to the manufacturer's protocol. The oligoamides were dissolved in 10 mM EDTA in water to prevent oxidation of the generated sulfhydryl groups, added to the prewashed gel and incubated for 1h. The supernatant contained the reduced oligoamides and was immediately used for the coupling reaction. Fluorescein-5-maleimide (Thermo Scientific Fisher) was used at a 15-fold molar excess and dissolved in DMF. For the coupling reaction the pH was adjusted to 6.8. After 2 h incubation the conjugate was purified by size exclusion chromatography using an Äkta purifier system (GE Healthcare Bio-Sciences AB, Uppsala, Sweden), a Sephadex G-10 column and water - acetonitrile 7 : 3 as solvent. The successful dye coupling was validated by MS.

2.2.8 Cy5 labeling of oligomer 454

Lipo-oligomer ***454*** were labeled using Cy5-NHS ester. To that extent, ***454*** (2.5 mg, 0.8 µmol) was dissolved in 0.5 mL of HEPES buffer (pH7.4). The pH was adjusted to 8.3 using 1 M NaOH. Cy5-NHS ester (0.4 mg, 0.6 µmol) was dissolved in DMSO and added to the lipo-oligomer solution. After 4 h reaction time at room temperature, the ***454***-Cy5 conjugate was purified by dialysis using a 1000 Da cut off membrane. The solution was lyophilized to yield ***454***-Cy5 as a blue powder.

2.2.9 Formation of drug incorporating *454* nanomicelles

Lipo-OAA ***454*** was dissolved in HEPES-buffered glucose (HBG, 20 mM HEPES, 5 % glucose [w/w], pH 7.4) at a concentration of 10 mg/mL. PT and MTX were dissolved in 10% DMSO, 90% HBG at a stock concentration of 10 mM. The drug solution was further diluted with HBG to final concentrations of 1 mM for MTX and 0.5 mM PT. The nanomicelle was formed by adding an equal volume of drug solution PT+MTX (0.5 mM + 1 mM) to the oligomer solution (10 mg/mL, 3 mM), and the solution was mixed by vigorous pipetting (Method A). This resulted in final concentrations of 250 µM PT, 500 µM MTX and 5 mg/mL (1.5 mM) lipo-oligomer ***454*** in the nanoparticle. Nanomicelles started to form immediately. Ratios of oligomer to drug concentrations and their effects on particle formation as described below are crucial for particle properties. Alternatively, micelles can be formed by dissolving dry lipo-OAA in a drug solution in HBG (Method B). Particle sizes and drug incorporations were comparable to particles formed from solution.[105]

2.2.10 Polyplex preparation

For polyplex formation, the siRNA was dissolved in 20 mM HEPES buffered 5% glucose pH 7.4 (HBG) at a concentration of 500 ng/µL. All polyplexes were prepared at a nitrogen/phosphate (N/P) ratio of 10, only protonatable nitrogens were considered in the N/P calculation. The lipo-oligomer ***1198*** solution was prepared in a separate tube in HBG. An equal volume of siRNA was added to the oligomer. The mixture was rapidly pipetted at least 5 x and incubated for 45 min at room temperature. The resulting polyplex solution contained 250 ng of siRNA/µL.

For PT containing polyplexes, PT in HBG was added to the siRNA solution to yield a PT+siRNA solution containing 0.156 ng PT/µL and 500 ng siRNA/µL. The siRNA+PT solution was added to the oligomer and again, the mixture was rapidly pipetted and left to incubate for 45 min. The polyplex contained 250 ng of siRNA/µL and 0.078 ng PT/µL.

For further experiments, e.g. MTT assays, the solution was further diluted. Twenty µL of polyplex solution containing 250 ng of siRNA and 0.078 ng of siRNA were added to 80 µL of medium in the well. This corresponded to molar concentrations of 185 nM siRNA and 1 nM of PT per well.

2.2.11 Post-modification of polyplexes with DBCO-PEG agents

For post-functionalization of ***1198*** siRNA polyplexes with click agents DBCO-PEG or DBCO-PEG-GE11, reagent solutions were prepared in ¼ of the volume of the polyplex solution. The concentration of the solution was calculated according to the respective equivalents (eq). Equivalents represent the molar ratio of shielding agents to oligomers in the polyplex solution. All polyplexes were modified with 0.75 eq. of click agent. The reaction time was 4 h.

2.2.12 Particle size and zeta potential

To determine particle size, nanomicelle complexes were formed as described above. ***454*** PT+MTX particles contained 250 µM PT, 500 µM MTX and 1500 µM lipo-OAA ***454***. ***1198*** polyplexes were freshly prepared as described above. Nanoparticle solution (60 µL) was transferred to a capillary cell (DTS1070) and measured using a Zetasizer Nano ZS with backscatter detection (Malvern Instruments, Worcestershire, UK).

For size measurements, the equilibration time was 0 min, the temperature was 25°C and an automatic attenuator was used. The refractive index of the solvent was 1.337 and the viscosity was 1.0336 mPa x s. Each sample was measured 3 times.

2.2.13 Transmission electron microscopy (TEM)

Transmission electron microscopy (TEM) images were taken by Dominik Loy (Pharmaceutical Biotechnology, LMU München). Carbon coated copper grids (300 mesh, 3.0 mm O. D.; Ted Pella, Inc. USA) were activated by plasma cleaning (420 V, 1 min, argon atmosphere). Afterwards, 5 µL of nanomicelle solution (250 µM PT, 500 µM MTX and 1500 µM lipo-OAA ***454***) were incubated on the grids for 3 min before it was removed and stained by a 1.0 % uranyl formate solution according to the following procedure: First, 5 µL uranyl formate solution were placed on the grid and removed immediately, second, 5 µL of the same solution were left on the grid for five seconds before removal. Afterwards, the grids were dried for 30 min at room temperature. The stained nanomicelles were visualized by a JEM/1011 transmission electron microscope with 80 kV acceleration voltage.

2.2.14 Drug incorporation efficiency

Incorporation efficiency was determined by ultrafiltration of nanoparticles and subsequent HPLC analysis of the filtrate. Nanoparticles were formed (***454*** PT+MTX: 250 µM PT, 500 µM MTX and 1500 µM lipo-OAA ***454***; ***1198*** siEG5+PT: N/P 10, 50 µg siRNA and 0.3 ng PT in 200 µL polyplex solution). Amicon Ultra – 0.5 mL (Ultracel 3 K) centrifugal filters were used according to the manufacturer's protocol. The filters were pre-rinsed with 200 µL of Millipore water. Particle solution in HBG (140-200 µL) was added to the filter, the filled device was inserted into a microcentrifuge tube and centrifuged at 18 000 g for 30 min. The filtrate was subjected to HPLC analysis (C-column, YMC column, HS-302, HS12S05-1546WT, 150 x 4.6 mm I.D., S-5 µm, 12 nm, YMC Europe GmbH, Dinslaken, Germany) with a gradient of 5% to 100% acetonitrile with 0.1 % TFA in 20 min. Unincorporated drugs PT and MTX were detected at 214 nm. Incorporation efficiency was calculated by comparing the peak areas of ultrafiltered, incorporated drug to the peak areas of ultrafiltered free drug. All experiments were performed in triplicates.

2.2.15 Stability of drug incorporation in HBG, 154 mM NaCl and FBS containing HBG.

The stability of drug incorporation in ***454*** PT+MTX nanomicelles incubated in HBG, 154 mM HBG and 10 % - 50 % FBS in HBG was determined at different temperatures and incubation time points. Nanomicellar PECs were prepared in HBG as previously described (250 µM PT, 500 µM MTX, 1500 µM lipo-OAA ***454***). Particle solution (100 µL) was added to the respective incubation medium (HBG, 308 mM NaCl and 20 – 100 % FBS in HBG). After incubation at room temperature or 37°C in a shaker for 1 h or 12 h, nanomicelles were ultrafiltered at 18 000 g for 30 min. Depending on the incubation medium, filtration devices with different cut offs were used. Amicon Ultra – 0.5 mL (Ultracel 3 K) were used to measure drug release upon incubation in serum-free HBG or NaCl solution. Due to interactions of PT and FBS components, filtration devices with a 100 K cut off (Amicon Ultra – 0.5 mL, Ultracel 100 K) were used in case of FBS containing solutions. Control experiments demonstrated that MTX or PT, only if released from nanomicelles, would be detectable in the filtrates in both settings. The filtrates were subjected to HPLC analysis (C18-column, YMC column, HS-302,

HS12S05-1546WT, 150 x 4.6 mm I.D., S-5 µm, 12 nm, YMC Europe GmbH, Dinslaken, Germany) with a gradient of 5% to 100% acetonitrile with 0.1 % TFA in 20 min. The amount of released drug upon incubation was determined for MTX and PT and calculated in relation to free PT+MTX which was incubated under the same conditions. The detection wavelength was 214 nm for PT and MTX monitoring. All experiments were performed in triplicates.

Alternatively, the release of MTX upon incubation of ***454*** PT+MTX in the different media was determined photometrically at 340 nm. Particles were formed to contain 125 µM PT, 250 µM MTX and 750 µM ***454*** and 100 µL particle solution was diluted with 100 µL of HBG, 308 mM NaCl and 20 % FBS in HBG. After ultrafiltration (Amicon Ultra – 0.5 mL Ultracel 3 K), 100 µL of filtrate were filled in a micro cuvette and the amount of released MTX was determined photometrically at 340 nm. Drug release was calculated in relation to ultrafiltered, free MTX.

2.2.16 Agarose gel shift assay

An agarose gel (1%) was prepared by dissolving agarose in TBE buffer (10.8 g of trizma base, 5.5 g of boric acid, 0.75 g of disodium EDTA, and 1 L of water) and subsequent boiling. After cooling down, GelRed™(Biotium, Inc., Hayward, CA, USA was added for siRNA detection. ***1198*** siEG5 polyplexes were prepared as described above containing 250 ng/µL and loading buffer, siRNA electrophoresis was performed at 80 V for 40 min.

2.2.17 Dihydrofolate reductase activity assay

The enzymatic activity of the enzyme dihydrofolate reductase (DHFR) in the presence of various MTX and FolA containing oligoamides was determined using a dihydrofolate reductase assay kit (Sigma-Aldrich) based on the NADPH dependent reduction of dihydrofolic acid to tetrahydrofolic acid. The assay was conducted according to the manufacturer's protocol. All tested compounds were dissolved in the provided assay buffer at final concentrations of 1000, 100, 10 and 1 nM. The reaction progress was monitored photometrically over a period of 5 min by measurement of NADPH absorption at 340 nm each 15 s. Control reactions in the absence of inhibitors were

carried out. Data points were fitted by linear regression and the gradient was determined. Relative enzyme activity was calculated as the ratio between the gradient of the reaction with test compound to the gradient of the control reaction without inhibition. The assay was carried out in triplicates for each oligoamide.

2.2.18 Cellular internalization determined by flow cytometry

2.2.18.1 Cellular internalization of oligoamide conjugates

Flow cytometry experiments to determine the uptake of the FR-targeted oligoamide-fluorescein conjugates were performed by Jasmin Kuhn (Pharmaceutical Biotechnology, LMU München).

KB cells were seeded on collagen-coated 24-well plates at a density of 5 x 10^4 cells/well 1 day before the experiment, medium was replaced with 450 µL of fresh growth medium either FolA-free or FolA-substituted at a concentration of 1.5 mM and cells were incubated for 30 min at 37 °C. L1210 cells were seeded 2 h prior to experiments at a density of 2 x 10^5 cells/well in 450 µL of FolA-free or FolA-substituted medium. Solutions of 20 µL oligoamide-fluorescein conjugates (at 1 µM calculated for the oligoamide), HBG or STOTDA-FITC (negative control) were added and incubated for 30 min. Medium was removed and cells were treated twice with PBS containing 100 IU heparin/mL for 15 min to remove non-internalized oligoamides. Cells were detached with Trypsin/EDTA, suspended in FACS buffer (PBS with 10 % FCS), centrifuged (2000 rpm, 5 min, 4 °C) and resuspended in 600 µL of FACS buffer. Internalization of the conjugates was measured by flow cytometry with CyanTM ADP (Dako, Hamburg, Germany) through excitation at 635 nm, and detection of emission at 665 nm. Dead cells were excluded by DAPI fluorescence detection. Data were analyzed by FlowJo® 7.6.5 flow cytometric analysis software.2.1.X. All experiments were performed in triplicates.

2.2.18.2 Cellular internalization of 1198 polyplexes

Flow cytometry experiments to determine the cellular internalization of ***1198*** polyplexes were performed by Dr. Wei Zhang and Dr. Yanfang Wang (Pharmaceutical Biotechnology, LMU München.) KB cells (5 x 10^4 cells/well) or Huh7 cells (8 x 10^4 cells/well) were seeded in 24-well plates at 24 h before the experiment. Medium was

changed. Subsequently, polyplexes (containing 1.5 µg siRNA per well including 20% Cy5 labeled siRNA) modified with DBCO-PEG-GE11 or DBCO-PEG were added into each well for 45 min at 37 °C in 5% CO_2. Cells were washed with PBS twice, then with 500 I.U. heparin to remove polyplexes non-specifically associated to the cell surface. After washing with PBS, cells were collected and resuspended in FACS buffer (PBS buffer with 10 % FBS). Internalization of the polyplexes was measured by flow cytometry with CyanTM ADP (Dako, Hamburg, Germany) through excitation at 635 nm, and detection of emission at 665 nm. Dead cells were excluded by DAPI fluorescence detection. Data were analyzed by FlowJo® 7.6.5 flow cytometric analysis software.2.1.X. All experiments were performed in triplicates.

2.2.19 Cellular internalization determined by confocal laser scanning microscopy

2.2.19.1 Cellular internalization of 454 PT+MTX

Confocal light scattering microscopy (CLSM) images were taken by Miriam Höhn (Pharmaceutical Biotechnology, LMU München). L1210 cells were seeded at a density of 1 × 10^5 cells/well (12-well plate, 960 µL cell suspension per well) 4 h prior to treatment. The cells were treated with 40 µL drug solution containing ***454***/***454***-Cy5 PT+MTX in HBG to a final drug concentration of 1 µM PT, 2 µM PT and 6 µM ***454***/***454***-Cy5 (50 % ***454***, 50 % ***454***-Cy5) on cells. After 4 h incubation time, cells were collected by centrifugation and washed with phosphate buffered saline (PBS). KB cells were seeded into eight-well µL-slides at a density of 1 x 102 in 300 µL of growth medium. After 4 h treatment with ***454***/***454***-Cy5 PT+MTX particles, medium was removed, and cells were washed with PBS. Cells were fixed with 4 % paraformaldehyde (PFA) in PBS for 45 min. After a PBS wash, the nucleus was stained with 4,6-diamidino-2-phenylindole (DAPI) and the actin skeleton with phalloidin-rhodamine for 45 min. The staining solution was removed, PBS was added to the KB cells in the chamber slides, which were then used for microscopy. L1210 cells were centrifuged and washed with PBS after the last staining step. PBS was removed and the cells were resuspended in 20 µL of mounting medium (Roti®-Mount FluorCare, Carl Roth). Five µL of the viscous cell suspension were added to a microscope slide, the cover slip was carefully placed on top of the drop. The cover slip was sealed with nail polish. After drying, the prepared

microscope slides were used for microscopy. Cellular internalization was observed by laser scanning confocal microscopy (Leica TCS SP8, Germany).

2.2.19.2 Cellular internalization of 1198 polyplexes

CLSM measurements to determine cellular internalization of ***1198*** polyplexes were performed by Dr. Wei Zhang, Dr. Yanfang Wang and Miriam Höhn (Pharmaceutical Biotechnology, LMU München). KB cells (2 x 10^4 cells/well) or Huh7 cells (2 x 10^4 cells/well) were seeded 24 h before the experiment in 8-well Ibidi µ-slides in 300 µL growth medium. Cells were incubated with polyplexes (containing 500 ng siRNA per well including 20% Cy5 labeled siRNA) for 45 min at 37 °C in 5% CO_2 after fresh medium was changed. Cells were washed twice with PBS and fixed with 4% paraformaldehyde solution for 30 min at room temperature. DAPI was used as nucleus staining probe, and actin cytoskeleton was stained with rhodamine phalloidin. Cellular internalization was observed by laser scanning confocal microscopy (Leica TCS SP8, Germany).

2.2.20 Influence of PT+MTX treatment on intracellular actin and tubulin determined by CLSM

CLSM images were taken by Miriam Höhn (Pharmaceutical Biotechnology, LMU München). L1210 cells were seeded at a density of 1 × 10^5 cells/well (12-well plate, 960 µL cell suspension per well) 4 h prior to treatment. The cells were treated with 40 µL drug solution containing PT, MTX and PT+MTX in HBG to a final drug concentration of 200 nM PT and 600 nM MTX on cells. After 24 h, 48 h or 72 h incubation time, cells were collected by centrifugation and washed with PBS. KB cells were seeded into eight-well µL-slides at a density of 1 x 102 in 300 µL of growth medium. After the respective incubation time, medium was removed and cells were washed with PBS. L1210 and KB cells were then extracted in Microtubule Stabilizing Buffer (80 mM PIPES pH 6.8, 1 mM MgCl2, 5mM EGTA-K, and 0.5% Triton X-100) for 30 seconds to remove monomeric and dimeric tubulin subunits. Glutaric aldehyde was added to a final concentration of 0.5% and cells were fixed for 10 minutes. A 0.1% solution of $NaBH_4$ in PBS was used for subsequent quenching of unreacted glutaric aldehyde (7 min). Next, cells were washed with PBS: L1210 cells were collected by centrifugation before washing, KB cells were washed in the chamber slides. To block unspecific

binding sites, cells were incubated with antibody dilution (AbDi)l solution (TBS-0.1% Triton X-100, 2% BSA 0.1% Azide) for 10 min. The cells were incubated with the primary α-tubulin antibody (Sigma-Aldrich, T9026) in AbDil solution for 45 min. After a TBS wash, the secondary antibody (Alexa Fluor 488) was added and left on the cells for another 45 min. Cells were washed with TBS and incubated with a solution of DAPI (nucleus staining reagent) and phalloidin-rhodamine (F-actin staining reagent) in AbDil for 15 min. The staining solution was removed, cells were washed with TBS and 100 µL of AbDil solution was added to the KB cells in the chamber slides, which were then used for microscopy. L1210 cells were centrifuged and washed with TBS after the last staining step. TBS was removed and the cells were resuspended in 20 µL of mounting medium (Roti®-Mount FluorCare, Carl Roth). 5 µL of the viscous cell suspension were added to a microscope slide, the cover slip was carefully placed on top of the drop. The cover slip was sealed with nail polish. After drying, the prepared microscope slides were used for microscopy.

2.2.21 GFP gene silencing

GFP gene silencing experiments were performed by Dr. Wei Zhang and Dr. Yanfang Wang (Pharmaceutical Biotechnology, LMU München). KB-eGFP-Luc cells (4 x 10^3 cells/well) or Huh7-eGFP-Luc cells (5 x 10^3 cells/well) were seeded in 96 well plates at 24 h before transfection. Cells were placed in fresh medium and incubated with 20 µL polyplex solution containing control siRNA or GFP siRNA (500 ng siRNA/well or 370 nM, N/P 10), alternatively siRNA co-formulated with 0.78 ng PT (results in elevated final concentration of 10 nM PT in well). Due to the short incubation time of 4+44 h, the concentration of PT was increased 10-fold in these experiments. Cells were cultured for 4 h, then the polyplex containing medium was replaced with fresh medium. Cells were incubated for a further 44 h. Afterwards, luciferase activity of cell lysates was measured using a Centro LB 960 plate reader luminometer (Berthold Technologies, Bad Wildbad, Germany) and a luciferin-LAR (1 M glycylglycine, 100 mM $MgCl_2$, 500 mM EDTA, DTT, ATP, coenzyme A) buffer solution at 48 h after transfection. The relative light units (RLU) were presented as percentage of the eGFP-luciferase gene expression obtained with buffer treated control cells. All experiments were performed in triplicates.

2.2.22 EG5 mRNA expression by qRT-PCR

To determine the mRNA level of the EG5 gene in transfected cells quantitative real time polymerase chain reactions (qRT-PCR) were performed by Dr. Yanfang Wang (Pharmaceutical Biotechnology, LMU München). KB cells (1.2 x 10^5 cells/well) and Huh7 cells (1.5 x 10^5 cells/well) were seeded in 2 mL of medium onto 6-well plates. After 24 h, medium was replaced with 900 µL of fresh medium. Cells were treated with 100 µL of polyplex solution containing 5 µg siEG5 or siCtrl (N/P 10) and incubated for 2 h. The medium was replaced with 1 mL of fresh growth medium. 24 h after transfection the total RNA was isolated with peqGOLD Total RNA Kit (Peqlab, Germany) followed by a reverse transcription using qScriptTM cDNA Synthesis Kit (Quanta Biosciences, USA) according to the manufacturers' protocols. Quantitative RT-PCR was performed in triplicates on a LightCycler 480 system (Roche, Mannheim, Germany) using UPL Probes (Roche, Mannheim, Germany) and Probes Master (Roche, Mannheim, Germany) with GADPH as housekeeping gene. The following probes and primer sequences were used: EG5, UPL Probe #53, left primer: CATCCAGGTGGTGGTGAGAT, right primer: TATTGAATGGGCGCTAGCTT; GAPDH, UPL Probe #45, left primer: TCCACTGGCGTCTTCACC, right primer: GGCAGAGATGATGACCCTTTT. Results were analyzed by the ΔCT method. CT values of GAPDH were subtracted from CT values of EG5. ΔCT values of siRNA-transfected cells were calculated as percentage relative to untreated control cells. All experiments were performed in triplicates.

2.2.23 Cell viability

L1210 suspension cells were seeded at a density of 5 x 10^3 cells/well (96-well plate) in 80 µL growth medium 4 h prior to addition of 20 µL treatment solution (refer to 2.2.23.1-4). KB cells were seeded at a density of 2.5 × 10^3 cells/well (96-well plate) in 100 µL of growth medium. Huh7 cells were seeded at a density of 5 x 10^3 cells/well (96-well plate) in 100 µL of growth medium. For KB and Huh7 cells, medium was replaced with 80 µL of fresh medium 1 h before treatment with 20 µL of treatment solution in 20 mM HBG. Cells were treated with free or formulated drugs for 2, 4, 24, 48 or 72 h in a cell culture incubator at 37 °C. After 2 and 4 h treatment, the cells were washed once with fresh medium. L1210 cells were washed by centrifuging the 96 well plate (1000 rpm, 7 min) and careful removal of the supernatant. Fresh medium (100 µL) was added, the plate was centrifuged again, and the medium was once more exchanged. After the

respective incubation times (see 2.2.23.1-4) 3-(4,5-dimethylthiazol-2-yl)-2,5-diphenyltetrazolium bromide (MTT, 10 µL, 5 mg/mL in PBS) was added to each well and cells were incubated for 2 h. For cell lysis of L1210 cells, a solution of 10 % sodium dodecyl sulfate (SDS) in 0.01 M hydrochloric acid (HCl) was added and incubated overnight. For KB cells and Huh7 cells, the medium was removed, cells were frozen at -80 °C for at least 30 min and DMSO was added to dissolve the formed formazan dye. In both cases, absorption was measured at a wavelength of 590 nm against a reference wavelength of 630 nm using a SpectraFluor™ Plus microplate reader (Tecan, Groedig, Austria). Cell viability was calculated as percentage of absorption compared to wells treated with HBG only. All experiments were performed in quintuplicates.

2.2.23.1 Cell viability of PT-oligoamide treated KB and L1210 cells

KB and L1210 cells were treated with PT-H-SS-Py, PT-H-C, PT-COOH (also known as PT) and PT-O-SS-Py, as well as PT-H oligoamide conjugates for 72 h. See x-axis label for treatment concentrations.

2.2.23.2 Cell viability of PT+MTX treated KB and L1210 cells

PT, MTX or PT+MTX in HBG were added, and plates were left to incubate for 72 h. See x-axis label for treatment concentrations.

2.2.23.3 Cell viability of 454 PT+MTX treated KB and L1210 cells

Cells were treated with free drug (PT, MTX, PT+MTX) or formulated drugs (***454*** PT, ***454*** MTX, ***454*** PT+MTX) for 4, 48 or 72 h. After 4 h treatment, the cells were washed once with fresh medium. L1210 cells were washed by centrifuging the 96 well plate (1000 rpm, 7 min) and careful removal of the supernatant. Fresh medium (100 µL) was added, the plate was centrifuged again, and the medium was once more exchanged. Cells were left to incubate for a further 44 or 68 h. KB cells treated for 4 h were also washed once with fresh medium, before being incubated for another 44 or 68 h.

2.2.23.4 Cell viability of 1198 PT+siEG5 treated KB and Huh7 cells

Twenty µL of free PT (0.078 ng) or the polyplexes containing 250 ng siRNA co-formulated with 0.078 ng PT were added to yield final concentrations of 185 nM siRNA and 1 nM PT and left on the cells for 48 h, 72 h or 2 h. In the last case, the treatment solution was replaced with fresh medium and cells were incubated for 70 h.

2.2.24 Cell cycle analysis

For cell cycle analysis, L1210 were seeded at a density of 1 x 10^5 L1210 (12-well plate, 940 µL cell suspension per well) 4 h prior to addition of 60 µL treatment solution (see 2.2.24.1 and 2.2.24.2 for specified content of treatment solution). Cells were incubated for 24 or 48 h, collected by centrifugation and washed with PBS. KB cells were seeded at a density of 5 x 10^4 cells/well. After 24 h, medium was changed and 960 µL of fresh medium were added, 30 min prior to addition of 40 µL drug solution. Cells were incubated for 24 or 48 h. KB cells were detached with T/E prior to collection and washed with PBS. Then, 100 µL of propidium iodide treatment solution (0.1% sodium citrate, 0.1% Triton-X100, 50 µg x mL−1 propidium iodide in Millipore water) were added and cells were incubated for 3 h on ice in dark. Cells were centrifuged after adding 1 mL of PBS, resuspended in 500 µL of PBS, and measured with the CyanTM ADP flow cytometer. Data were analyzed by FlowJo 7.6.5 flow cytometric analysis software. All experiments were performed in triplicates.

2.2.24.1 Cell cycle analysis of PT+MTX treated L1210 and KB cells

The cells were treated with PT, MTX and PT+MTX in HBG to a final drug concentration of 200 nM PT and 600 nM MTX on cells.

2.2.24.2 Cell cycle analysis of 454 PT+MTX treated L1210 cells

The treatment solution contained free or formulated drug or free oligomer at the following final concentrations on cells: 200 nM PT, 400 nM MTX, 800 nM lipo-OAA ***454***.

2.2.25 Apoptosis analysis

L1210 cells were seeded at a density of 1 × 10^5 cells/well (12-well plate, 960 µL cell suspension per well) 4 h prior to treatment. The cells were treated with 40 µL drug solution containing PT, MTX and PT+MTX in HBG to a final drug concentration of 200 nM PT and 600 nM MTX on cells. KB cells were seeded at a density of 5 × 104 cells/well (12-well plate, 1 mL cell suspension per well). After 24 h, medium was changed and 960 µL of fresh medium were added, 30 min prior to addition of 40 µL drug solution containing PT, MTX and PT+MTX in HBG to a final drug concentration of 200 nM PT and 600 nM MTX on cells. The cells were incubated for 24, 48 or 72 h.

L1210 cells were collected by centrifugation, KB cells were detached using T/E prior to collection. After a PBS wash, apoptosis was detected with an Annexin V-FITC/PI assay (BioVision) by Cyan ADP flow cytometry. Data were analyzed by FlowJo 7.6.5 flow cytometric analysis software. Cells in different apoptotic stages were visualized with the dyes annexin V-fluorescein isothiocyanate (FITC)/propidium iodide (PI). Annexin V has a high affinity for membrane phosphatidylserine (PS), thus FITC-labeled annexin V can be used for the detection of outer membrane translocated PS in apoptotic cells. PI can intercalate in the DNA. It can reach the DNA as soon as the cell membrane has started to disintegrate. No dye can bind to healthy cells, they are therefore Annexin V-FITC –/PT – (Q4). When cells start to undergo apoptosis, annexin V binds PS. PI, however, cannot yet reach the DNA. Cells are Annexin V-FITC +/PI – (Q3). In late apoptosis or necrosis, cells are Annexin V-FITC +/ PI + (Q2). When the cell membrane is very badly deformed, Annexin V cannot bind PS anymore even though PI can still stain the DNA (Annexin V-FITC –/PI +, Q1). All experiments were performed in triplicates.

2.2.26 *In vivo* experiments

Animal experiments were performed by Dr. Sarah Kern (Pharmaceutical Biotechnology, LMU München). Mice were housed in isolated ventilated cages under specific pathogen-free conditions with a 12 h day/night interval and food and water ad libitum. After a minimum of 7 days of acclimation time, tumor cells were subcutaneously injected into the left flank of female, 6-week-old mice, RJ: NMRI-nu (nu/nu) (Janvier, Le-Genest-St-Isle, France). After tumor cell inoculation, weight and general well-being were monitored continuously. Tumor size was measured with a caliper and determined by formula $a \times b^2 / 2$ (a = longest side of the tumor; b = widest side vertical to a). All animal experiments were performed according to the guidelines of the German law for the protection of animal life and were approved by the local animal ethics committee.

2.2.26.1 Murine leukemia tumor model

L1210 cells (0.5×10^6 cells in 150 µL PBS) were injected subcutaneously into the left flank of female 6-week-old mice, RJ: NMRI-nu (nu/nu) (Janvier, Le-Genest-St-Isle, France) after a minimum of 7 days of acclimation time prior to experiments.

2.2.26.2 Xenograft animal model

KB-wt cells (5×10^6) suspended in 150 µL PBS were injected subcutaneously into the left flank of female 6-week-old mice, RJ: NMRI-nu (nu/nu) (Janvier, Le-Genest-St-Isle, France) after a minimum of 7 days of acclimation time prior to experiments.

2.2.26.3 4-arm MTX-H-PT treatment study

The animals were randomly divided into 4 groups (n=8). Two days after inoculation of tumor cells, the animals were injected intratumorally with 50 µL of native PT (PT-COOH), the 4-arm structure 4-arm E4-MTX and the corresponding conjugate with PT-hydrazide 4-arm E4-MTX-H-PT. Treatments were repeated on days 2, 5, 7, 9, 12 and 14. Tumor sizes of the animals were monitored daily. Animals were sacrificed after the tumor size reached 1000 mm^3 in the control and 4-arm E4-MTX groups.

2.2.26.4 Treatment experiment in L1210 tumor model

Three days after tumor cell inoculation, animals were randomly divided into 3 groups (n = 6). Intravenous treatments were performed 8 times (on days 3, 5, 7, 10, 12, 14, 17 and 19). Animals were injected via tail vein injection with 250 µL of PT+MTX (PT: 2 mg/kg, MTX: 2.5 mg/kg), the corresponding nanomicelle ***454*** PT+MTX or HBG buffer control. Mice were sacrificed by cervical dislocation once their tumor reached 1500 mm^3 or in case of severely affected well-being (e.g. continuous weight loss, apathy, visibly enlarged lymph nodes or spleen) for reasons of animal welfare.

2.2.27 MALDI-TOF mass spectrometry

One µL matrix consisting of a saturated solution of Super-DHB (mixture of 2,5-dihydroxybenzoic acid and 2-hydroxy-5-methoxybenzoic acid) in acetonitrile / water (1:1) containing 0.1% (*v*/*v*) trifluoroacetic acid was applied on a MTP AnchorChip (Bruker Daltonics, Bremen, Germany). After the Super-DHB matrix dried and crystalized, one µL of the sample solution (10 mg/mL in water) was added to the matrix spot. Samples were analyzed using an Autoflex II mass spectrometer (Bruker Daltonics, Bremen, Germany). Spectra were partly recorded by Dr. Sören Reinhard and Dr. Stephan Morys (Pharmaceutical Biotechnology, LMU München) after positive or negative ionization.

2.2.28 Proton NMR spectroscopy

^{1}H-NMR spectra were recorded using an AVANCE III HD500 (500 MHz) by Bruker with a 5 mm CPPBBO probe. Spectra were recorded without TMS as internal standard and therefore all signals were calibrated to the residual proton signal of the deuterium oxide (D_2O) solvent. Chemical shifts are reported in ppm and refer to the solvent as internal standard (D_2O at 4.79). Integration was performed manually. The spectra were analyzed using MestreNova (Ver.9.0 by MestReLab Research). Integrals were normalized to the succinic acid peaks.

2.2.29 Analytical RP-HPLC

Reversed-phase HPLC (RP-HPLC) was carried out with a VWR-Hitachi Chromaster 5160 Pump System (VWR, Darmstadt, Germany), VWR-Hitachi Chromaster 5260 Autosampler (VWR, Darmstadt, Germany) and a Diode Array Detector (VWR-Hitachi Chromaster 5430; VWR, Darmstadt, Germany) at 214 nm detection wavelength. As a column either a YMC Hydrosphere 302 C18 (YMC Europe, Dinslaken, Germany) or a Waters Sunfire C18 (Waters, Saint-Quentin en Yvelines Cedex, France) was used. A gradient starting at 95 : 5 (water / acetonitrile) to 0 : 100 within 20 min was applied. All solvents were supplemented with 0.1% trifluoroacetic acid.

2.2.30 Statistical analysis

The results are presented as mean values of experiments performed in at least triplicates. Unless stated otherwise, error bars display standard deviation (SD). Statistical analysis of the results (mean ± SD) was evaluated by unpaired t test: *$p < 0.05$; **$p<0.01$; ***$p < 0.001$; ****$p < 0.0001$. Calculations and graphical presentation were performed with Prism 6 (GraphPad Software Inc.).

3 Results

3.1 Sequence-defined oligoamide drug conjugates of pretubulysin and methotrexate for folate receptor targeted cancer therapy

This chapter was adapted from:

Truebenbach, I.; Gorges, J.; Kuhn, J.; Kern, S.; Baratti, E.; Kazmaier, U.; Wagner, E.; Lächelt, U., Sequence-Defined Oligoamide Drug Conjugates of Pretubulysin and Methotrexate for Folate Receptor Targeted Cancer Therapy. Macromol Biosci 2017, 17 (10).

The novel tubulin binding drug PT was shown to have antitumoral[9-11, 16] and antiangiogenic properties, vascular disrupting effects[19] as well as antimetastatic potential.[9] Nevertheless, medium sized drugs can suffer from short systemic circulation time, suboptimum intracellular uptake and undesired toxicity at non-target sites.[106, 107] The conjugation of small molecule drugs to receptor targeted, sequence-defined oligoamides can help overcome some of these obstacles.

In this chapter, a set of FolA- and MTX-oligoamides with varied topology (linear, 2-arm, 4-arm) and different numbers of FolA or MTX as ligands was synthesized by solid-phase-assisted synthesis. All oligoamides contained a cysteine for conjugation with thiol-reactive drug cargos to serve as a module in SMDC. In the first part, structure activity relationships of the sole oligoamides was assessed in different *in vitro* assays. The identification of MTX derivatives with high affinity toward the FR and cytotoxic potency despite covalent modification was the main objective. Promising compounds were then used for subsequent covalent attachment of PT to generate FR-targeted combination therapy drug conjugates. In case of the MTX containing molecules, their combination therapy effect was assessed.

3.1.1 Oligoamide design and synthesis

Several structural motifs were crucial in the design of the drug delivery vehicles (see Scheme 5). To couple thiol containing drug cargos to the carrier system via a disulfide bond, a C-terminal cysteine (C) was introduced as the starting point for solid-phase supported oligoamide synthesis. Next, the monodisperse PEG_{12} unit (with amine and

carboxylic acid functional end groups) was incorporated into the linear oligoamides to increase the size and hydrophilicity, thus also solubility of the constructs, and to decrease unspecific cellular interactions. The *N*-Fmoc-*N″*-succinyl-4,7,10-trioxa-1,13-tridecanediamine (Fmoc-STOTDA) was included in the 2- and 4-arm structures. The STOTDA building block contains three ethylene glycol units and has therefore similar functions as the PEG block. The derivatization with a Fmoc protection group as well as a carboxylic acid functionality enables direct usage for solid phase synthesis.

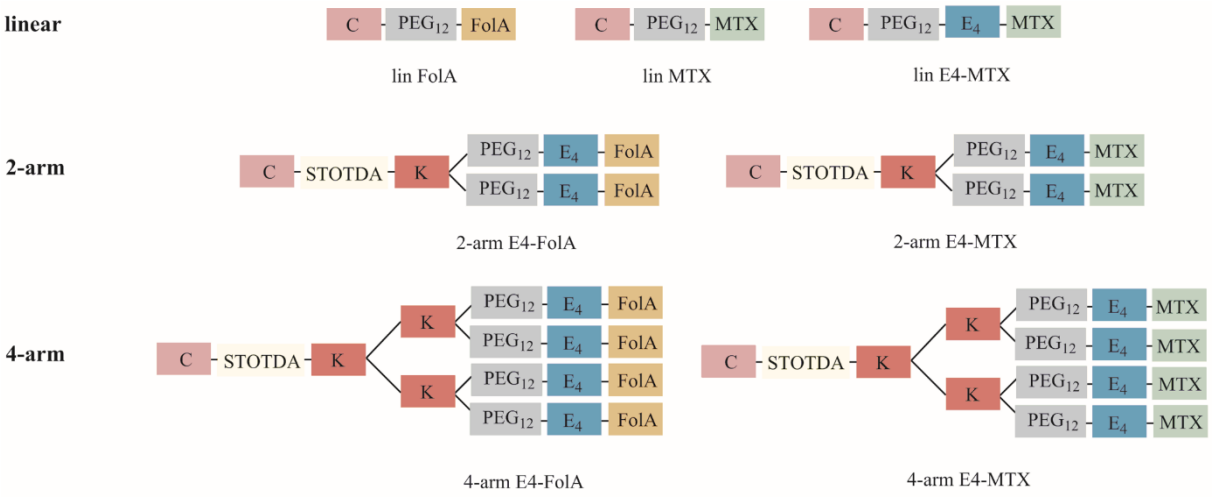

Scheme 5. Schematic illustration of synthesized, sequence-defined FR-targeting oligoamides: The linear structures contain one targeting ligand, ligand multivalency is introduced in the 2-arm and 4-arm structures. C, K, E indicate α-amino acids in one letter code; STOTDA abbreviates the short ethylene glycol linker *N*-succinyl-4,7,10-trioxa-1,13-tridecanediamine; PEG_{12} indicates a discrete polyethylene glycol unit assembled from 12 ethylene oxide units; FolA and MTX indicate ligands.

Next, lysine (K) was introduced in the assembly of 2-arm and 4-arm structures. Containing two primary amines, K can act as a symmetrical branching point in the synthesis of the branched structures. One K was integrated in case of 2-arm structures, in case of 4-arm structures two consecutive K couplings were conducted. The targeting ligands MTX and FolA were also introduced as their tetraglutamatylated forms (E_4) since the polyglutamylated derivatives of free low molecular weight MTX/FolA are generated intracellularly by the enzyme folylpolyglutamate synthase and represent the biologically active metabolites.[7, 54] The glutamates were linked via the γ-carboxylic acid function of the glutamate molecule since this corresponds to the naturally occurring γ-

linkage. In the last step, the targeting ligand FolA, consisting of glutamate and pteroic acid, or the corresponding MTX were also introduced on solid phase.

3.1.2 Effect of MTX and FolA containing oligoamides on DHFR activity

Aside from intracellular transport, the inhibition of the target enzyme of MTX, the dihydrofolate reductase (DHFR), can influence the effects of linear and branched polymers on cells. The DHFR catalyzes the reduction of dihydrofolate (DHF) to tetrahydrofolate (THF), which is vital for nucleotide biosynthesis. This explains the mechanism of action and the wide applicably of the drug MTX in diseases associated with rapid cell division.[7]

Figure 1 shows the influence of the number of MTX ligands on cell-free enzyme inhibition.

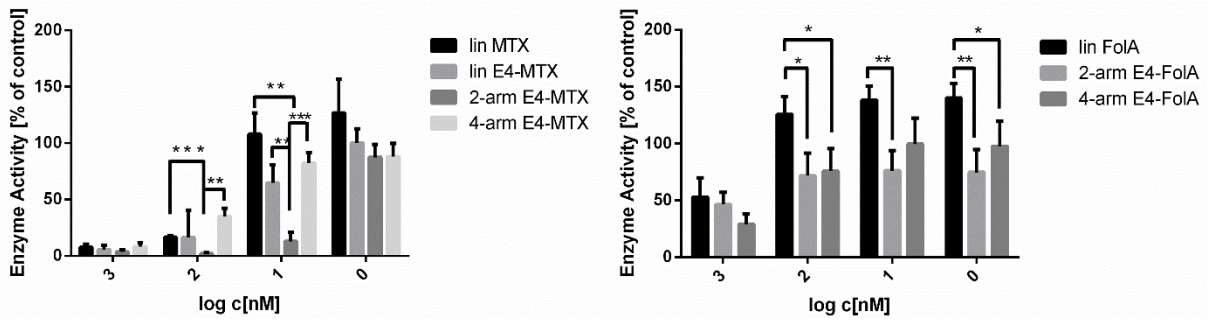

Figure 1. DHFR inhibition. The effect of oligoamides on DHFR activity was investigated in a cell free enzymatic assay. At high concentrations, all MTX-oligoamides inhibit the DHFR-catalyzed NADPH dependent reduction of dihydrofolic acid to tetrahydrofolic acid (left). The 2-arm E4-MTX molecule shows the highest enzyme inhibition potency. All FolA counterparts mediate lower DHFR inhibition (right).

The enzyme's activity was inhibited by all MTX containing oligoamides. The 2-arm oligoamide exhibited the strongest inhibition potential, reducing the enzyme activity to 13 %, even at a low concentration of 10 nM. The elevated MTX-concentration of the 4-arm oligoamide did not increase the inhibitory effect. To inhibit the enzyme, the MTX molecules have to reach the active site of the DHFR. The spacious 4-arm structure might therefore not fit into the enzyme pocket as good as the linear and 2-arm

counterparts. The 2-arm structure in turn increased enzyme inhibition with its doubled MTX-content, compared to the linear derivatives. Comparing lin MTX and lin E4-MTX, we could see an effect of polyglutamylation on enzyme inhibition, which has already been shown by Lächelt et al..[54] Also the analogous FolA derivatives affected enzyme activity to some extent. Especially the 2-arm and 4-arm structure seemed to bind the active site of the enzyme and influenced the reduction reaction, however with much lower potency than the MTX containing analogues.

3.1.3 Cellular uptake and FR-specificity of MTX and FolA containing oligoamides

To evaluate the impact of structural variation, such as type of ligand and valency, on receptor binding and cellular uptake, the latter was evaluated in FR and RFC expressing cell lines by flow cytometry. All oligoamide structures were therefore labeled with fluorescein-5-maleimide.

Figure 2 A depicts the cellular uptake of the different oligoamides into KB cells. When comparing FolA and MTX as targeting ligands, the natural ligand of the FR, FolA, was clearly the better receptor ligand than its structural derivative. This can be seen for all structures and has already been shown in previous work.[54, 79] The lin FolA molecule showed the best receptor uptake, the inclusion of another FolA molecule did not increase intracellular delivery. In contrast, for the MTX containing oligoamides introduction of multivalent ligands clearly improved internalization of the conjugates.

Also on L1210 cells, the FolA ligand was superior to MTX (Figure 2 B). Here however, we found an additional impact of the introduction of another ligand. The 2-arm and the 4-arm FolA or MTX derivatives were taken up better than the linear structures. Since L1210 cells are suspension cells, the FR can be accessed by the ligands from all sites and can eventually facilitate a better binding of bigger structures. In both cases of FolA- or MTX-oligoamides, the representative 2-arm structure was taken up to a slightly higher extent than the 4-arm counterpart was.

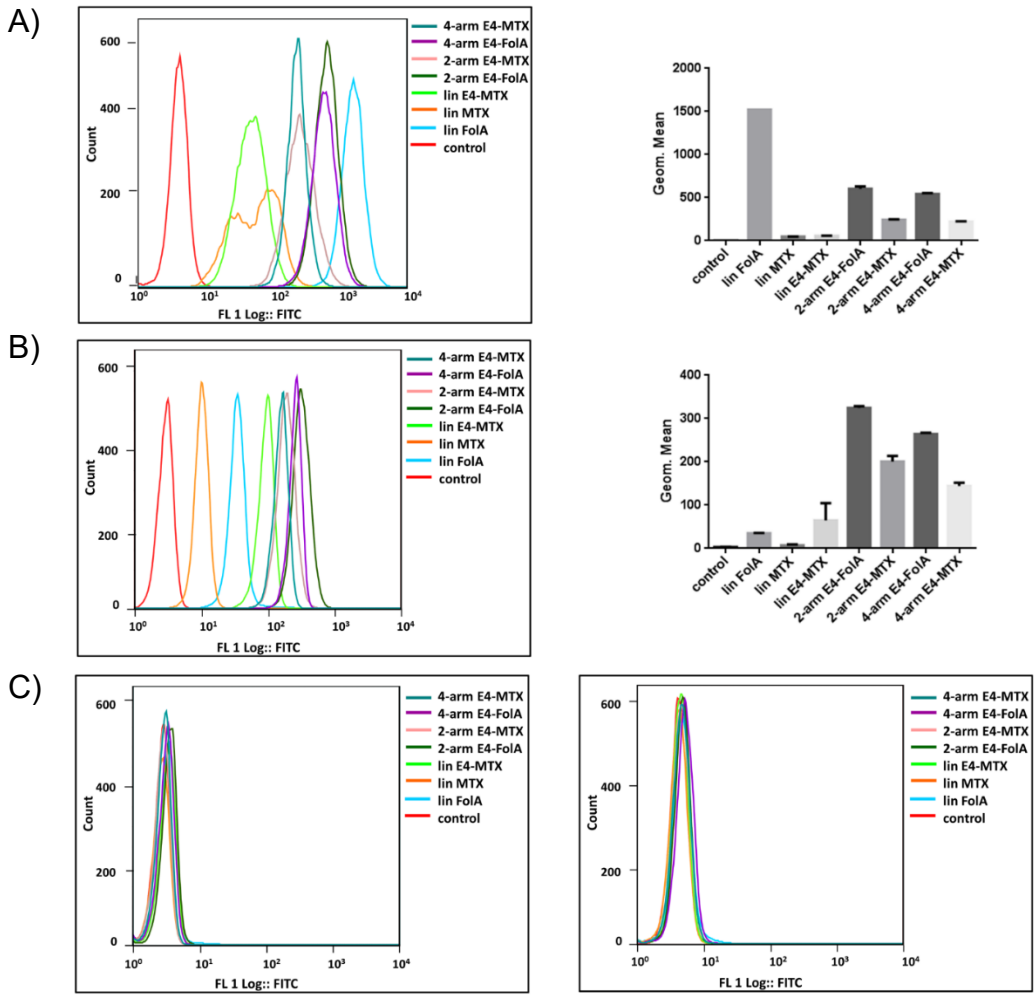

Figure 2. Cellular uptake of fluorescein labelled FR-targeted oligoamides after 30 min incubation determined by flow cytometry. HBG buffer is used as control. (A) On KB cells the FolA ligand is superior to MTX, the lin FolA structure shows the highest cellular uptake compared to the branched oligoamides. For MTX containing oligoamides, multivalent ligands improve cellular uptake. (B) Also on L1210 cells, the FolA ligand is superior to MTX. The branched structures, however, mediate a stronger uptake compared to the linear structure. The 2-arm oligoamides exhibit highest cellular uptake. (C) FR uptake is blocked by pre-incubation with FolA substituted medium on KB (left) as well as L1210 cells (right). Flow cytometry experiments were performed by Jasmin Kuhn (Pharmaceutical Biotechnology, LMU München).

To block the FR-specific uptake of the oligoamides, both cell lines were preincubated with 1.5 mM FolA in RPMI-1640 medium. Here, the receptors bind their natural ligand FolA and the uptake of the oligoamides is blocked. The complete blockage of oligomer uptake by FolA competition supported the expected FR-specific uptake route of the compounds. Additionally, STOTDA-FITC (fluorescein isothiocyanate) served as a

negative control without FR ligand and did not mediate observable cellular uptake into any of the two cell lines (see Figure 3).

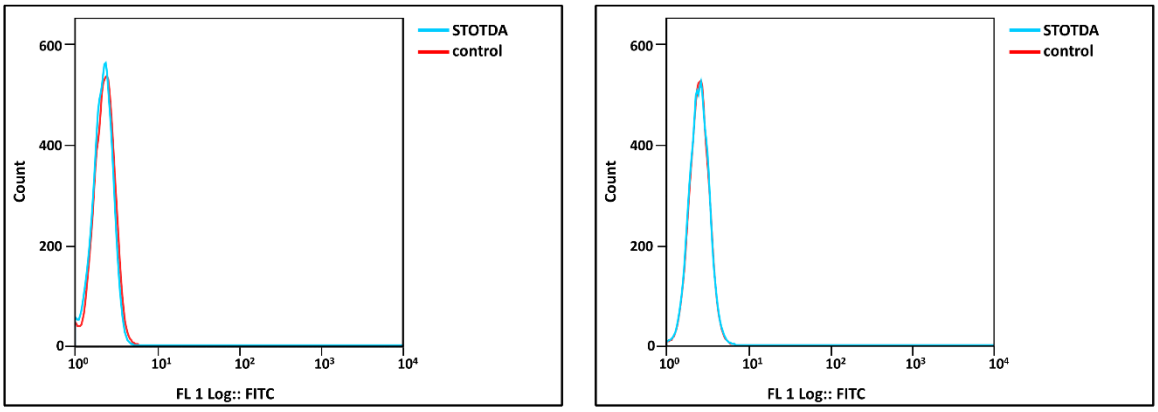

Figure 3. Cellular uptake of non-targeted control oligomer STOTDA-FITC on KB cells (left) and L1210 cells (right). The labelled conjugate, which does not contain the ligands FolA or MTX, is not internalized into KB or L1210 cells. Flow cytometry experiments were performed by Jasmin Kuhn (Pharmaceutical Biotechnology, LMU München).

3.1.4 Cytotoxicity of differently branched MTX and FolA containing oligoamides

The effects of FolA- and MTX-oligoamides on FR-overexpressing cell lines were evaluated on KB and L1210 cells and can be seen in Figure 4.

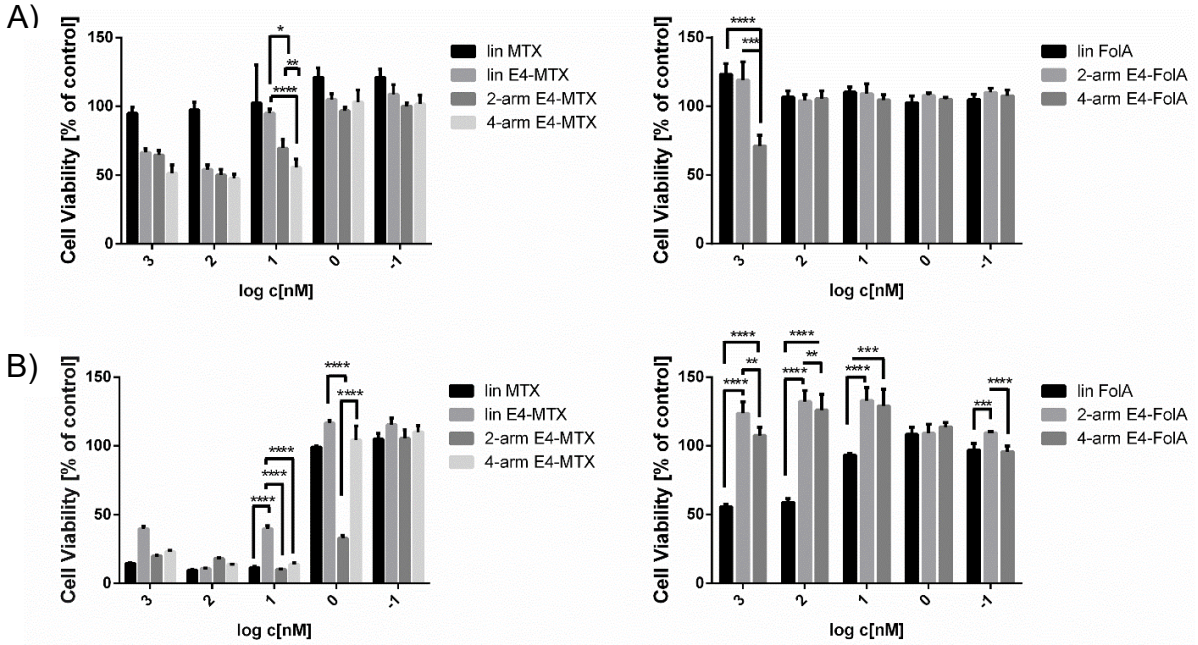

Figure 4. (A) Viability of KB cells after 72 h treatment with different FolA and MTX containing oligoamides determined by MTT assay. Overall MTX sensitivity of the cell line is low. Nevertheless, the tetravalent construct 4-arm E4-MTX exhibits highest toxicity. The folate analogs show no obvious effect on cell viability. (B) Viability of L1210 cells after 72 h treatment with different FolA and MTX containing oligoamides determined by MTT assay. The MTX-sensitivity is very high, the 2-arm structure 2-arm E4-MTX show the greatest effect on cell viability as can be seen especially at a concentration of 1 nM. The linear FolA structure exhibits low toxicity at the highest concentrations.

Figure 4 A, left, depicts the low MTX-sensitivity of the KB cell line. Cell viability was not reduced to any further than 50% even at a high concentration of 1000 nM. Comparing the MTX containing oligoamides, the effect on cell viability seemed to correlate with ligand multivalency and polyglutamylation. At a concentration of 1 nM, the toxic effect followed the order 4-arm E4-MTX > 2-arm E4-MTX > lin E4-MTX > lin MTX, presumably due to an increased number and therefore concentration of the anti-folate drug MTX. In accordance with previous findings from Lächelt et.al.[54], the glutamate

unit was beneficial for the activity of MTX conjugates since no effect of the lin MTX-oligoamide on cell viability could be observed. The FolA-oligoamides (Figure 4 A right) seemed to be fairly non-toxic, only the 4-arm E4-FolA showed a very low effect on KB cells at highest concentration of 1000 nM.

The effect of the oligoamides on cell viability of L1210 cells looked very differently (Figure 4 B). The general MTX-sensitivity was high: cell viability was decreased to around 10 % for almost all MTX-containing oligoamides at 1000 nM and even to around 40 % at a very low concentration of 1 nM of 2-arm E4-MTX. The comparably higher concentration of MTX in the 4-arm did not lead to an increase in toxicity. This corresponded to the lack of additional inhibitory effect of the 4-arm in the DHFR activity assay (Figure 1). Interestingly, polyglutamylation did not have a beneficial effect on the efficiency of the linear oligoamides on this cell line. Cytotoxicity is the result of several independent processes, such as cellular absorption and target interaction. The results of the cell viability assay in comparison to the previously examined cellular uptake and DHFR-inhibition, that help elucidate the potential of the oligoamides in individual delivery stages in an isolated fashion, showed this clearly. The high potency of the 2-arm E4-MTX correlated with the highest DHFR inhibition (Figure 1) and most efficient uptake of the MTX containing analogs into L1210 cells (Figure 2). While we saw accordance in the case of L1210 cells, the highest effect of the 4-arm E4-MTX on KB cells seemed to be independent from DHFR inhibition and cellular uptake.

3.1.5 The conjugation chemistry influences the toxicity of PT

The potent cancer chemotherapeutic PT was selected as possible cargo for FR-targeted conjugates and MTX oligoamide combinations. Figure 5 A shows the different PT derivatives used in this study.

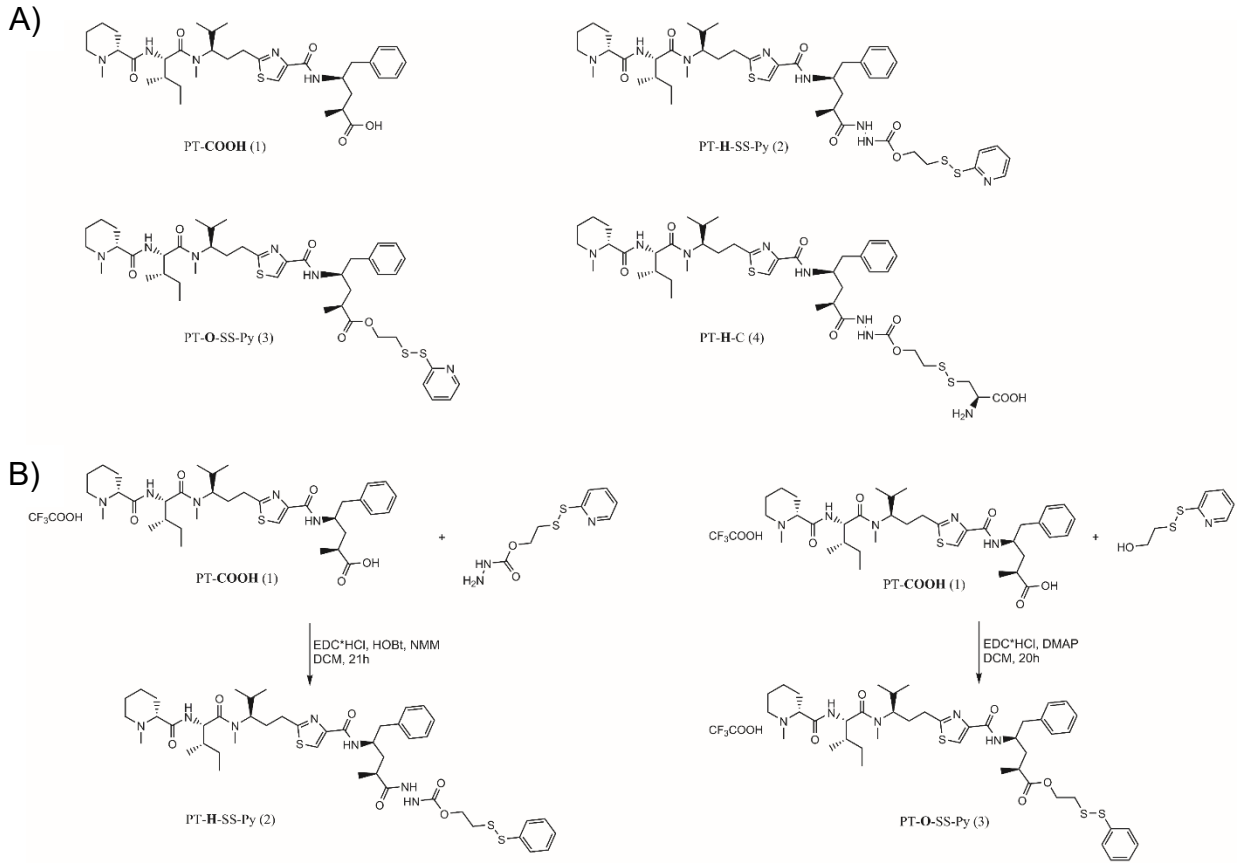

Figure 5. (A) Chemical structures of the four PT-derivatives that were used in the study. Structure (1) depicts the native PT-molecule. The carboxyl group was functionalized either by hydrazide (2) or ester (3) linker containing an activated disulfide bond. Structure (4) represents the cysteine (C)-coupled PT-hydrazide. (B) Synthesis scheme of the PT-hydrazide (2) and PT-ester (3) from the PT-COOH TFA salt. PT derivatives were synthesized by Dr. Jan Gorges (Organic Chemistry, Saarland University).

The naturally occurring PT-COOH (1) was derivatized chemically to provide an anchor point for covalent conjugation of carrier systems. A disulfide bond facilitated selective intracellular cleavage of a PT-carrier conjugate and drug release due to an increased

concentration of cytosolic glutathione.[108, 109] A thiol reactive disulfide bond was introduced via the conjugation of 2-mercaptoethanol to the carboxylic acid function of the PT molecule via an ester or hydrazide bond. Previous studies have shown that structural alterations of the PT basic structure lead to a loss in functionality. Nevertheless, derivatizations at the carboxylic acid position can still leave PT with substantial anticancer activity.[16]

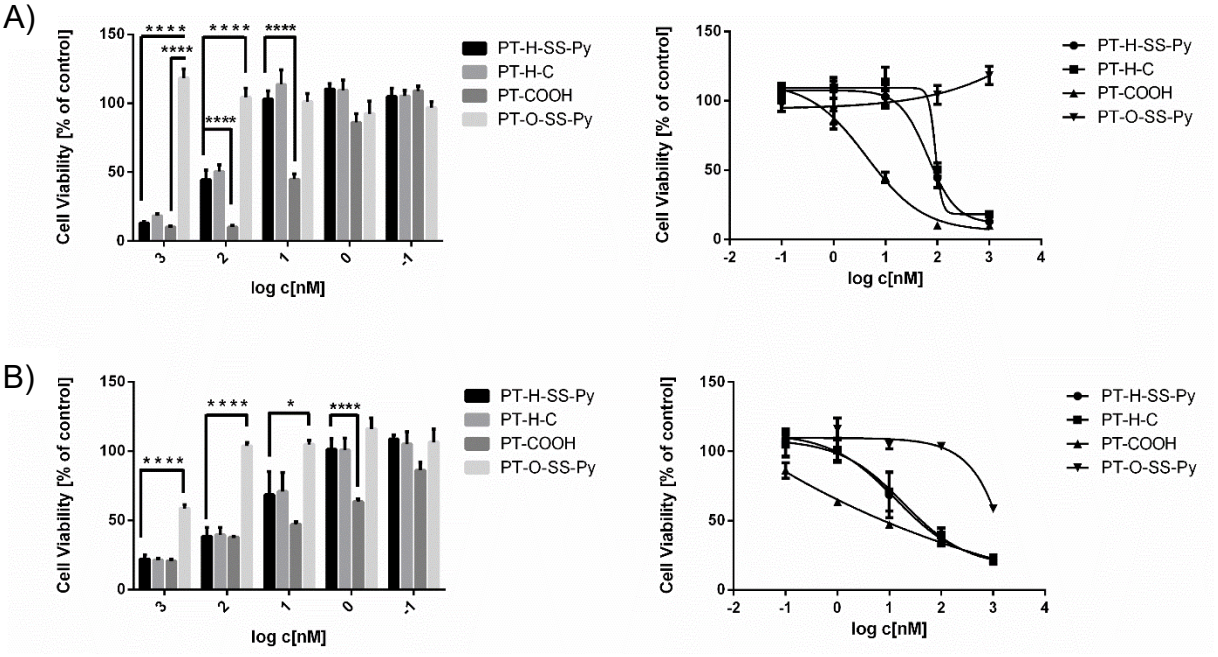

Figure 6. MTT assay to examine the influence of linker chemistry on cell viability of (A) KB cells and (B) L1210 cells. The native PT-COOH (1) exhibits the highest effect on both cell lines. The ester derivatization leads to a loss of cytotoxicity whereas the hydrazide moiety still induces concentration dependent cytotoxicity.

The MTT assay shows the great influence of the chosen linker chemistry on the toxicity of PT on L1210 as well as KB cells (Figure 6). An ester functionalization (PT-O-SS-Py) led to a complete loss of toxicity of derivative (3), presumably due to a higher stability of an ester bond compared to a hydrazide bond (PT-H-SS-Py) as in derivative (2). The beneficial hydrazide linker is similar to the linker strategy of a published folate-tubulysin conjugate which was investigated in a phase I clinical trial.[72, 93, 110, 111] The hydrazine carbamate unit constituted a second breaking point which facilitated the release of active PT at the target site. Nevertheless, the hydrazide derivatization (PT-H) diminished PT's activity compared to the naturally occurring PT-COOH to some extent.

This was especially visible for KB cells, with relative IC_{50} values of 66.12 nM for PT-H-SS-Py (2) and 4.34 nM for PT-COOH (1), and to a lesser extent for L1210 cells with relative IC_{50} values of 13.21 nM for PT-H-SS-Py (2) and 2.53 nM for PT-COOH (1) (Figure 6). The hydrazide derivatized PT-H-SS-Py (2) was used for further experiments and coupled to different oligoamide structures.

3.1.6 Toxicity of PT oligoamide conjugates

Additionally to examining the structure activity relationships of the individual oligoamide structures, they were tested for their effects on toxicity after conjugation with the activated PT derivative.

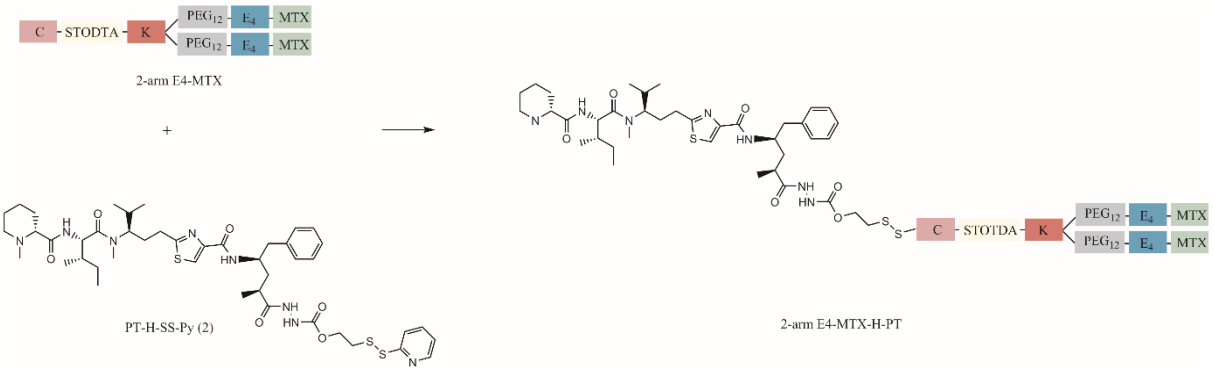

Scheme 6. Representative reaction scheme of PT-H-SS-Py (2) conjugation with C-containing oligoamide 2-arm E4-MTX.

PT-H-SS-Py was coupled to FolA- and MTX-containing oligoamides (Scheme 6) to facilitate FR-specific PT delivery and, for MTX, to exploit combinatorial therapeutic effects. The successful conjugation was verified by RP-HPLC monitoring of the reaction between PT-H-SS-Py and the 2-arm E4-MTX oligomer (Figure 7) as well as detection of the conjugation product by mass spectrometry (Figure 8). The resulting conjugate showed stability in phosphate-buffered saline during 24 hours incubation (Figure 9) but rapid cleavage upon incubation with the reducing agent tris(2-carboxyethyl)phosphine (TCEP) (Figure 10).

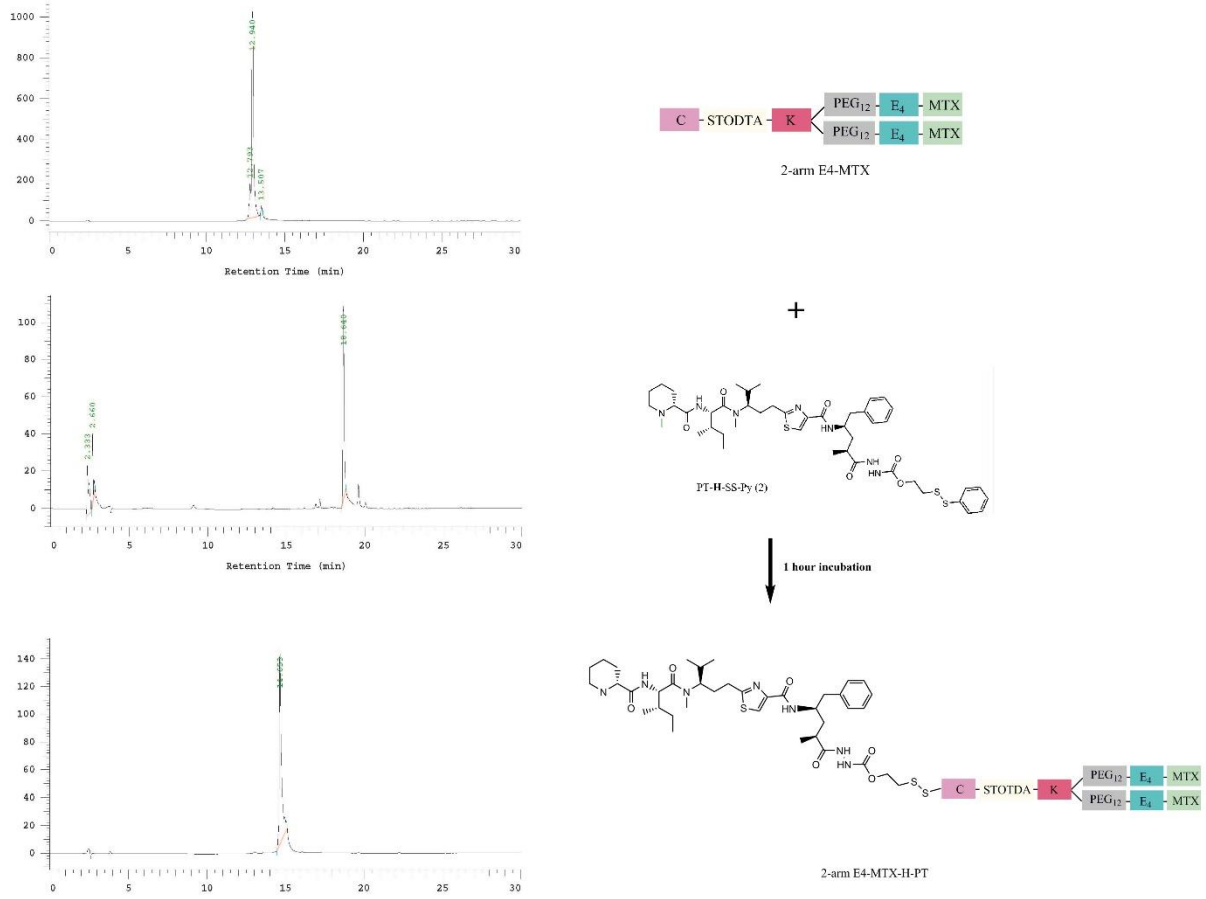

Figure 7. RP-HPLC monitoring of PT-oligomer conjugation reaction with oligomer 2-arm E4-MTX. The compounds PT-H-SS-Py and oligomer 2-arm E4-MTX were analyzed before and after conjugation by RP-HPLC using a VWR Hitachi Chromaster HPLC system (5160 pump module, 5260 auto sampler, 5310 column oven, 5430 diode array detector), a C18-column (YMC column, HS-302, HS12S05-1546WT, 150 x 4.6 mm I.D., S-5 µm, 12 nm, YMC Europe GmbH, Dinslaken, Germany) column and a gradient of 5 % to 100 % acetonitrile with 0.1 % TFA in 30 min. Elution was monitored photometrically at 214 nm. The PT-oligomer conjugate was then purified by HPLC under the conditions mentioned above. The retention time of PT-H-SS-Py is 18.6 min (top), the retention time of the oligomer is 12.9 min (middle). After conjugation and purification, the isolated construct has a retention time of 14.7 min (bottom).

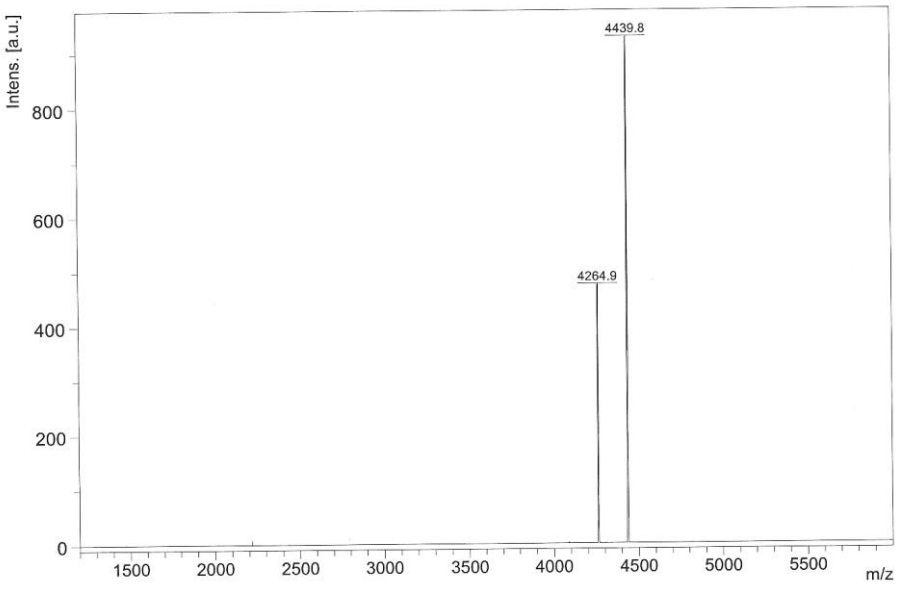

Figure 8. MS-spectrum of 2-arm E4-MTX-H-PT and its chemical structure. Additionally to the HPLC-analysis of construct 2-arm E4-MTX-H-PT, the conjugation reaction was verified via MS.

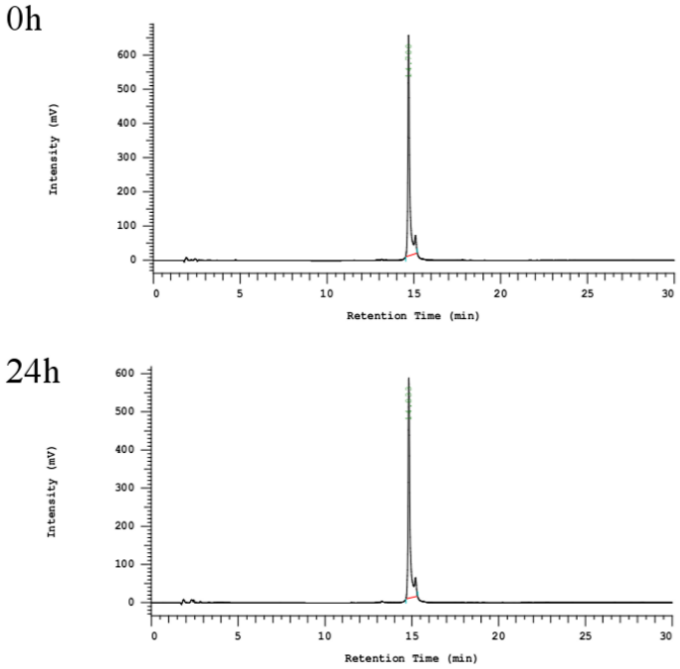

Figure 9. Stability of the 2-arm E4-MTX-H-PT construct in PBS over 24h: 2-arm E4-MTX-H-PT was dissolved in PBS and immediately (top) or after 24 h incubation at room temperature (bottom) the solution was diluted in HPLC solvent H_2O with 0.1% TFA and analyzed with the RP-HPLC system that is described in Figure 7. According to the HPLC spectrum, no degradation occurred over the course of 24h.

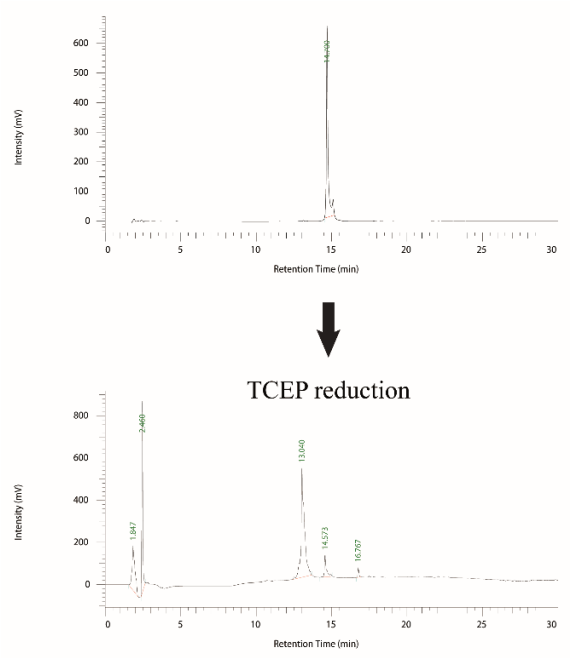

Figure 10. Reductive cleavage of the 2-arm E4-MTX-H-PT construct upon incubation with the reducing agent tris(2-carboxyethyl)phosphine (TCEP).

Cell viability after 72 h incubation was assessed for the constructs on KB and L1210 cells and results can be seen in Figure 11. PT reduced cell viability to below 10 % at its highest concentrations for both cell lines and therefore, strongly increased MTX-effects on cells, especially on KB cells (see Figure 11 A and Figure 4 A). Comparing the conjugates to PT-hydrazides (2) and (4) on KB cells (Figure 11 A), the conjugation to the 2-arm and 4-arm MTX structures affected the anticancer potential with significant higher tumor cell killing at 1 nM concentration. Also on L1210 cells, the conjugation of PT to the 2-arm and 4-arm MTX structures strongly increased the antitumoral activity of PT (Figure 11 B). Especially the 2-arm structure seemed to be a valid candidate for PT-MTX codelivery, as it induced substantial cell killing even at a low concentration of 1 nM. In both cell lines, the identification of most potent candidates (4-arm E4-MTX-H-PT in KB cells, 2-arm E4-MTX-H-PT in L1210 cells) correlated with the previous cytotoxicity evaluation of oligoamides alone. PT conjugates with the FolA containing oligoamides did not show an increased cytotoxic effect compared to the PT derivative without conjugation (Figure 12). The data indicates that the covalent linkage of MTX and PT yields conjugates of two drugs with combined activity and potential for FR-targeted combination therapy approaches.

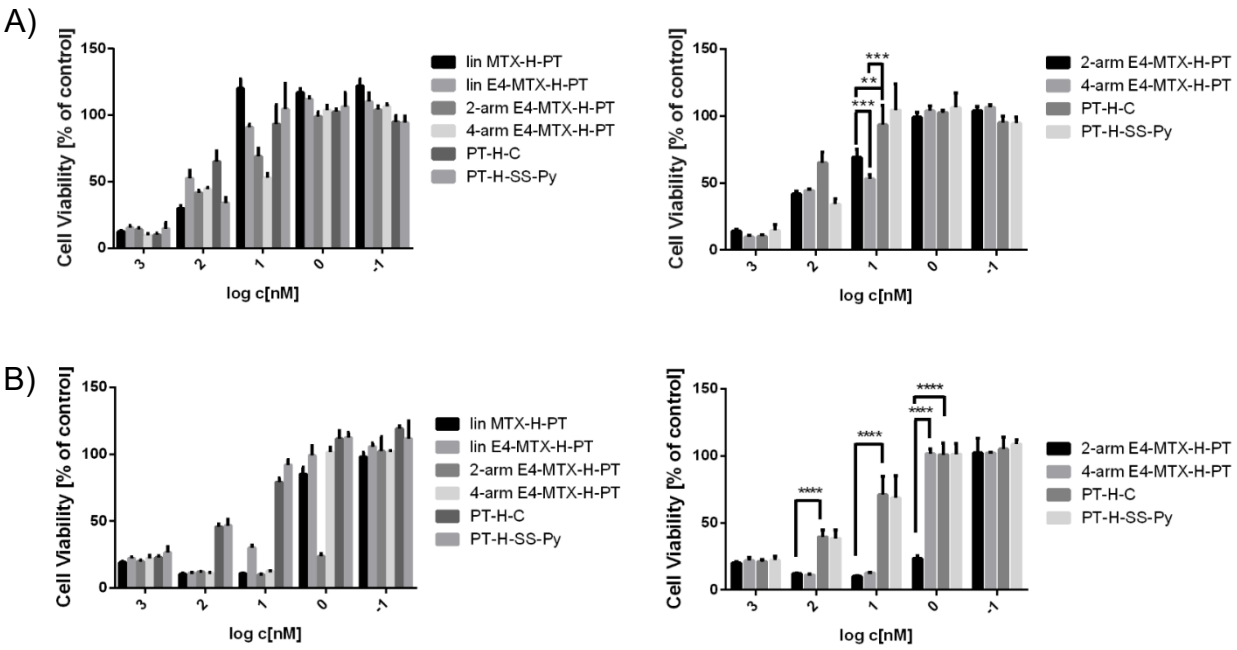

Figure 11. Cell viability after 72 h treatment with MTX-oligoamide PT conjugates. Effects of all MTX containing oligoamides (left panel) and rearranged overview over the results (same experiment) achieved with the 2-arm E4-MTX-H-PT and 4-arm E4-MTX-H-PT only (right panel). (A) KB cells: The 4-arm E4-MTX-H-PT construct exhibits highest effects on cell viability, especially compared to PT-hydrazides (PT-H-C and PT-H-SS-Py) and 4-arm E4-MTX (Figure 4 A) (B) L1210 cells. The 2-arm E4-MTX-H-PT is superior to all other MTX containing PT-conjugates.

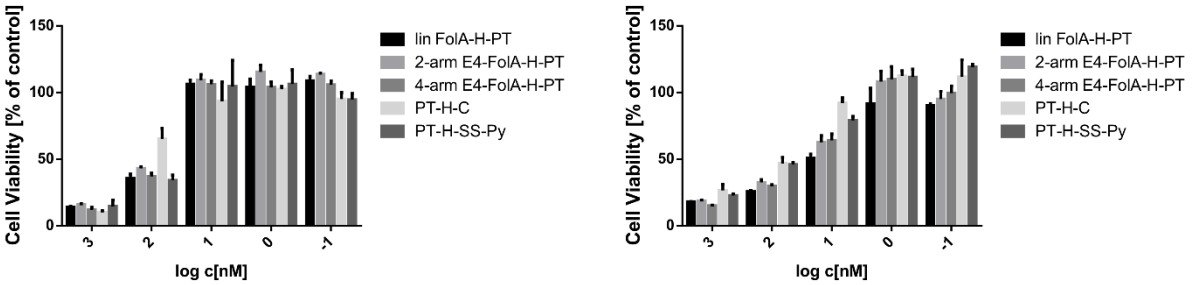

Figure 12. Viability of KB cells (left) and L1210 cells (right) after 72 h treatment with FolA-oligomer PT conjugates. The FolA-containing oligomers were conjugated to PT and the conjugates were compared to free PT (as PT-H-SS-Py or PT-H-C) for their cytotoxic effect. In KB cells (left) no increased cytotoxicity of FolA-oligomer PT conjugates was observed. In L1210 cells, cell viability was slightly decreased for the targeted conjugates compared to the free PT especially at 100 and 10 nM. This could be due to receptor specific PT-uptake into the L1210 suspension-cells.

3.1.7 Combinatorial treatment with 4-arm E4-MTX-H-PT conjugate *in vivo*

To investigate the antitumoral potency of E4-MTX-H-PT conjugate in an *in vivo* situation, a mouse xenograft model with subcutaneous FR-overexpressing KB tumors was chosen. The mice were divided into four groups of 8 mice; intratumoral injections were started at day 2 after tumor inoculation and repeated at days 5, 7, 9, 12 and 14. The conjugate of PT-H-SS-Py and the 4-arm E4-MTX oligomer, 4-arm E4-MTX-H-PT was compared to the natural PT-COOH and the bare oligomer 4-arm E4-MTX. The 4-arm construct was chosen as it showed the best combination effects and highest potency in the cell viability assay on KB-cells (see Figure 11 A). Figure 13 shows the tumor volume over the time course of the experiment.

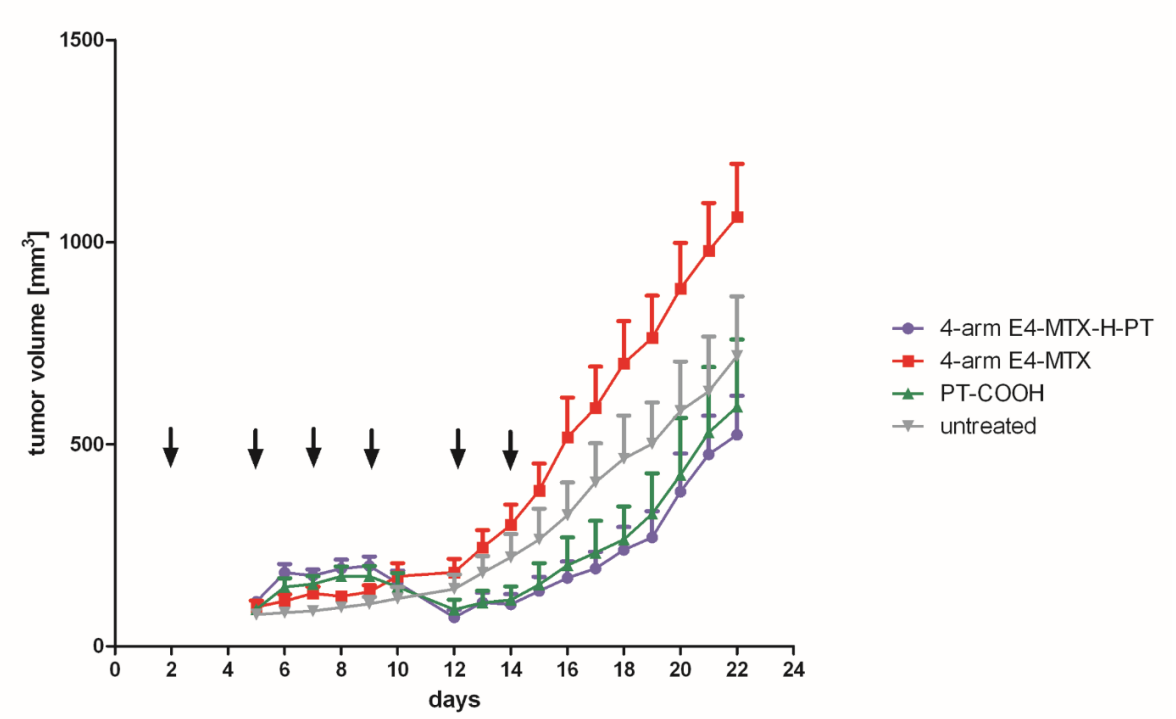

Figure 13. Growth of subcutaneous KB tumors in a murine xenograft model after repeated treatments with bare 4-arm E4-MTX oligomer, native PT-COOH and the 4-arm E4-MTX-H-PT conjugate (n=8 per group). Intratumoral injections were administered at day 2, 5, 7, 9, 12 and 14 after tumor cell inoculation (arrows) whereas the untreated mice were not injected. Tumor volumes were determined based on caliper measurements. Animal experiments were performed by Dr. Sarah Kern (Pharmaceutical Biotechnology, LMU München).

The 4-arm E4-MTX oligomer alone did not inhibit tumor growth. The size difference compared to the untreated group could be explained by the absence of post-injection swelling of untreated tumors as well as the coincidentally slow initial tumor growth

within the control group. However, the absence of an inhibitory effect of the MTX oligomer alone in the KB tumor model correlated with previous findings from Lee et al.[79] In contrast, both PT formulations mediated distinct antitumoral effects and clearly attenuated tumor growth during the treatment phase. After the last treatment, tumors showed a relapse and increase in tumor volume over time again. Native PT-COOH has been shown to have a growth retarding effect on several tumor types when applied systemically before[9, 19], which was now confirmed also in the case of local injections into KB tumors. The FR-targeting conjugate 4-arm E4-MTX-H-PT showed a comparable therapeutic effect on tumor growth as the native PT-COOH. Since the conjugate contained the chemically modified hydrazide PT-derivative which has been found to be less potent *in vitro* (Figure 6), with an approximately 15-fold higher IC_{50}-value in KB cells, the therapeutic effect *in vivo* was considered to be a promising result. Both the native and conjugated PT-H derivative showed similar effects on tumor growth after direct local intratumoral injection and there can be hope for an additional advantage due to receptor targeting of the conjugate in case of a systemic route of administration, as it was reported for the folate-tubulysin conjugate.[72, 110, 111] However, in the current study, no advantage over the native drug could be shown in this experimental setup. Finally, monitoring of body weights resulted in no obvious signs for adverse effects or pathological findings; all treatments seemed to be well tolerated by the animals (Figure 14).

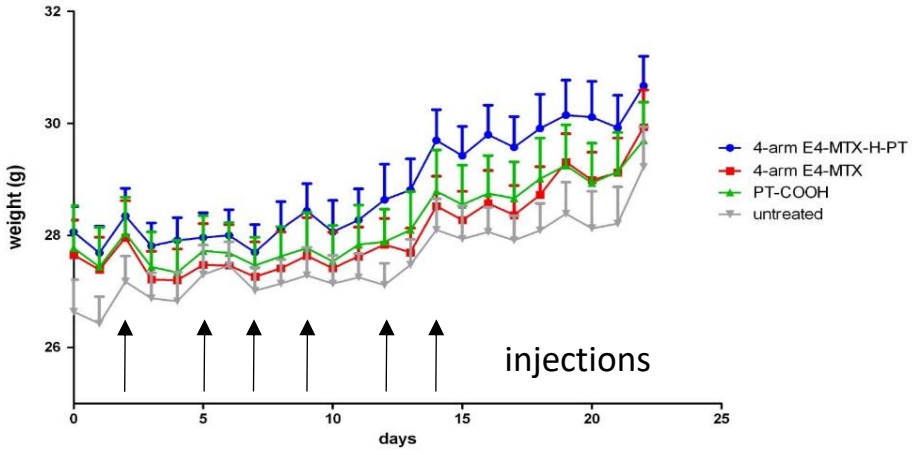

Figure 14. The body weight of the animals (n=8) receiving different formulations was monitored on a daily basis throughout the experiment. The treatments were tolerated well, no drastic loss in body weight could be observed. Animal experiments were performed by Dr. Sarah Kern (Pharmaceutical Biotechnology, LMU München).

3.2 Combined antitumoral effects of pretubulysin and methotrexate

This chapter was adapted from:

Kern, S.; Truebenbach, I.; Höhn, M.; Gorges, J.; Kazmaier, U.; Zahler, S.; Vollmar, A. M.; Wagner, E., Combined antitumoral effects of pretubulysin and methotrexate. Pharmacol Res Perspect 2019, 7 (1), e00460.

In the previous chapter, the novel tubulin inhibitor PT was conjugated with MTX-containing oligomers for FR-targeted delivery. The native PT was functionalized via a hydrazide bond to enable covalent linkage of PT to the SMDC. The dual delivery systems displayed a clear antitumoral combination effect.

In this chapter, the free drug combination of PT+MTX was evaluated against both free PT and MTX in different *in vitro* experiments to elucidate possible reasons for the combinatorial behavior.

3.2.1 *In vitro* antitumoral activity of PT, MTX or PT+MTX

L1210 and KB cells were treated with PT and MTX for 72 h at a set drug molar ratio of 1 to 3, and cell viability of drug-treated cells was determined by MTT assay (Figure 15). In case of L1210 cells (Figure 15 A) both the single drugs as well as their combination induced strong effects already at low nanomolar concentrations. The IC_{50} values of the single drugs in the 96-well format were around 1 nM (PT: 1.3 ± 0.067; MTX: 1.984 ± 0.49; PT+MTX: 0.215 ± 0.01), and a beneficial effect of PT+MTX over PT and MTX alone was visible. The combination effect was especially predominant at a concentration of 1 nM of PT and 3 nM MTX, and could also be seen when comparing the IC_{50} values.

As stated in the previous chapter, KB cells (Figure 15 B) were partly resistant to MTX, with a minimum cell viability of 40% remaining at high MTX concentrations. PT alone exhibited strong antitumoral effects on KB cells, with an IC_{50} in the low nanomolar region. The combination formulation was similarly potent as the single drug PT, as can be seen for the IC_{50} values in Table 14 B. At doses below 40 nM of PT, the combination PT+MTX was significantly more potent than PT alone.

A)

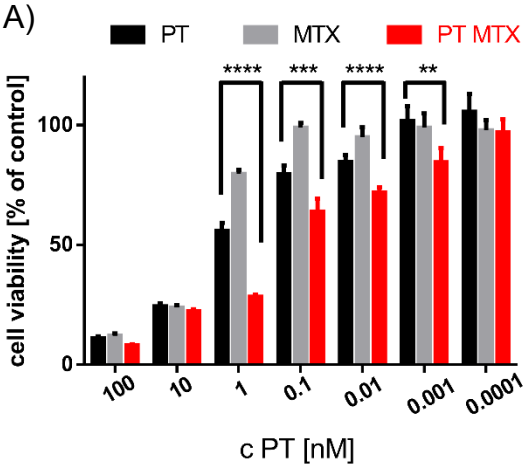

	PT	MTX	PT+MTX
IC 50 [nM]	1.3 ± 0.67	1.984 ± 0.49	0.215 ± 0.01

B)

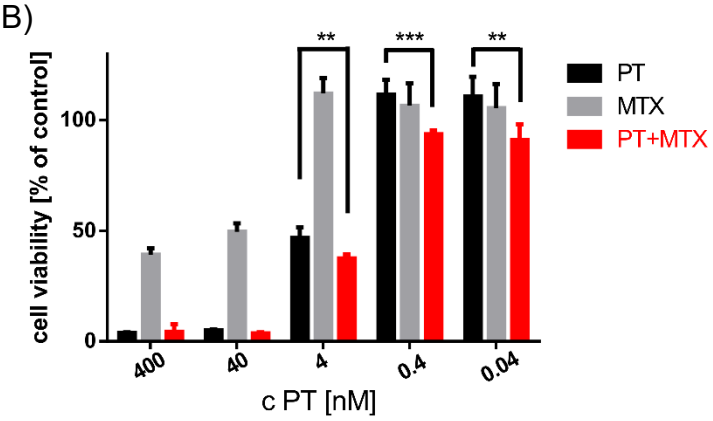

	PT	MTX	PT+MTX
IC 50 [nM]	3.16 ± 0.67	-	2.975 ± 0.95

Figure 15. Combination effect of PT and MTX on cultured L1210 cells but not KB cells. Cell viability and $IC5_0$ values of drug-treated (A) L1210 cells and (B) KB cells. Cell viability was measured with an MTT assay after 72 h treatment and is presented as the mean + SD (n = 5) in % relative to buffer (HBG) treated cells. c [nM] refers to the concentration of PT, the concentration is 3-fold higher for MTX, due the 1:3 molar drug ratio (*p < 0.05; **p < 0.01; ***p < 0.001; ****p < 0.0001).

Furthermore, also different molar ratios of MTX to PT were investigated. While the PT dose was left constant, the MTX dose was gradually increased from equimolar to a 10-fold molar surplus of MTX to PT. Figure 16 A depicts the MTT data of drug treated L1210 cells at the different ratios. As expected, an increase in the MTX dose led to a reduction in cell viability of the MTX sensitive L1210 cells when looking at the graphs

from left to right. For all dose ratios, the combination of PT+MTX exceeded PT and MTX in terms of cell killing.

Cell viability after drug treatment of KB cells with different molar ratios of PT, MTX or PT+MTX is shown in Figure 16 B. Also here, a steady increase of MTX increased the number of dead cells. The cell viability of MTX resistant KB cells, however, could not be reduced to less than 40% cell viability, even at the highest dose of 1 µM of MTX. At the low molar ratios (1 to 1 and 1 to 3) the combination seemed to be slightly superior to the single drugs. That effect was not observed for the higher MTX concentrations at the ratios 1 to 5 and 1 to 10 though. The dose ratio of 1 to 3 was chosen for all further experiments due to the treatment study described in the previous chapter where said ratio led to a promising retardation in tumor growth.[17]

A)

B)

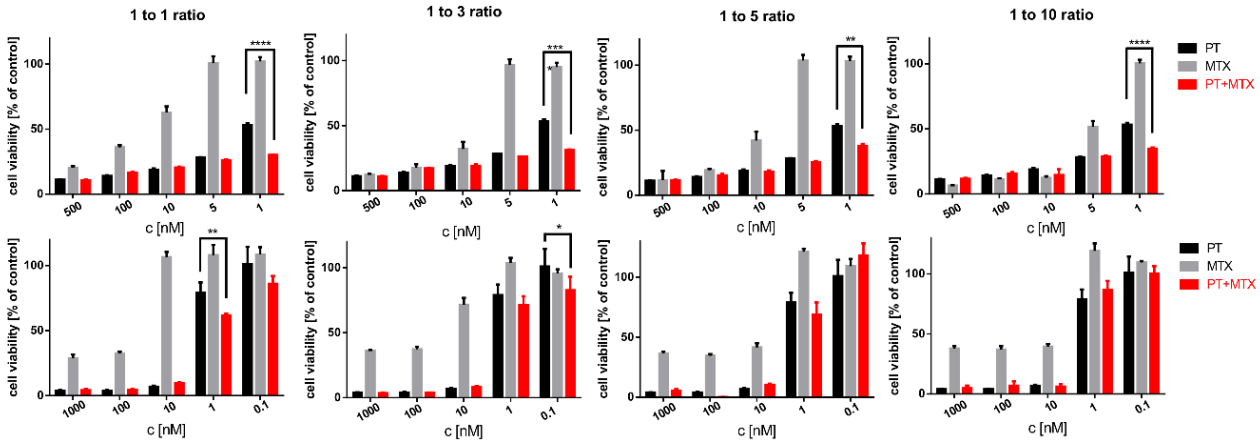

Figure 16. Evaluation of different dose ratios of MTX to PT by MTT assay. Cell viability of drug treated (A) L1210 and (B) KB cells. Cells were treated with PT, MTX and the combination PT+MTX at different molar ratios. Cell viability was measured with an MTT assay after 72 h incubation time and is presented as the mean + SD (n = 5) in % relative to HBG treated cells.

Different conditions were used to determine the *in vitro* effects of PT, MTX and PT+MTX. The MTT assays to determine IC50 values of drugs and their possible combination effects were performed in 96 well plates in accordance to previous work on cellular effects of PT, with drug concentrations ranging from 0.0001 nM up to 100 nM of PT.[9, 17, 18]

For flow cytometry experiments, higher numbers of cells were needed. Hence, experimental conditions were modified. Cells were seeded in 12-well plates and suitable concentrations of PT and MTX were determined. The effect of 200 nM PT and 600 nM MTX on L1210 and KB cells were determined by MTT-assay. Figure 17 A depicts the time-dependent effects of drugs on L1210 cells. As expected, cell viability decreased over the time course of the experiment; with only 11% viable L1210 cells left after 72 h of PT+MTX treatment, 16% viable cells after PT treatment and 17% viable cells after MTX treatment. The antitumoral effect of PT was already well visible after 24 h, whereas the onset of MTX toxicity could be seen after 48 h. The combination effect of PT+MTX over PT was already prominent after 24 h treatment.

The weaker overall effect of the drugs on KB cells could be seen in Figure 17 B. After 72 h incubation, cell viability was reduced to 22% (PT+MTX), 20% (PT) or 57% (MTX). No significant combination effect is visible in this setting. A time-dependent effect of drugs on cell viability could also be determined here.

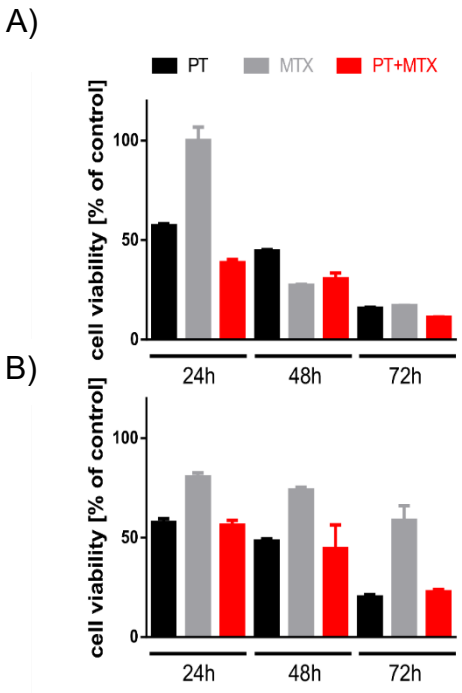

Figure 17. MTT assay of drug treated L1210 (A) and KB cells (B) at 24, 48 and 72 h incubation time. Cell viability is presented as mean + SD (n = 5) in % relative to buffer (HBG) treated cells.

3.2.2 The effect of PT, MTX or PT+MTX treatment on tumor cell cycle

L1210 and KB cells were treated with HBG, PT, MTX or PT+MTX and left to incubate for 24 h or 48 h. Time points and drug concentrations were adjusted to the 12-well plate culture conditions. Cells were stained with the DNA intercalating dye propidium iodide and measured by flow cytometry (Figure 18). After 24 h treatment of L1210 cells (Figure 18 A), PT induced the expected strong G2/M arrest (83% arrest in G2/M), whereas MTX induced a strong G1/S arrest (86% in G1). With regard to PT+MTX co-treatment, the pattern at 24 h (81% arrest in G2/M) equaled treatment with only PT. Interestingly, after 48 h the G2/M effect of PT treated cells was reduced (55% G2/M, 30% G1), whereas MTX still induced a strong 75% G1/S arrest. In contrast, no comparable G1/S arrest was found in the PT+MTX combination group, but a stronger G2/M arrest of cells (64% G2/M, only 11% G1) was seen when compared to the single drug PT. In sum, in the combination group, the G2/M effect of PT seemed to be predominant, and the effect was even supported by MTX co-treatment.

For KB cells (Figure 18 B), changes in cell cycle are in general delayed as compared with the faster growing L1210 cells. No significant alterations could be noted after 24 h incubation. With time, PT treatment started to build up some G2/M arrest (41% G2/M at 48 h), MTX treated cells were largely in G1 phase. In sharp contrast to the single drug treatments, the PT+MTX combination induced a strong G2/M arrest already after 24 h, and much stronger (78% G2/M) also after 48 h than PT alone.

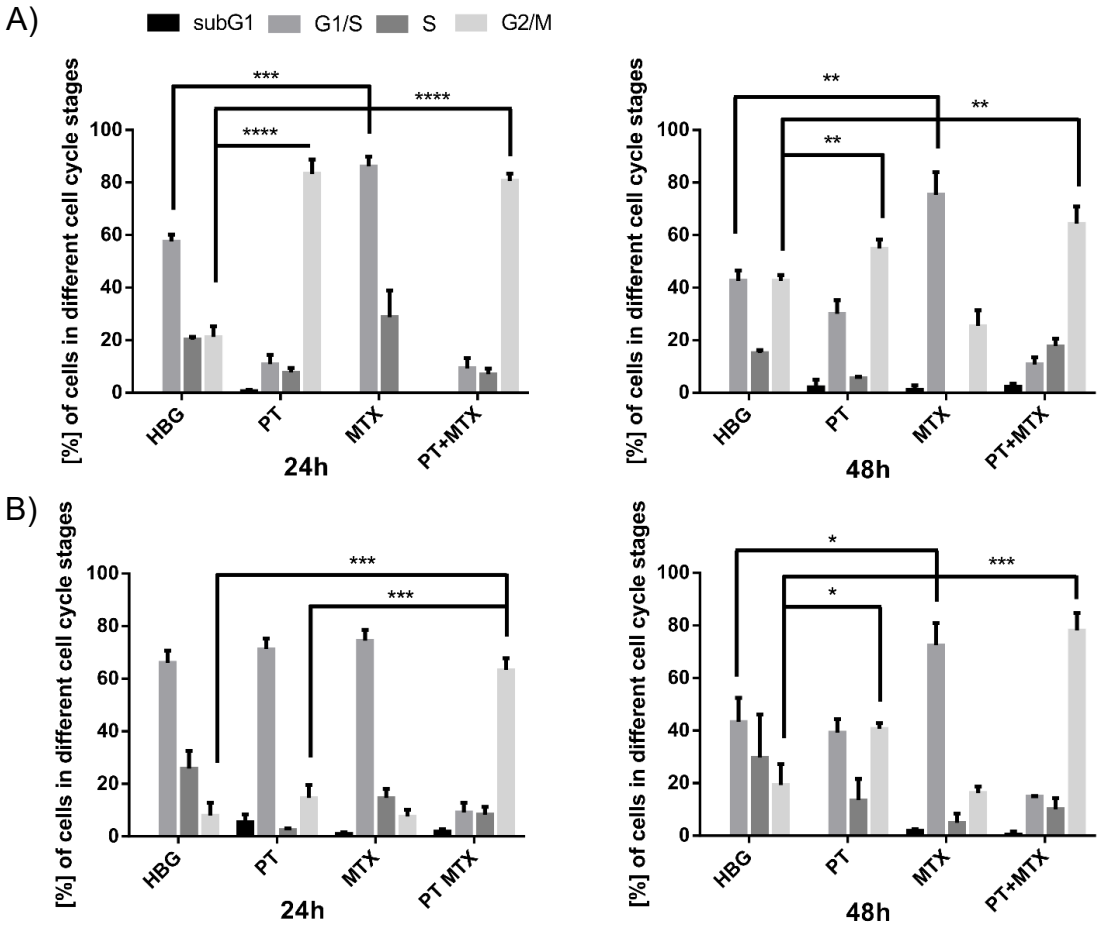

Figure 18. Cell cycle analysis of drug-treated cells. (A) L1210 cells and (B) KB cells were treated with HBG buffer control, 200 nM PT, 600 nM MTX, or the combination PT+MTX (200+600 nM). Cells were incubated for 24 h, respectively 48 h. Cells were stained with propidium iodide and analyzed by flow cytometry. Treatments were performed in triplicates.

3.2.3 Induction of apoptosis by PT, MTX or PT+MTX

The effect of drug treatment on apoptosis of L1210 (Figure 19 A and Figure 20) and KB cells (Figure 19 B and Figure 21) was monitored with an annexin V-fluorescein isothiocyanate (FITC)/propidium iodide (PI) assay. L1210 and KB cells were treated with HBG control buffer, PT, MTX or PT+MTX and left to incubate for 24, 48 or 72 h. Cells were collected, stained with annexin V-FITC and PI and analyzed by flow cytometry. For L1210 cells (Figure 19 A and Figure 20), HBG and MTX treatment for 24 h did not trigger any signs of apoptosis (Q4), whereas PT and PT+MTX induced apoptosis in 10% of cells (Q1-Q3). After 48 h, 30% of MTX treated and 30-40% of PT or PT+MTX treated L1210 cells were apoptotic. After 72 h incubation time, 80% of MTX treated cells and 70% of PT or PT+MTX treated cells showed signs of apoptosis.

Combining PT and MTX did not increase the number of apoptotic cells in comparison to the single drugs. Apoptotic cells are mainly in the Q2 quadrant, reflecting that cells are in the late apoptotic or necrotic phase.

After treatment of KB cells (Figure 19 B and Figure 21) for 24 h, MTX treated cells did not show apoptotic signs (Q4), whereas PT and PT+MTX treated cells were 20% or 30% apoptotic (Q1 Q3). The number of PT or PT+MTX treated apoptotic cells steadily increased over the time course of the experiment, with only around 15% of healthy cells remaining. In contrast to L1210 cells, the majority of apoptotic KB cells were FITC – / PI + (Q1), indicating that the cell membrane of KB cells was too heavily destroyed to bind annexin V. Consistent with MTT and cell cycle data, the MTX resistance of KB cells was also noted in the apoptosis analysis; only 20% of MTX treated cells had undergone apoptosis after 72 h treatment. Like for L1210 cells, the combination PT+MTX did not enhance the number of apoptotic KB cells over the single drug treatments.

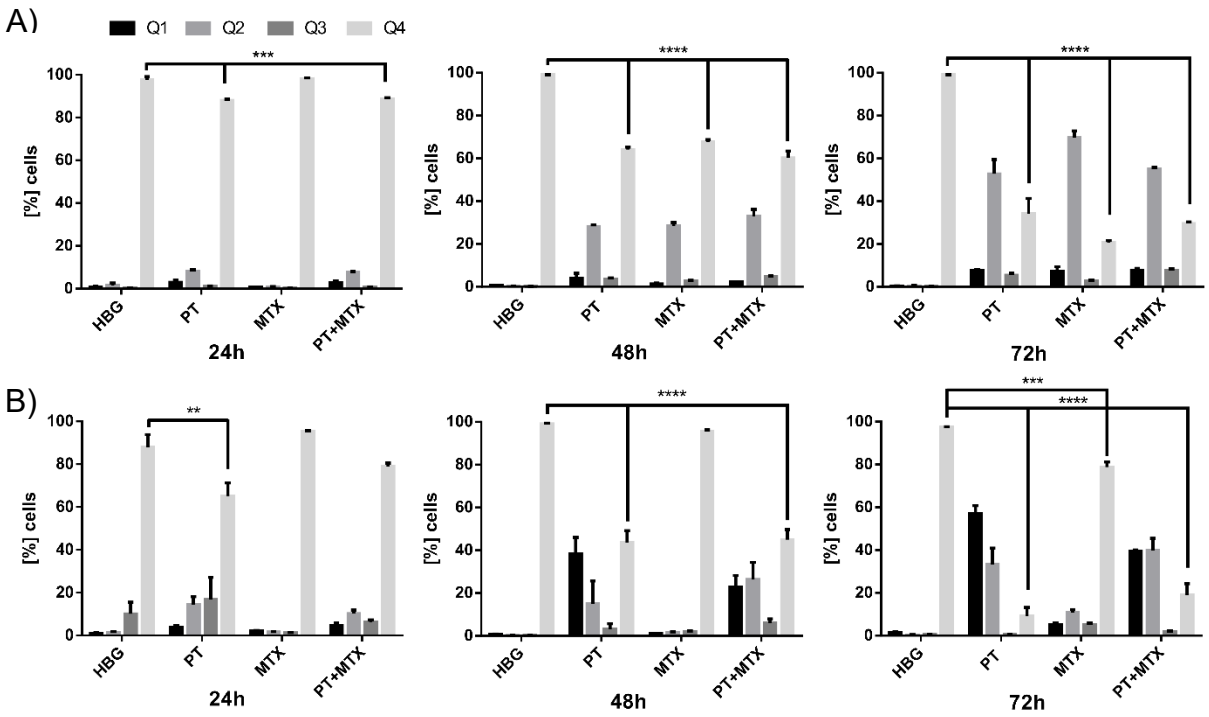

Figure 19. Apoptosis in drug-treated L1210 cells (A) or KB cells (B). Cells were treated with control buffer HBG, PT, MTX or PT+MTX and incubated for 24, 48 and 72 h, respectively. Cells were stained with annexin V-FITC and propidium iodide and analyzed by flow cytometry. Treatments were performed in triplicates. Q1: Annexin V-FITC – / PI +; Q2: Annexin V-FITC +/PI + ; Q3: Annexin V-FITC +/PI – ; Q4: Annexin V-FITC –/PI –

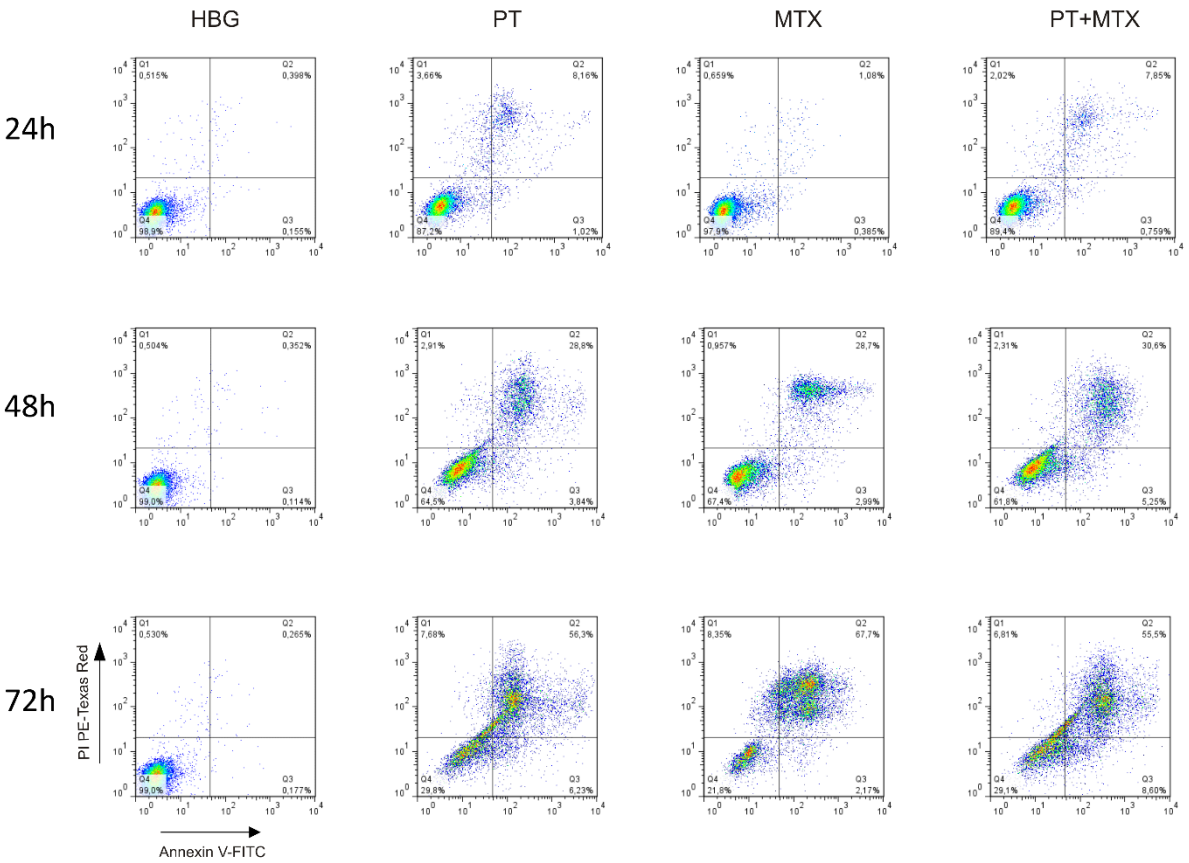

Figure 20. Flow cytometric analysis of apoptosis in drug treated L1210 cells. L1210 cells were treated with HBG, PT, MTX and PT+MTX and incubated for 24, 48 and 72 h respectively. Cells were stained with annexin V-FITC and propidium iodide and analyzed by flow cytometry. Treatments were performed in triplicates (n = 3). Q1: FITC – / PI + Q2: FITC +/PI + Q3: FITC +/PI – Q4: FITC –/PI –

.

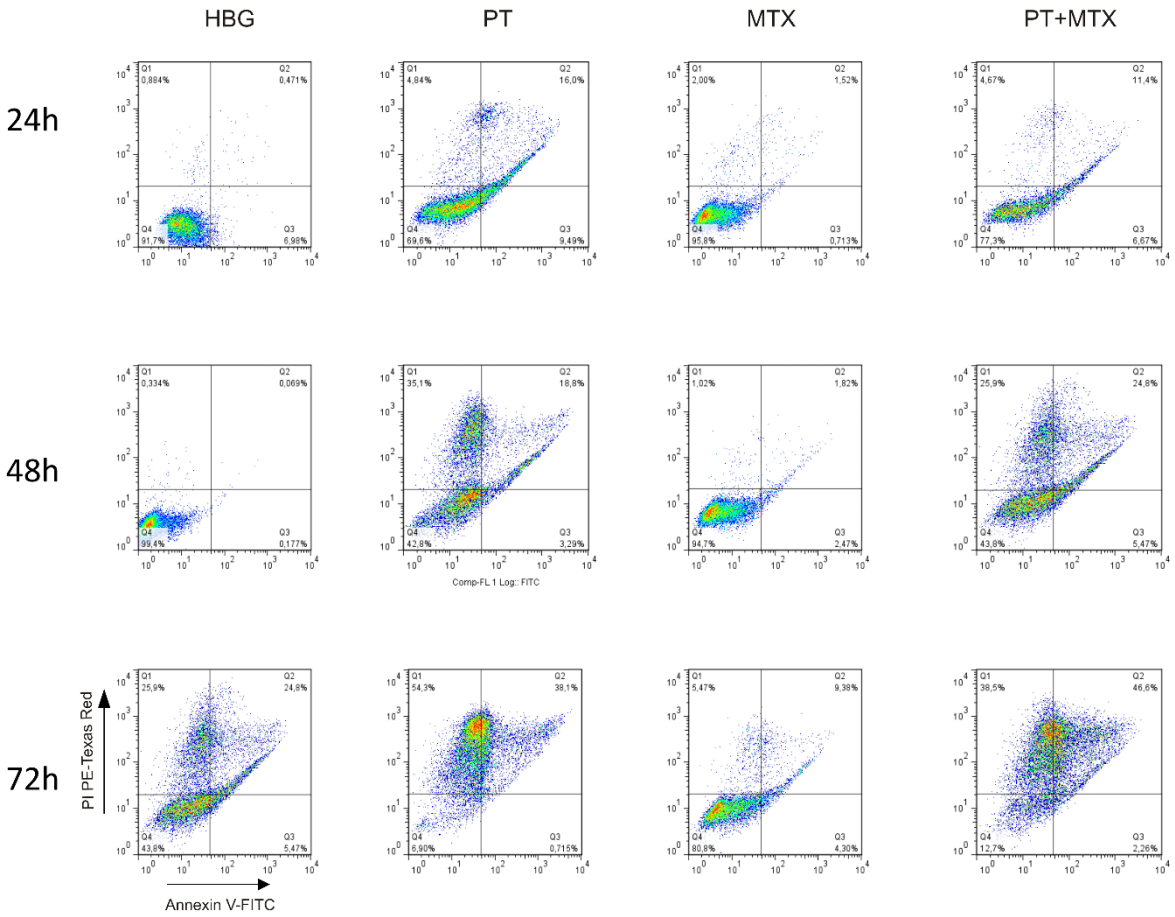

Figure 21. Flow cytometric analysis of apoptosis in drug treated KB cells. KB cells were treated with HBG, PT, MTX or PT+MTX and incubated for 24, 48 and 72 h respectively. Cells were stained with annexin V-FITC and propidium iodide and analyzed by flow cytometry. Treatments were performed in triplicates (n = 3). Q1: FITC – / PI + Q2: FITC +/PI + Q3: FITC +/PI – Q4: FITC –/PI –

3.2.4 Confocal laser scanning microscopy of drug-treated cells

The effects of PT, MTX and PT+MTX on the DNA, the actin cytoskeleton and on the microtubules of L1210 and KB cells were determined by confocal laser scanning microscopy (CLSM). Figure 21 depicts the disruption of the microtubule network of L1210 and KB cells caused by PT treatment, already after 24 h treatment (see also Figure 22 for non-merged images). L1210 cells (Figure 22 A) have lost their structural integrity, the microtubule network seems to be located extracellularly. PT also induced nuclear fragmentation of L1210 cell nuclei. Moreover, a change in the F-actin cytoskeleton upon MTX treatment could be seen especially for KB cells (Figure 22 B).

Cell morphology changed, as cells became elongated over the 72 h time course. In comparison to HBG treatment, MTX treatment led to an accumulation of actin in the cell periphery and the formation of pseudopodia. L1210 cells treated with MTX have completely lost their structural integrity after 72 h. Furthermore, L1210 cell morphology was changed. Cells were shaped less spherical in comparison to HBG treated cells. This effect was, however, less pronounced than for KB cells. PT+MTX treated L1210 cells displayed signs of apoptosis already after 24 h. Cell integrity was lost, nuclei are fragmented and the microtubule network was destroyed. The toxic effects of the drug combination were equally pronounced on KB cells.

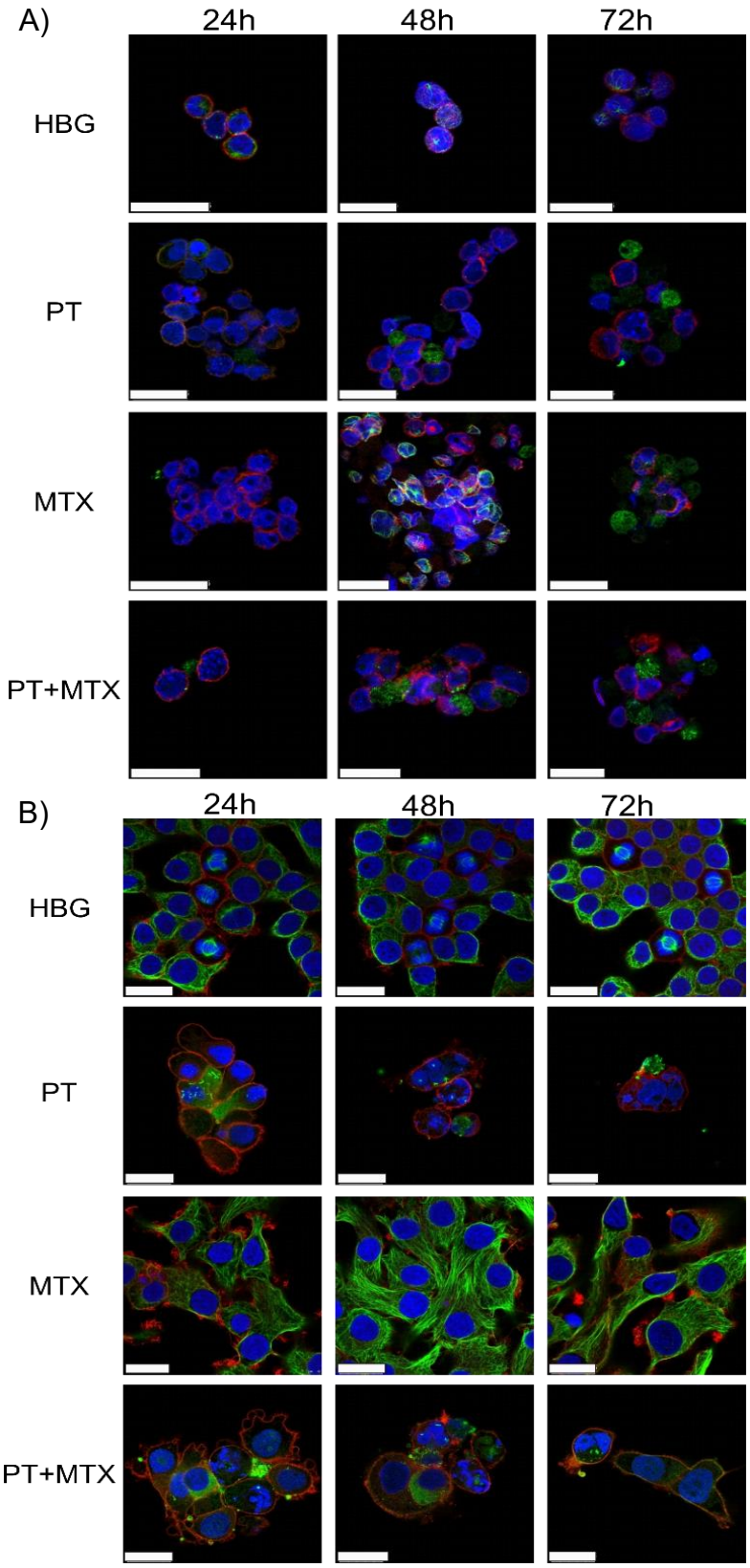

Figure 22. Fluorescence microscopy images of drug-treated L1210 (A) or KB (B) cells. DNA was stained with DAPI (blue), the F-actin was stained with phalloidin-rhodamine (red) and tubulin was visualized using an α-tubulin primary antibody and an AlexaFluor 488 coupled secondary antibody (green). Pictures show the merged staining, scale bar is 25 µm. CLSM images were taken by Miriam Höhn (Pharmaceutical Biotechnology, LMU München).

A)

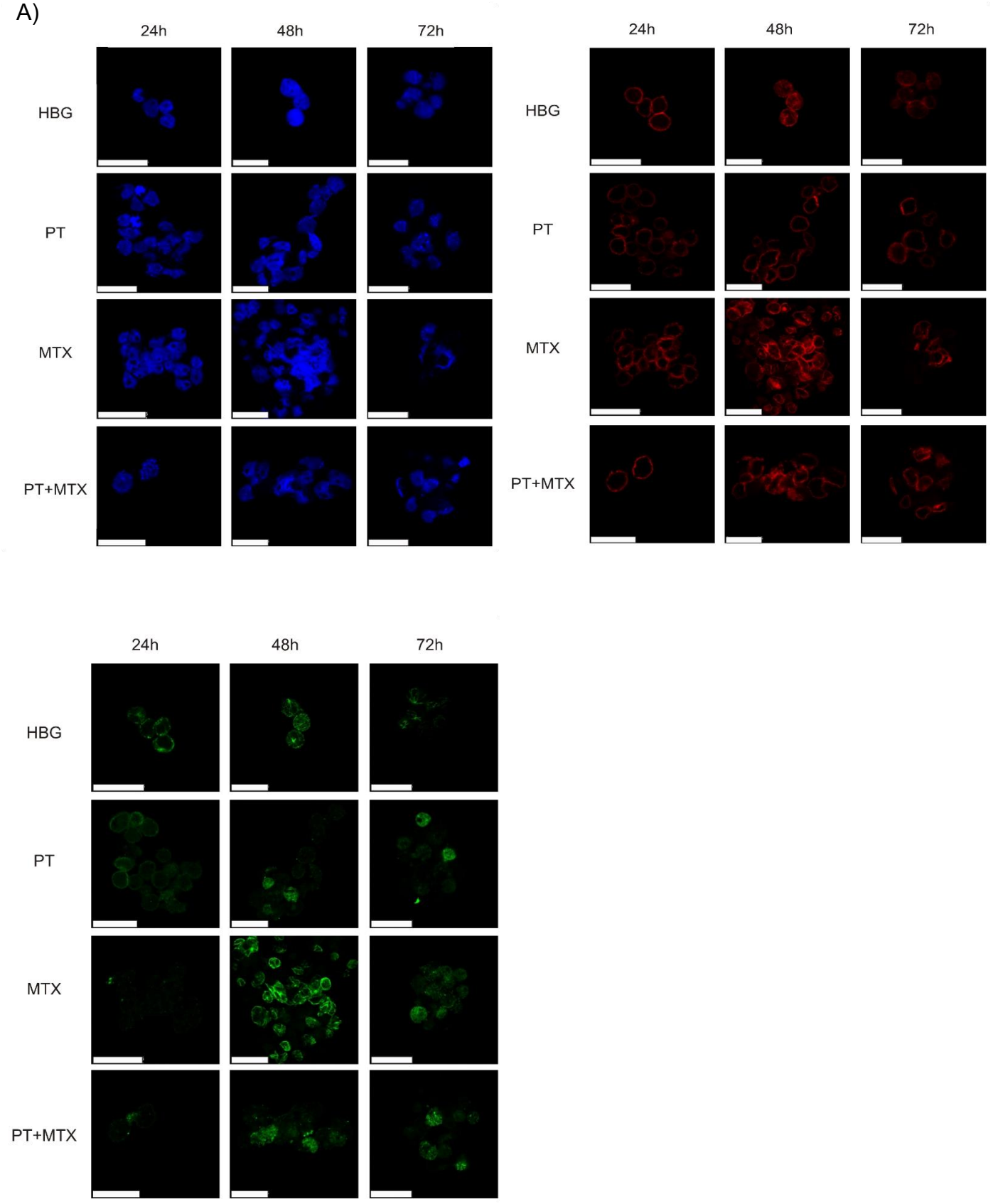
24h
48h
72h
HBG
PT
MTX
PT+MTX
24h
48h
72h
HBG
PT
MTX
PT+MTX
24h
48h
72h
HBG
PT
MTX
PT+MTX

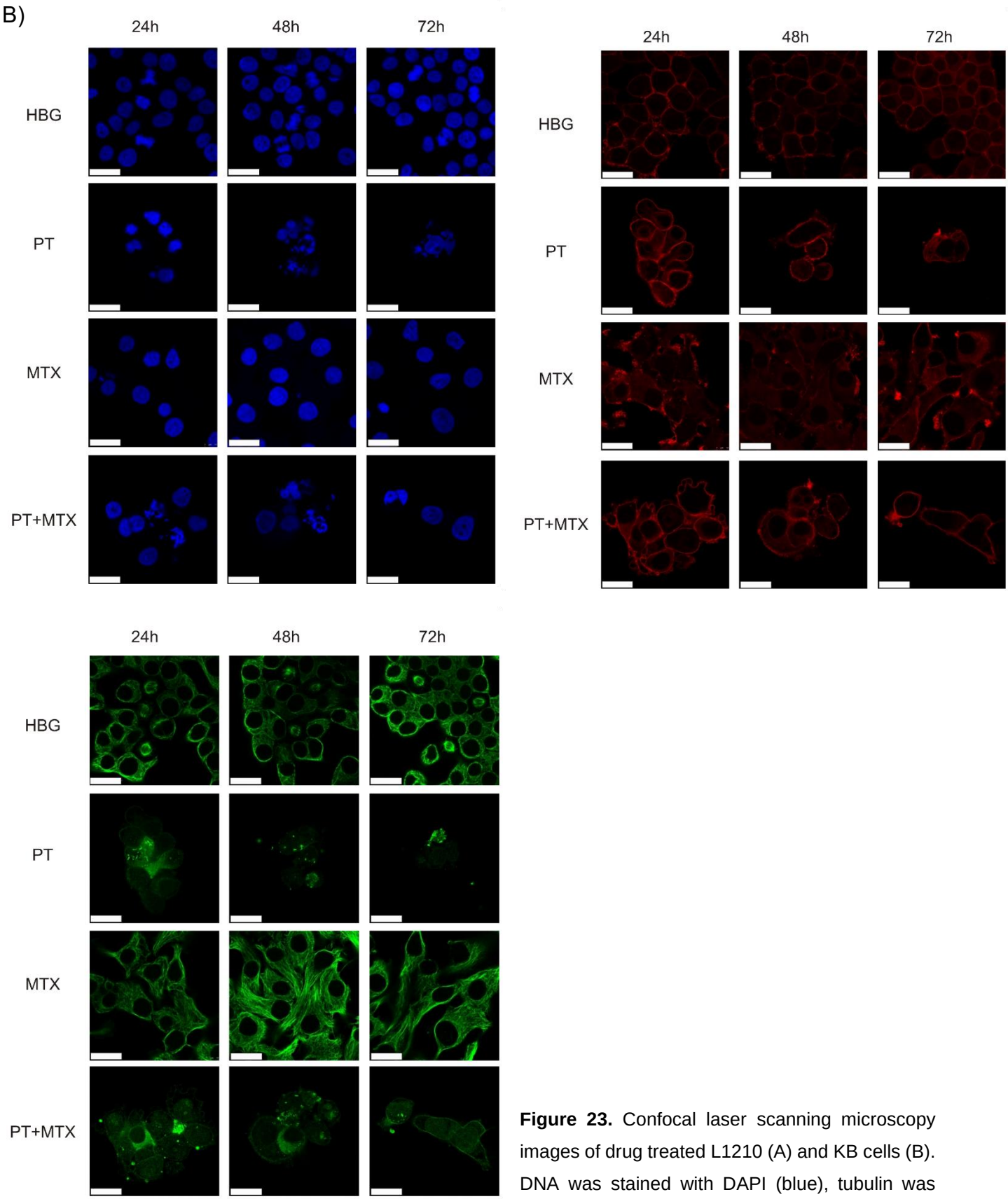

Figure 23. Confocal laser scanning microscopy images of drug treated L1210 (A) and KB cells (B). DNA was stained with DAPI (blue), tubulin was visualized using an α-tubulin primary antibody and an AlexaFluor 488 coupled secondary antibody (green), the actin cytoskeleton was stained with phalloidin-rhodamine (red). CLSM images were taken by Miriam Höhn (Pharmaceutical Biotechnology, LMU München).

3.3 Combination chemotherapy of L1210 tumors in mice with pretubulysin and methotrexate lipo-oligomer nanoparticles

This chapter was adapted from:

*Truebenbach, I.; Kern, S.; Loy, D. M.; Höhn, M.; Gorges, J.; Kazmaier, U.; Wagner, E., Combination Chemotherapy of L1210 Tumors in Mice with Pretubulysin and Methotrexate Lipo-Oligomer Nanoparticles. Mol Pharm 2019,*16 (6), 2405-2417*. Copyright (2019) American Chemical Society.*

The beneficial properties of the drug combination PT+MTX were evaluated in the second chapter of this thesis. To unify the different pharmacokinetic behavior of two drugs after *in vivo* administration, drugs can be co-delivered to the tumor site by formulation into a nanoparticle. In the third chapter of this thesis, PT and MTX were co-incorporated into a delivery system using the previously established lipo-oligoaminoamide (lipo-OAA) ***454***. Containing hydrophobic and hydrophilic segments, the cationizable lipo-OAA ***454*** spontaneously self-assembles into micellar structures in aqueous solution. Four units of the artificial amino acid succinoyl tetraethylene pentamine (Stp) serve as a hydrophilic protonatable segment in ***454***. Being partially protonated at physiological pH, the Stp units facilitate the polyelectrolyte complex (PEC) formation with negatively charged cargo molecules, such as MTX, via electrostatic interaction. The zwitterionic lipophilic PT interacts with ***454*** independently from PEC formation, presumably via hydrogen bonding, hydrophobic, or other interactions.[98] Upon cell uptake, additional protonation of the Stp units under acidifying endosomal conditions promote escape of complexes out of these intracellular vesicles.[51] In addition to the ionic building blocks, lipo-OAA ***454*** contains two oleic acid chains (OleA), and tyrosine tripeptide units which might serve as a further stabilizing domain of the micellar structures by hydrophobic or aromatic π-π stacking interactions.[91, 101] N- and C-terminal cysteines were shown to stabilize siRNA containing complexes due to their disulfide crosslinking potential.[87, 89]

3.3.1 Formation and characterization of 454 nanomicelle complexes

In this study, lipo-OAA ***454*** and antimetabolite MTX were used to form polyelectrolyte complexes (PECs) which were co-loaded with the potent tubulin binding drug PT (Scheme 7).

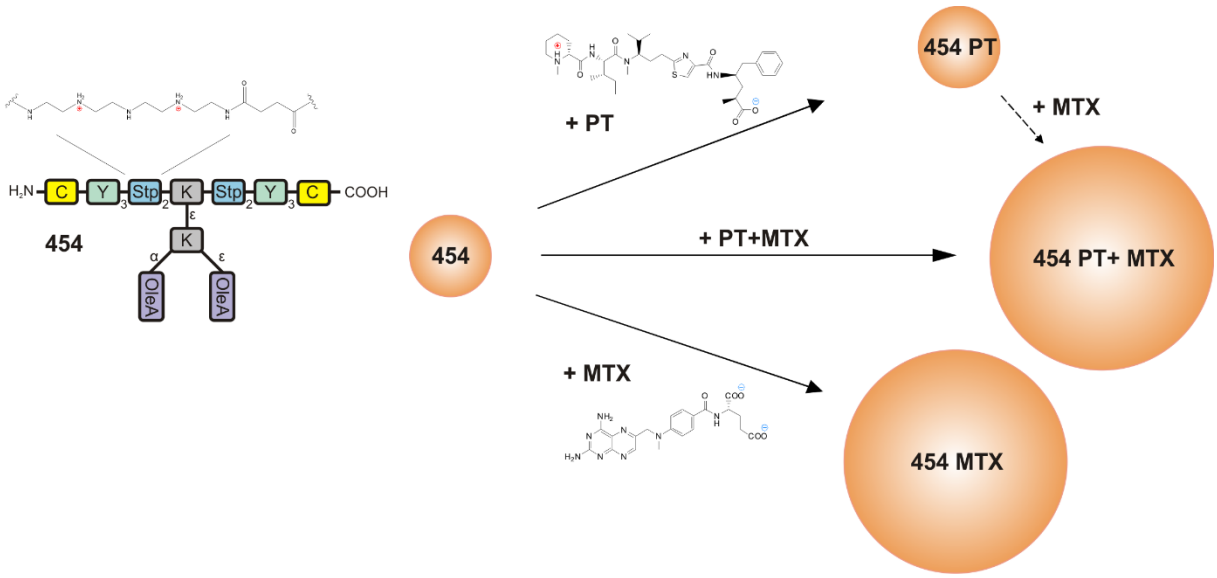

Scheme 7. Schematic representation of nanomicelle complex formation based on lipooligomer ***454***, MTX, and PT. The positively charged sequence-defined lipo-oligoamino amide ***454*** self-assembles into nanomicellar structures with particle sizes of 20 nm. The zwitterionic natural product PT can incorporate into the amphiphilic structures without detectable change in nanomicelle size. Upon addition of the negatively charged MTX to ***454***, a polyelectrolyte complex (PEC) of 150 nm is formed. PEC formation in the presence of MTX and PT results in co-incorporation of the zwitterionic PT by noncovalent interactions, such as hydrogen bonding, or hydrophobic forces.53 The different structural segments of the lipo-oligomer are represented in different colors: hydrophilic regions: blue (Stp), hydrophobic: purple (oleic acid) and aromatic: green (tyrosine). Additional nanoparticle stabilization is facilitated by disulfide crosslinkages (yellow: cysteine).

To enable the successful formation of PECs it is crucial to determine an ideal ratio of both oppositely charged components. Thus, different ratios of oligomer to MTX were investigated to determine a composition that yielded reproducible particles (Figure 24 A). Steinborn et al. have previously examined the particle properties of MTX and ***454***

or polyglutamylated analogs of MTX.[48] In the current study, dynamic light scattering (DLS) measurements revealed that a 10-fold molar surplus of oligomer ***454*** over MTX led to the formation of a heterogeneous mixture of two nanoparticle populations, one small at 24 nm, and another big one at 540 nm (Figure 24 A). By decreasing the ratio of oligomer to MTX, particle properties could be optimized. At a 5-fold surplus of oligomer, ***454*** MTX were found to be of 150 nm in size with a polydispersity index (PDI) of 0.2. By further lowering oligomer amounts to a molar ratio of 3 to 1 or 1 to 1, the PDI of the ***454*** MTX particles decreased further to < 0.2. The particle size slightly increased to 160 nm. The ratio of oligomer to drug was inversed using a 3-fold excess of MTX. This however, led to particle agglomeration and precipitation (not shown). Therefore, a 3:1 molar ratio was used for subsequent ***454*** MTX PEC formation studies.

Before PEC formation studies, several different ratios of ***454*** to PT were screened (Figure 24 A). Different from ***454*** MTX PECs and similar as empty ***454*** nanomicelles, ***454*** PT particle sizes ranged from 15-20 nm with PDIs of 0.3-0.4 independently of the oligomer ratios tested. A ratio of 6 to 2 to 1 of oligomer ***454*** to MTX to PT was finally selected, since Kern et al. described that an excess of MTX over PT was favorable for the drug combination in terms of antitumoral activity and tumor growth *in vivo*.[8]

Nanoparticle sizes and morphology of the ***454*** MTX scaffold and its PT loaded counterpart ***454*** PT+MTX at the optimized oligomer to drug ratio were compared by DLS (Figure 24 B) and transmission electron microscopy (TEM, Figure 24 C). While the particle size of ***454*** MTX nanoparticles at a 3 to 1 ratio (150 nm) slightly increased upon co-assembly with PT (170 nm), the PDI stayed unchanged. TEM images show ***454*** MTX and ***454*** PT+MTX PECs to be uniform and spherical in shape. Data correspond well with DLS measurements in terms of particle size. MTX particles revealed sizes around 100 nm. ***454*** PT+MTX particles were considerably bigger than 100 nm. The particle size and morphology of lipo-oligomer ***454***, which can assemble into particle-like structures in aqueous medium due to its zwitterionic character, and ***454*** PT is depicted in Figure 25**.** Furthermore, the influence of the addition of MTX to existing ***454*** PT particles was investigated. This resulted in the formation of PECs of 165 nm (Figure 26).

Particles which are smaller than 5-10 nm are reported to be rapidly cleared by the kidneys, whereas particles with sizes above 200 nm are recognized by the

reticuloendothelial system (RES) and degraded by macrophages.[112, 113] Particle sizes between 10 and 200 nm have previously been shown to passively target tumors by the EPR effect.[65] Klein et al. demonstrated that targeted and shielded siRNA polyplexes of 190 nm can reach subcutaneous L1210 tumors *in vivo* after systemic administration, which is the same *in vivo* model as used in the current studies.[49] Hence, ***454*** PT+MTX particles with a size of 175 nm should be applicable for intravenous delivery into L1210 leukemia tumors *in vivo*.

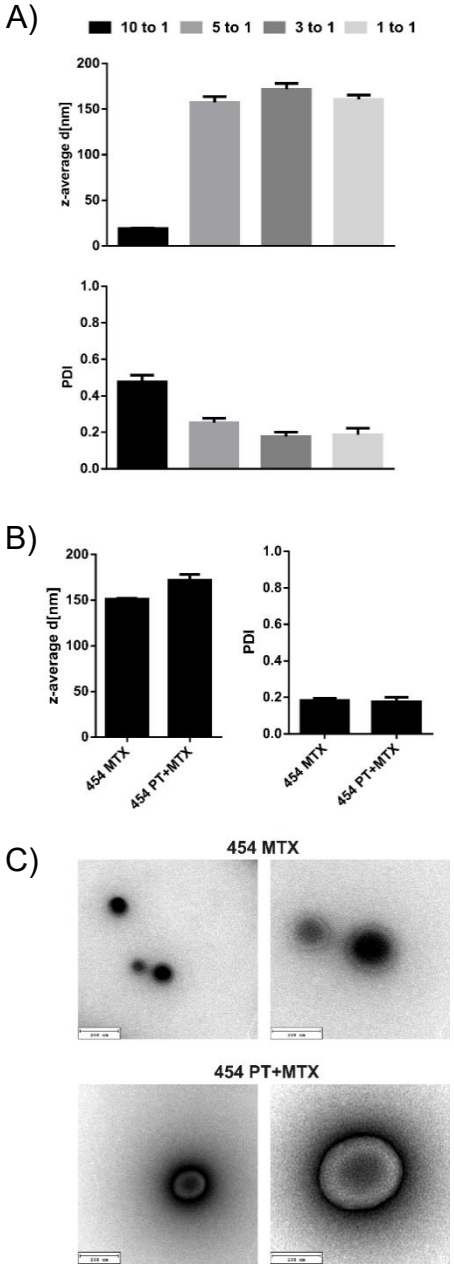

Figure 24. Size and morphology of ***454*** MTX and PT loaded ***454*** PT+MTX. (A) PEC sizes and uniformities are dependent on molar ratios of lipo-OAA to MTX. ***454*** MTX scaffolds were formed in HBG, particle size (z-average) and polydispersity index (PDI) were determined by DLS. (B) Hydrodynamic

diameter (z-average) and PDI of ***454*** MTX and the PT loaded counterpart ***454*** PT+MTX were determined by DLS and are shown as mean ± SD (n=3). (C) TEM images of nanoparticles. The scale bar in the left pictures is 200 nm, in the right 100 nm. TEM images were taken by Dominik Loy (Pharmaceutical Biotechnology, LMU München).

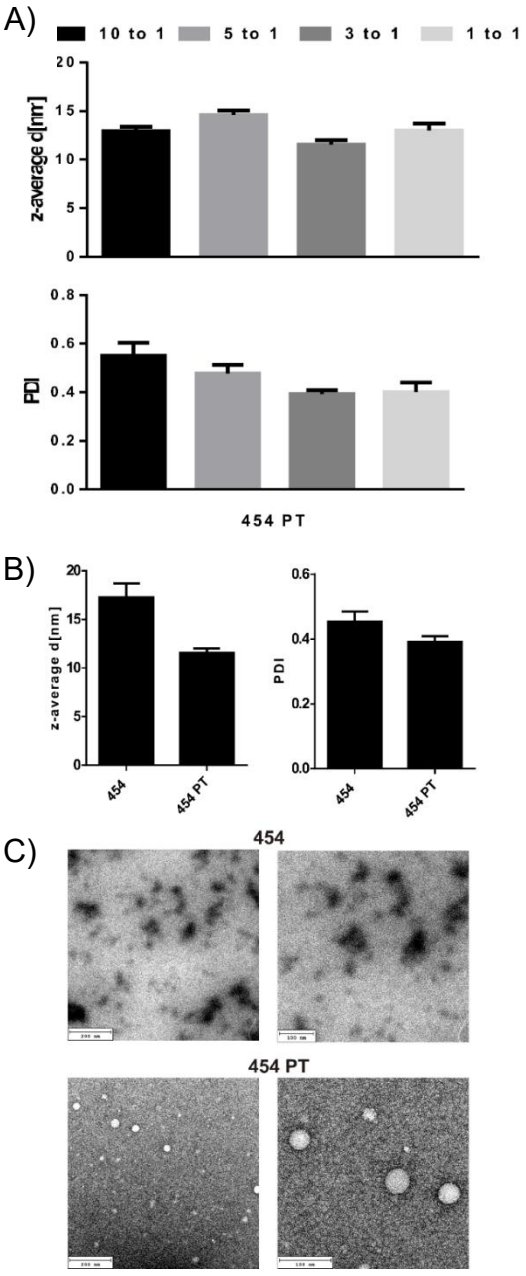

Figure 25. (A) Different ratios of lipo-OAA ***454*** to PT were tested towards its influence on particle size and polydispersity. Nanoparticle size (z-average) and uniformities (PDI) were determined by DLS and are independent from molar ratios of lipo-OAA to PT. (B) Hydrodynamic diameter (z-average) and polydispersity index (PDI) of ***454*** and the PT loaded counterpart ***454*** PT were determined by DLS and are shown as mean ±SD (n=3). Measurements reveal particle sizes of 12 – 20 nm and relatively high PDIs of 0.4. (C) TEM images of nanoparticles. While no uniform particles can be detected on the grid

for an aqueous ***454*** solution, TEM images depict ***454*** PT particles to be homogenous and spherical. The scale bar in the left pictures is 200 nm, in the right 100 nm. TEM images were taken by Dominik Loy (Pharmaceutical Biotechnology, LMU München).

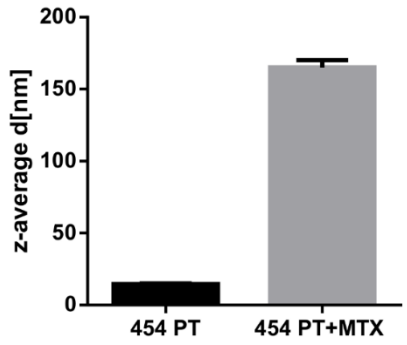

Figure 26. Influence of subsequent MTX addition on particle size of pre-formed ***454*** PT nanoparticles. ***454*** PT particles were formed as described before. After 30 min incubation time, 30 µL of ***454*** PT solution where diluted with 30 µL MTX solution to yield ***454*** PT+MTX particles at a final concentration of 250 µM PT, 500 µM MTX and 1500 µM ***454***. Alternatively, 30 µL of HBG were added to ***454*** PT. Hydrodynamic diameters (z-average) were determined by DLS and revealed particle sizes of 15 nm for ***454*** PT. Upon addition of the anionic MTX, polyelectrolyte complex (PEC) formation resulted in particle sizes of 165 nm. The hydrodynamic diameter is presented as mean ±SD (n=3).

3.3.2 Drug incorporation efficiency of *454*

A nanoparticle system with maximal drug loading and a high incorporation efficiency will reduce the quantity of carriers required for the administration of sufficient amount of active compound and is crucial for the therapeutic effect.[114] The incorporation of MTX and PT+MTX into ***454*** nanomicelles was determined by ultrafiltration. Nanoparticles were formed and ultrafiltered using centrifugal filters with a cut off of 3 kDa. The filtrate, containing non-incorporated drug, was analyzed by HPLC for drug content. Figure 27 represents the amounts of incorporated drug. At the optimized molar ratio (***454***: MTX : PT – 6:2:1), lipo-OAA ***454*** incorporates 84% of MTX and 71% of PT. Upon increasing the amount of PT to ratios of 3:1:1, the incorporation efficiency of the PECs stays unchanged. At higher doses of PT (ratio 3:1:3) however, the incorporation efficiency decreases.

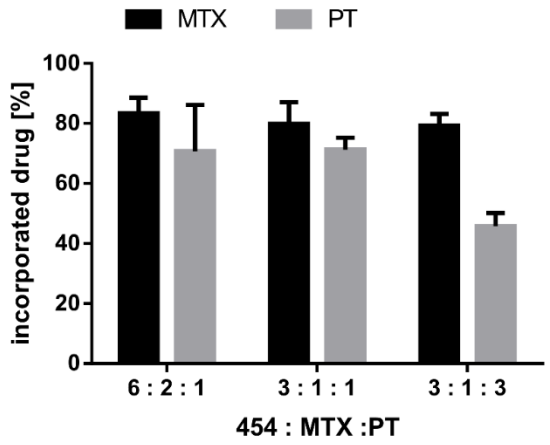

Figure 27. Drug incorporation efficiency of ***454***. Nanomicelle PECs were formed at a fixed molar ratio of oligomer ***454*** to MTX of 3:1, and the PT ratio was increased stepwise. Incorporation efficiency of drugs was determined by analytical reverse phase HPLC (C18 column of 5% to 100% gradient of acetonitrile in 0.1 % aqueous TFA, detection wavelength 214 nm) of the filtrate after removal of nanomicelles by ultrafiltration (Amicon Ultracel 3K) in HBG and is presented as mean ± SD (n=3).

The ability of lipo-OAA ***454*** to incorporate MTX (***454*** MTX) and PT (***454*** PT) is shown in Figure 28. Additionally, the drug loading capacity, i.e. the amount of incorporated drug per nanoparticle, was calculated (Table 9). One mg of ***454*** PT+MTX contained 0.028 mg of PT and 0.038 mg of MTX.

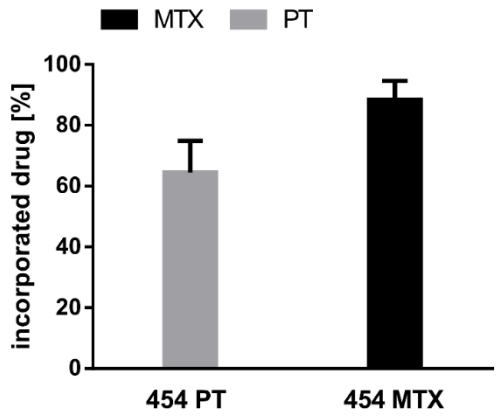

Figure 28. Drug incorporation efficiency of ***454*** PT and ***454*** MTX. Incorporation efficiency was determined by analytical reverse phase HPLC (C18 column of 5% to 100% gradient of acetonitrile in 0.1 % aqueous TFA, detection wavelength 214 nm) of the filtrate after ultrafiltration of ***454*** PT and ***454*** MTX nanoparticles (Amicon Ultracel 3K) in HBG and is presented as mean ± SD (n=3). The incorporation efficiency of the single drug formulations does not differ from the PT loaded ***454*** MTX+PT nanoparticles.

Drug loading capacity [%]	PT	MTX
454 PT	**2.7**	
454 MTX		**4.2**
454 PT+MTX	**2.8**	**3.8**

Table 9. Drug loading capacity of ***454*** PT, ***454*** MTX and ***454*** PT+MTX in [w/w %]. The drug loading capacity was calculated as the amount of incorporated drug divided by the total nanoparticle weight. For ***454*** PT+MTX, 1 mg of nanoparticle contains 0.028 mg of PT and 0.038 mg of MTX.

3.3.3 Stability of *454* PT+MTX Nanomicelle PECs

It is essential to ensure the stability of a micelle under physiological conditions. Different parameters, like salt changes and contact with numerous proteins, endanger its structural integrity.[115] To determine whether ***454*** particles were stable upon exposure to different media, ***454*** PT+MTX nanomicelles were incubated in HBG, physiological NaCl solution (154 mM NaCl) and 10% FBS in HBG. After the respective incubation time points, the particles were ultrafiltered. Different filtration devices were used to separate released PT+MTX from the nanomicelle-bound forms. To determine stability in HBG or physiological NaCl solution, filters with a cut off of 3 K served to investigate the drug release for both MTX and PT. For FBS containing media, filters with a 100 K cut off were used to determine amounts of free PT+MTX. Since PT binds to FBS components (Figure 29), it cannot pass an ultrafiltration membrane with a small cut off of 3 K.

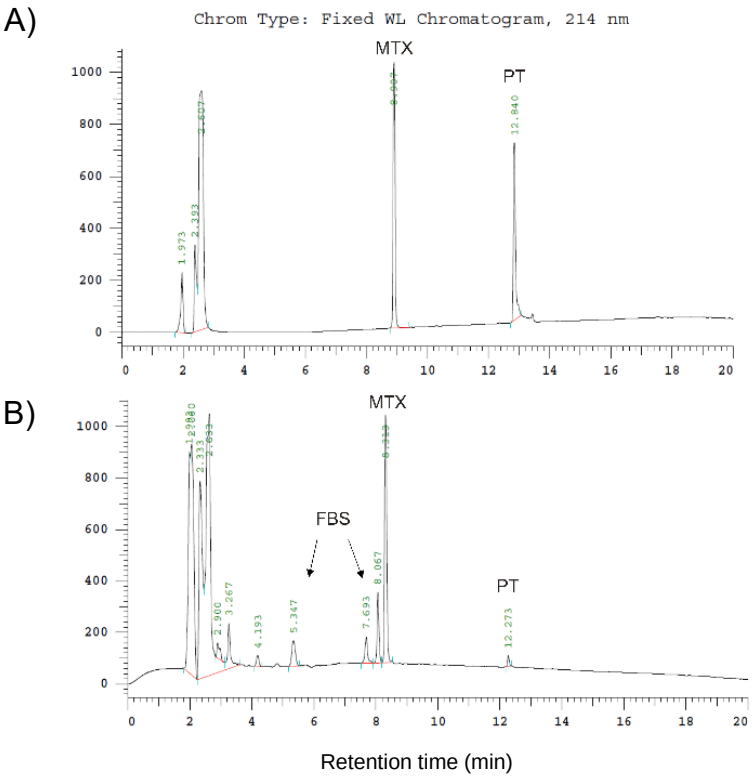

Figure 29. HPLC chromatogram of free PT+MTX incubated with 90% FBS. In order to determine possible interactions of free drugs PT and MTX with serum components, the drug solution in HBG was incubated with 90% FBS at room temperature for 1 h. The sample was ultrafiltered and the filtrate was evaluated by HPLC for free, unbound drug. (A) Chromatogram of ultrafiltered, free drugs PT+MTX at monitoring wavelength 214 nm. (B) Chromatogram of FBS incubated and ultrafiltered PT+MTX at 214 nm. Free MTX does not interact with serum components and can therefore be recovered in the filtrate. Free PT however binds to FBS and can thus not pass the ultrafiltration membrane. Some serum components ('FBS'), which are small enough to pass the 3 kDa molecular weight cut-off ultrafiltration membrane, appear in the HPLC trace at a monitoring wavelength of 214 nm.

In contrast, released PT, even if FBS bound, can pass the ultrafiltration barrier of the 100 K cut off filters and can be detected in the filtrate. The amount of released PT+MTX in the respective filtrates was determined by HPLC analysis and compared to drug content of analogously treated free drug solution incubated in the presence of the respective medium (upper chromatogram of Figure 30 A and B).

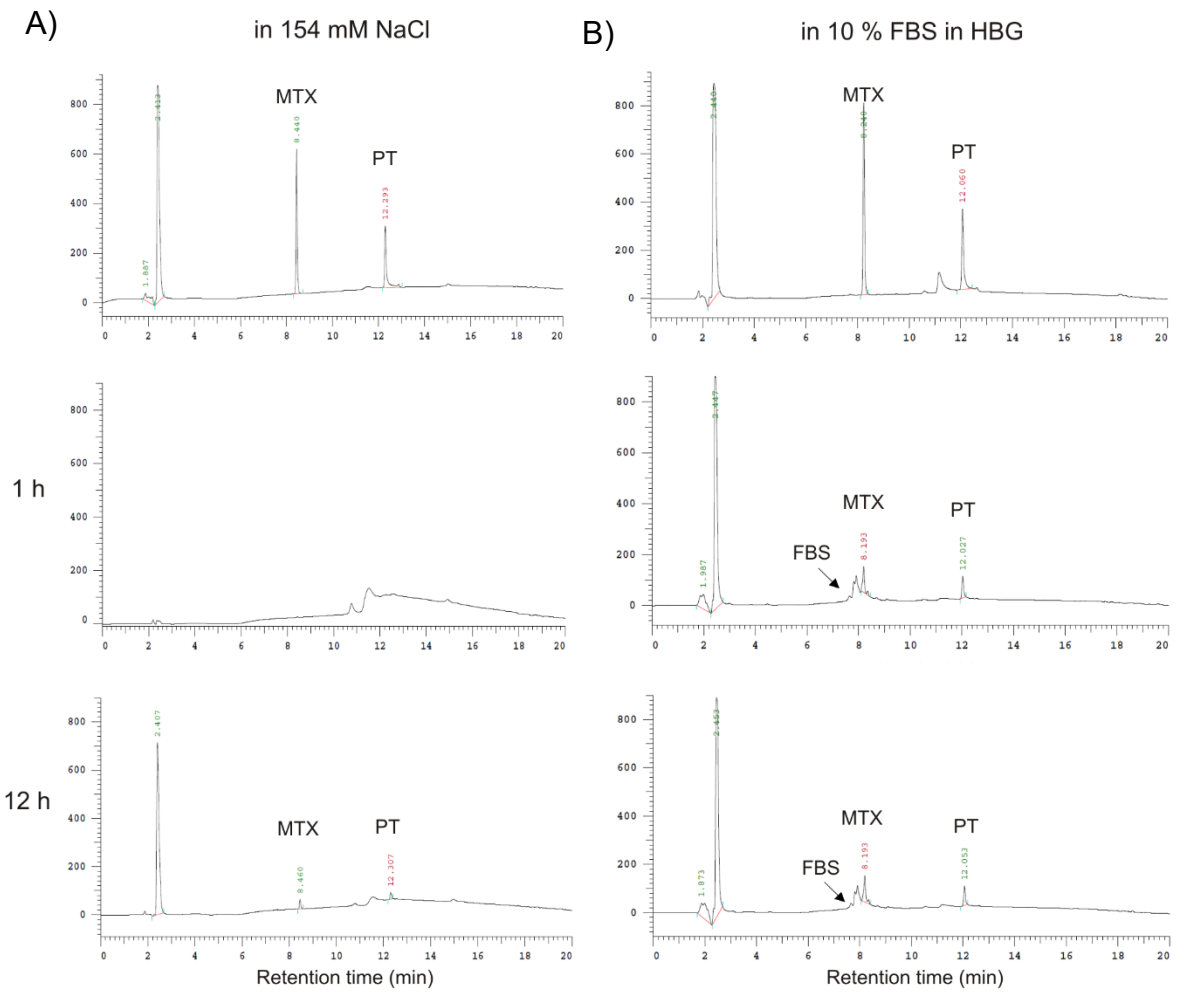

Figure 30. Stability of PT+MTX drug incorporation into ***454*** nanomicelles upon exposure to (A) 154 mM NaCl solution and (B) 10% serum containing HBG at room temperature. HPLC chromatograms (C18 column, 5% to 100% acetonitrile gradient in 0.1 % aqueous TFA in 20 min, detection wavelength 214 nm) of PT+MTX or ***454*** PT+MTX particles after ultrafiltration. Nanoparticle solution (250 µM PT, 500 µM MTX, 1500 µM ***454***; 100 µL) was diluted with 100 µL of incubation medium (308 mM NaCl, 20 % FBS containing HBG). PECs were incubated at final concentrations of 154 mM NaCl and 10 % FBS for 1 h or 12 h at room temperature and ultrafiltered. For nanoparticles incubated in physiological NaCl solution (A), filters with a 3 K cut off (Amicon Ultracel 3K) were used to separate the nanoparticle from free, unincorporated drug. In case of 10 % FBS as the stability medium (B), filters with a 100 K cut off (Amicon Ultracel 100 K) served to separate the free drug. The respective filtrates were evaluated by HPLC for released drug. (A) Stability of ***454*** PT+MTX under physiological salt conditions (154 mM NaCl). The upper chromatogram serves as a concentration standard to calculate free, unincorporated drug. The two bottom chromatograms depict the amount of released drug upon exposure to 154 mM NaCl for 1 or 12 h. (B) Stability of ***454*** PT+MTX in 10 % FBS containing HBG. The upper chromatogram serves as a concentration standard to calculate free, unincorporated drug. The two bottom chromatograms depict the amount of released drug upon exposure to 10 % FBS for 1 or 12 h.

Upon incubation with physiological NaCl solution (Figure 30 A), only 5 % of MTX and PT were freed over the incubation duration of 12 h. Exposure to 10 % FBS led to a release of 9 % of MTX and PT alike over the 12 h time course of the experiment at room temperature (Figure 30 B). Hence, more than 90 % of PT+MTX were stably incorporated into the delivery system. Upon incubation of ***454*** PT+MTX in NaCl solution and 10 % FBS at body temperature, 10 – 15 % of drug was released (Figure 31).

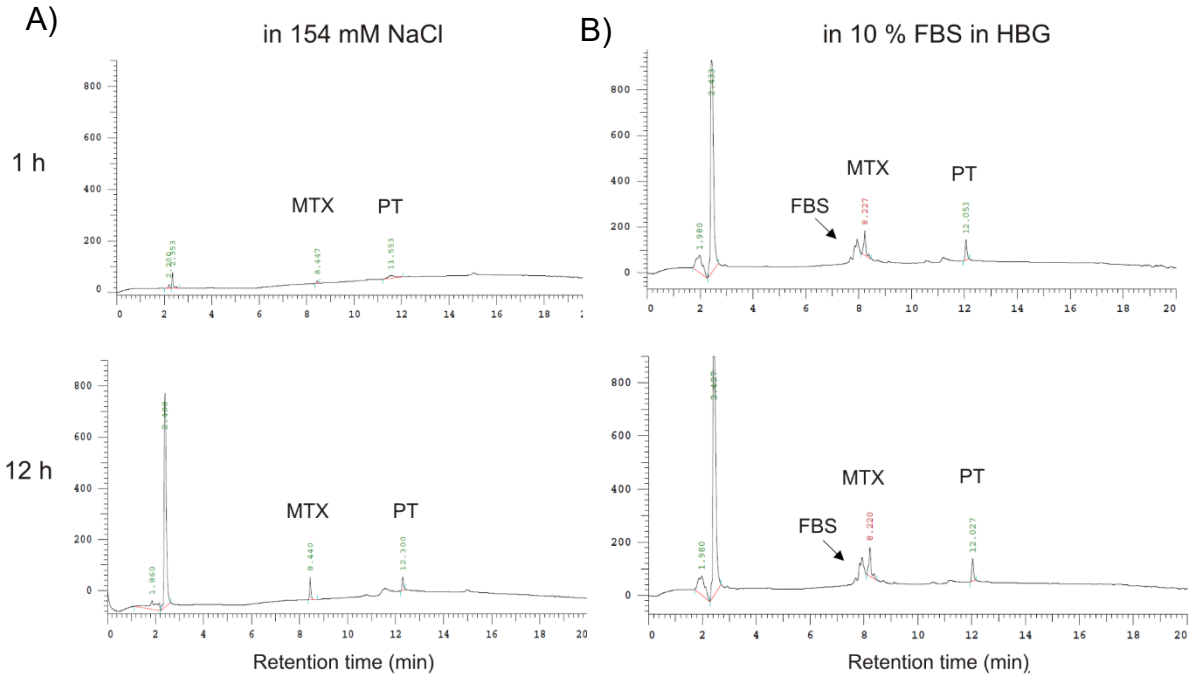

Figure 31. Stability of PT+MTX drug incorporation into ***454*** nanomicelles upon exposure to (A) 154 mM NaCl solution and (B) 10% serum containing HBG at 37 °C. HPLC chromatograms (C18 column, 5% to 100% acetonitrile gradient in 0.1 % aqueous TFA in 20 min, detection wavelength 214 nm) of ***454*** PT+MTX particles after ultrafiltration. Nanoparticle solution (250 µM PT, 500 µM MTX, 1500 µM ***454***; 100 µL) was diluted with 100 µL of incubation medium (308 mM NaCl, 20 % FBS containing HBG). PECs were incubated at final concentrations of 154 mM NaCl and 10 % FBS for 1 h or 12 h at 37 °C and ultrafiltered with filtration devices with a cut off of 3 K for 154 mM NaCl (Amicon Ultracel 3K) or 100 K (Amicon Ultracel 100 K) for FBS containing buffer. The respective filtrates were evaluated by HPLC for released drug. (A) Stability of ***454*** PT+MTX under physiological salt conditions. The chromatograms depict the amount of released drug upon exposure to 154 mM NaCl for 1 or 12 h at 37 °C. Less than 5 % of PT+MTX were released at both time points. (B) Stability of ***454*** PT+MTX in 10 % FBS containing HBG. The chromatograms show the released drug upon exposure to 10 % FBS for 1 or 12 h. Approximately 10 % of PT+MTX were released upon incubation in FBS containing HBG.

An increase in FBS content to 50 % in the incubation medium led to an elevated drug release for both drugs (Figure 32). While particles were stable upon exposure to 20 % FBS for 1 h at 37 °C, an increase in FBS levels to 50 % induced a release of 80 % of MTX and 71 % of PT. The anionic nature of MTX might facilitate the lower stability of MTX incorporation than PT incorporation since anionic albumin molecules in FBS might replace MTX.

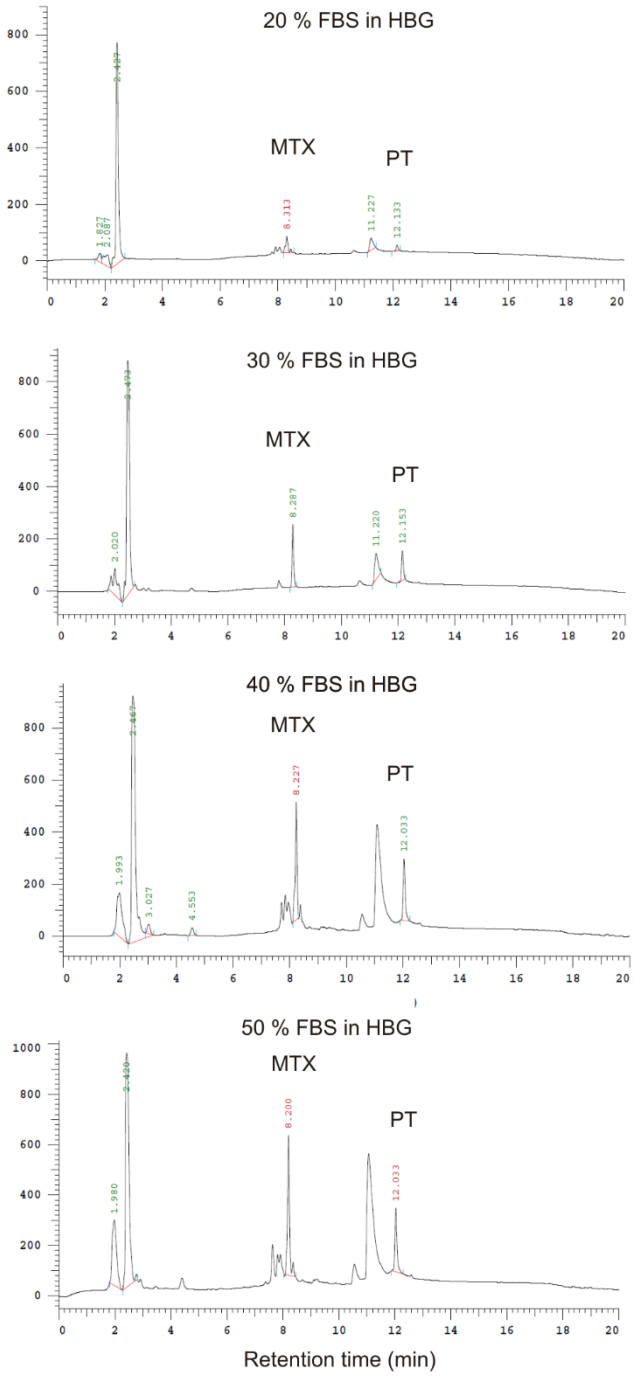

Figure 32. Stability of PT+MTX drug incorporation into ***454*** nanomicelles upon exposure to increasing concentrations of FBS. HPLC chromatograms (C18 column, 5% to 100% acetonitrile gradient in 0.1 % aqueous TFA in 20 min, detection wavelength 214 nm) of ***454*** PT+MTX particles (PECs) after incubation in FBS containing media and ultrafiltration. Nanoparticle solution (250 µM PT, 500 µM MTX, 1500 µM ***454***; 100 µL) was diluted with 100 µL of incubation medium (40% FBS, 60 % FBS, 80 % FBS and 100 % FBS). PECs were incubated at final concentrations of 20 %, 30 %, 40 % and 50 % FBS in HBG at 37 °C and 1 h incubation time. The solution was ultrafiltered using a filtration device with a 100 K cut off (Amicon Ultracel 100 K), the respective filtrates were evaluated by HPLC for free PT+MTX. Drug release increased with elevated levels of FBS. Particles were stably incorporating 90 % of PT+MTX at 20 % FBS. Upon exposure to 30 % FBS, drug incorporation levels decreased to 74 % for both drugs. Only 36 % of PT+MTX were stably incorporated into ***454*** PT+MTX upon incubation in 40 % FBS. A final increase to 50 % FBS in HBG led to a further particle destabilization. 20 % of MTX and 29 % of PT remained incorporated into PECs. FBS components, which are smaller in size than 100 K, also pass the ultrafiltration membrane and are visible in the HPLC trace. With increasing amounts of FBS, more FBS components appear in the HPLC spectra.

Several serum components, which are smaller than 100 K Da, also pass the ultrafiltration membrane and are visible in the HPLC trace. Nanoparticles were stable in HBG buffer for at least 12 h (Figure 33).

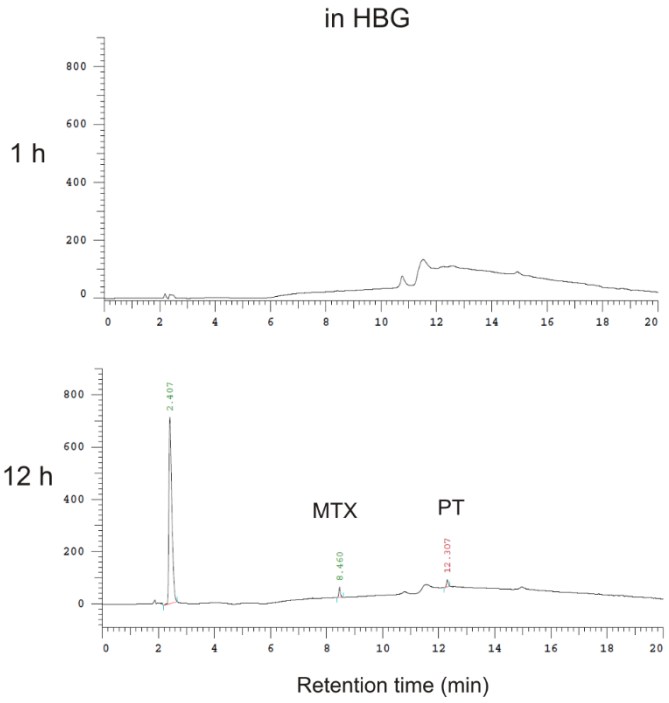

Figure 33. Stability of ***454*** PT+MTX nanoparticles in HBG at 37 °C. In order to determine the stability of ***454*** PT+MTX nanomicelles in HBG, 100 µL of nanoparticle solution (250 µM PT, 500 µM MTX, 1500 µM ***454***) was diluted with 100 µL HBG. Particles were incubated at 37 °C for 1 h or 12 h, respectively. Samples were ultrafiltered (Amicon Ultracel 3K) and the filtrate was evaluated by HPLC for released free PT+MTX. HPLC chromatograms (C18 column, 5% to 100% acetonitrile gradient in 0.1 % aqueous TFA in 20 min, detection wavelength 214 nm) show no release of both drugs over the time course of 12 h.

The MTX release of ***454*** PT+MTX PECs upon incubation at 1 h, 12 h and 24 h in HBG, 154 mM NaCl and 10 % FBS was additionally determined in a photometric assay, as shown in Figure 34. MTX release was examined after ultrafiltration and subsequent photometric analysis of the filtrate for MTX at 340 nm. Over the duration of 24 h, nanoparticles were stably incorporating MTX in HBG. A burst release of 10 % MTX occurred upon incubation with 10 % FBS. Nevertheless, 90 % of MTX were stably incorporated for a further 24 h. Also in NaCl solution, no more than 10 % MTX were released in 24 h.

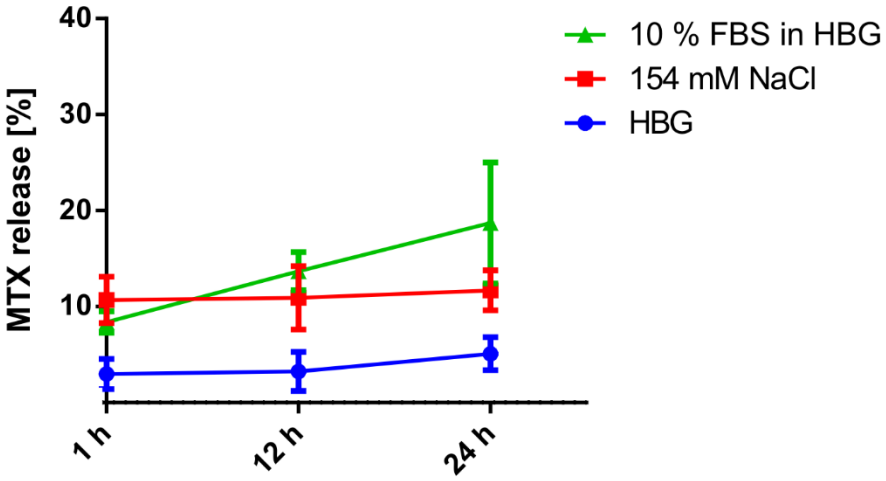

Figure 34. MTX release over time upon incubation of ***454*** PT+MTX in HBG, 154 mM NaCl and 10 % FBS in HBG at 37 °C. ***454*** PT+MTX particles (125 µM PT, 250 µM MTX, 750 µM ***454***) were formed in HBG. Nanoparticle formulations (100 µL) were added to the respective incubation medium (100 µL of HBG, 308 mM NaCl or 20 % FBS in HBG). Upon incubation for 1 h, 12 h or 24 h the solution was transferred to the ultrafiltration device (Amicon Ultracel 3K) and ultrafiltered. The amount of released MTX in the filtrate was determined UV-metrically at a wavelength of 340 nm. Drug release was calculated in comparison to drug content of the filtrate of free PT+MTX, incubated under the same

conditions and subsequently ultrafiltered. In HBG, particles were stable for at least 24 h. Upon incubation of ***454*** PT+MTX in physiological NaCl solution, 10 % MTX was released. No further release occurred over the duration of 24 h. In a solution containing 10 % FBS and 90 % HBG, 10 % of MTX were released upon 1 h incubation time. Throughout the duration of the release study, the MTX release increased to 17 %.

3.3.4 Cellular uptake studies of *454* nanomicelle complexes

The cellular internalization of ***454*** PT+MTX was determined by confocal light scattering microscopy (CLSM) of Cy5 labeled nanoparticles (Figure 35). In the first step, the lipo-oligomer ***454*** was covalently conjugated to Cy5-NHS ester. The secondary amines of the Stp units react readily with the dye. After purification, nanoparticles were formed from 50 % ***454*** and 50 % ***454***-Cy5 as well as the drug combination PT+MTX. L1210 (Figure 35 A) and KB cells (Figure 35 B) were treated with ***454***/***454***-Cy5 PT+MTX for 4 h. The nanoparticle-containing medium was removed; cells were washed with PBS and fixed with PFA (4 % in PBS). After staining the nucleus with DAPI and the actin skeleton with rhodamine-phalloidin, cellular uptake was determined. The CLSM images show the successful intracellular delivery of the nanoparticles into L1210 and KB cells alike.

The incorporation of drugs inside a carrier system enables the delivery of high amounts across the cell membrane to their target site.[116] The successful uptake of ***454*** PT+MTX facilitates the drugs to exercise an increased therapeutic effect intracellularly.

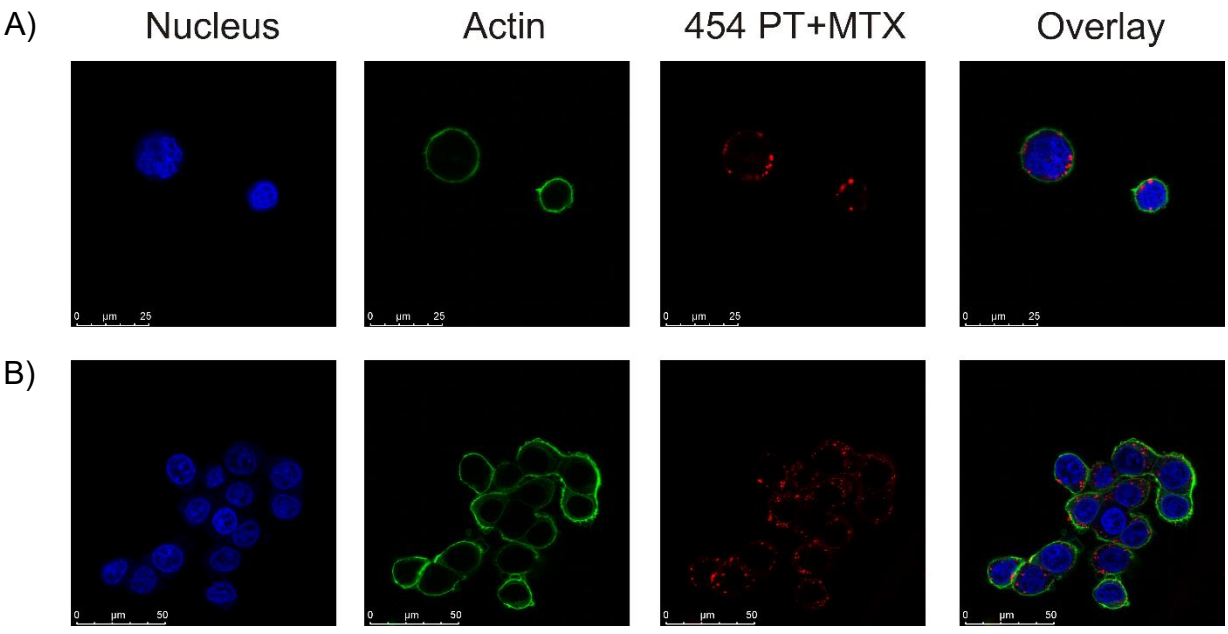

Figure 35. Fluorescence microscopy images of ***454*** PT+MTX PECs treated L1210 cells (A) and KB cells (B). Cells were treated with Cy5 labeled PECs for 4 h. Cells were washed with PBS, fixed with PFA, the nucleus was stained with DAPI, the actin cytoskeleton with rhodamine-phalloidin. CLSM images were taken by Miriam Höhn (Pharmaceutical Biotechnology, LMU München).

3.3.5 *In vitro* antitumoral activity of free or formulated PT, MTX or PT+MTX

PT has a strong antiproliferative effect on L1210 leukemia and KB cervix carcinoma cells *in vitro* and *in vivo*. L1210 cells are very sensitive to MTX treatment and the combination effect of PT+MTX has already been demonstrated.[8] While KB cells have been shown to be partly MTX resistant,[8, 54] PT+MTX however, also displays considerable toxicity.[8] The antitumoral effect of PT+MTX loaded nanomicelle PECs was evaluated in comparison to the free drugs by MTT assay (Figure 36) at different incubation time points. In a short time incubation time set up, PECs were incubated on cells for 4 h. After a wash with fresh medium, the nanoparticles were left on cells for a further 44 or 68 h. Under these conditions, most the free drugs are washed off the cells, while the positively charged ***454*** PT+MTX particles which are associated to the negatively charged cell membrane stay on the cells. In a long time incubation time set up, L1210 and KB cells were treated with ***454*** PT+MTX or PT+MTX for 48 or 72 h respectively. The IC_{50} values were calculated upon 72 h incubation and are shown in Table 9.

For PT+MTX, ***454*** incorporation strongly increased the antitumoral effects on L1210 cells and KB cells alike, especially at lower concentrations (Figure 36). As expected, the overall antitumoral effect is higher, if drugs are left on cells for a longer time (48 h, 72 h). The IC_{50} value PT+MTX (0.2 nM) could be lowered by more than a factor of ten to 0.0195 nM (Table 10). ***454*** PT+MTX killed 50% of KB cells at 0.48 nM, as opposed to the free drug combination PT+MTX (2.773 nM).

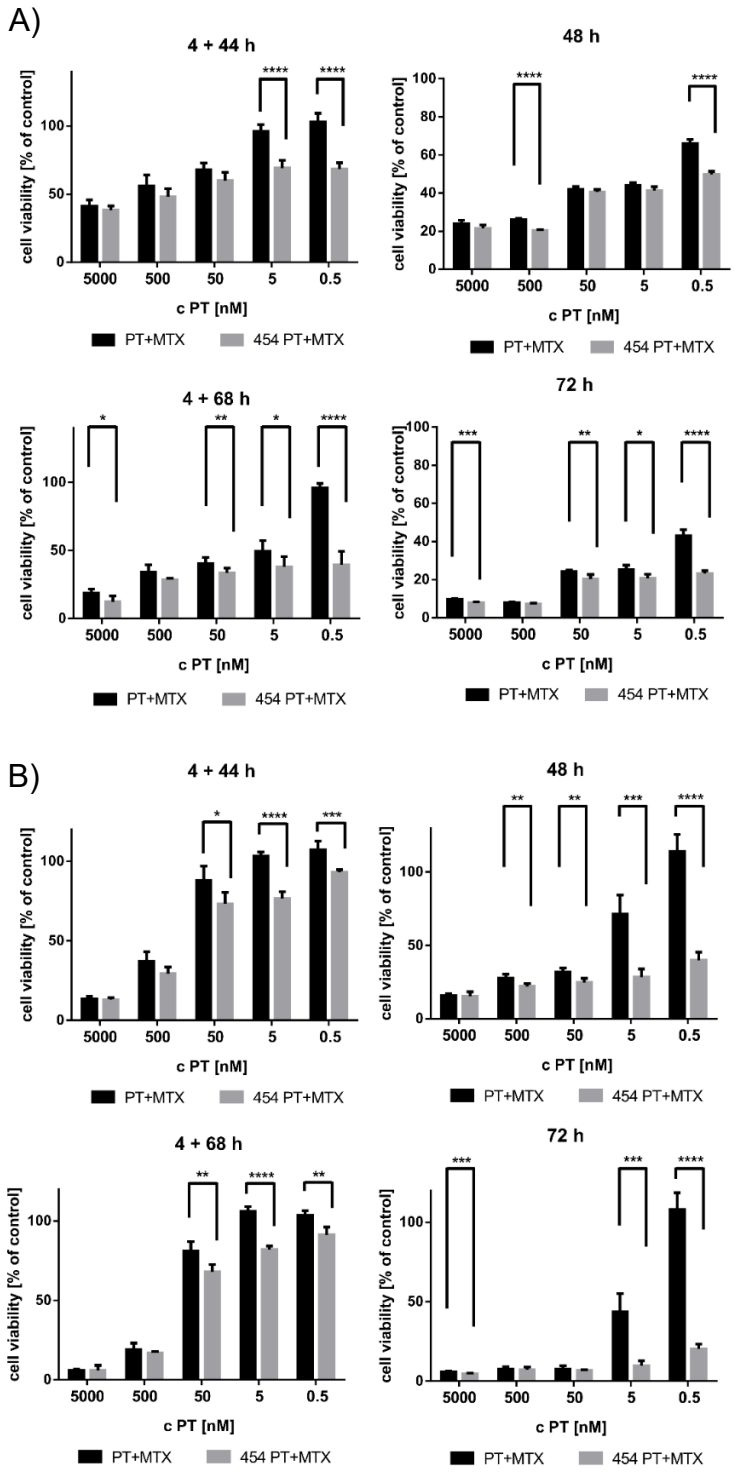

Figure 36. Cell viability of (A) L1210 or (B) KB cells upon treatment with free or formulated drugs. Different incubation conditions were used to determine the effect of nanoparticulate incorporation on antitumoral activity of PT+MTX. Cells were either treated with nanoparticles for 4 h. After non-associated PECs were washed away with fresh medium, medium was added and cells were left to incubate for a further 44 or 68 h. In the second case, ***454*** PT+MTX or PT+MTX remained on the cells for a full 48 or 72 h. Cell viability was measured with an MTT assay and is presented as the mean ± SD (n= 5) in %

relative to buffer (HBG) treated cells. c [nM] refers to the concentration of PT. The molar ratios of oligomer to drugs are 6 : 2 : 1 (***454*** : MTX : PT).

IC 50 [nM]	L1210 cells	KB cells
PT+MTX	0.219	2.773
454 PT+MTX	0.019	0.048

Table 10. IC 50 values of free and formulated drugs on (A) L1210 or (B) KB cells.

Figure 37 shows the antitumoral efficiency of ***454*** PT, ***454*** MTX and ***454*** PT+MTX after 72 h incubation time at lower concentrations. The increased tumor cell killing effects of the ***454*** formulations over the free drugs could not be attributed to lipo-OAA toxicity, which was negligible (Figure 38).

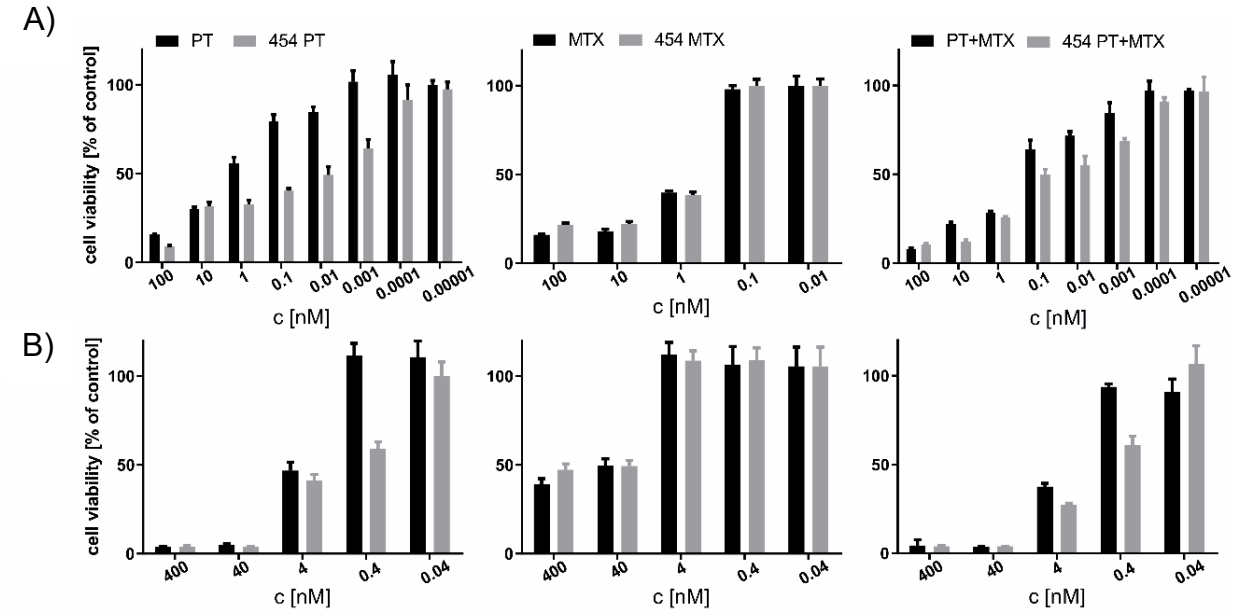

Figure 37. Cell viability of (A) L1210 leukemia or (B) KB cervix carcinoma cells upon treatment with free or formulated drugs. Cell viability was measured with an MTT assay 72 h after treatment and is presented as the mean ± SD (n= 5) in % relative to buffer (HBG) treated cells. c [nM] refers to the concentration of PT and MTX; their concentrations are set at an equimolar ratio. The molar ratios of oligomer to drugs are 6 : 2 : 1 (***454*** : MTX : PT). The data in this graph was used for calculation of IC 50 values (Table 10 and Table 11). While nanoparticulate formulation strongly enhanced antitumoral activity for PT and PT+MTX, it stayed unchanged for MTX.

IC 50 [nM]	L1210 cells	KB cells
PT	0.644	3.195
454 PT	0.002	0.6
MTX	0.637	-
454 MTX	0.428	-

Table 11. IC 50 values of PT, MTX, ***454*** PT and ***454*** MTX on L1210 and KB cells. IC 50 values were determined upon 72 h treatment, see Figure 37. For PT, incorporation into a delivery system increased its antitumoral potency to nanomolar regions. Incorporation of MTX affected the cytotoxic effects of MTX only slightly. Since KB cells are partly MTX resistant, no IC 50 values were calculated for MTX treated KB cells.

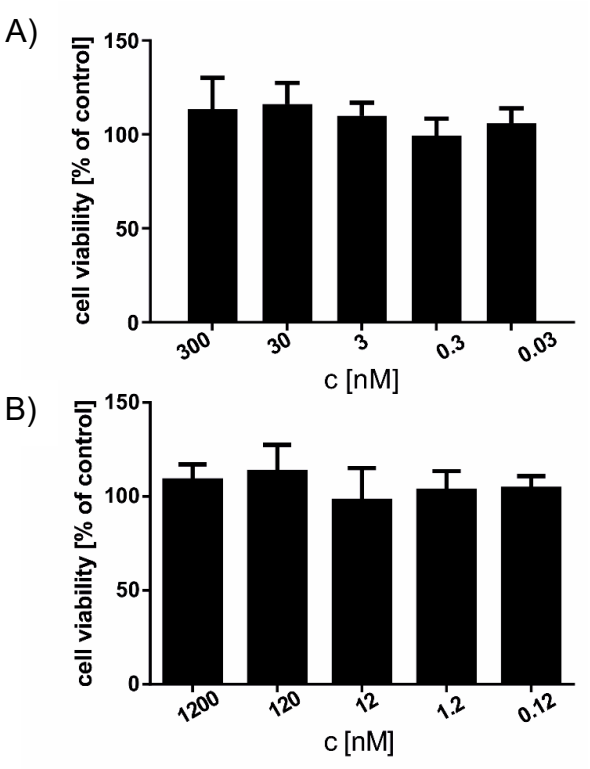

Figure 38. Cell viability of (A) L1210 or (B) KB cells treated with free lipo-OAA ***454***. Cell viability was measured with an MTT assay after 72 h treatment and is presented as the mean ± SD (n= 5) in % relative to buffer (HBG) treated cells, c [nM] refers to the concentration ***454***. Toxic effects were not observed in both cell lines.

The successful delivery of a drug into the cytosol is crucial. An effective strategy is necessary which enables the therapeutic agent to cross the biological membranes and

subsequently protects it against the hostile environment of the endosome and lysosome.[117] Even though PT already displays a considerable antitumoral activity on its own, the formulation with ***454*** strongly increases its potency. Up to date, very little is known about the intracellular uptake mechanism of the peptide-like drug PT. Since ***454*** particles are efficiently loaded with high amounts of PT, particles display a positive surface charge of 30 mV (Figure 39), and Figure 35 shows that PT loaded PECs are readily internalized into L1210 and KB cells, nanomicellar formulation might facilitate an increased uptake of larger quantities of PT and thereby account for the higher antitumoral potency of the nanoparticle over the free drug.[118-120] Free MTX is mainly taken up into the cell via the reduced folate carrier (RFC).[121] The nanomicellar incorporation does not seem to increase the intracellular amount of drug and does therefore not enhance the therapeutic effect of MTX alone (see Figure 37).

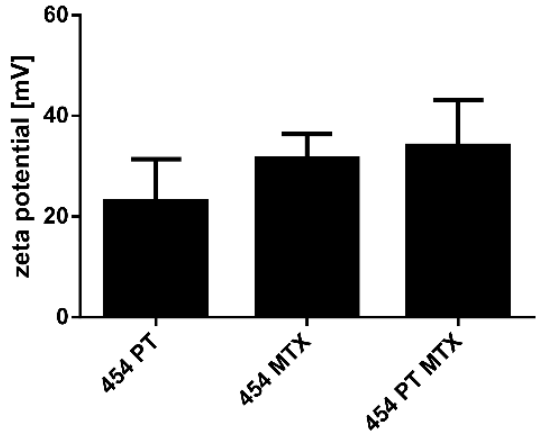

Figure 39. Zeta potential of ***454*** nanomicelles as measured by DLS. The zeta potential for ***454*** nanomicelles is positive (between 20 and 35 mV).

3.3.6 Effect of nanomicellar formulation on cell cycle changes induced by PT+MTX

The effect of PT, MTX and PT+MTX on the cell cycle of different tumor cell lines has recently been investigated.[8] While the tubulin binding agent PT leads to considerable G2/M arrest[8, 9, 18] cells remain in the G1/S phase upon MTX treatment, as the

antimetabolite inhibits the de novo synthesis of nucleotides. For the drug combination PT+MTX at a 3-fold surplus of MTX, the effect of PT on the cell cycle is more prominent. Hence, a considerable G2/M arrest could be observed for PT+MTX treated cells.[8] Also at a 2-fold excess of MTX over PT, the G2/M arrest inducing effect of PT was predominant (Figure 40). In order to determine a possible change in cellular effects due to the incorporation of the drugs into a delivery system, the effect of the nanoformulation 454 PT+MTX on the cell cycle was investigated next to the free drug combination PT+MTX. Formulation of PT+MTX did neither impact the cell cycle upon 24 h treatment, nor after 48 h treatment. Additionally, also lipo-OAA 454 alone and the incorporation of PT and MTX into 454 PT or 454 MTX did not affect the cell cycle (Figure 41). The predominant G2/M-effect of PT and PT+MTX or G1/S-effect of MTX was still observed for the drug formulation.

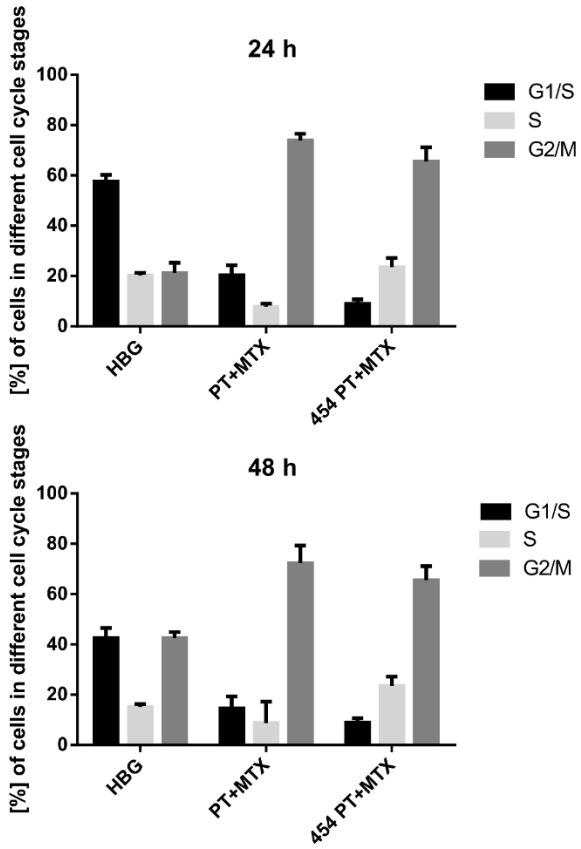

Figure 40. Influence of ***454***, the free drug combination PT+MTX and its nanoparticulate formulation on L1210 cells after 24 h or 48 h treatment. L1210 cells were treated with HBG buffer control, the combination PT+MTX (200+400 nM) or the PT loaded ***454*** MTX nanomicelle complexes (***454*** PT+MTX). Nanomicelles were formed as previously described, at a dose ratio of 6 : 2 : 1 of oligomer : MTX : PT. Cells were incubated for 24 h or 48 h, respectively. Cells were stained with propidium iodide and analyzed by flow cytometry. Treatments were performed in triplicates (n=3), results are presented as the mean ± SD.

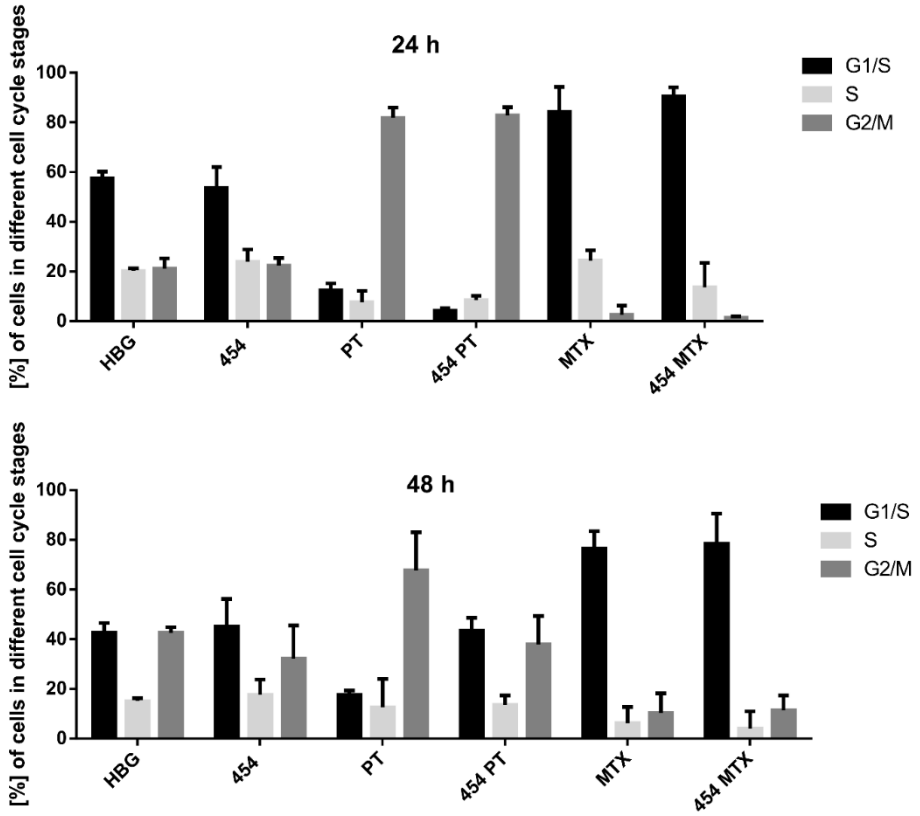

Figure 41. Influence of ***454***, free drugs PT and MTX and their nanomicellar formulations on L1210 cells after 24 h or 48 h treatment. L1210 cells were treated with HBG buffer control, 200 nM PT, 400 nM MTX, or drug containing nanoparticles. Nanomicelles were formed as previously described, at a dose ratio of 6 : 1 for ***454*** : PT or 3 : 1 for ***454*** MTX. Cells were incubated for 24 h or 48 h, respectively. Cells were stained with propidium iodide and analyzed by flow cytometry. Treatments were performed in triplicates (n=3), results are presented as the mean ± SD. While PT induces a strong G2/M arrest, MTX induces a strong S phase arrest. Nanoparticulate incorporation does not affect the cellular effects of both drugs.

3.3.7 Treatment of L1210 leukemia bearing mice with *454* nanomicelles

The ***454*** PT+MTX nanomicelle PECs and the free drug counterpart PT+MTX were investigated *in vivo* for their effects on tumor growth in a subcutaneous L1210 model (Figure 42 A). Due to the high sensitivity of L1210 cells towards PT and MTX *in vitro*, they were chosen over KB cells for the *in vivo* treatment study. L1210 tumor bearing mice were injected intravenously with buffer control (HBG), free drug combination PT+MTX or ***454*** PT+MTX. The dose of PT was set at 2 mg/kg. In case of MTX, a dose of 2.5 mg/kg was chosen as higher doses led to precipitation of the formulation. Treatments were repeated three times per week, with a maximum of 8 injections in total. Animals were sacrificed after reaching the criteria critical tumor size of 1500 mm^3 and Kaplan Meier survival was analyzed. To monitor animal well-being mice were weighed daily. Considerable weight loss occurred in several animals of the ***454*** PT+MTX group after the first treatment. Nevertheless, mice tolerated all further injections well and the weight development was unobtrusive throughout the rest of the experiment. Animals displayed a rather constant weight whereas after the end of treatments, all surviving mice started to steadily gain weight (Figure 43).

The tumor growth throughout the treatments with buffer control (HGB), ***454*** PT+MTX and PT+MTX is shown in Figure 42 A. Tumors of the HBG group started to grow 8 days after tumor cell inoculation. Several animals reached the critical tumor size of 1500 mm^3 already 4-5 days later. Tumors of PT+MTX treated animals started growing on day 14. Encouragingly, mice treated with ***454*** PT+MTX exhibited the strongest tumor growth delay as tumor growth onset did not start before day 18. The beneficial effect of ***454*** PT+MTX over PT+MTX was most prominent on day 20 (Figure 42 B). The Kaplan-Meier curve (Figure 42 C) demonstrates a statistically significant longer survival of the mice in the ***454*** PT+MTX nanoparticle group. Nanoparticle formulation of PT+MTX with ***454*** increased survival of mice by more than 100% compared to the HBG treated group. Overall survival of animals of the ***454*** PT+MTX group was significantly longer compared to animals of PT+MTX group (log rank test of Kaplan Meier curve PT+MTX vs. ***454*** PT+MTX: 0.013) longer than mice of all other groups with the last animal being sacrificed on day 38 after tumor cell inoculation (Figure 42 C).

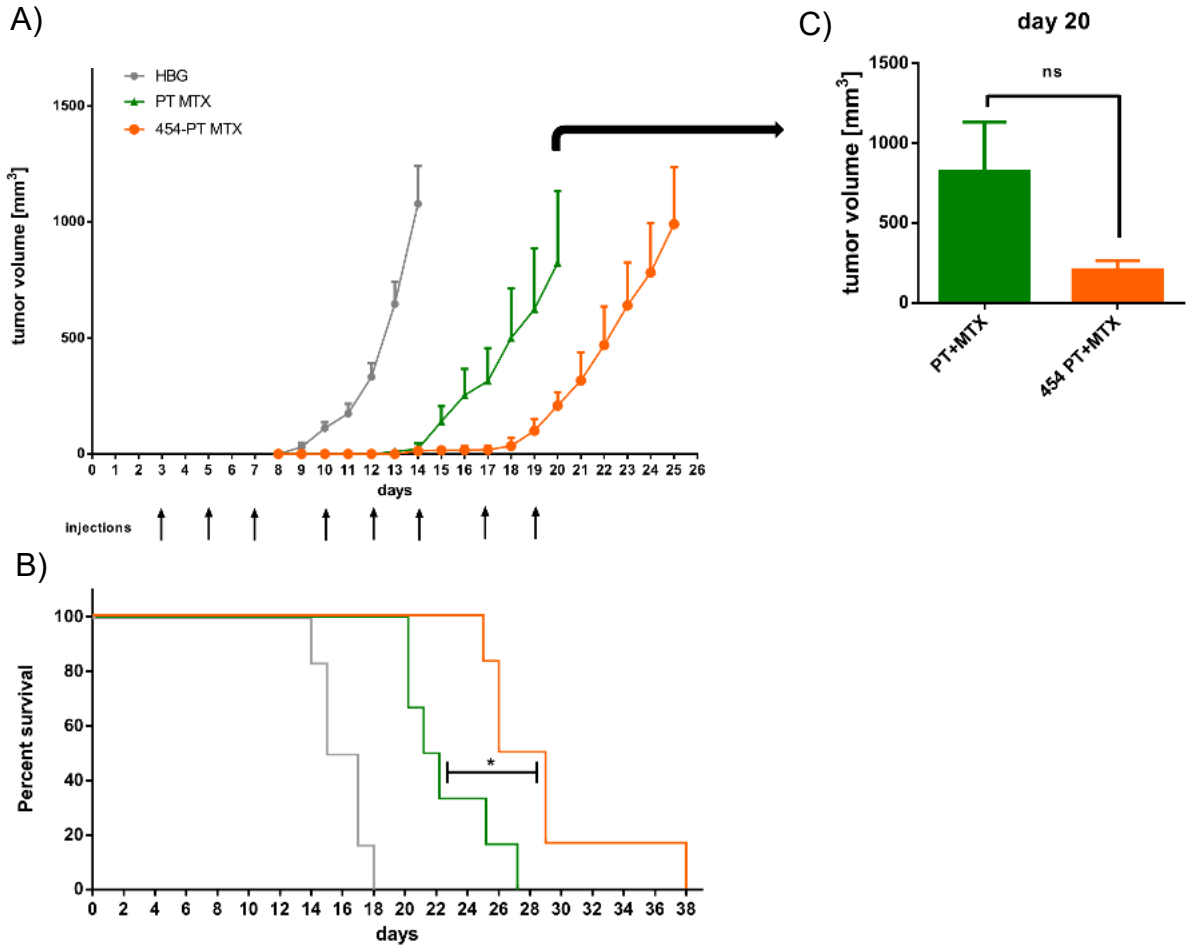

Figure 42. Treatment of subcutaneous L1210 tumors. (A) Tumor volume of subcutaneous L1210 tumors throughout the experiment (mean + SEM; n = 6 mice per group). Animals were treated intravenously with 250 µL of HBG, PT+MTX or ***454*** PT+MTX (2 + 2.5 mg/kg). (B) Tumor volume of PT+MTX and ***454*** PT+MTX on day 20 after tumor inoculation. (C) Kaplan Meier survival curve of animals treated with HBG, PT+MTX or ***454*** PT+MTX (n = 6 mice per group). Significance of the results was evaluated using log rank test (*: p = 0.0131). Animal experiments were performed by Dr. Sarah Kern (Pharmaceutical Biotechnology, LMU München).

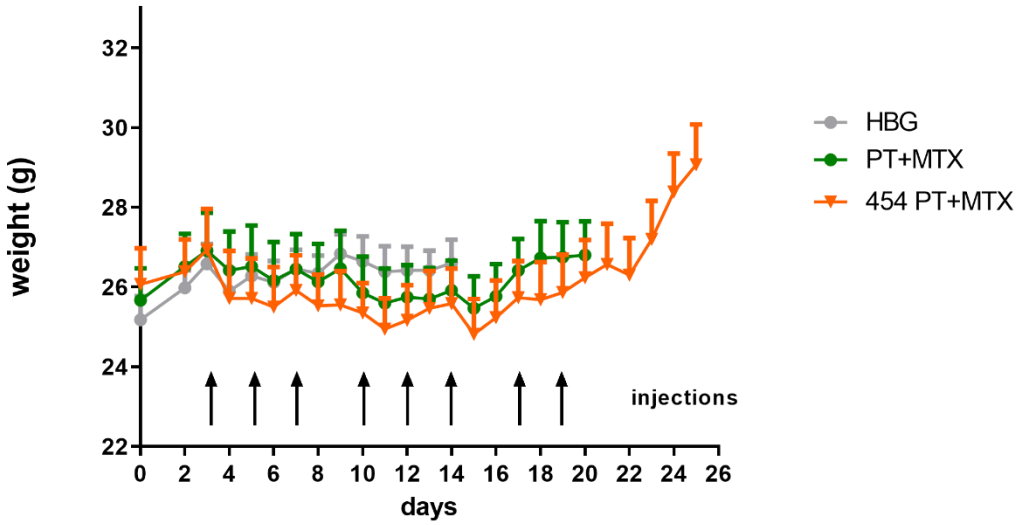

Figure 43. Weight development of mice during systemic treatment with HBG, PT+MTX and ***454*** PT+MTX in L1210 tumor bearing animals, starting on day 0 with tumor cell inoculation. Represented is the mean weight + SEM of 6 mice per group. Some weight loss occurred in several animal of the ***454*** PT+MTX group after the first treatment. Nevertheless, mice of the ***454*** PT+MTX group tolerated all further injections well and the weight development was unobtrusive throughout the rest of the experiment. After the last injection, the surviving mice (***454*** PT+MTX) gained weight steadily. Animal experiments were performed by Dr. Sarah Kern (Pharmaceutical Biotechnology, LMU München).

3.4 Co-delivery of pretubulysin and siEG5 to EGFR overexpressing carcinoma cells

This chapter was adapted from:

Truebenbach, I.; Zhang, W.; Wang, Y.; Kern, S.; Höhn, M.; Reinhard, S.; Gorges, J.; Kazmaier, U.; Wagner, E., Co-delivery of pretubulysin and siEG5 to EGFR overexpressing carcinoma cells. Int J Pharm 2019, 569, 118570.

The final chapter of this thesis examines the combination of PT with the therapeutic siRNA siEG5. Several different drug combinations with siRNA polyplexes have already been investigated. In a first study, siEG5 was combined with the well-established antimetabolite drug methotrexate.[48] Even though the combination exhibited a beneficial antitumoral efficiency, acquired resistances to MTX are common. Therefore, MTX was substituted with the potent tubulin binding drug PT; Klein et al. investigated a combination of free drug PT and folate receptor targeted polyplexes containing siEG5.[49] This drug combination displayed antitumoral effects. In the current work as a next step, PT and siEG5 were co-incorporated into a nanoparticle to enable their controlled and simultaneous delivery to the target cell. The polyplexes containing the two antitumoral entities, i.e. the microtubule inhibitor PT and the mitotic arrest inducing EG5 siRNA, were formed using lipo-oligomer ***1198***, the azide bearing analog of the previously described ***454***. This sequence-defined lipo-oligoaminoamide was sequentially assembled via SPS and optimized towards intracellular delivery of nucleic acids. The different structural units of ***1198***, which facilitate the successful co-incorporation of siEG5 and PT, are shown in Scheme 8. The lipo-oligomer contains the cationizable artificial amino acid Stp for complexation of the siRNA component and endosomal buffering.[90] Tyrosine tripeptide motifs (Y3) provide polyplex stabilization via π-stacking effects.[91, 122, 123] C- and N-terminal cysteines (C) stabilize the polyplex through disulfide crosslinking potential.[87, 89] T-shaped lipo-oligomers such as ***1198*** contain a further hydrophobic domain branching off the cationic backbone. Two fatty acids, oleic acid in this case, improve polyplex stability via hydrophobic stabilization and cause endosomal membrane destabilization.[87, 100] The different structural units of the polymer ***1198*** enable the successful co-incorporation of the rather lipophilic peptide-like natural product derivative PT. Hydrophobic interactions with the oleic acid

domains, possibly also aromatic interactions, with the Y_3 motif, and also hydrogen bonds with the oligoaminoamide Stp units may facilitate a successful incorporation of PT inside the polyplex.

The azide moiety enables the covalent attachment of a shielding and/ or targeting agent onto the surface of the polyplex (Scheme 8 A) via copper free click chemistry.[49] The reaction partner dibenzocyclo-octyne (DBCO) was successfully incorporated into the shielding agent DBCO-PEG and the targeting agent DBCO-PEG-GE11 via SPS. A bifunctional monodisperse PEG molecule with 24 ethylene oxide monomer units was used in the current study. The orthogonal nature of the click reaction enables the selective and efficient modification of the polyplex surface.[49, 124, 125] The chemical structures of the shielding agent DBCO-PEG and the targeting agent DBCO-PEG-GE11 are shown in Scheme 8 B. The ***1198*** polyplexes, containing either siRNA or the siRNA and drug combination, were thus functionalized with PEG or PEG-GE11 respectively.

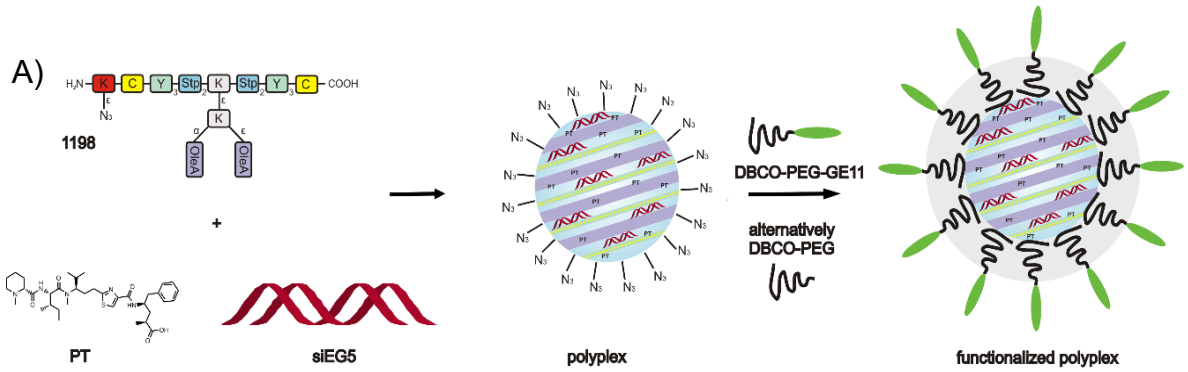

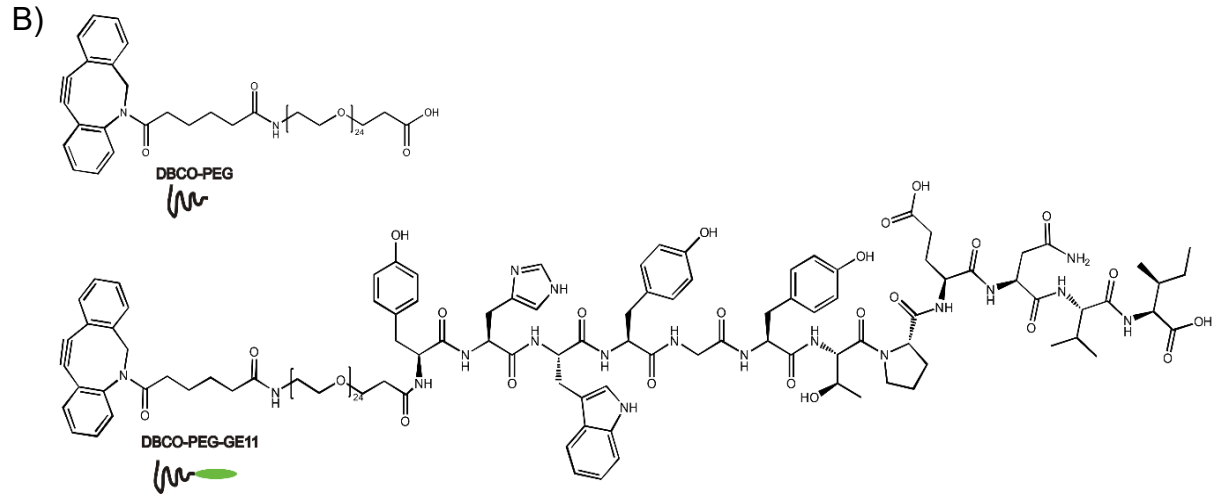

Scheme 8. (A) Illustration of polyplex formation. Azide containing lipo-oligomer ***1198*** and siEG5 and PT form a lipo-polyplex. In the second step, the lipo-polyplex surface is functionalized via click-chemistry; (B) chemical structures of the DBCO containing shielding agent DBCO-PEG and targeting agent DBCO-PEG-GE11.

3.4.1 Drug incorporation efficiency and siRNA binding

As PT on its own already shows great potential as a new microtubule inhibitor in cancer therapy, the combined incorporation of PT with antitumoral siRNA into a delivery system aims at elevating the therapeutic effect. To this effect, PT needs to be sufficiently incorporated into the siRNA lipopolyplex. Thus, the drug incorporation efficiency of the ***1198*** siEG5+PT particles was determined. Polyplexes were formed as described above and ultrafiltered (using a membrane with a molecular weight cut-off of 3 kDa) to separate residual, unincorporated PT. The filtrate was then analyzed by HPLC to determine the amount of free PT. As a concentration standard, a solution containing free PT was ultrafiltered and the filtrate was subjected to HPLC analysis (Figure 44 A, upper chromatogram). After polyplex incorporation, only small amounts of free PT were determined in the filtrate (Figure 44 A, bottom chromatogram). By relating the peak areas of the PT peaks at 12.5 nm, the drug incorporation efficiency of the ***1198*** siEG5+PT polyplex was calculated to be 84%.

Cationizable oligomers are able to complex nucleic acids into polyplexes via electrostatic interactions and thus enable the intracellular delivery of the negatively charged cargo across the cell membrane.[126] Ensuring a sufficient binding affinity between siRNA and the delivery material is crucial. The siRNA compaction efficiency of the ***1198*** oligomer was determined with a gel shift experiment (Figure 44 B). The ***1198*** siEG5 polyplex, PEG-GE11 targeted ***1198*** siEG5 and the PEGylated ***1198*** siEG5 all sufficiently bind siRNA at an N/P ratio of 10. In summary, ***1198*** facilitated the successful incorporation of both the natural product PT and siEG5.

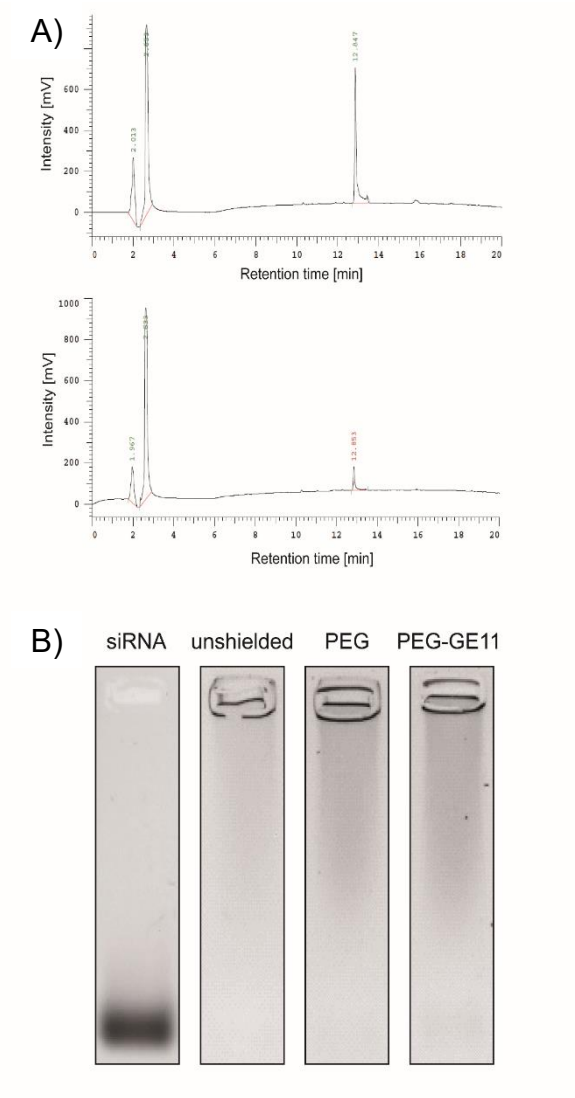

Figure 44. Drug incorporation efficiency and siRNA binding of ***1198*** polyplexes. (A) The incorporation efficiency of PT into ***1198*** siEG5 polyplexes (N/P ratio 10, 50 µg siRNA, 0.3 ng PT in 200 µL HBG) was determined by ultrafiltration of drug loaded polyplexes and subsequent HPLC analysis (C18 column, 5% to 100% acetonitrile gradient in 0.1 % aqueous TFA in 20 min, detection wavelength 214 nm) of the filtrate for free PT. A solution containing free, ultrafiltered PT served as the concentration standard (upper chromatogram). After formation of the PT loaded polyplexes (***1198*** siEG5+PT), ultrafiltration was performed to remove residual, unincorporated free PT. The filtrate was analyzed by HPLC for the residual drug (lower chromatogram). The amount of free PT was determined in relation to the concentration standard. (B) The siRNA binding of ***1198*** siEG5 polyplexes was determined by gel shift assay for the unshielded, PEG modified or PEG-GE11 functionalized polyplexes. ***1198*** polyplexes were formed at an N/P ratio of 10 and contained 250 ng siRNA. Polyplexes were post-functionalized with 0.75 eq. of PEG or PEG-GE11 and incubated for 4 h. For the unshielded formulation, the respective amount of HBG was added. A 1% agarose gel was prepared in TBE buffer, GelRed was added for siRNA detection. Gels were run at 80 mV for 45 min.

3.4.2 Particle size, polydispersity and zeta potential

The particle size, polydispersity and zeta potential of the polyplexes containing siEG5 or siEG5+PT were determined by dynamic light scattering (DLS). Furthermore, the effect of post-functionalization on the biophysical particle properties was evaluated. Figure 45 A depicts the hydrodynamic diameter of the polyplexes. Particle sizes ranged from 185 nm to 200 nm (Figure 45 A). While the additional incorporation of PT slightly decreased particle size, functionalization of the polyplex with PEG and PEG-GE11 did not impact particle size. The PDI of PT containing particles (***1198*** siEG5+PT) was slightly lower in comparison to siEG5 formulations (***1198*** siEG5, Figure 2b) ranging from 0.16 (***1198*** siEG5+PT PEG-GE11) to 0.25 (***1198*** siEG5 unshielded). Post-modification of the ***1198*** polyplexes with PEG or PEG-GE11 did not considerably influence the polydispersity. The zeta potential of ***1198*** polyplexes is shown in Figure 45 B. Here, PT incorporation slightly increased the positive surface charge of the polyplexes, albeit not significantly. The zeta potential of the unshielded formulation was 22 mV (***1198*** siEG5), respectively 24 mV (***1198*** siEG5+PT). The efficient shielding effect of PEG is clearly visible here, with zeta potentials decreasing to 6 mV (***1198*** siEG5) or 7 mV (***1198*** siEG5+PT). Post-functionalization of particles with PEG-GE11 led to an increase in positive surface charge to values of 18 mV (***1198*** siEG5) and 20 mV (***1198*** siEG5+PT) negating the shielding effect of PEG.

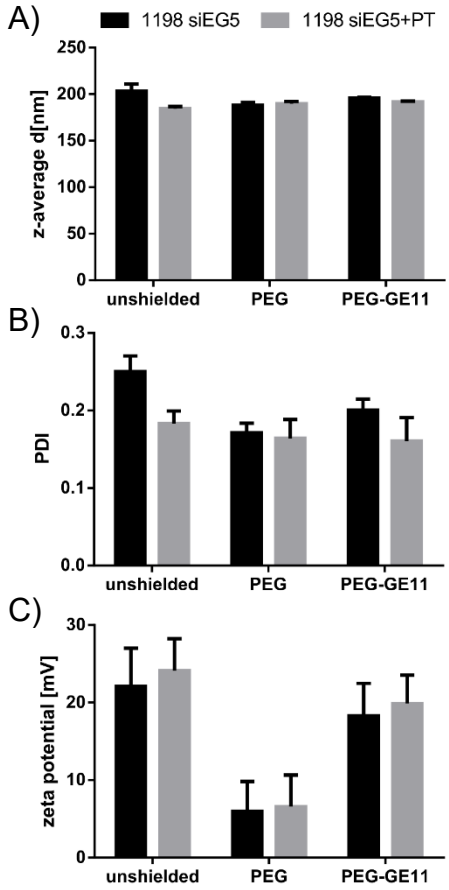

Figure 45. Drug incorporation efficiency and siRNA binding of ***1198*** polyplexes. (A) The incorporation efficiency of PT into ***1198*** siEG5 polyplexes (N/P ratio 10, 50 µg siRNA, 0.3 ng PT in 200 µL HBG) was determined by ultrafiltration of drug loaded polyplexes and subsequent HPLC analysis (C18 column, 5% to 100% acetonitrile gradient in 0.1 % aqueous TFA in 20 min, detection wavelength 214 nm) of the filtrate for free PT. A solution containing free, ultrafiltered PT served as the concentration standard (upper chromatogram). After formation of the PT loaded polyplexes (***1198*** siEG5+PT), ultrafiltration was performed to remove residual, unincorporated free PT. The filtrate was analyzed by HPLC for the residual drug (lower chromatogram). The amount of free PT was determined in relation to the concentration standard. (B) The siRNA binding of ***1198*** siEG5 polyplexes was determined by gel shift assay for the unshielded, PEG modified or PEG-GE11 functionalized polyplexes. ***1198*** polyplexes were formed at an N/P ratio of 10 and contained 250 ng siRNA. Polyplexes were post-functionalized with 0.75 eq. of PEG or PEG-GE11 and incubated for 4 h. For the unshielded formulation, the respective amount of HBG was added. A 1% agarose gel was prepared in TBE buffer, GelRed was added for siRNA detection. Gels were run at 80 mV for 45 min.

3.4.3 Cellular internalization of *1198* siRNA polyplexes

The incorporation of siRNA into a nanoparticle facilitates the intracellular delivery of the spacious and negatively charged cargo. The functionalization of the nanoparticle surface with the shielding agent PEG or the EGFR targeting peptide GE11 influences the uptake profile of the nanoparticles into the EGFR overexpressing cell lines. The effect of the shielding agent PEG and the targeting ligand PEG-GE11 on cellular internalization of the ***1198*** siRNA polyplexes was determined by flow cytometry (Figure 46 A-B) and confocal laser scanning microscopy (CLSM) (Figure 46 C-D). Several studies have demonstrated the GE11 peptide to be an effective active targeting agent in nanoparticle delivery.[81, 82, 127-130] Polyplexes containing Cy5 labeled siRNA (red) were prepared, left unshielded or equipped with the shielding agent (PEG) or the targeting agent (PEG-GE11) and incubated on the cells for 45 min to enable the cells to actively internalize polyplexes bound to their surface. Subsequently, cellular uptake was determined.

For flow cytometry studies, cells were washed with PBS and heparin before quantifying the Cy5 intensity. The wash with negatively charged heparin largely dissociates remaining lipopolyplex material from the cell membranes and thus, only internalized Cy5 siRNA is detected. The mean fluorescence intensity (MFI) of the targeted formulation (PEG-GE11) over the shielded formulation (PEG) and the unshielded formulation was significantly increased on KB cells (Figure 46 A) and Huh7 cells (Figure 46 B) proving the effectiveness of the GE11 ligand. Additionally, PEG functionalization decreased cellular uptake compared to the unshielded formulation for both cell lines.

The functionalization with the GE11 targeting peptide increased polyplex uptake into KB cells, especially in comparison to the PEG group (Figure 46 C). PEG shielding decreased the cellular internalization of the polyplexes in comparison to both the unshielded and targeted group. On Huh7 cells (Figure 46 D), the CLSM images confirmed a higher intracellular delivery of the PEG-GE11 group over the PEG group and also the unshielded group. In summary, by functionalization of the particle surface with EGFR targeting GE11 peptide, the receptor mediated uptake of ***1198*** siRNA polyplexes into KB and Huh7 cells was increased.

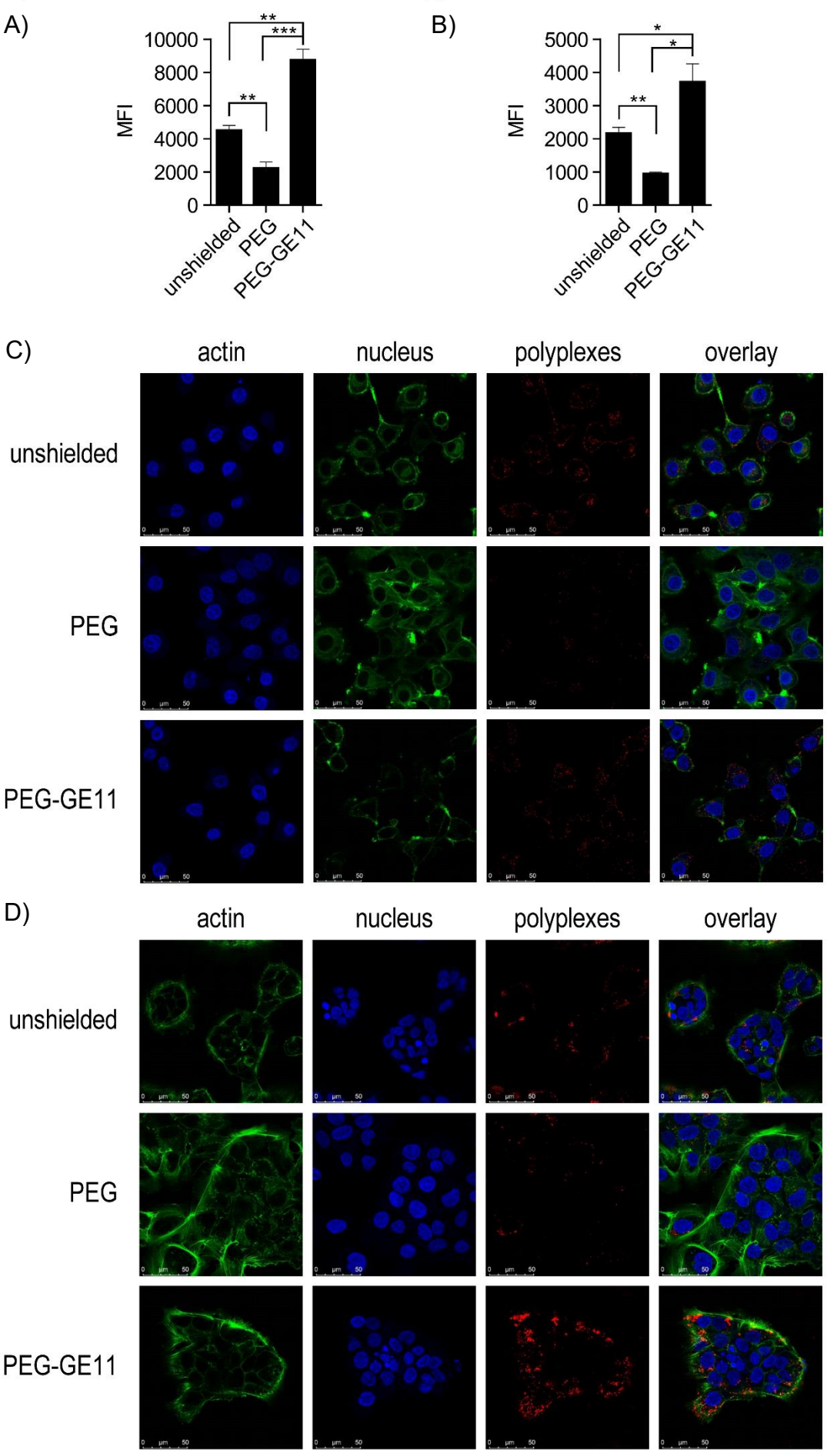
A)
MFI
10000
8000
6000
4000
2000
0
**
***
**
unshielded
PEG
PEG-GE11
B)
MFI
5000
4000
3000
2000
1000
0
*
*
**
unshielded
PEG
PEG-GE11
C)
actin
nucleus
polyplexes
overlay
unshielded
PEG
PEG-GE11
D)
actin
nucleus
polyplexes
overlay
unshielded
PEG
PEG-GE11

Figure 46. Internalization of polyplexes was monitored with flow cytometry (A-B) or confocal laser scanning microscopy (CLSM, C-D). For flow cytometry experiments, polyplexes were incubated on cells for 45 min in a cell culture incubator. Cells were washed with PBS and heparin. Cellular uptake was determined by flow cytometry; (A) Cellular internalization of ***1198*** polyplexes into KB cells; (B) Cellular internalization of polyplexes into Huh7 cells. Polyplexes contained 1.5 µg siRNA per well (1 mL) including 20% Cy5 labelled siRNA. Mean fluorescence intensity (MFI) is presented as the mean ± SD (n=3). For CLSM experiments, KB cells (C) or Huh7 cells (D) were incubated with 300 µL of polyplex solution containing 500 ng siRNA per well including 20% Cy5-siRNA (red color) for 45 min at 37 °C. Nuclei were stained with DAPI (blue) and the actin cytoskeleton was stained with rhodamine phalloidin (green); polyplexes are visualized by Cy5 labeled siRNA (red). The white scale bars indicate 25 µm. Flow cytometry experiments were performed by Dr. Wei Zhang and Dr. Yanfang Wang (Pharmaceutical Biotechnology, LMU München). CLSM images were taken by Miriam Höhn (Pharmaceutical Biotechnology, LMU München).

3.4.4 GFP gene silencing

Gene silencing experiments were performed using the KB-eGFP-Luc or Huh7-eGFP-Luc cells (Figure 47). Polyplexes were formed from GFP siRNA (siGFP) or control siRNA (siCtrl) and lipo-oligomer ***1198***. They were further equipped with the shielding agent PEG or the targeting peptide PEG-GE11. Cells were incubated with polyplexes for 4 h, GFP gene silencing was quantified after 48 h by reduced luciferase activity of the eGFP-Luc fusion protein. The influence of the functionalization on GFP gene silencing was investigated.

The ***1198*** siGFP polyplex facilitated successful silencing of the GFP gene in KB-eGFP-Luc cells (Figure 47 A). The unmodified polyplex reduced luciferase activity to below 40 %. PEGylation decreased GFP gene silencing activity, probably due to reduced cellular uptake of the shielded formulations. The introduction of the EGFR targeting peptide PEG-GE11 strongly increased the silencing efficiency to below 20% luciferase activity. The luciferase expression activity in cells treated with ***1198*** siCtrl was not altered, which ruled out potential intrinsic cytotoxicity of the polyplex.

Also on Huh7 cells, ***1198*** siGFP reduced luciferase activity to below 60 % (Figure 47 B). The PEG shielded formulation was not internalized and did therefore not silence the GFP gene. The introduction of the GE11 targeting peptide only slightly improved the gene silencing activity of the polyplex.

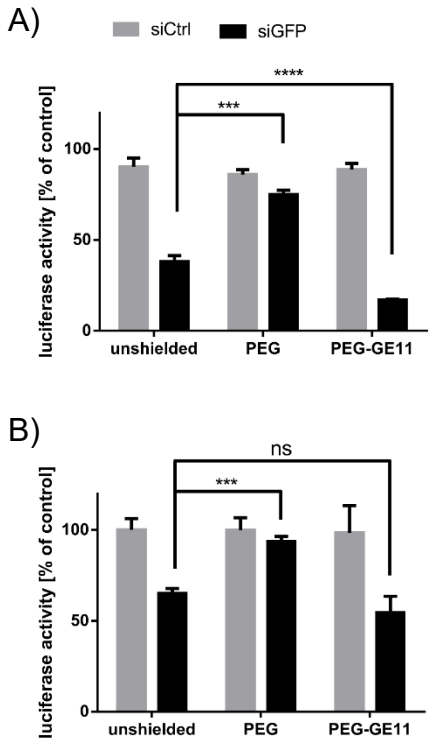

Figure 47. GFP gene silencing in A) KB-eGFP-Luc and B) Huh7-eGFPLuc cells with ***1198*** siGFP or siCtrl polyplexes. Polyplexes were formed at an N/P of 10 and either left unshielded or post-modified with 0.75 eq. of PEG or PEG-GE11. For transfections, 20 µL of polyplexes (500 ng siRNA) were incubated with the cells for 2 h in 100 µL medium. Medium was changed and the eGFP-luciferase marker gene expression was measured at 48 h after transfection using a standard luciferase assay. Marker gene activities are presented as the mean ± SD (n= 3) in % relative to untreated cells. GFP gene silencing experiments were performed by Dr. Yanfang Wang (Pharmaceutical Biotechnology, LMU München).

Theoretically, PT as a microtubule inhibitor might interfere with cellular dynamics such as nanoparticle delivery and subsequent processes in gene silencing. Therefore, a potential influence of co-incorporation of PT into the ***1198*** polyplex on GFP gene silencing was investigated (Figure 48). The concentration of PT was increased 10-fold in comparison to the cell viability determination since polyplexes were left on the cells for only 4 h. Under these short time conditions, 1 nM of PT would be unlikely to affect cellular mechanisms. Also at an elevated concentration of 10 nM, PT did not influence luciferase gene silencing activity of ***1198*** siGFP polyplexes.

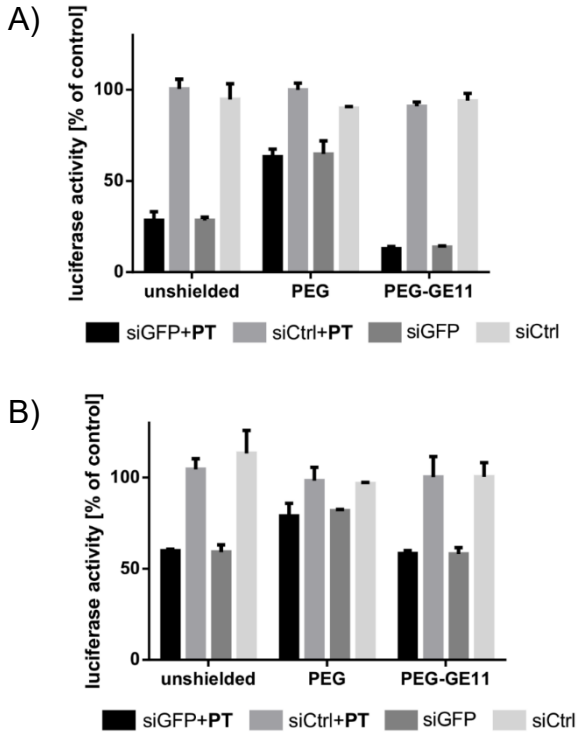

Figure 48. Influence of PT on GFP gene silencing of ***1198*** siGFP or siCtrl polyplexes on (A) KB and (B) Huh7 cells. Polyplexes were formed at an N/P of 10 and were either left unshielded or post-modified with 0.75 eq. of PEG or PEG-GE11. For transfections, 20 µL of polyplexes containing 500 ng siRNA and 0.78 ng PT were incubated on the cells in a final volume of 100 µL, which yielded concentrations of 370 nM siRNA and 10 nM PT, for 4 h. Medium was changed and the eGFP-luciferase marker gene expression was measured at 48 h after transfection using a standard luciferase assay. Marker gene activities are presented as the mean ± SD (n= 3) in % relative to untreated cells. PT does not influence the GFP gene silencing activity of ***1198*** siGFP. GFP gene silencing experiments were performed by Dr. Yanfang Wang (Pharmaceutical Biotechnology, LMU München).

3.4.5 qRT-PCR

The successful intracellular delivery of EG5 siRNA leads to the degradation of the respective EG5 mRNA. To determine the influence of ***1198*** siEG5 on EG5 expression in KB and Huh7 cells, they were incubated with siEG5 or siCtrl containing ***1198*** polyplexes for 2 h. EG5 mRNA expression was determined 22 h later by quantitative real time polymerase chain reaction (qRT-PCR).

Figure 49 A represents the relative EG5 mRNA expression of transfected KB cells. The mRNA expression was efficiently downregulated by treatment with all EG5 containing polyplexes. EGFR targeted polyplexes (siEG5 PEG-GE11) induced an almost

complete downregulation of EG5 to mRNA levels below 3 %. The respective PEGylated formulation (siEG5 PEG) still facilitated an mRNA knockdown of almost 70 %. The effect of the targeted control formulation (siCtrl PEG-GE11) was negligible. Effects of ***1198*** polyplexes on Huh7 followed a similar trend (Figure 49 B). EG5 mRNA expression was sufficiently downregulated to 24 % by transfection with siEG5 containing ***1198*** polyplexes, PEG functionalization hindered the uptake of the shielded formulations and therefore EG5 expression was higher. Targeted control formulation did not induce any unspecific effects.

The target specific gene silencing activity of EG5 siRNA could be demonstrated on the mRNA level for both cell lines. Additionally, a beneficial effect of the targeting agent PEG-GE11 could be demonstrated.

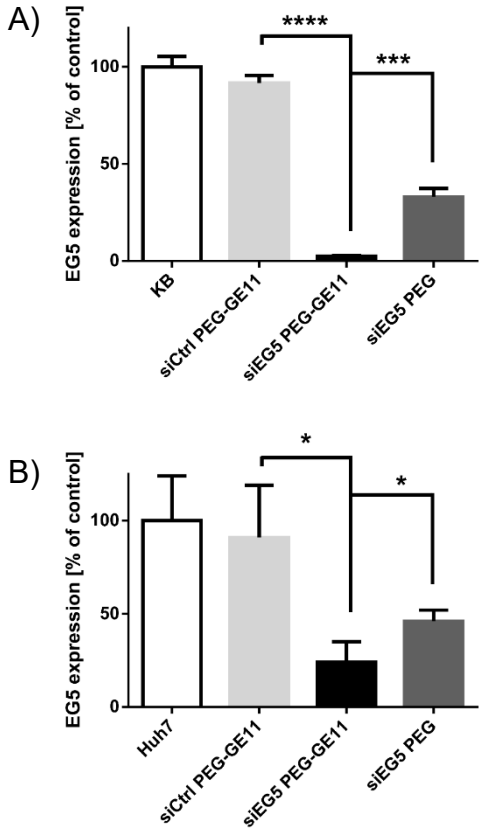

Figure 49. qRT-PCR experiments were performed to determine siEG5 gene silencing activity on the mRNA level. KB cells (A) or Huh 7 cells (B) were treated with siEG5 or siCtrl containing ***1198*** polyplex (N/P ratio of 10, 0.75 eq. of functionalization agent, 5 µg of siRNA in 2 mL growth medium per well) for 2 h. After 24 h incubation, mRNA expression levels were determined. GAPDH was used as housekeeper for all experiments. EG5 mRNA expression is depicted as the mean ± SD (n=3). QRT-PCR experiments were performed by Dr. Yanfang Wang (Pharmaceutical Biotechnology, LMU München).

3.4.6 Antitumoral efficiency

The motor protein EG5 is crucial for centrosome separation during mitosis. Thus, EG5 gene silencing induces tumor cell apoptosis through cell cycle arrest in the G2 stage.[131] The tubulin inhibitor PT binds to the β-subunit of tubulin inhibiting tubulin polymerization. The resulting G2 arrest by PT has been demonstrated on several cell lines.[8, 9, 18, 19] Huh7 and KB cells were chosen for the cytotoxicity assessment due to their overexpression of EGFR[48, 82] and their sensitivity towards siEG5 and PT (Figure 50). Different concentrations of siEG5 and PT were tested on KB (Figure 50 A) and Huh7 cells (Figure 50 B) to determine optimum doses for the combination formulation. For siEG5, 250 ng of siRNA induced potent cell killing in both cell lines. The nanomolar potency of PT on KB cells has been demonstrated before.[8] A low dose of 1 nM was chosen since higher concentrations, such as 10 nM, displayed potent antitumoral activity on their own. At the selected doses, formulated 250 ng siEG5 and 1 nM PT already showed substantial cell killing activity on their own, whilst leaving sufficient margin to elucidate a possible combination effect of both therapeutic modalities.

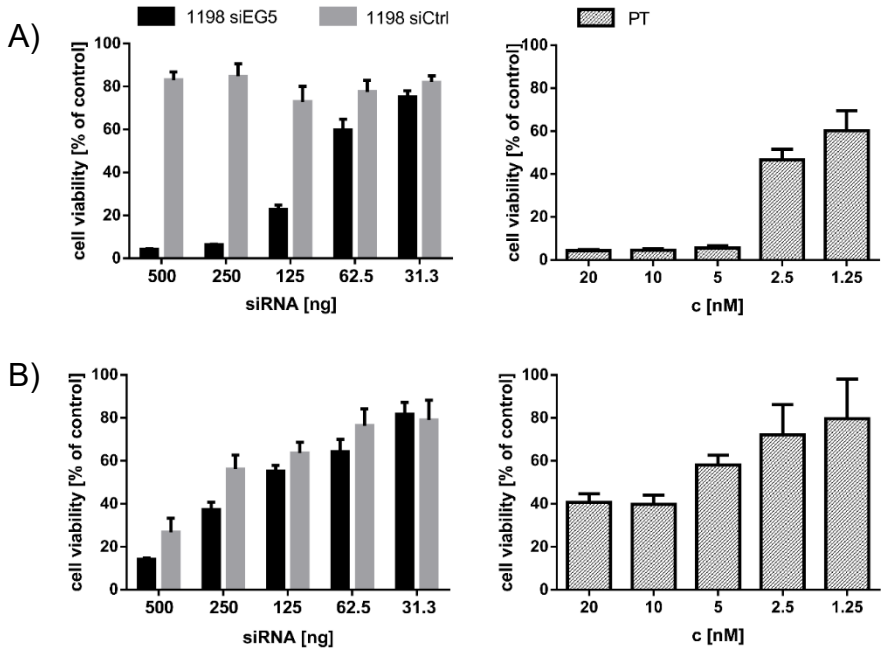

Figure 50. Cell killing of (A) KB and (B) Huh7 cells by ***1198*** siEG5 polyplexes or PT. Cells were treated with different concentrations of unshielded ***1198*** siEG5, ***1198*** siCtrl or PT. Cell viability was measured with an MTT assay after 72 h treatment and is presented as the mean ± SD (n= 5) in % relative to buffer (HBG) treated cells. Interestingly, after these long-term incubations for 3 days, in KB cells a siEG5

specific dose dependent cell killing was observed; in Huh7cells dose dependent cell killing was also observed with siCtrl formulations.

Higher doses of PT were combined with a dose of 250 ng siEG5 (see Figure 51) but led to an early onset of cytotoxicity and were therefore not applicable to investigate a combinatorial effect of the two therapeutic modalities.

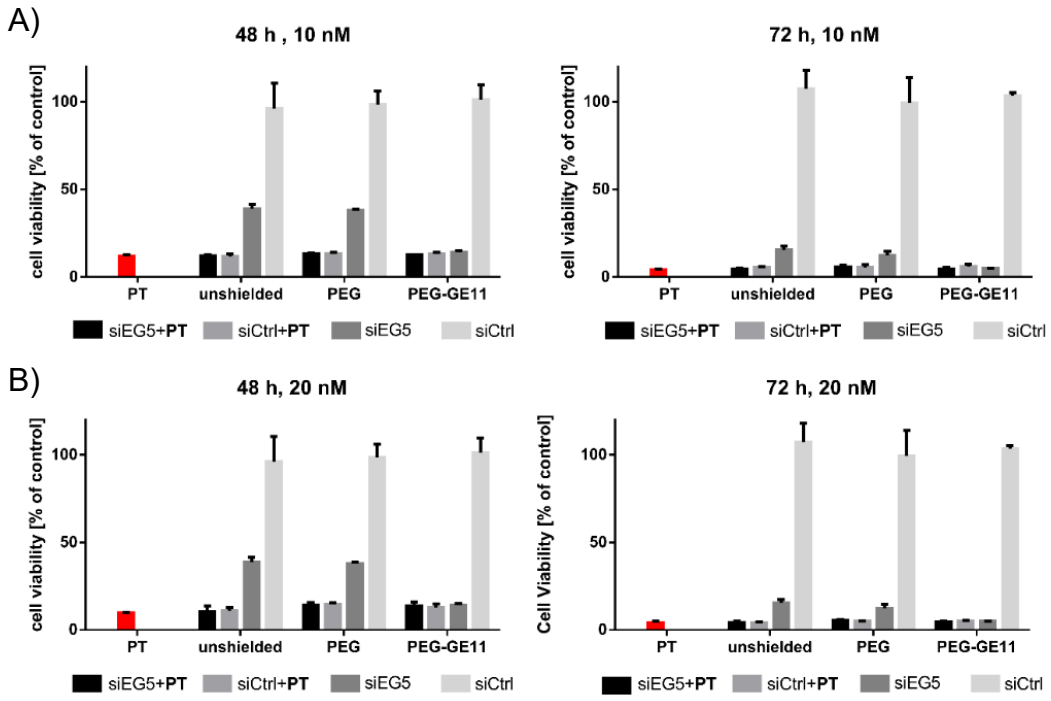

Figure 51. The antitumoral activity of free PT or polyplexes containing siEG5 and siEG5+PT was determined by MTT assay at 48 h and 72 h incubation time using (A) KB cells or (B) Huh7 cells. Polyplexes were formed in 20 µL of HBG at an N/P ratio of 10, contained 250 ng siRNA and 0.78 ng PT (10 nM per well) or 1.56 ng PT (20 nM per well) and were left unshielded or post-functionalized with 0.75 eq. of targeting ligand PEG-GE11 or shielding agent PEG. Twenty µL of polyplex solution or free PT were added to 80 µL growth medium for 48 h or 72 h. Cell viability was measured with an MTT assay after 72 h incubation time and is presented as the mean ±SD (n= 3) in % relative to buffer (HBG) treated cells. After 48 and 72 h treatment, the PT induced toxicity is too strong to determine combinatorial activity.

KB and Huh7 carcinoma cells were treated with polyplexes containing the single formulations ***1198*** siEG5 and ***1198*** siCtrl, the combination formulation ***1198*** siEG5+PT, the control formulation ***1198*** siCtrl+PT, as well as the equivalent dose of 1nM free drug

PT. Cell viability was assessed after 48 h and 72 h incubation time by MTT assay (Figure 52). On KB cells (Figure 52 A), siEG5 formulations (*third bars in each group*) displayed a time-dependent cell killing activity leading to a reduction of cell viability to less than 10 % for the last time point. The control formulation siCtrl did not induce cell killing, indicating no ***1198*** related toxicity. The functionalization of the polyplexes with PEG did not significantly alter the antitumoral activity of the siRNA polyplexes. The introduction of the targeting agent GE11, however, enhanced cell killing for ***1198*** siEG5 after 48 h incubation time. The low dose of free 1 nM PT showed only a moderate cell killing effect. In contrast, co-formulation with siCtrl (*second bar of each group*) resulted in substantial cell killing, similar or slightly less than the siEG5 groups, presumably due to an increased intracellular uptake of PT. The combination of siEG5 plus incorporated PT (*first bar of each group*) in general resulted in the best cell killing, with a combination effect demonstrated for the unshielded and PEGylated groups.

Treatment with siEG5 containing polyplexes also facilitated time-dependent killing of Huh7 hepatocarcinoma cells (Figure 52 B). The polyplex functionalization with PEG decreased levels of cell killing upon 48 h treatment, whereas the targeting peptide agent PEG-GE11 strongly increased the antitumoral potential of the siEG5 containing groups. Upon 72 h treatment, cell viability levels were reduced to below 10 %. Interestingly however, at the longest incubation time point all groups post-functionalized with PEG-GE11 were cytotoxic, even the siCtrl without PT group.

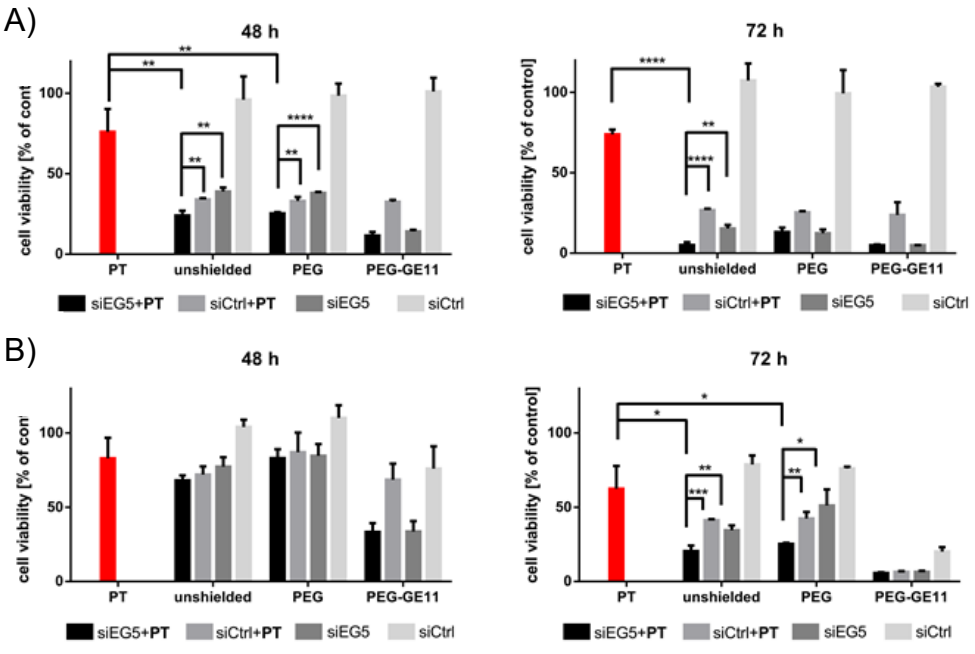

Figure 52. The antitumoral activity of free PT or polyplexes containing siEG5 and siEG5+PT was determined by MTT assay at 48 h and 72 h incubation time using (A) KB cells or (B) Huh7 cells. Polyplexes were formed in HBG at an N/P ratio of 10, and left unshielded or post-functionalized with 0.75 eq. of targeting ligand PEG-GE11 or shielding agent PEG. Cells were seeded in 96-well plates in 100 µL medium. After a medium change (80 µL fresh medium), 20 µL of polyplex solution containing 250 ng siRNA and 0.078 ng PT were added to the cells, which resulted in a final concentration of 185 nM siRNA and 1 nM PT per well. Cells were treated with polyplexes or free PT for 48 h or 72 h. Cell viability was measured with an MTT assay after 72 h incubation time and is presented as the mean ±SD (n= 3) in % relative to buffer (HBG) treated cells.

The unexpected long-term toxicity of the PEG-GE11 modified ***1198*** polyplexes on Huh7 cells was further investigated. Huh7 cells were treated with lipo-oligomer ***1198*** and the conjugates PEG ***1198*** or PEG-GE11 ***1198*** without siRNA for 72 h (Figure 53 A). Only the PEG-GE11 ***1198*** conjugate group induced a mild cytotoxicity. The functionalization agents PEG and PEG-GE11 alone did not reduce cell viability (Figure 53 B). Thus, improved intracellular uptake of the lipo-oligomer ***1198*** was suspected to cause the time-dependent toxic effects. Since the modification of the lipo-oligomer ***1198*** or its polyplexes with the GE11 targeting construct induced an increased intracellular delivery of ***1198***, the EGFR targeted groups displayed the highest cytotoxic effects. After 72 h incubation time, this effect was most obvious as large quantities of oligomer were internalized. Figure 51 supports the hypothesis, that higher intracellular levels of ***1198*** cause cell death of Huh7 cells. The dose titration showed that with higher amounts of siRNA, and hence also higher levels of ***1198,*** cell viability decreased in a dose-dependent manner in this particular Huh7 cancer cell line but not in KB cells.

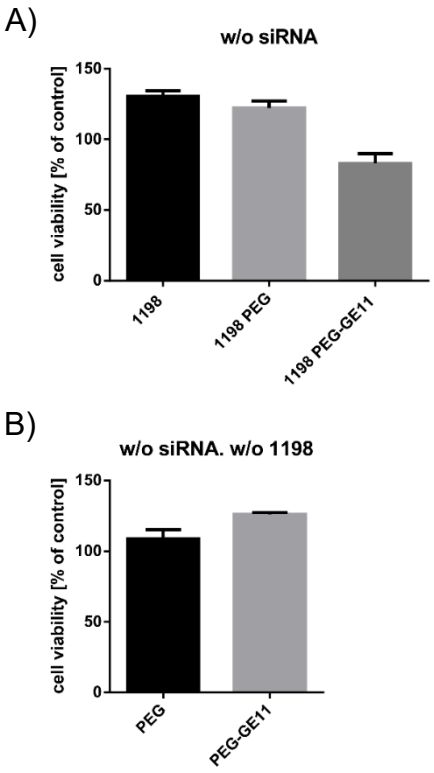

Figure 53. The cytotoxicity of (A) lipo-oligomer ***1198***, lipo-oligomer ***1198*** DBCO-PEG conjugate or ***1198*** DBCO-PEG-GE11 conjugate, and alternatively (B) DBCO-PEG and DBCO-PEG-GE11 on Huh7 cells as determined by MTT assay. Amounts of ***1198*** and functionalization agents DBCO-PEG and DBCO-PEG-GE11 were equivalent to those in the corresponding siRNA polyplexes. Cells were treated for 72 h, cell viability is shown as the mean ± SD (n=3) relative to HBG treated controls. Only ***1198*** DBCO-PEG-GE11 conjugate induced a mild toxicity. The conjugate of the lipo-oligomer with the GE11 targeting construct presumably induces an increased uptake of the lipo-oligomer which induces cytotoxic effects in Huh7 cells. Cytotoxicity was assessed by Dr. Wei Zhang (Pharmaceutical Biotechnology, LMU München).

The cytotoxicity of ***1198*** siRNA polyplexes was compared to the respective pDNA formulations (Figure 54). Neither ***1198*** siCtrl nor the respective pDNA formulation induced cytotoxicity. On Huh7 cells however, polyplexes of the ***1198*** PEG-GE11 were toxic. Even though siRNA polyplexes led to an overall higher cell killing, also the pDNA polyplex induced cytotoxicity. In pDNA polyplexes, the nucleic acid cargo is more firmly compacted into the nanoparticle than in siRNA formulation. Thus, we speculate that less oligomer ***1198*** might be released upon cellular pDNA polyplex internalization, as a possible explanation for the differing cytotoxicity.

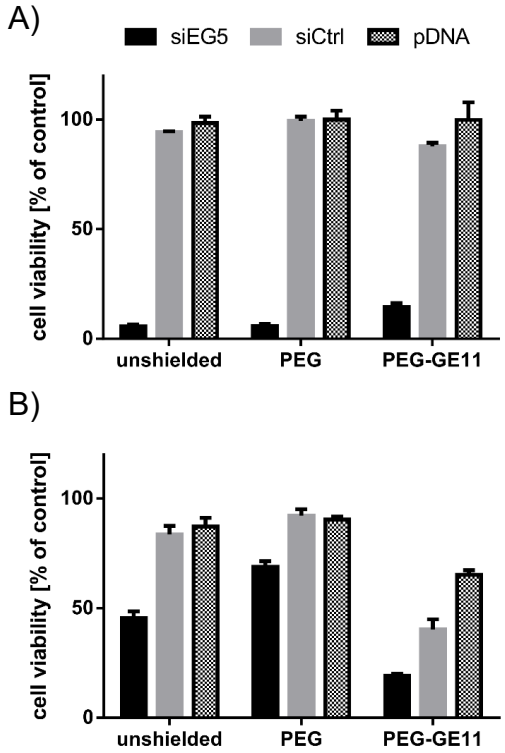

Figure 54. The cytotoxicity of ***1198*** siRNA polyplexes was compared to the respective pDNA formulations. Polyplexes were formed at N/P 10 and contained 500 ng siRNA or 200 ng pDNA. KB cells (A) or Huh 7 cells (B) were treated with 20 µL of polyplex solution for 72 h. Cell viability was determined by MTT assay and is depicted as the mean ± SD. On KB cells, ***1198*** siEG5 displayed efficient antitumoral activity. Neither ***1198*** siCtrl nor the respective pDNA formulation induced cytotoxicity. On Huh7 cells however, polyplexes of the ***1198*** PEG-GE11 were toxic. Even though siRNA polyplexes led to an overall higher cell killing, also the pDNA polyplex induced cytotoxicity. In pDNA polyplexes, the nucleic acid cargo is more firmly compacted into the nanoparticle than in siRNA formulation. Thus, we speculate that less oligomer ***1198*** might be released upon cellular pDNA polyplex internalization, as a possible explanation for the differing cytotoxicity. Cytotoxicity was assessed by Dr. Wei Zhang (Pharmaceutical Biotechnology, LMU München).

A time-dependent cell killing by PT effect was also found for Huh7 cells. Also here, polyplex formulation into ***1198*** siCtrl+PT increased the antitumoral potency of PT for the unshielded, PEGylated and EGFR targeted group. The combination activity of siEG5 and PT is less pronounced, a beneficial combination effect is only visible after 72 h treatment in the unshielded and PEGylated group.

In summary, siEG5 and PT upon lipopolyplex formulation displayed antitumoral potency on KB and Huh7 cells. A combination effect of both therapeutics could be demonstrated. The introduction of the targeting-peptide GE11 increased antitumoral efficacy, presumably by facilitating an increased intracellular delivery of both compounds. On Huh7 cells, the functionalization with the GE11 targeting peptide induced an additional cytotoxic effect, most likely based on enhanced cell-associated oligomer dose.

4 Discussion

4.1 Sequence-defined oligoamide drug conjugates of pretubulysin and methotrexate for folate receptor targeted cancer therapy

This chapter was partly adapted from:

Truebenbach, I.; Gorges, J.; Kuhn, J.; Kern, S.; Baratti, E.; Kazmaier, U.; Wagner, E.; Lächelt, U., Sequence-Defined Oligoamide Drug Conjugates of Pretubulysin and Methotrexate for Folate Receptor Targeted Cancer Therapy. Macromol Biosci 2017, 17 (10).

In the first chapter, several FolA and MTX containing oligoamides for potential conjugation with drug payloads were synthesized and differences in structure-activity properties concerning target enzyme DHFR inhibition, FR-specific cellular uptake and cytotoxicity, were investigated. Interestingly, the studies on adherent human KB carcinoma cells and murine leukemia L1210 suspension cells resulted in identification of diverging most promising compounds. In KB cells, the 4-arm E4-MTX with a tetravalent tetraglutamyl-MTX ligand exhibited highest cytotoxic activity in MTT assays, whereas 2-arm E4-MTX with a divalent tetraglutamyl-MTX ligand was most promising in L1210 cells. Potency of the latter directly correlated with the results of the DHFR activity assay and cellular uptake experiments. Notably, cellular uptake of all oligoamides could be blocked by FolA competition, which supports the FR-specific endocytosis pathway. The FolA containing analogues did not mediate distinct effects on cell viability, despite a remarkably high cellular uptake. The cysteine containing oligoamides were used for conjugation to a PT hydrazide derivative with an activated thiol and beneficial combined potency was observed with 4-arm E4-MTX-H-PT in KB tumor bearing mice and 2-arm E4-MTX-H-PT in L1210 cells. An *in vivo* experiment in KB cells showed a growth retarding effect of the 4-arm E4-MTX-H-PT conjugate and the native PT-COOH when administered intratumorally.

4.2 Combined antitumoral effects of pretubulysin and methotrexate

This chapter was adapted from:

Kern, S.; Truebenbach, I.; Höhn, M.; Gorges, J.; Kazmaier, U.; Zahler, S.; Vollmar, A.; Wagner, E., Combined Antitumoral Effects of Pretubulysin and Methotrexate. Pharmacology Res Perspect 2019, e00460.

Based on the previous chapter examining conjugates of PT with MTX-containing oligomers[17], the drug combination was further characterized. The effects of the free drugs PT, MTX and the combination PT+MTX were assessed in terms of cytotoxicity in MTT assays and apoptosis analyses. Cell cycle changes as well as differences in cytoskeleton architecture upon drug treatment were evaluated.

The *in vitro* cytotoxicity studies demonstrated the favorable combination effect of PT and MTX on both cell lines at different drug ratios. The only moderate cytotoxic effects of MTX on KB cells are not surprising, as chemoresistance of KB cells to MTX has previously been reported.[132, 133]

Regarding the effects of the drugs on the cell cycle, our experiments confirm the expected G2/M arrest of PT treated cells[9, 10, 19] and G1/S arrest by MTX.[134, 135] Remarkably, G2/M arrest mediated by PT+MTX combination went far beyond the effect of PT alone. One explanation for the predominance of the PT effect on the cell cycle might be its more direct way of interference. PT binds to tubulin and thereby directly affects the working of the cell division cycle. MTX on the other hand influences the G1/S stage of the cell cycle more indirectly. MTX is essentially a prodrug. In order to bind its target enzyme DHFR, MTX must be polyglutamylated intracellularly. After polyglutamylation, MTX inhibits the synthesis of the co-factor tetrahydrofolate and thus, the C1 metabolism. As a result, no nucleotides are synthesized which would be essential for DNA synthesis. Furthermore, PT does not have to be converted into its active form before carrying out its toxic effect. The earlier onset in toxicity leads to a G2/M arrest, and arrested cells cannot in turn be affected by MTX anymore.

With regard to drug-induced apoptotic events in L1210 or KB cells, treatment with PT or MTX alone resulted in a steady increase of apoptotic cells, which is in accordance

with previous work.[9, 10, 136, 137] Yet, apoptosis could not be further enhanced by combining both agents.

Previous studies show PT induced depolymerization of microtubules in different cell lines[9, 19], which could be confirmed for L1210 and KB cells using CLSM. Encouragingly, the combination was equally potent as PT alone. Furthermore, we could show the impairment of the cellular actin skeleton mediated by MTX. This is in line with various reports about MTX influence on the actin cytoskeleton.[138, 139] Furthermore, levels and distribution of globular actin (G-actin) and/or filamentous actin (F actin) and total actin were changed upon MTX treatment. Mazur et al. postulate that polyglutamylated MTX inhibits specific enzymes, resulting in increased levels of adenosine.[140] These have in turn been shown to inhibit actin polymerization.[139, 141] It has been demonstrated previously that microtubule inhibitors can influence the actin cytoskeleton.[142-144] Treatment with microtubule depolymerizing drugs increases contractility in fibroblasts. Additionally, rapid restoration of actin-containing stress fibers is induced, even after their previous disruption.[142] The authors offer several possible explanations. Firstly, they postulate that cellular forces are redistributed due to the drug-induced imbalance where the pushing force of microtubules is decreased. This might lead to increased tension and could cause actin to become bundled in stress fibers. Secondly, microtubules may modulate and exert inhibitory control over actin architecture. Microtubules can weaken contractility and organization of actin. Microtubule disruption releases actin from inhibition.[142] As to a PT+MTX combination effect, one may hypothesize that actin stress fibers might be required in the cellular survival response upon microtubule inhibition by PT. MTX treatment has been shown to prevent such actin stress fibers. Thus, in the PT+MTX combination, one can assume that the cell rescue effect by actin is prevented by MTX, leading to a combined loss in microtubule as well as actin cytoskeleton function and thus enhanced cell killing. In addition to the qualitative analysis of CLSM, more quantitative experiments will be required to further analyze the underlying molecular mechanisms.

To investigate whether the combination effect could be translated to *in vivo* experiments, the drug combination PT+MTX was tested in both the L1210 and KB tumor models.[145] In contrast to cell culture cytotoxicity on L1210 cells, a lack of antitumoral activity of MTX was observed *in vivo* at the applied dosage of 5 mg/kg. An acquired chemoresistance against MTX could be excluded, since the MTX treated

tumors are still MTX sensitive in cell culture.[8] PT on the other hand exhibited a clear antitumoral effect on L1210 tumors *in vivo* at 2 mg/kg. The favorable PT effect was further enhanced by co-administration with a low dose of 5 mg/kg MTX which resulted in a significantly retarded tumor growth in the combination group. Considering the lack of antitumoral effects, the boosting effect of low dose MTX is remarkable.

The first chapter of the thesis already demonstrated the antitumoral effect of PT in the KB human cervix carcinoma tumor model. Kern et al. confirmed the antitumoral activity of 2 mg/kg PT, while MTX only slightly inhibited KB tumor growth. This is consistent with the known *in vitro* chemoresistance of KB cells to MTX and *in vivo* studies.[54] Importantly, also in this tumor model, the co-administration of 5 mg/kg MTX resulted in a significantly enhanced antitumoral effect of PT+MTX over PT alone. Very similar findings were made in a subcutaneous Huh7 hepatocellular model in NMRI-nude mice, with MTX showing negligible effects, whereas both PT containing groups exhibited significantly inhibited tumor growth and survival of all animals for 22 days for PT vs. 25 days for PT+MTX.[145]

The combination of MTX with Vinca alkaloids as another class of tubulin binders has been demonstrated as favourable for cancer therapy both in a leukemia mouse model and in the clinics.[33, 146] Thus, the combination of the novel potent tubulin inhibitor PT with MTX might present a new interesting clinical direction in cancer chemotherapy.

4.3 Combination chemotherapy of L1210 tumors in mice with pretubulysin and methotrexate lipo-oligomer nanoparticles

This chapter was adapted from:

Truebenbach, I.; Kern, S.; Loy, D. M.; Höhn, M.; Gorges, J.; Kazmaier, U.; Wagner, E., Combination Chemotherapy of L1210 Tumors in Mice with Pretubulysin and Methotrexate Lipo-Oligomer Nanoparticles. Mol Pharm 2019, 16 (6), 2405-2417*. Copyright (2019) American Chemical Society.*

In the next study, the drug combination PT+MTX was co-incorporated into a nanoparticulate delivery system to enable the controlled co-delivery of both compounds to the tumor site. Polyelectrolyte complexes were formed through electrostatic interactions between the anionic MTX and cationizable ***454***, PT was co-incorporated by different hydrophobic and hydrophilic interactions. Particle sizes ranged from 20 nm to 175 nm which rendered nanoparticles applicable for intravenous delivery into L1210 leukemia tumors *in vivo*. Drug incorporation into PECs was determined to be slightly higher for MTX than for PT. Electrostatic interactions between ***454*** and MTX seemed to facilitate higher levels of drug incorporation. In the next step, stability of nanomicelles was investigated upon exposure to physiological NaCl solution and FBS. Upon incubation with FBS containing buffer, PT was more stably incorporated into the nanoparticles. The anionic nature of MTX might explain the lower stability of MTX incorporation since anionic albumin molecules in FBS might replace MTX. The overall stability of the delivery system in FBS containing media was, unfortunately, rather low.

The beneficial combination effect of PT+MTX, which is described in the previous chapter of this thesis, could be further improved both *in vitro* and *in vivo* by incorporating PT+MTX into nanomicellar PECs. While ***454*** incorporation strongly increased the *in vitro* antitumoral effects of PT+MTX and PT on L1210 cells and KB cells alike, nanomicellar incorporation did not improve antitumoral properties of MTX. While MTX uptake via the RFC is well characterized, nothing is known about the cellular uptake route of PT. Nanomicellar formulation might facilitate an increased uptake of larger quantities of PT.[118-120] *In vivo*, the formulation of PT+MTX into ***454***

PT+MTX PECs slowed down tumor growth. Furthermore, mice of the ***454*** PT+MTX group demonstrated a statistically significant longer survival. The mechanism behind the favorable effect of drug nanoformulation on tumor size and mouse survival is currently still unclear. Nanoparticle based combination therapy could unify the different pharmacological profiles of PT+MTX and enable their joint delivery.[57] An increase in drug accumulation at the tumor site via the EPR effect[65] is rather unlikely due to lack of surface shielding of the current nanomicelle PECs. Another explanation could be a prolonged systemic availability of the drugs by the nanoformulation.[147-149] To clarify the mechanism, future efforts will be required to study the pharmacokinetics of PT in the current or further stabilized and shielded systems. One obvious opportunity to further optimize the PEC system in terms of *in vivo* antitumoral potency will be improved stabilization through strengthened electrostatic interactions, such as by replacing MTX by polyglutamylated analogs or including polyanionic siRNA.[48] Furthermore, drug incorporation and stability might be increased by including further hydrophobic stabilization domains, like extended tyrosine motifs.[101] A further option presents the provision of ***454*** PT+MTX nanomicelle PECs with targeting ligands[150] or shielding agents.[64, 151, 152] For example, Klein et al.[49] have demonstrated that an introduction of a folate ligand plus PEG shield can substantially improve the biodistribution and tumor targeting of a siRNA lipo-polyplex.

4.4 Co-delivery of pretubulysin and siEG5 to EGFR overexpressing carcinoma cells

Building on the work of Klein et al.[49], PT was combined with the potent antitumoral siEG5. To enable a joint intracellular delivery of both compounds, a suitable co-delivery system was developed. SiEG5 and azide bearing lipo-oligomer ***1198*** formed polyplexes by electrostatic interactions, PT was co-incorporated. While the stability of ***454*** PT+MTX PECs upon exposure to FBS was problematic, the polyanionic nature of siEG5 was thought to yield a more stable co-delivery vehicle. The polyplexes were functionalized further by click chemistry to introduce a PEG shielding domain and the GE11 peptide as an EGFR targeting moiety. While the PEG shielding domain successfully reduced particle surface charge as well as cellular internalization, the GE11 peptide facilitated higher cellular internalization of polyplexes into EGFR overexpressing KB and Huh7 carcinoma cells. The activity of both antitumoral components was demonstrated separately and in combination. While siEG5 on its own mediated EG5 gene silencing and cell killing, it increased the antitumoral efficacy of the co-delivered microtubule inhibitor PT, and a combination effect could be shown on both investigated carcinoma cell lines.

Klein et al. successfully combined FR-targeted, siEG5 containing polyplexes and free, unincorporated PT to treat L1210 tumor bearing mice resulting in significant tumor growth inhibition and prolonged survival.[49] Therefore, the co-delivery system based on ***1198*** and the GE11-targeting peptide was tested for an *in vivo* antitumoral effect in a subcutaneous Huh7 model, against the targeted ***1198*** siEG5 and ***1198*** siCtrl and free PT.[145] Tumor growth could be stopped throughout treatments in all PT containing groups. Nevertheless, differences in tumor sizes were less pronounced within these groups. The important effect of PT on the Huh7 tumor model *in vivo* has previously been demonstrated.[19] While treatment of L1210 tumors with siEG5 successfully slowed down tumor growth, this effect could not be reproduced for Huh7 tumors. Further investigations in the *in vivo* co-delivery of PT and siEG5 to other tumor models are necessary to evaluate the full potential of the promising co-delivery system.

A surprising GE11-mediated toxic effect on Huh7 cells was demonstrated. This effect seemed to be related to a higher intracellular concentration of the cationizable lipo-oligomer ***1198*** in the targeted group. Although cationic polymers, like poly

ethyleneimine (PEI), enable the efficient intracellular delivery of their payload, they often show toxicity in a time- and concentration-dependent manner.[126, 153] Additionally, fatty acid containing carrier systems can have membrane lytic activity. Their cytotoxicity can be reduced by introducing biodegradable motifs which facilitate degradation of the toxic material upon successful entry into the cytosol.[100] Reinhard et al. introduced enzymatic cleavage sides into the oligomers via SPS, which reduced the cytotoxic activity of siRNA containing polyplexes, whilst enabling sufficient gene silencing ability.[154] The introduction of an enzymatic cleavage site into co-delivery system might negate the oligomer related cytotoxic effects seen for the GE11-targeted group and help better characterize the combination effect of PT and siEG5 on this cell line.

5 Summary

Combinations of drugs with different intracellular targets are routinely used in tumor chemotherapy due to their increased efficiency and reduced risk for chemoresistance. In this thesis, the novel tubulin binding drug pretubulysin (PT) was investigated in combination with two different therapeutic modalities. To enable tumor-specific delivery, the drugs were co-incorporated in delivery systems.

In the first chapter, folic acid (FolA) and methotrexate (MTX) containing oligoamides were synthesized and differences in structure-activity properties concerning dihydrofolate reductase (DHFR) inhibition, folic acid receptor (FR)-specific cellular uptake and cytotoxicity, were investigated. In KB cells, the 4-arm E4-MTX exhibited highest cytotoxic activity, whereas the 2-arm E4-MTX was most promising in L1210 cells. Potency of the latter directly correlated with the results of the DHFR activity assay and cellular uptake experiments. Oligoamines were conjugated to a PT hydrazide derivative. A beneficial combined potency was observed with 4-arm E4-MTX-H-PT in KB cells and 2-arm E4-MTX-H-PT in L1210 cells. An *in vivo* experiment in KB tumors showed a growth retarding effect of the 4-arm E4-MTX-H-PT conjugate and the native PT-COOH when administered intratumorally.

In the second part of the study, the free drugs PT and MTX were further evaluated for a combination effect on KB and L1210 cells. While both PT and MTX alone showed a potent antitumoral effect on L1210 cells *in vitro*, the drug combination PT+MTX exceeded the effects of single drugs. A slight combination effect was also visible on L1210 cells. Cell cycle analysis confirmed the expected arrest in G1/S for MTX treatment and G2/M for PT. In both cell lines, the PT+MTX combination induced a stronger G2/M arrest than free PT. The combination PT+MTX did not increase rates of apoptotic L1210 and KB cells compared to the single drug applications. CLSM images show the microtubule disruption and nuclear fragmentation associated with PT treatment on both cell lines. MTX treatment seemed to change F-actin structure. PT+MTX combined the effects of both drugs on tubulin and actin architecture.

In the third chapter, the previously investigated combination PT+MTX was co-formulated into nanoparticles. Polyelectrolyte complexes (PECs) were formed from the cationizable lipo-oligomer ***454*** and the anionic drug MTX, PT was co-incorporated via

different hydrophobic and hydrophilic interactions. Particle sizes were determined to be favorable for passive tumor targeting. Both drugs were co-incorporated to a high extent. Nanoparticles were stable in up to 20 % fetal bovine serum (FBS) containing buffer and physiological NaCl solution. Cellular internalization of ***454*** PT+MTX into L1210 and KB cells was confirmed by confocal laser scanning microscopy (CLSM). The incorporation of PT+MTX into the delivery systems strongly increased the antitumoral efficiency of the free drug combination. Systemic treatment of NMRI nun/nu mice bearing subcutaneous L1210 tumors with ***454*** PT+MTX resulted in a more efficient delay in tumor growth and a significant increase in mice survival compared to the free drug combination PT+MTX.

In the fourth chapter, small interfering RNA (siRNA) against the kinesin related mRNA eglin 5 gene (siEG5) and the microtubule inhibitor PT were co-formulated into polyplexes using azide-containing lipo-oligomer ***1198***. Nanoparticle surfaces were further modified by click reaction using shielding agent DBCO-PEG or EGFR targeting peptide GE11 (DBCO-PEG-GE11). Polyplexes displayed efficient payload incorporation and homogenous particle sizes of 200 nm. The biological effects of the unmodified and surface-functionalized polyplexes were investigated. The successful GE11-mediated intracellular delivery of siRNA into the EGFR overexpressing KB and Huh7 cell lines facilitated potent silencing of an EGFP-luciferase reporter gene by GFP siRNA. Specific downregulation of EG5 mRNA by siEG5 resulted in the expected antitumoral activity. The combination formulation ***1198*** siEG5+PT provided superior antitumoral activity over free PT and ***1198*** siEG5.

Overall, two pretubulysin-based combination chemotherapies were evaluated in this thesis. Both PT+MTX and PT+siEG5 were co-incorporated into delivery systems and investigated for combination benefits *in vitro* and *in vivo*. All dual delivery vehicles showed beneficial combination effects in different *in vitro* and *in vivo* settings.

6 Appendix

6.1 Abbreviations

AbDil	Antibody dilution
ACN	Acetonitrile
ATP	Adenosine Triphosphate
BSA	Bovine serum albumin
CLSM	Confocal laser scanning microscopy
Cy5	Cyanine 5
DAPI	4′,6-diamidino-2-phenylindole
DBCO	Dibenzo cycloocytne
DCM	Dichloromethane
DDS	Drug delivery system
DHFR	Dihydrofolate reductase
DIPEA	*N,N*-Diisopropylethylamine
DLS	Dynamic light scattering
DMEM	Dulbecco's modified Eagle's medium
DMF	*N,N*-Dimethylformamide
DMSO	Dimethyl sulfoxide
DNA	Desoxyribonucleic acid
DTT	Dithriothreitol
EDC	1-Ethyl-3-(3-dimethylaminopropyl)carbodiimide
EDT	1,2-Ethandithiol
EDTA	Ethylenediaminetetraacetic acid
EG5	Eglin 5
EGF	Epidermal growth factor
EGFR	Epidermal growth factor receptor
EPR	Enhanced permeation and retention
FBS	Fetal bovine serum
FITC	Fluorescein isothiocyanate
Fmoc	Fluorenylmethoxycarbonyl protecting group
FolA	Folic acid

FR	Folate receptor
G1	Gap phase 1
G2	Gap phase 2
GFP	Green fluorescent protein
GSH	Glutathion
HCl	Hydrochloric acid
HBG	Hepes-buffered glucose
HBTU	2-(1H-benzotriazole-1-yl)-1,1,3,3-tetramethyluronium hexafluorophosphate
HEPES	*N*-(2-hydroxethyl) piperazine-N‘-(2-ethansulfonic acid)
HOBt	1-Hydroxybenzotriazole
IC 50	Half maximal inhibitory concentration
kDa	Kilodalton
MALDI-MS	Matrix-assisted laser desorption/ionization mass spectrometry
mM	Millimolar
mRNA	Messenger RNA
MTBE	Methyl *tert*-butyl ether
MTT	3-(4,5-dimethylthiazol-2-yl)-2,5-diphenyltetrazolium bromide
MTX	Methotrexate
MWCO	Molecular weight cut-off
$NaBH_4$	Sodium borohydride
NaOH	Sodium hydroxide
NADPH	Nicotinamide adenine dinucleotide phosphate
N/P	Nitrogen to phosphate ratio
NHS	*N*-Hydroxysuccinimide
nm	Nanometer
NMP	*N*-Methyl-2-pyrrolidone
NMR	Nuclear magnetic resonance
OAA	Oligoaminoamide
OleA	Oleic acid
PBS	Phosphate buffered saline
PDI	Polydispersity index
PEC	Polyelectrolyte complex
PEI	Polyethylenimine

PEG	Polyethylene glycol
PI	Propidium iodide
PIPES	Piperazine-N,N'-bis(2-ethanesulfonic acid)
Poly (I:C)	Polyinosinic:polycytidylic acid
PS	Phosphatidyl serine
PT	Pretubulysin
PyBOP	Benzotriazol-1-yloxy-tripyrrolidinophosphonium hexafluorophosphate
RFC	Reduced folate carrier
RLU	Relative light units
RNA	Ribonucleic acid
RNAi	RNA interference
RP-HPLC	Reversed-phase high-performance liquid chromatography
RPMI	Rosewell Park Memorial Institute
RT	Room temperature
S	Synthesis phase
SDS	Sodium dodecyl sulfate
SEC	Size-exclusion chromatography
siRNA	Small interfering RNA
SMDC	Small molecule drug conjugate
SPAAC	Strain-promoted alkyne-azide cycloaddition
SPS	Solid-phase synthesis
Stp	Succinoyl-tetraethylene pentamine
STOTDA	*N*-Fmoc-*N*″-succinyl-4,7,10-trioxa-1,13-tridecanediamine
TBE	Tris-boric acid-EDTA buffer
TBS	Tris-buffered saline
TCEP	Tris(2-carboxyethyl)phosphine
TFA	Trifluoroacetic acid
TEM	Transmission electron microscopy
TIS	Triisopropylsilane
qRT-PCR	Quantitative real time polymerase chain reaction

6.2 Analytical data

6.2.1 NMR spectra of PT derivatives

6.2.1.1 Pretubulysin hydrazide (PT-H-SS-Py, 2)

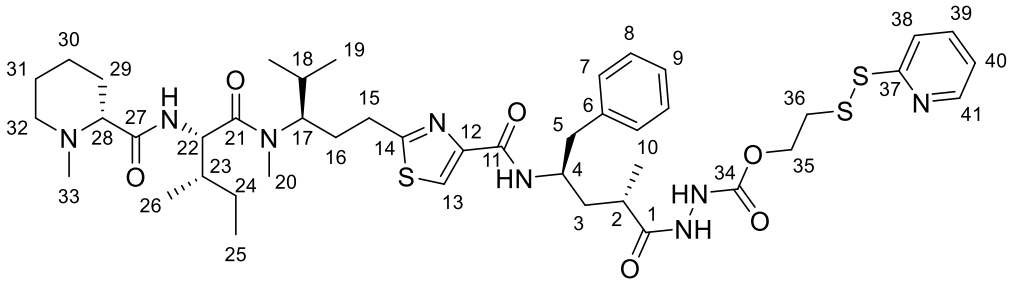

^{1}H-NMR (500 MHz, $CDCl_3$): δ = 0.77 (d, *J* = 6.6 Hz, 3 H, 19-H), 0.88 (t, *J* = 7.3 Hz, 3 H, 25-H), 0.96 (m, 6 H, 19-H', 26-H), 1.10 (d, *J* = 6.6 Hz, 3 H, 10-H), 1.17 (m, 2 H, 24-H_a, 30-H_a), 1.36 (m, 1 H, 29-H_a), 1.59 (m, 6 H, 3-H_a, 18-H, 24-H_b, 30-H_b, 31-H), 1.84 (m, 3 H, 16-H_a, 23-H, 29-H_b), 2.00 (m, 2 H, 3-H_b, 32-H_a), 2.11 (m, 1 H, 16-H_b), 2.22 (s, 3 H, 33-H), 2.39 (m, 1 H, 2-H), 2.49 (dd, *J* = 11.0 Hz, 3.2 Hz, 1 H, 28-H), 2.88 (m, 5 H, 5-H, 15-H, 32-H_b), 3.01 (s, 3 H, 20-H), 3.05 (m, 2 H, 36-H), 4.38 (m, 3 H, 17-H, 35-H), 4.72 (m, 1 H, 4-H), 4.77 (dd, *J* = 9.3 Hz, 8.4 Hz, 1 H, 22-H), 6.85 (s, 1 H, N-H), 7.07 (m, 2 H, 40-H, N-H), 7.21 (m, 5 H, 7-H, 8-H, 9-H), 7.56 (d, *J* = 9.5 Hz, 1 H, N-H), 7.67 (m, 2 H, 38-H, 39-H), 7.91 (s, 1 H, 13-H), 8.45 (m, 1 H, 41-H), 9.83 (s, 1 H, N-H).

^{13}C-NMR (125 MHz, $CDCl_3$): δ = 10.9 (C-25), 15.9 (C-26), 17.7 (C-10), 19.6 (C-19), 20.1 (C-19'), 23.2 (C-30), 24.6 (C-24), 25.0 (C-31), 29.3 (C-16), 29.7 (C-20), 30.0 (C-15), 30.1 (C-18), 30.4 (C-29), 35.1 (C-2), 37.1 (C-23), 37.3 (C-3), 37.6 (C-36), 41.6 (C-5), 44.8 (C-33), 48.6 (C-4), 53.0 (C-22), 55.3 (C-32), 58.5 (C-17), 63.5 (C-35), 69.6 (C-28), 119.7 (C-38), 120.8 (C-40), 123.2 (C-13), 126.6 (C-9), 128.5 (C-8), 129.3 (C-7), 137.0 (C-39), 137.2 (C-6), 148.9 (C-41), 149.6 (C-12), 155.9 (C-34), 159.7 (C-37), 162.2 (C-11), 170.1 (C-14), 173.3 (C-21), 174.3 (C-27), 176.2 (C-1).

^{1}H-NMR spectrum

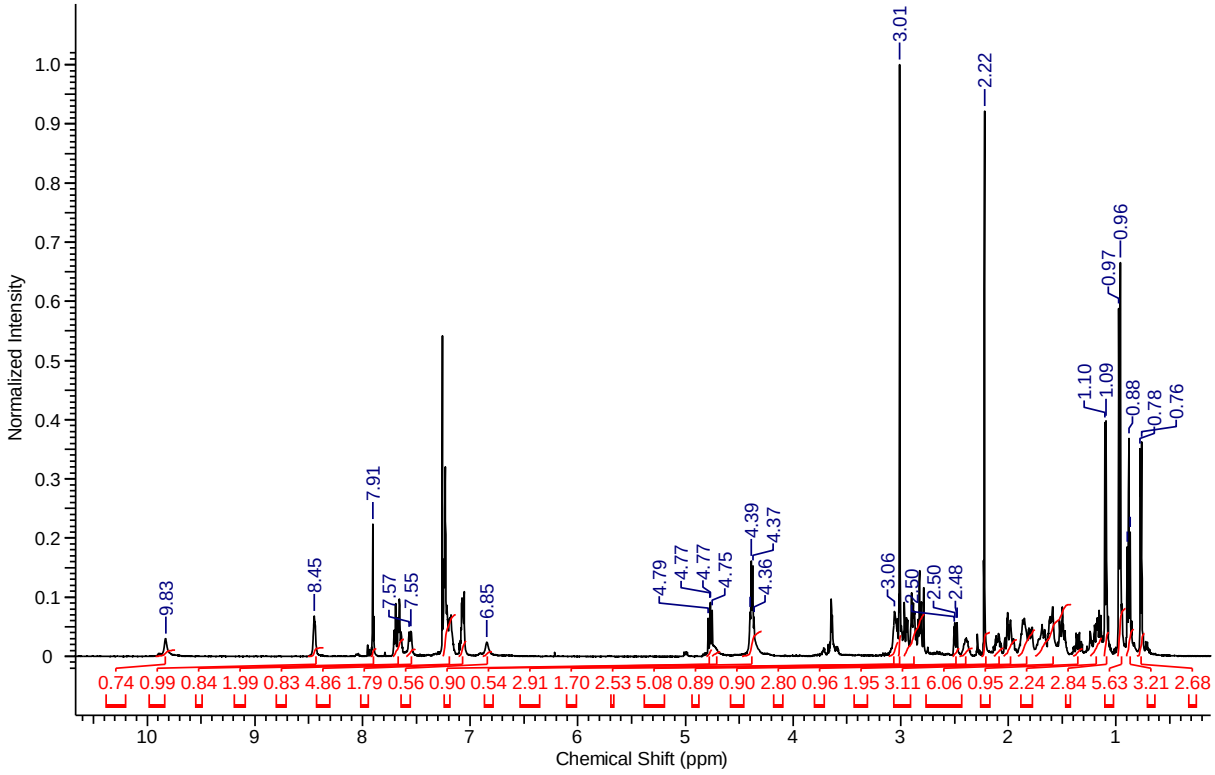

^{13}C-NMR spectrum

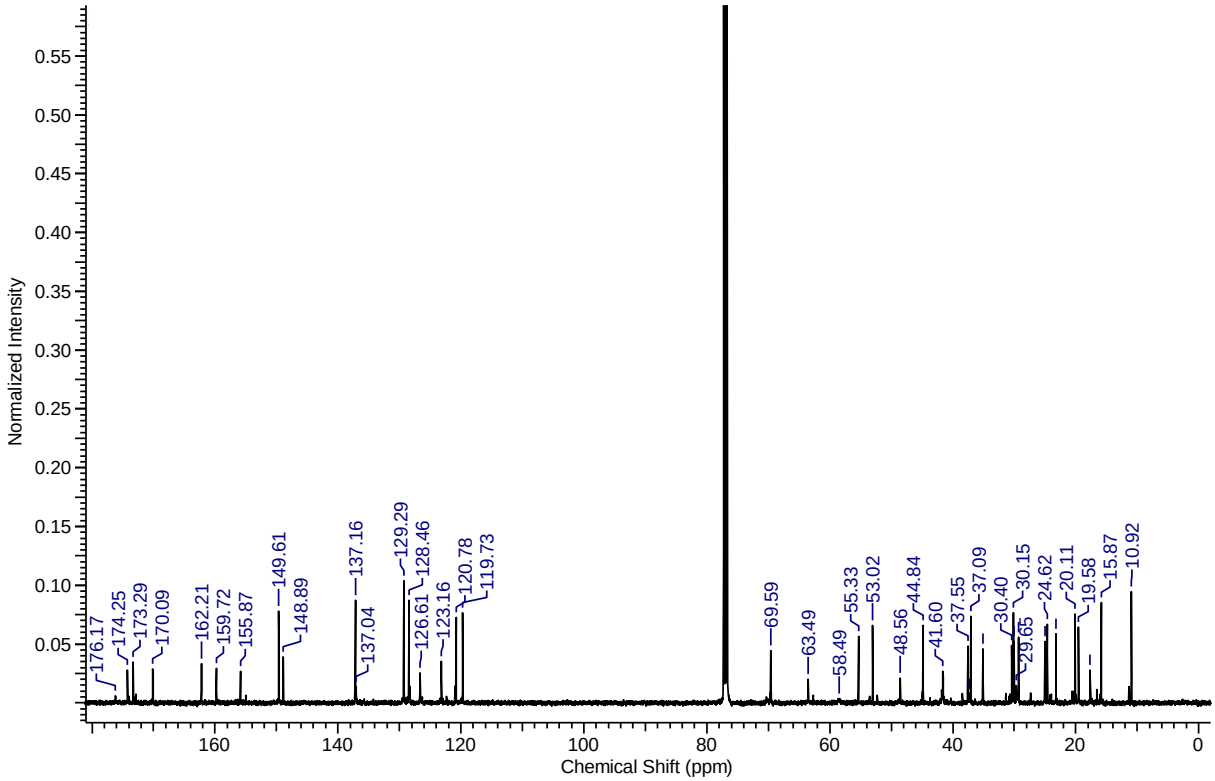

6.2.1.2 Pretubulysin ester (PT-O-SS-Py, 3)

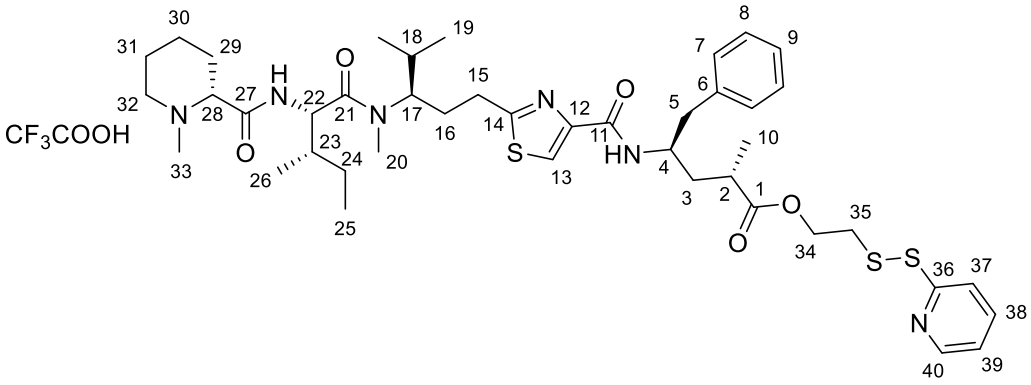

^{1}H-NMR (400 MHz, $CDCl_3$): δ = 0.77 (d, *J* = 6.6 Hz, 3 H, 19-H), 0.88 (t, *J* = 7.4 Hz, 3 H, 25-H), 0.96 (d, *J* = 6.3 Hz, 3 H, 19-H'), 0.98 (d, *J* = 6.6 Hz, 3 H, 26-H), 1.16 (d, *J* =7.1 Hz, 3 H, 10-H), 1.17 (m, 1 H, 24-H_a), 1.35 (m, 2 H, 29-H_a, 30-H_a), 1.59 (m, 6 H, 3-H_a, 18-H, 24-H_b, 30-H_b, 31-H), 1.84 (m, 3 H , 16-H_a, 23-H, 29-H_b), 2.01 (m, 2 H, 3-H_b, 32-H_a), 2.10 (dtd, *J* = 14.2 Hz, 8.2 Hz, 3.5 Hz, 1 H, 16-H_b), 2.23 (s, 3 H, 33-H), 2.49 (dd, *J* =10.8 Hz, 2.6 Hz, 1 H, 28-H), 2.62 (m, 1 H, 2-H), 2.89 (m, 5 H, 5-H, 15-H, 32-H_b), 2.98 (m, 2 H, 35-H), 3.01 (s, 3 H, 20-H), 4.25 (dt, *J* =11.4 Hz, 6.5 Hz, 1 H, 34-H_a), 4.32 (dt, *J* =11.4 Hz, 6.3 Hz, 1 H, 34-H_b), 4.40 (m, 2 H, 4-H, 17-H), 4.78 (dd, *J* = 9.4 Hz, 8.1 Hz, 1 H, 22-H), 7.05 (m, 1 H, N-H), 7.08 (ddd, *J* = 7.2 Hz, 4.9 Hz, 1.1 Hz, 1 H, 39-H), 7.22 (m, 5 H, 7-H, 8-H, 9-H), 7.41 (d, *J* = 9.3 Hz, 1 H, N-H), 7.62 (ddd, *J* = 8.1 Hz, 7.3 Hz, 1.8 Hz, 1 H, 38-H), 7.68 (ddd, *J* = 8.1 Hz, 1.0 Hz, 1.0 Hz, 1 H, 37-H), 7.88 (s, 1 H, 13-H), 8.45 (ddd, *J* = 4.7 Hz, 1.6 Hz, 0.8 Hz, 1 H, 40-H).**^{13}C-NMR** (100 MHz, $CDCl_3$): δ = 11.0 (C-25), 15.9 (C-26), 18.0 (C-10), 19.6 (C-19), 20.1 (C-19'), 23.3 (C-30), 24.6 (C-24), 25.1 (C-31), 29.4 (C-16), 29.6 (C-20), 30.0 (C-15), 30.2 (C-18), 30.5 (C-29), 36.6 (C-2), 37.2 (C-23), 37.3 (C-3), 37.8 (C-35), 41.6 (C-5), 44.0 (C-33), 48.5 (C-4), 53.0 (C-22), 55.4 (C-32), 58.4 (C-17), 62.0 (C-34), 69.7 (C-28), 119.7 (C-37), 120.7 (C-39), 122.3 (C-13), 126.4 (C-9), 128.4 (C-8), 129.5 (C-7), 137.0 (C-38), 137.7 (C-6), 149.7 (C-40), 149.8 (C-12), 159.8 (C-36), 160.7 (C-11), 169.6 (C-14), 173.2 (C-21), 174.3 (C-27), 175.8 (C-1).

^{1}H-NMR spectrum

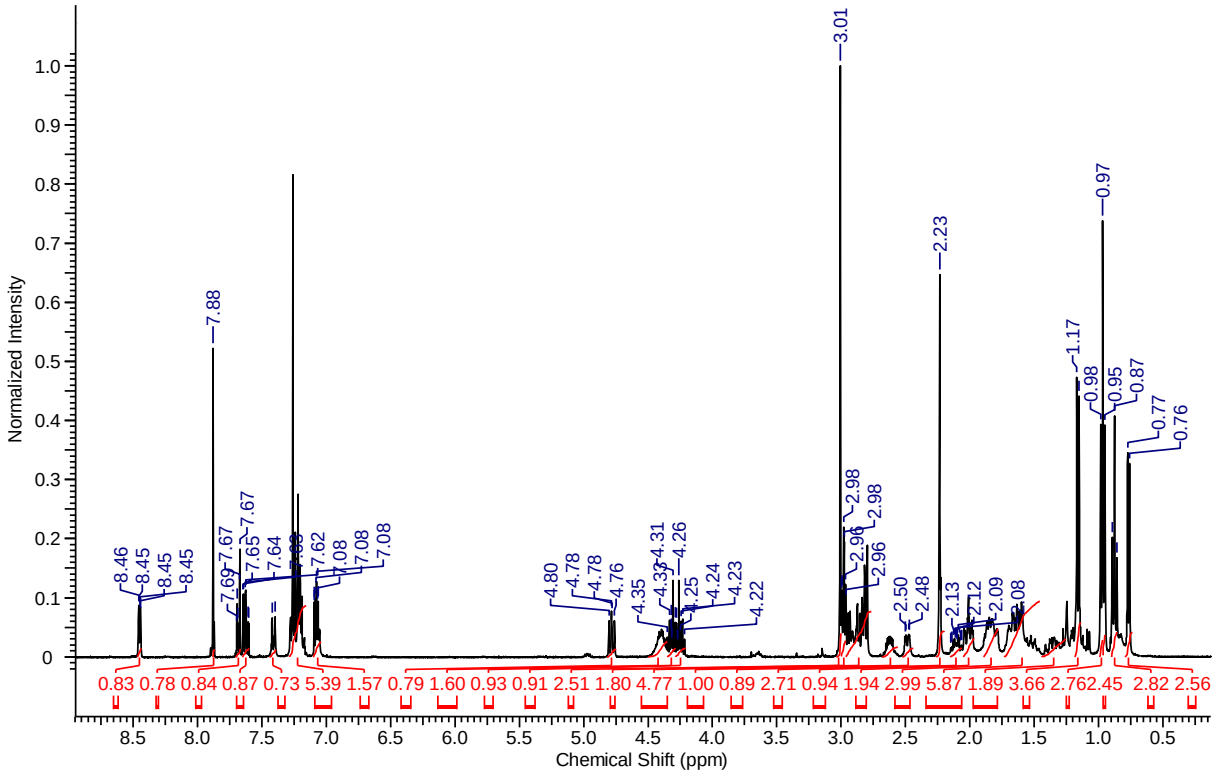

^{13}C-NMR spectrum

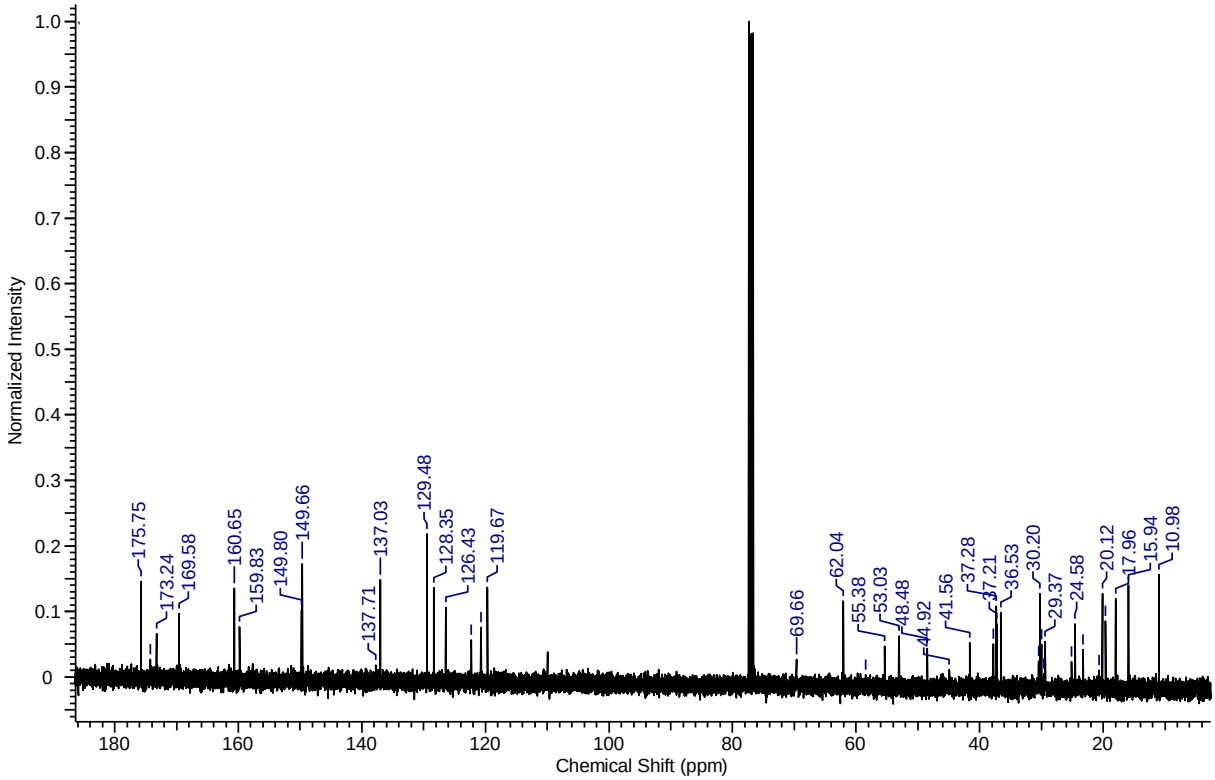

6.2.2 Analytical data of oligomers and post-modification agents

Oligomer	Molecular formula	$[M+H]^+$ calc.	$[M+H]^+$ found
454	$C_{72}H_{119}N_{19}O_{12}S_2$	3072.9	3069.9
883 **(lin FolA)**	$C_{49}H_{78}N_9O_{20}S$	1144.5	1143.5
884 **(lin MTX)**	$C_{50}H_{81}N_{10}O_{19}S$	1157.5	1156.5
948 **(lin E_4-MTX)**	$C_{70}H_{109}N_{14}O_{31}S$	1673.7	1672.3
950 **(2-arm E_4-MTX)**	$C_{157}H_{248}N_{31}O_{66}S$	3655.7	3654.5
951 (4-arm E_4-MTX)	$C_{303}H_{474}N_{61}O_{125}S$	7014.2	7007.1
1002 **(2-arm E_4-FolA)**	$C_{155}H_{242}N_{29}O_{68}S$	3628.6	3623.8
1052 **(4-arm E_4-FolA)**	$C_{300}H_{466}N_{57}O_{130}S$	6979.1	not found
1198	$C_{162}H_{264}N_{36}O_{28}S_2$	3229.2	3226.7
1138 **(DBCO-PEG)**	$C_{72}H_{120}N_2O_{28}$	1483.7	1483.4
1415 **(DBCO-PEG-GE11)**	$C_{145}H_{210}N_{18}O_{47}$	2955.5	2952.96

Table 11. summarizing mass data of oligomers. Mass data were recorded with a Bruker MALDI-TOF instrument.

6.2.2.1 454[91]

Sequence (C→N): C-Y_3-Stp_2-K-ε[K-α,ε$(OleA)_2$]αStp_2-Y_3-C

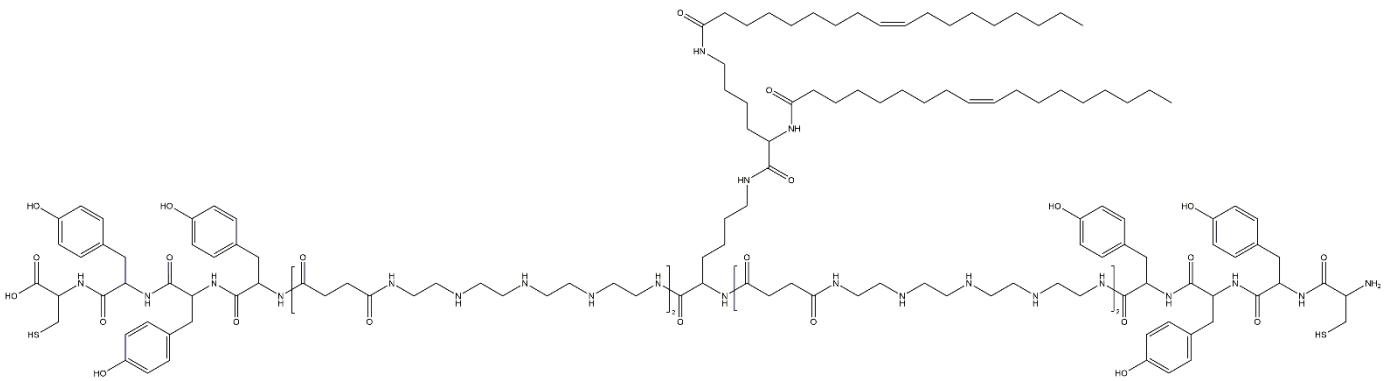

MALDI-MS

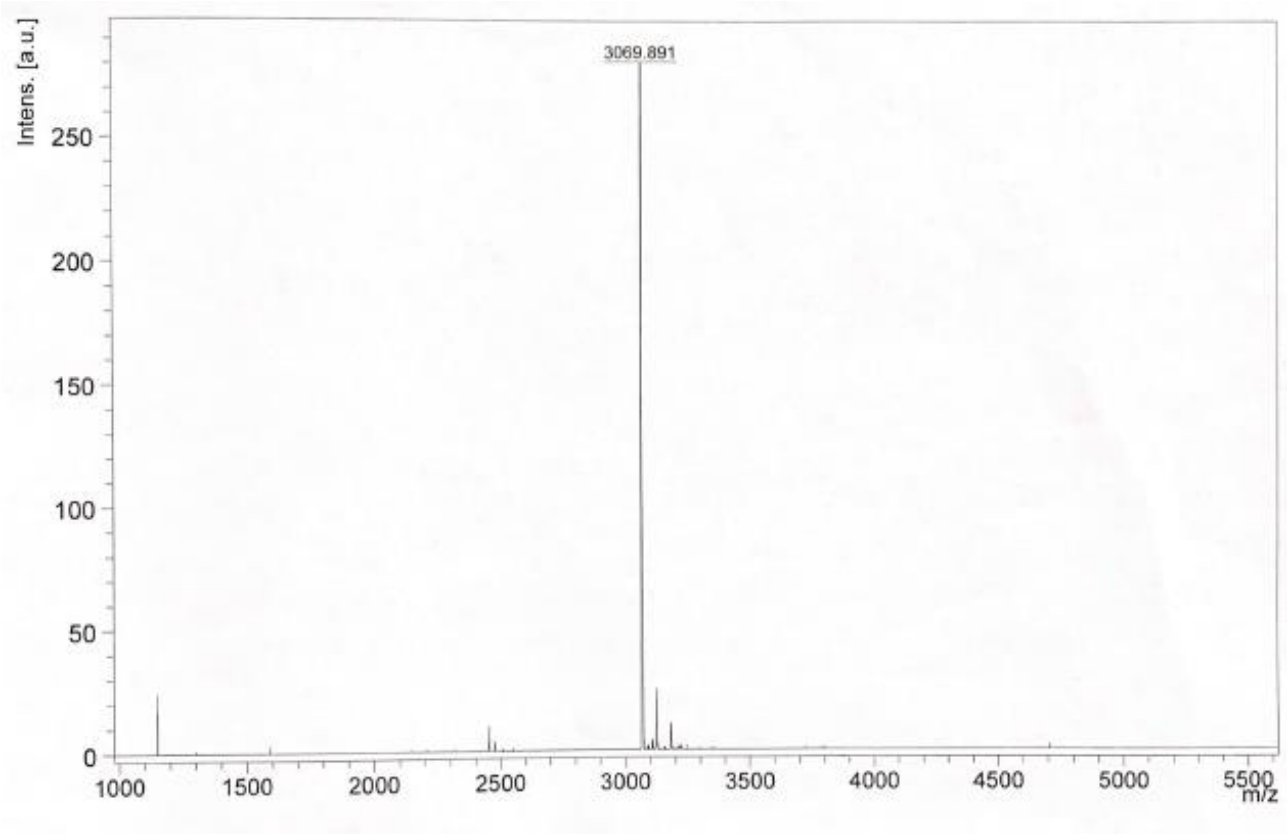

6.2.2.2 883 (linFolA):

Sequence (C→N): C-STOTDA-E_4-FolA

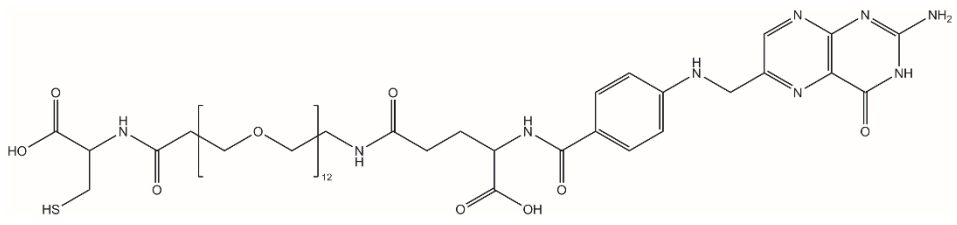

MALDI-MS

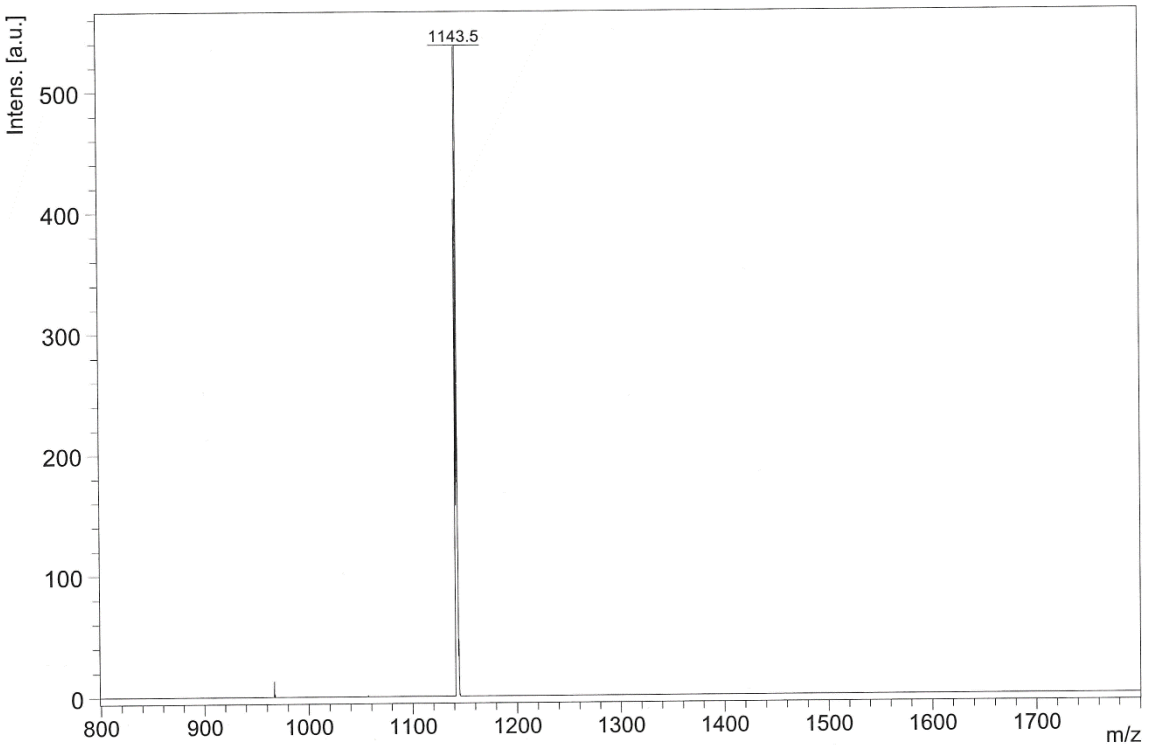

^{1}H-NMR (400 MHz, D_2O): δ (ppm) = 2.1-2.6 (6H, βγH glutamate, -CO-CH_2- PEG_{12}), 3.2-3.7 (52H, βH cysteine, -C-CH_2- PEG_{12}, -N-CH_2- PEG_{12}), 4.3-4.5 (4H αH glutamate/ cysteine, -CH_2- pteroic acid), 6.7 (d, 2H, Ar-H pteroic acid), 7.6 (d, 2H, Ar-H pteroic acid), 8.6 (s, 1H, Ar-H pteroic acid)

HPLC

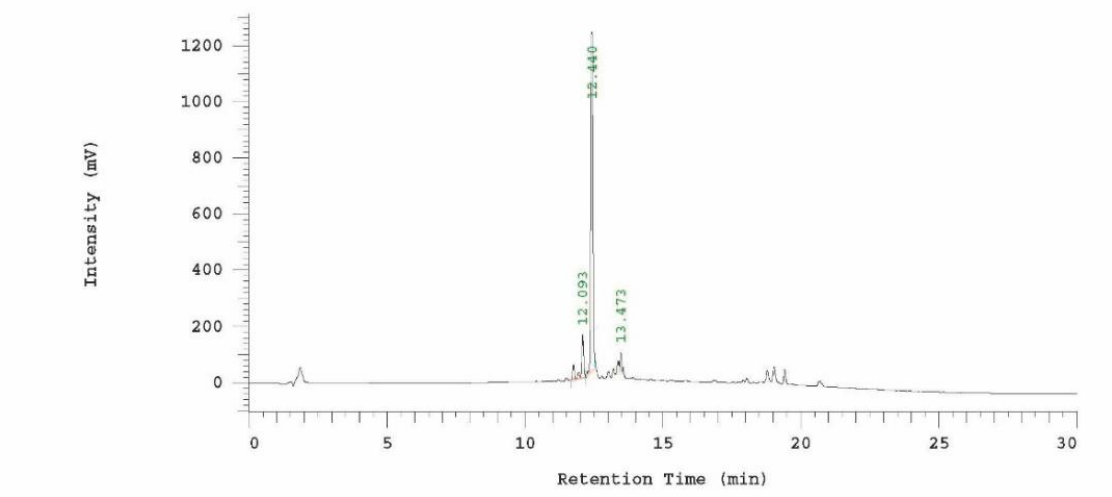

6.2.2.3 884 (linMTX):

Sequence (C→N): C-STOTDA-MTX

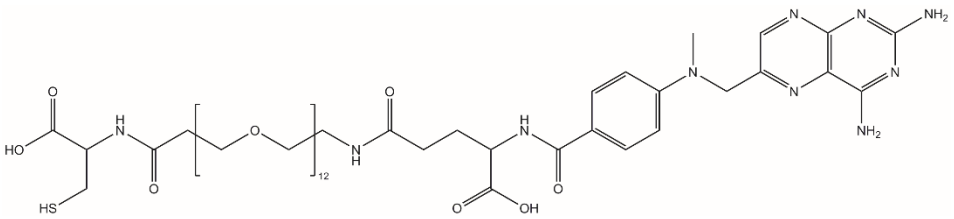

MALDI-MS

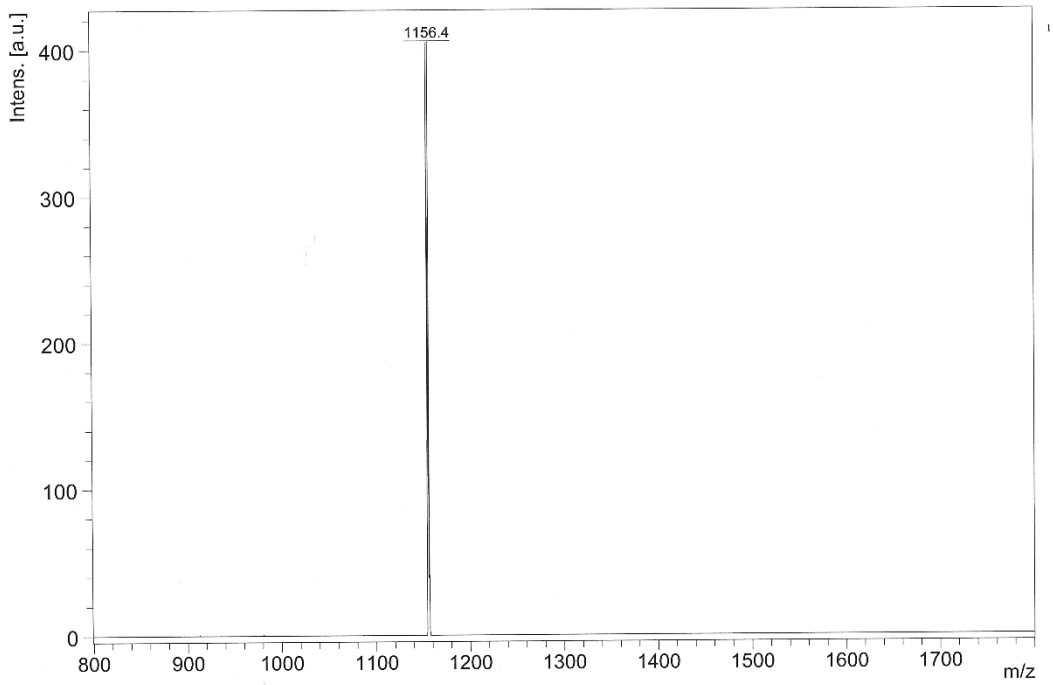

^{1}H-NMR (400 MHz, D_2O): δ (ppm) = 2.0-2.6 (6H, βγH glutamate, -CO-CH_2- PEG_{12}), 3.2-3.7 (52H βH cysteine, -C-CH_2- PEG_{12}, -N-CH_2- PEG_{12}), 4.3-4.5 (4H, αH glutamate/ cysteine, -CH_2- pteroic acid), 6.7 (d, 2H, Ar-H pteroic acid), 7.7 (d, 2H, Ar-H pteroic acid), 8.6 (s, 1H, Ar-H pteroic acid)

HPLC

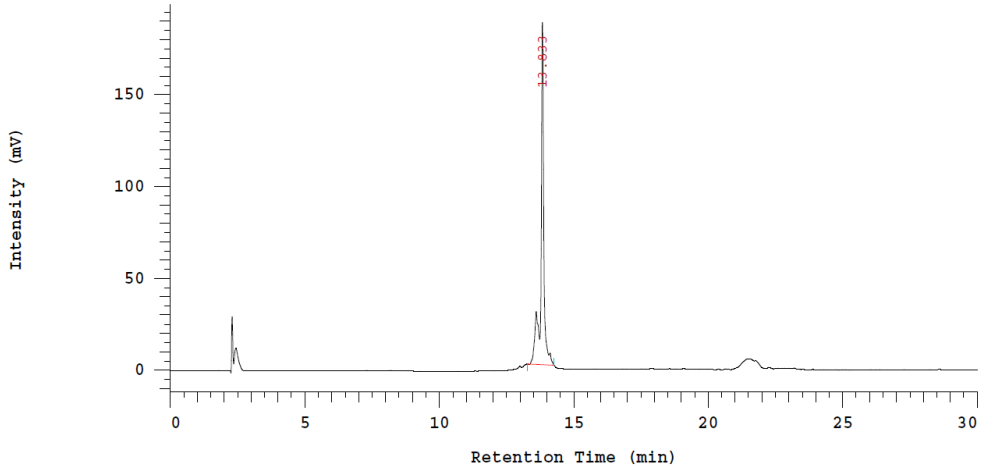

6.2.2.4 948 (linE$_4$MTX):

Sequence (C→N): C-STOTDA-E$_4$-MTX

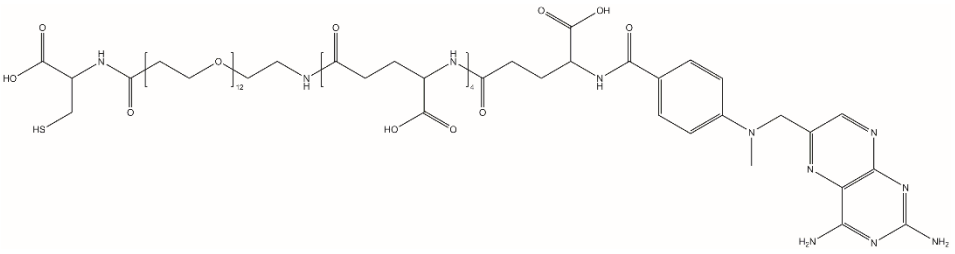

MALDI-MS

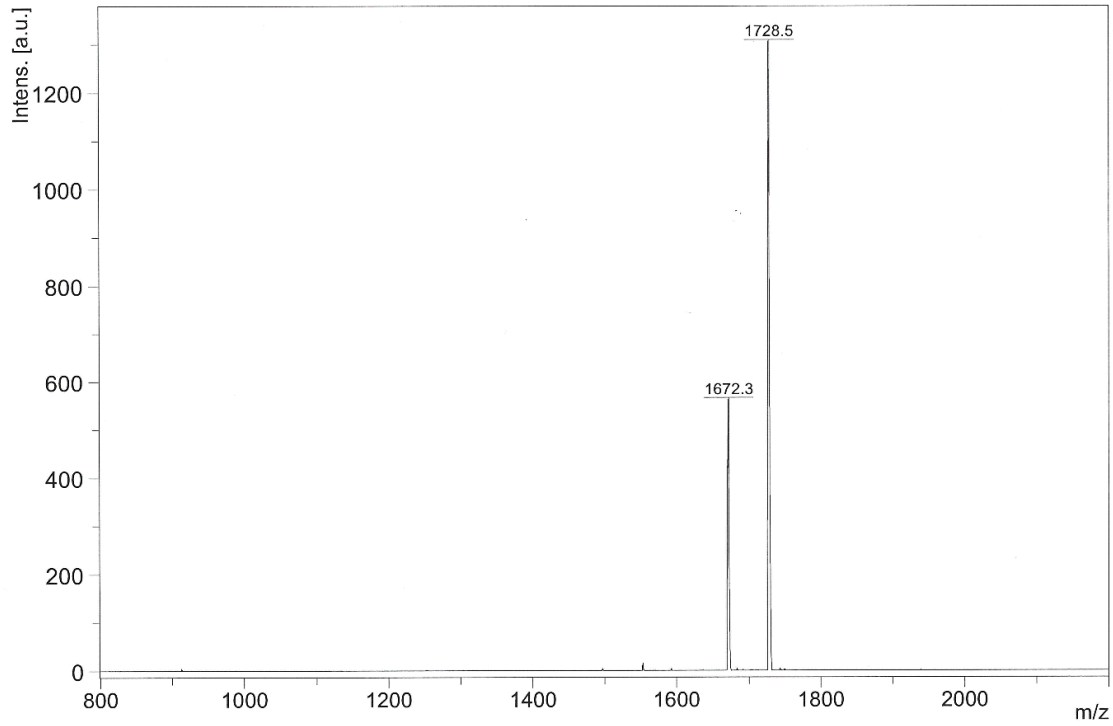

^{1}H-NMR (400 MHz, D_2O): δ (ppm) = 1.95-2.6 (22H, βγH glutamate, -CO-CH_2- PEG_{12}), 3.3-3.6 (52H, βH cysteine, -O-CH_2- PEG_{12}, -N-CH_2- PEG_{12}), 4.0-4.4 (8H, αH glutamate/ cysteine, -CH_2- pteroic acid), 6.8 (d, 2H, Ar-H pteroic acid), 7.7 (d, 2H, Ar-H pteroic acid), 8.6 (s, 1H, Ar-H pteroic acid)

HPLC

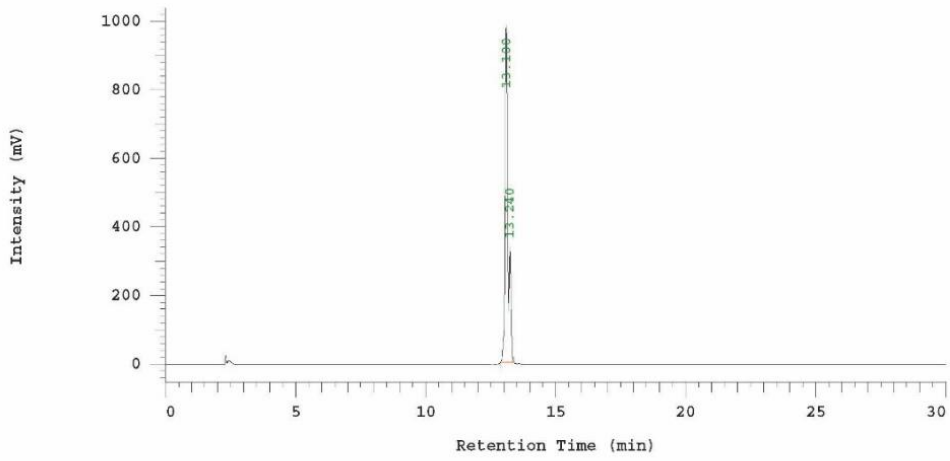

6.2.2.5 1002 (2-arm E4-FolA):

Sequence (C→N): C-STOTDA-K-$_{\alpha,\varepsilon}$[PEG$_{12}$-E$_4$-FolA]$_2$

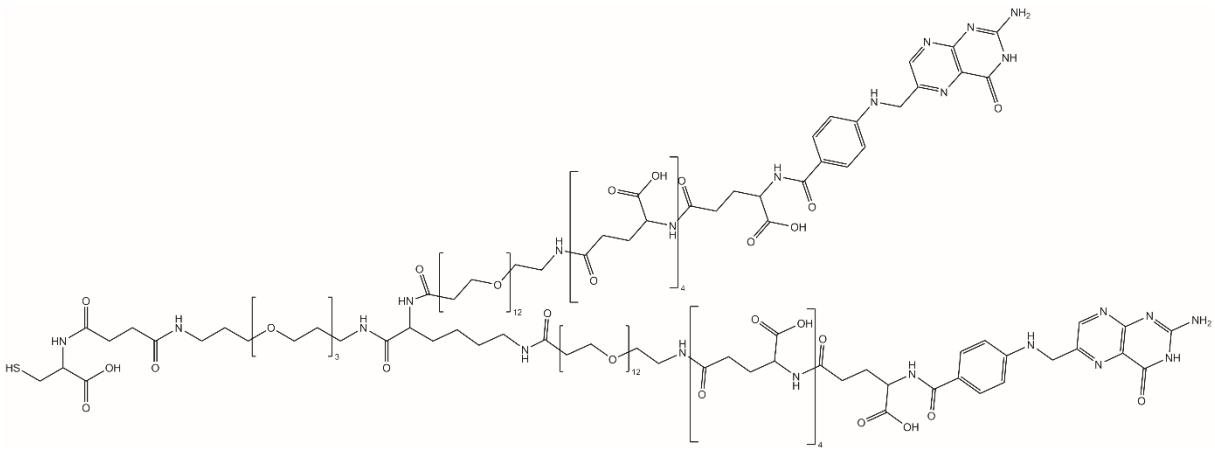

MALDI-MS

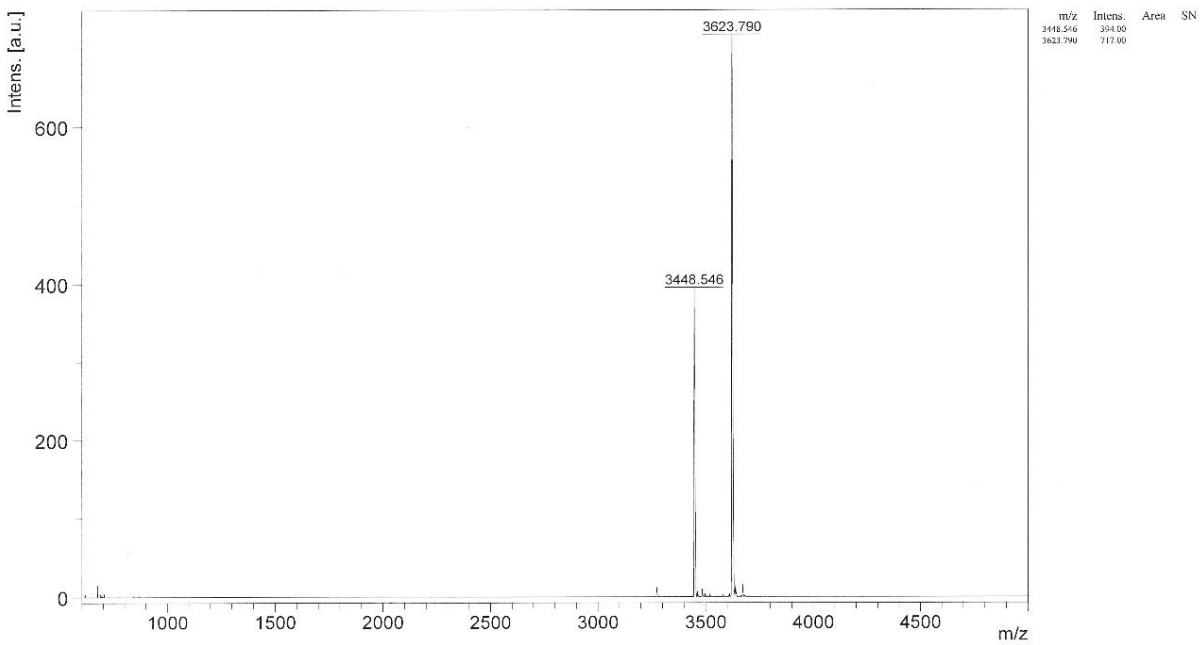

^{1}H-NMR (400 MHz, D_2O): δ (ppm) = 1.7-2.4 (56H, βγH glutamate, βγδH lysine, -CO-CH_2- PEG$_{12}$, -C-CH_2-C- STOTDA, -CO-CH_2-CH_2-CO- STOTDA), 3.3-3.6 (120H, βH cysteine, εH lysine, -O-CH_2- PEG$_{12}$, -N-CH_2- PEG$_{12}$, -O-CH_2- STOTDA, -N-CH_2- STOTDA), 4.0-4.4 (16H, αH glutamate/ cysteine/ lysine, -CH_2- pteroic acid), 6.73 (d, 4H, Ar-H pteroic acid), 7.6 (d, 4H, Ar-H pteroic acid), 8.6 (s, 2H, Ar-H pteroic acid)

HPLC

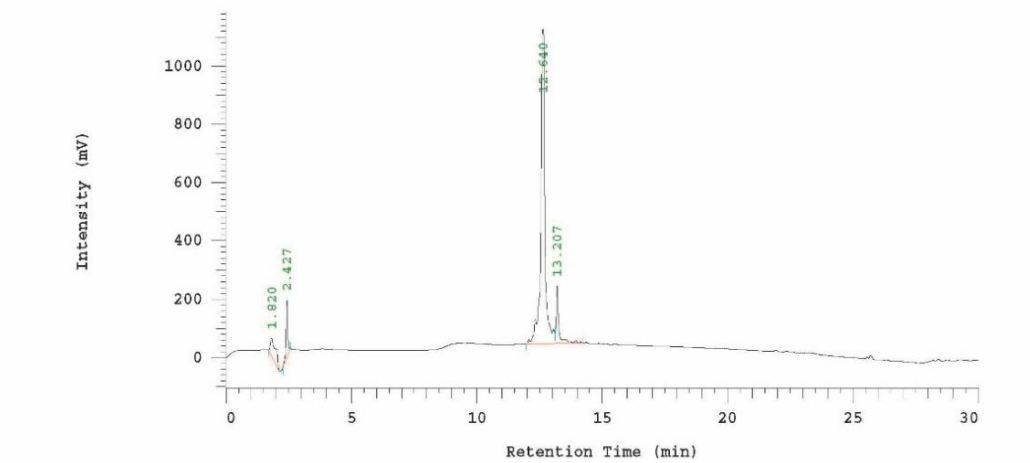

6.2.2.6 950 (2-arm E_4-MTX):

Sequence (C→N): C-STOTDA-K-$_{\alpha,\varepsilon}$[PEG_{12}-E_4-MTX]$_2$

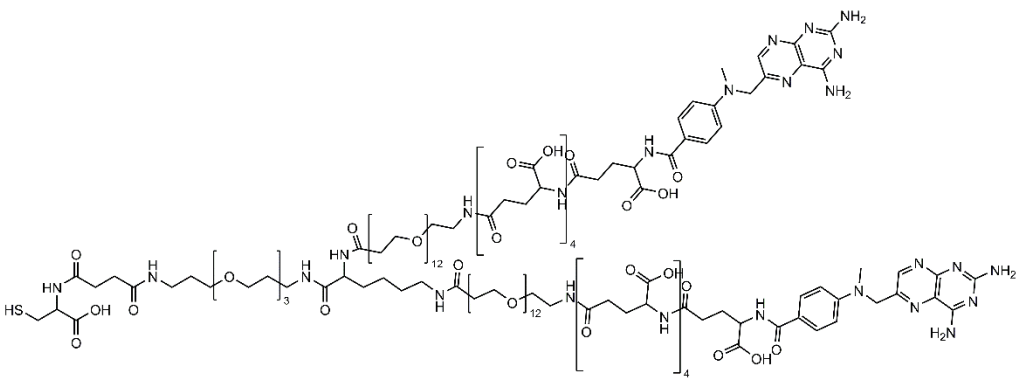

MALDI-MS

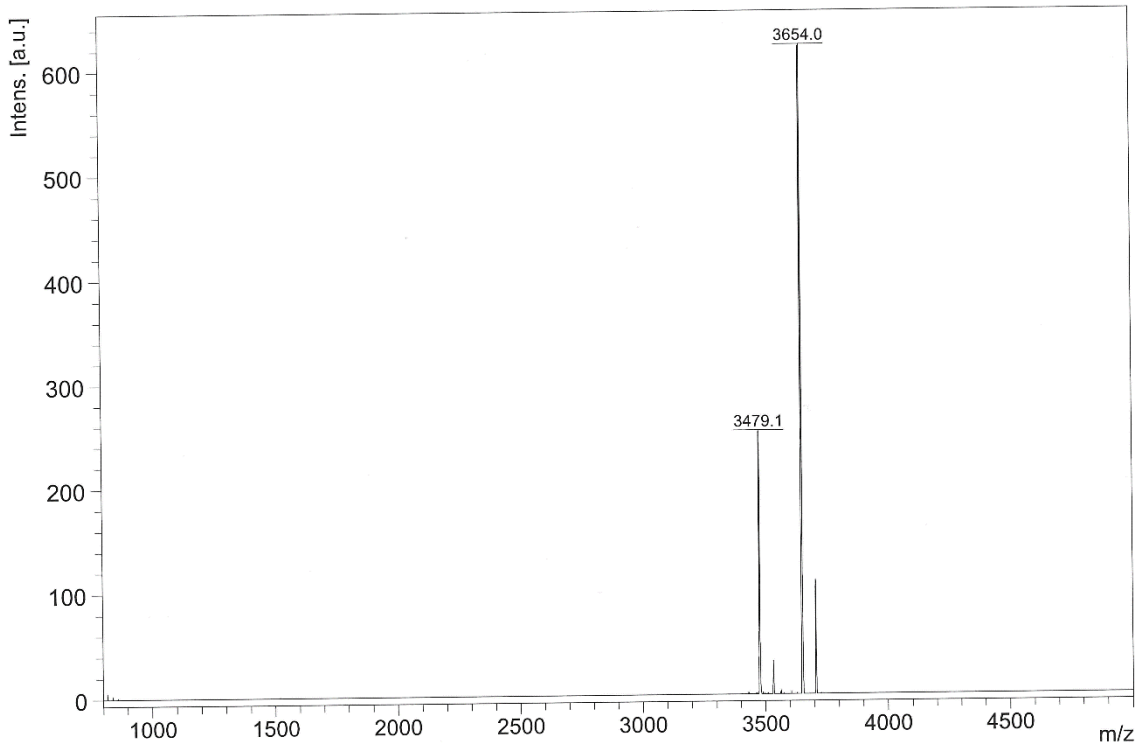

^{1}H-NMR (400 MHz, D_2O): δ (ppm) = 1.8-2.4 (56H βγH glutamate, βγδH lysine, –CO-CH_2- PEG_{12}, -C-CH_2-C- STOTDA, -CO-CH_2-CH_2-CO- STOTDA), 3.2-3.6 (120H, βH cysteine, εH lysine, -O-CH_2- PEG_{12}, -N-CH_2- PEG_{12}, -O-CH_2- STOTDA, -N-CH_2- STOTDA), 4.0-4.4 (16 αH glutamate/ cysteine/ lysine, -CH_2- pteroic acid), 6.6 (d, 4H, Ar-H pteroic acid), 7.5 (d, 4H, Ar-H pteroic acid), 8.6 (s, 2H, Ar-H pteroic acid)

HPLC

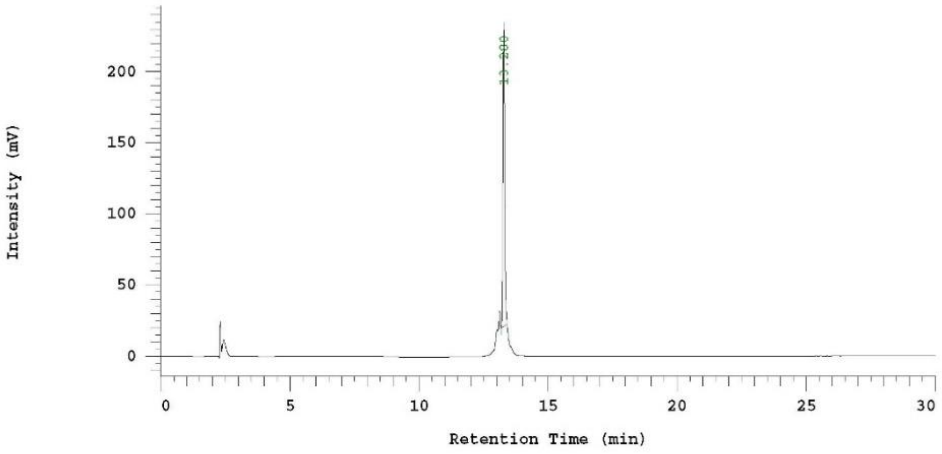

6.2.2.7 951 (4-arm E_4-MTX):

Sequence (C→N): C-STOTDA-K-α,ε[K-α,ε(PEG12-E4-MTX)$_4$]$_2$

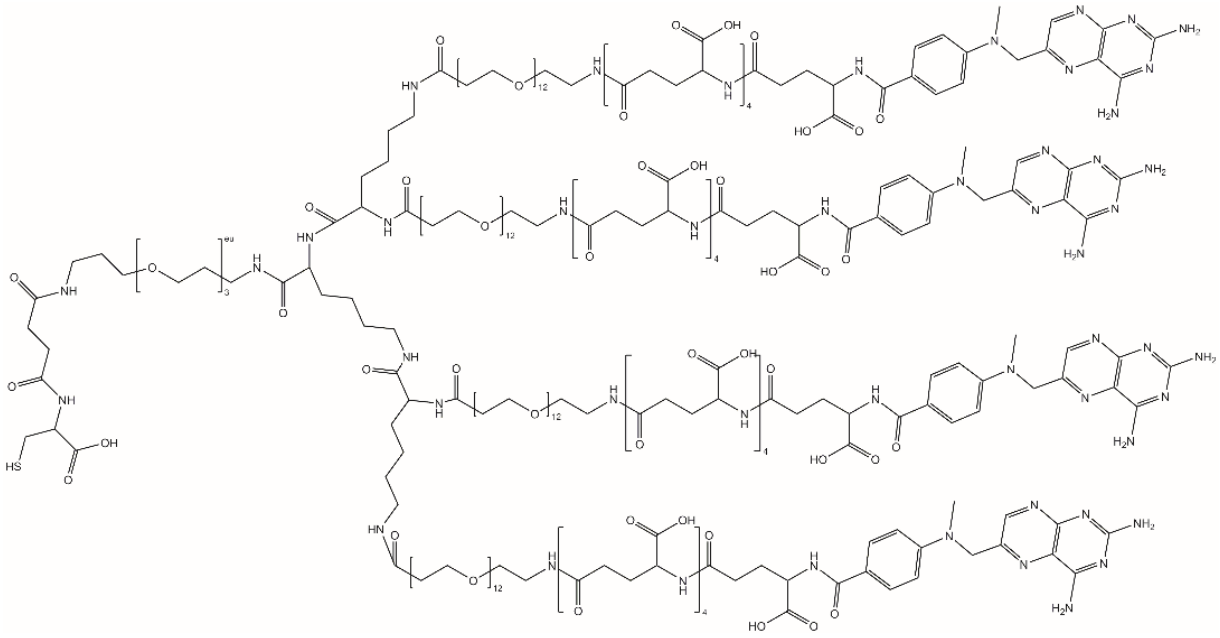

MALDI-MS

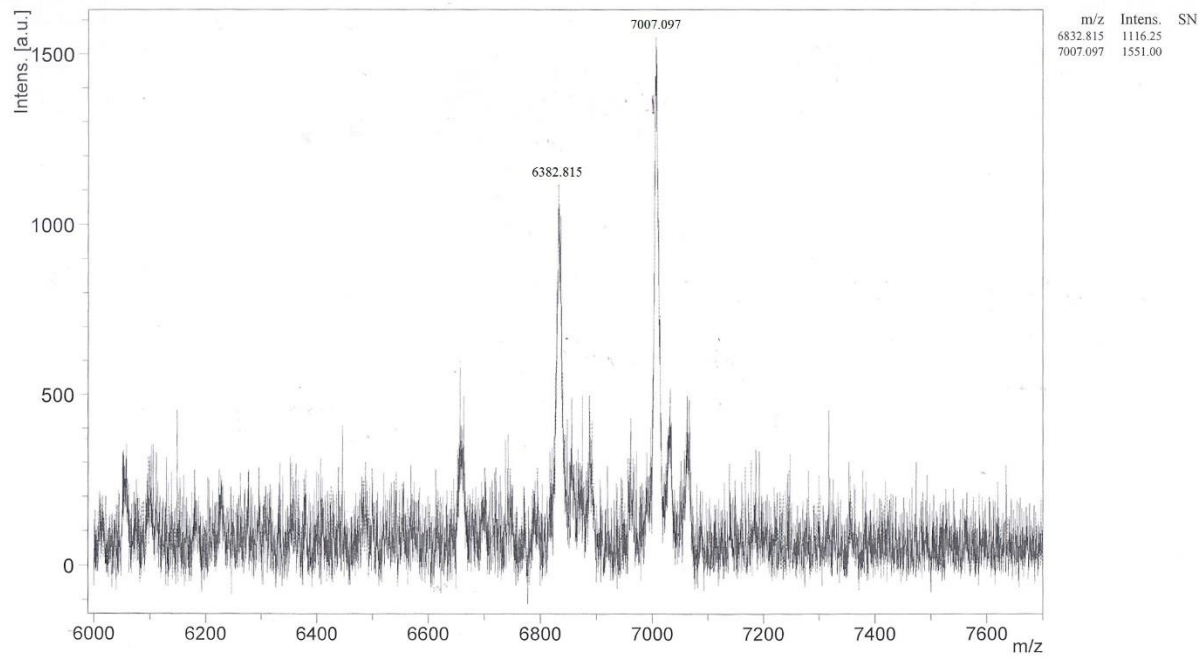

HPLC

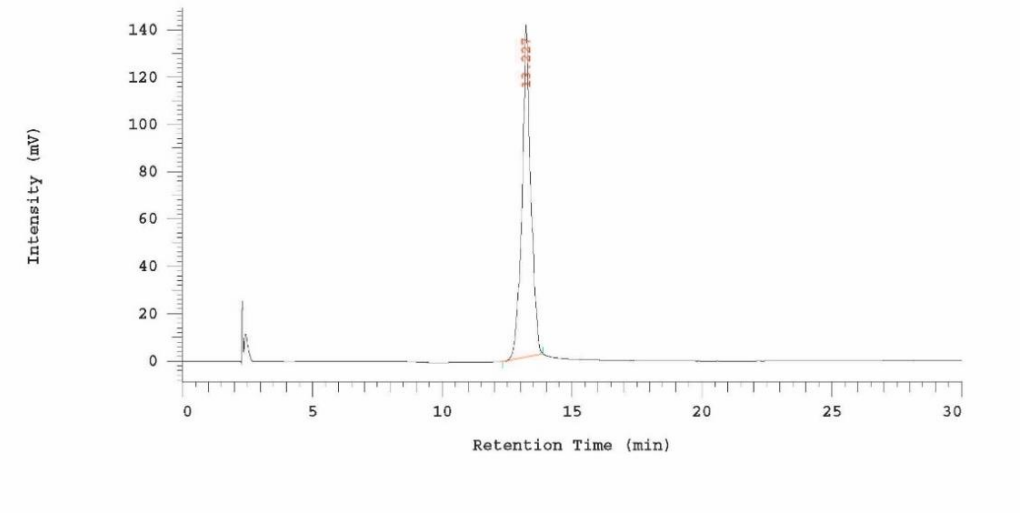

6.2.2.8 1052 (4-arm E_4-FolA):

Sequence (C→N): C-STOTDA-K-$_{\alpha,\varepsilon}$[K-$_{\alpha,\varepsilon}$(PEG12-E4-MTX)$_4$]$_2$

^{1}H-NMR (400 MHz, D2O): δ (ppm) = 1.7-2.4 (114H βγH glutamate, 18H βγδ lysine, -CO-CH2- PEG12, -C-CH2-C- STOTDA, -CO-CH2-CH2-CO- STOTDA), 3.4-3.7 (224H, βH cysteine, εH lysine, -O-CH2- PEG12, -N-CH2- PEG12, -O-CH2- STOTDA, -N-CH2- STOTDA), 4.0-4.3 (32H, αH glutamate/ cysteine/ lysine, -CH2- pteroic acid), 6.8 (d, 8H, Ar-H pteroic acid), 7.6 (d, 8H, Ar-H pteroic acid), 8.5 (s, 4H, Ar-H pteroic acid)

HPLC

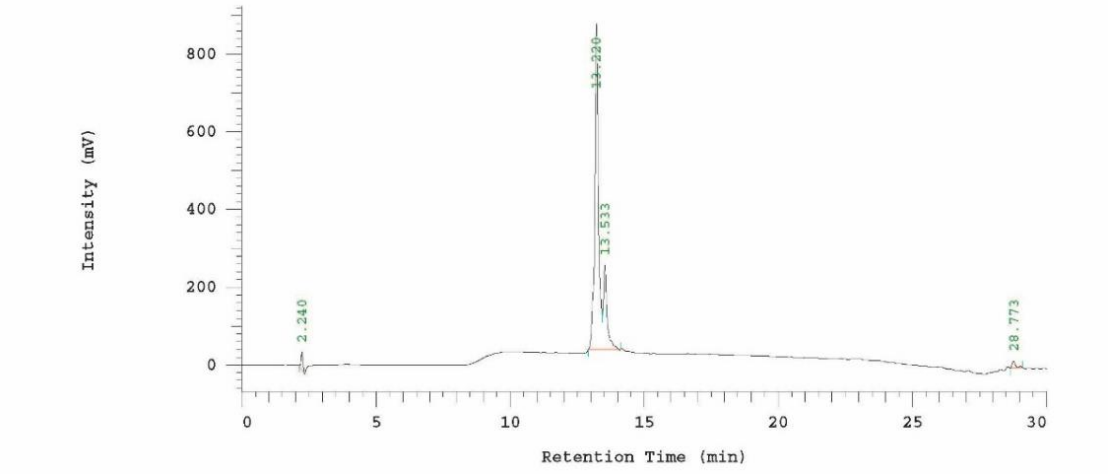

6.2.2.9 1198 (T-shape) [155]

Sequence (C→N): C-Y_3-Stp_2-K-ε[K-α,ε$(OleA)_2$]αStp_2-Y_3-C-K(N_3)

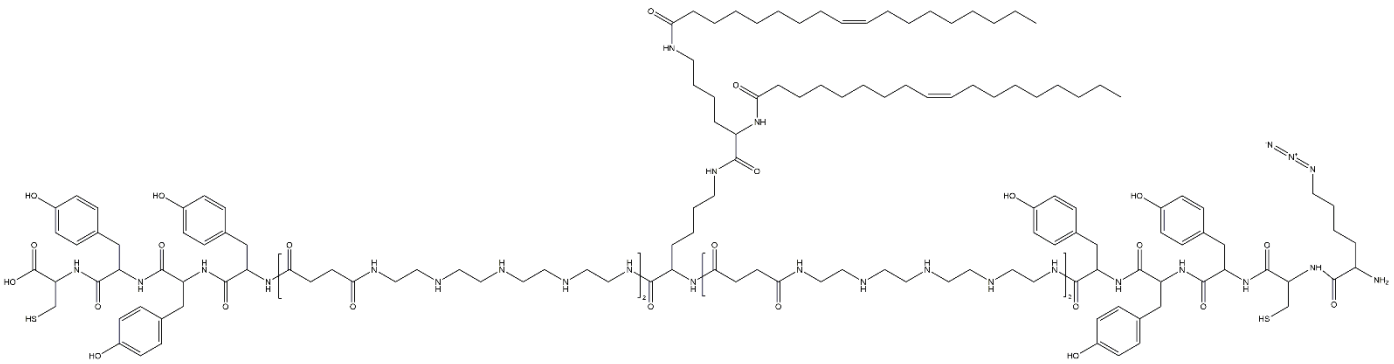

MALDI-MS

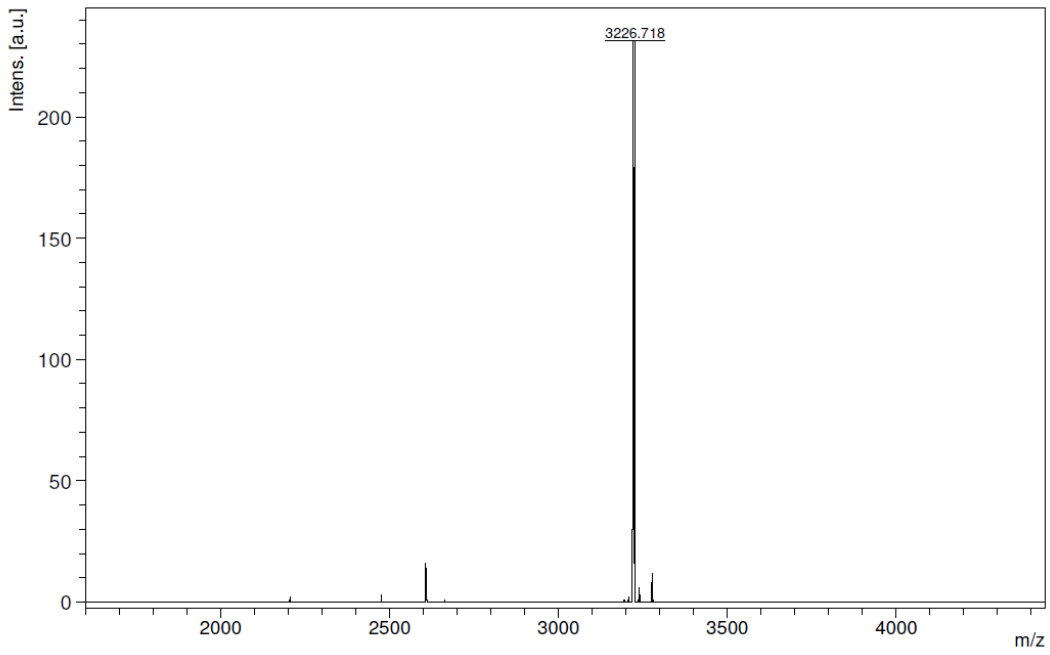

6.2.2.10 1138 (DBCO-PEG)

Sequence (C→N): PEG_{24}-DBCO

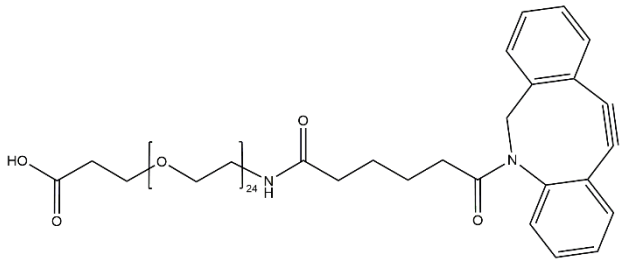

MALDI-MS

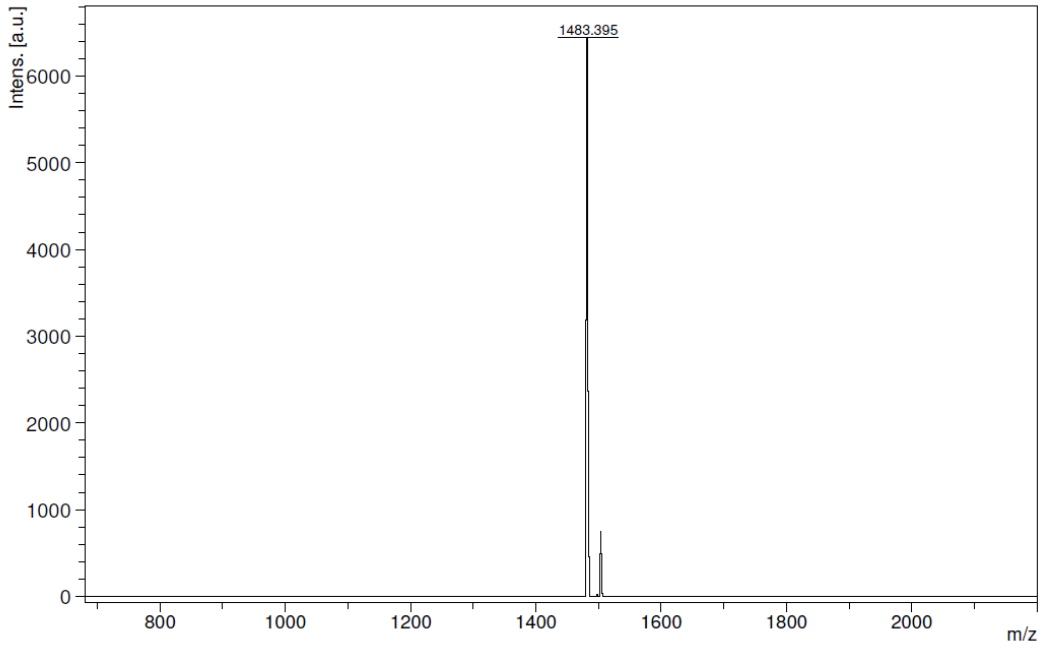

6.2.2.11 1415 (DBCO-PEG-GE11)

Sequence (C→N): IVNQPTYGYWHY-PEG_{24}-DBCO

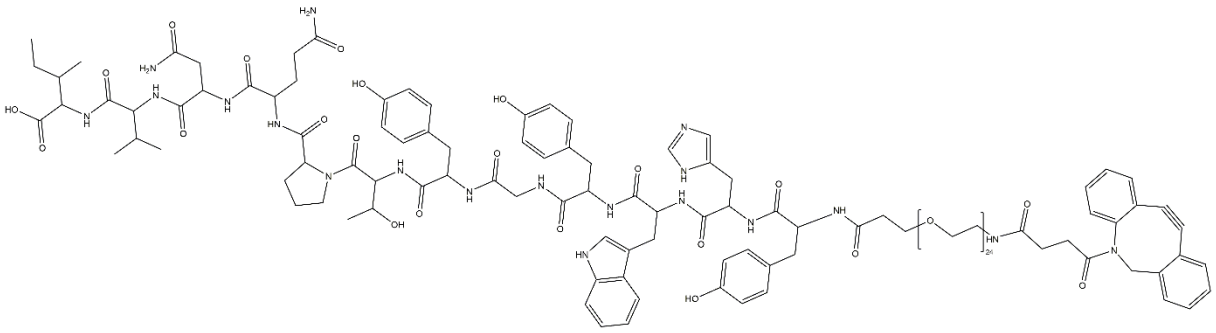

MALDI-MS

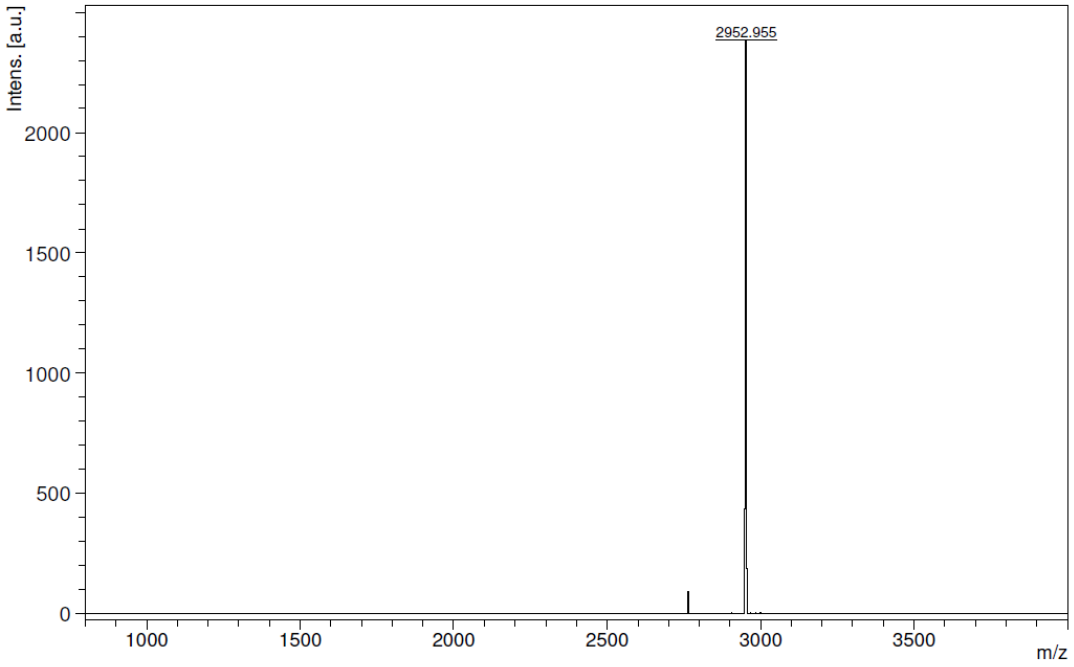

7 References

1. Yap, T. A.; Omlin, A.; de Bono, J. S., Development of therapeutic combinations targeting major cancer signaling pathways. *J Clin Oncol* **2013,** *31* (12), 1592-605.
2. Janku, F.; Hong, D. S.; Fu, S.; Piha-Paul, S. A.; Naing, A.; Falchook, G. S.; Tsimberidou, A. M.; Stepanek, V. M.; Moulder, S. L.; Lee, J. J.; Luthra, R.; Zinner, R. G.; Broaddus, R. R.; Wheler, J. J.; Kurzrock, R., Assessing PIK3CA and PTEN in early-phase trials with PI3K/AKT/mTOR inhibitors. *Cell Rep* **2014,** *6* (2), 377-87.
3. Zoli, W.; Ricotti, L.; Tesei, A.; Barzanti, F.; Amadori, D., In vitro preclinical models for a rational design of chemotherapy combinations in human tumors. *Crit Rev Oncol Hematol* **2001,** *37* (1), 69-82.
4. Mayer, L. D.; Janoff, A. S., Optimizing combination chemotherapy by controlling drug ratios. *Mol Interv* **2007,** *7* (4), 216-23.
5. Bayat Mokhtari, R.; Homayouni, T. S.; Baluch, N.; Morgatskaya, E.; Kumar, S.; Das, B.; Yeger, H., Combination therapy in combating cancer. *Oncotarget* **2017,** *8* (23), 38022-38043.
6. Frei, E., 3rd; Karon, M.; Levin, R. H.; Freireich, E. J.; Taylor, R. J.; Hananian, J.; Selawry, O.; Holland, J. F.; Hoogstraten, B.; Wolman, I. J.; Abir, E.; Sawitsky, A.; Lee, S.; Mills, S. D.; Burgert, E. O., Jr.; Spurr, C. L.; Patterson, R. B.; Ebaugh, F. G.; James, G. W., 3rd; Moon, J. H., The effectiveness of combinations of antileukemic agents in inducing and maintaining remission in children with acute leukemia. *Blood* **1965,** *26* (5), 642-56.
7. Chabner, B. A.; Roberts, T. G., Jr., Timeline: Chemotherapy and the war on cancer. *Nat Rev Cancer* **2005,** *5* (1), 65-72.
8. Kern, S.; Truebenbach, I.; Höhn, M.; Gorges, J.; Kazmaier, U.; Zahler, S.; Vollmar, A.; Wagner, E., Combined Antitumoral Effects of Pretubulysin and Methotrexate. *Pharmacology Res Perspect* **2019**, e00460.
9. Braig, S.; Wiedmann, R. M.; Liebl, J.; Singer, M.; Kubisch, R.; Schreiner, L.; Abhari, B. A.; Wagner, E.; Kazmaier, U.; Fulda, S.; Vollmar, A. M., Pretubulysin: a new option for the treatment of metastatic cancer. *Cell Death Dis* **2014,** *5*, e1001.
10. Herrmann, J.; Elnakady, Y. A.; Wiedmann, R. M.; Ullrich, A.; Rohde, M.; Kazmaier, U.; Vollmar, A. M.; Muller, R., Pretubulysin: from hypothetical biosynthetic intermediate to potential lead in tumor therapy. *PLoS One* **2012,** *7* (5), e37416.
11. Ullrich, A.; Chai, Y.; Pistorius, D.; Elnakady, Y. A.; Herrmann, J. E.; Weissman, K. J.; Kazmaier, U.; Müller, R., Pretubulysin, a potent and chemically accessible tubulysin precursor from Angiococcus disciformis. *Angew Chem Int Ed Engl* **2009,** *48* (24), 4422-5.
12. Schwenk, R.; Stehning, T.; Bischoff, I.; Ullrich, A.; Kazmaier, U.; Fürst, R., The pretubulysin-induced exposure of collagen is caused by endothelial cell retraction that results in an increased adhesion and decreased transmigration of tumor cells. *Oncotarget* **2017,** *8* (44), 77622-77633.
13. Eirich, J.; Burkhart, J. L.; Ullrich, A.; Rudolf, G. C.; Vollmar, A.; Zahler, S.; Kazmaier, U.; Sieber, S. A., Pretubulysin derived probes as novel tools for monitoring the microtubule network via activity-based protein profiling and fluorescence microscopy. *Mol Biosyst* **2012,** *8* (8), 2067-75.
14. Khalil, M. W.; Sasse, F.; Lünsdorf, H.; Elnakady, Y. A.; Reichenbach, H., Mechanism of Action of Tubulysin, an Antimitotic Peptide from Myxobacteria. *ChemBioChem* **2006,** *7* (4), 678-683.

15. Sasse, F.; Steinmetz, H.; Heil, J.; Hofle, G.; Reichenbach, H., Tubulysins, new cytostatic peptides from myxobacteria acting on microtubuli. Production, isolation, physico-chemical and biological properties. *J Antibiot (Tokyo)* **2000,** *53* (9), 879-85.
16. Ullrich, A.; Herrmann, J.; Müller, R.; Kazmaier, U., Synthesis and Biological Evaluation of Pretubulysin and Derivatives. *European Journal of Organic Chemistry* **2009,** *2009* (36), 6367-6378.
17. Truebenbach, I.; Gorges, J.; Kuhn, J.; Kern, S.; Baratti, E.; Kazmaier, U.; Wagner, E.; Lächelt, U., Sequence-Defined Oligoamide Drug Conjugates of Pretubulysin and Methotrexate for Folate Receptor Targeted Cancer Therapy. *Macromolecular bioscience* **2017,** *17* (10).
18. Kubisch, R.; von Gamm, M.; Braig, S.; Ullrich, A.; Burkhart, J. L.; Colling, L.; Hermann, J.; Scherer, O.; Müller, R.; Werz, O.; Kazmaier, U.; Vollmar, A. M., Simplified pretubulysin derivatives and their biological effects on cancer cells. *J Nat Prod* **2014,** *77* (3), 536-42.
19. Rath, S.; Liebl, J.; Fürst, R.; Ullrich, A.; Burkhart, J. L.; Kazmaier, U.; Herrmann, J.; Müller, R.; Gunther, M.; Schreiner, L.; Wagner, E.; Vollmar, A. M.; Zahler, S., Anti-angiogenic effects of the tubulysin precursor pretubulysin and of simplified pretubulysin derivatives. *Br J Pharmacol* **2012,** *167* (5), 1048-61.
20. Li, M. C.; Hertz, R.; Spencer, D. B., Effect of Methotrexate Therapy upon Choriocarcinoma and Chorioadenoma. *Proceedings of the Society for Experimental Biology and Medicine* **1956,** *93* (2), 361-366.
21. Hertz, R., Five years' experience with the chemotherapy of metastatic choriocarcinoma and related trophoblastic tumors in women. *Cancer Chemother Rep* **1962,** *16*, 341.
22. Zhao, P.; Hou, J.; Wu, H.; Zhong, M., Analysis of genetic polymorphism of methylenetetrahydrofolate reductase in a large ethnic Hakka population in southern China. *Medicine (Baltimore)* **2018,** *97* (50), e13332.
23. Ross, J. F.; Chaudhuri, P. K.; Ratnam, M., Differential regulation of folate receptor isoforms in normal and malignant tissues in vivo and in established cell lines. Physiologic and clinical implications. *Cancer* **1994,** *73* (9), 2432-43.
24. Spinella, M. J.; Brigle, K. E.; Sierra, E. E.; Goldman, I. D., Distinguishing between folate receptor-alpha-mediated transport and reduced folate carrier-mediated transport in L1210 leukemia cells. *J Biol Chem* **1995,** *270* (14), 7842-9.
25. Weitman, S. D.; Lark, R. H.; Coney, L. R.; Fort, D. W.; Frasca, V.; Zurawski, V. R., Jr.; Kamen, B. A., Distribution of the folate receptor GP38 in normal and malignant cell lines and tissues. *Cancer research* **1992,** *52* (12), 3396-401.
26. Parker, N.; Turk, M. J.; Westrick, E.; Lewis, J. D.; Low, P. S.; Leamon, C. P., Folate receptor expression in carcinomas and normal tissues determined by a quantitative radioligand binding assay. *Analytical biochemistry* **2005,** *338* (2), 284-93.
27. Kremer, J. M., Toward a better understanding of methotrexate. *Arthritis and rheumatism* **2004,** *50* (5), 1370-82.
28. Chabner, B. A.; Allegra, C. J.; Curt, G. A.; Clendeninn, N. J.; Baram, J.; Koizumi, S.; Drake, J. C.; Jolivet, J., Polyglutamation of methotrexate. Is methotrexate a prodrug? *J Clin Invest* **1985,** *76* (3), 907-12.
29. Bertino, J. R.; Goker, E.; Gorlick, R.; Li, W. W.; Banerjee, D., Resistance Mechanisms to Methotrexate in Tumors. *The Oncologist* **1996,** *1* (4), 223-226.
30. Zhao, R.; Goldman, I. D., Resistance to antifolates. *Oncogene* **2003,** *22* (47), 7431-57.
31. Gorlick, R.; Goker, E.; Trippett, T.; Steinherz, P.; Elisseyeff, Y.; Mazumdar, M.; Flintoff, W. F.; Bertino, J. R., Defective transport is a common mechanism of

acquired methotrexate resistance in acute lymphocytic leukemia and is associated with decreased reduced folate carrier expression. *Blood* **1997,** *89* (3), 1013-8.
32. Bertino, J. R., Karnofsky memorial lecture. Ode to methotrexate. *J Clin Oncol* **1993,** *11* (1), 5-14.
33. Park, K. H.; Choi, Y. J.; Kim, K. W.; Ro, K. H.; Kang, C. H.; Song, S. H.; Park, J. H., Combination chemotherapy with methotrexate and vinblastine for surgically unresectable, aggressive fibromatosis. *Jpn J Clin Oncol* **2016,** *46* (9), 845-9.
34. Cipriani, P.; Ruscitti, P.; Carubbi, F.; Liakouli, V.; Giacomelli, R., Methotrexate: an old new drug in autoimmune disease. *Expert Review of Clinical Immunology* **2014,** *10* (11), 1519-1530.
35. Gavrilov, K.; Saltzman, W. M., Therapeutic siRNA: principles, challenges, and strategies. *Yale J Biol Med* **2012,** *85* (2), 187-200.
36. Chakraborty, C.; Sharma, A. R.; Sharma, G.; Doss, C. G. P.; Lee, S.-S., Therapeutic miRNA and siRNA: Moving from Bench to Clinic as Next Generation Medicine. *Mol Ther Nucleic Acids* **2017,** *8*, 132-143.
37. Garber, K., Alnylam launches era of RNAi drugs. *Nature Biotechnology* **2018,** *36*, 777.
38. Haussecker, D., Current issues of RNAi therapeutics delivery and development. *J Control Release* **2014,** *195*, 49-54.
39. Davis, M. E.; Zuckerman, J. E.; Choi, C. H.; Seligson, D.; Tolcher, A.; Alabi, C. A.; Yen, Y.; Heidel, J. D.; Ribas, A., Evidence of RNAi in humans from systemically administered siRNA via targeted nanoparticles. *Nature* **2010,** *464* (7291), 1067-70.
40. Chou, S. T.; Mixson, A. J., siRNA nanoparticles: the future of RNAi therapeutics for oncology? *Nanomedicine (Lond)* **2014,** *9* (15), 2251-4.
41. Edinger, D.; Klager, R.; Troiber, C.; Dohmen, C.; Wagner, E., Gene silencing and antitumoral effects of Eg5 or Ran siRNA oligoaminoamide polyplexes. *Drug Deliv Transl Res* **2014,** *4* (1), 84-95.
42. Judge, A. D.; Robbins, M.; Tavakoli, I.; Levi, J.; Hu, L.; Fronda, A.; Ambegia, E.; McClintock, K.; MacLachlan, I., Confirming the RNAi-mediated mechanism of action of siRNA-based cancer therapeutics in mice. *J Clin Invest* **2009,** *119* (3), 661-73.
43. Valentine, M. T.; Fordyce, P. M.; Block, S. M., Eg5 steps it up! *Cell Div* **2006,** *1*, 31.
44. Zhou, J.; Shum, K. T.; Burnett, J. C.; Rossi, J. J., Nanoparticle-Based Delivery of RNAi Therapeutics: Progress and Challenges. *Pharmaceuticals (Basel)* **2013,** *6* (1), 85-107.
45. Pecot, C. V.; Calin, G. A.; Coleman, R. L.; Lopez-Berestein, G.; Sood, A. K., RNA interference in the clinic: challenges and future directions. *Nat Rev Cancer* **2011,** *11* (1), 59-67.
46. Wang, J.; Lu, Z.; Wientjes, M. G.; Au, J. L. S., Delivery of siRNA therapeutics: barriers and carriers. *AAPS J* **2010,** *12* (4), 492-503.
47. Kozielski, K. L.; Tzeng, S. Y.; Green, J. J., Bioengineered nanoparticles for siRNA delivery. *Wiley Interdiscip Rev Nanomed Nanobiotechnol* **2013,** *5* (5), 449-68.
48. Steinborn, B.; Truebenbach, I.; Morys, S.; Lächelt, U.; Wagner, E.; Zhang, W., Epidermal growth factor receptor targeted methotrexate and small interfering RNA co-delivery. *J Gene Med* **2018,** *20* (7-8), e3041.
49. Klein, P. M.; Kern, S.; Lee, D. J.; Schmaus, J.; Höhn, M.; Gorges, J.; Kazmaier, U.; Wagner, E., Folate receptor-directed orthogonal click-functionalization of siRNA lipopolyplexes for tumor cell killing in vivo. *Biomaterials* **2018,** *178*, 630-642.
50. Pittella, F.; Cabral, H.; Maeda, Y.; Mi, P.; Watanabe, S.; Takemoto, H.; Kim, H. J.; Nishiyama, N.; Miyata, K.; Kataoka, K., Systemic siRNA delivery to a

spontaneous pancreatic tumor model in transgenic mice by PEGylated calcium phosphate hybrid micelles. *J Control Release* **2014,** *178*, 18-24.
51. Lächelt, U.; Wagner, E., Nucleic Acid Therapeutics Using Polyplexes: A Journey of 50 Years (and Beyond). *Chem Rev* **2015,** *115* (19), 11043-78.
52. Nakamura, K.; Abu Lila, A. S.; Matsunaga, M.; Doi, Y.; Ishida, T.; Kiwada, H., A double-modulation strategy in cancer treatment with a chemotherapeutic agent and siRNA. *Mol Ther* **2011,** *19* (11), 2040-7.
53. Gandhi, N. S.; Tekade, R. K.; Chougule, M. B., Nanocarrier mediated delivery of siRNA/miRNA in combination with chemotherapeutic agents for cancer therapy: current progress and advances. *J Control Release* **2014,** *194*, 238-56.
54. Lächelt, U.; Wittmann, V.; Müller, K.; Edinger, D.; Kos, P.; Höhn, M.; Wagner, E., Synthetic polyglutamylation of dual-functional MTX ligands for enhanced combined cytotoxicity of poly(I:C) nanoplexes. *Mol Pharm* **2014,** *11* (8), 2631-9.
55. Zhuang, C.; Guan, X.; Ma, H.; Cong, H.; Zhang, W.; Miao, Z., Small molecule-drug conjugates: A novel strategy for cancer-targeted treatment. *European Journal of Medicinal Chemistry* **2019,** *163*, 883-895.
56. Ventola, C. L., The nanomedicine revolution: part 2: current and future clinical applications. *P T* **2012,** *37* (10), 582-591.
57. Hu, C. M.; Zhang, L., Nanoparticle-based combination therapy toward overcoming drug resistance in cancer. *Biochem Pharmacol* **2012,** *83* (8), 1104-11.
58. Andresen, T. L.; Jensen, S. S.; Jorgensen, K., Advanced strategies in liposomal cancer therapy: problems and prospects of active and tumor specific drug release. *Prog Lipid Res* **2005,** *44* (1), 68-97.
59. Dutta, R. C., Drug carriers in pharmaceutical design: promises and progress. *Curr Pharm Des* **2007,** *13* (7), 761-9.
60. Mayer, L. D.; St-Onge, G., Determination of free and liposome-associated doxorubicin and vincristine levels in plasma under equilibrium conditions employing ultrafiltration techniques. *Anal Biochem* **1995,** *232* (2), 149-57.
61. Iyer, A. K.; Khaled, G.; Fang, J.; Maeda, H., Exploiting the enhanced permeability and retention effect for tumor targeting. *Drug Discov Today* **2006,** *11* (17-18), 812-8.
62. Zhang, L.; Gu, F. X.; Chan, J. M.; Wang, A. Z.; Langer, R. S.; Farokhzad, O. C., Nanoparticles in medicine: therapeutic applications and developments. *Clin Pharmacol Ther* **2008,** *83* (5), 761-9.
63. Krauss, A. C.; Gao, X.; Li, L.; Manning, M. L.; Patel, P.; Fu, W.; Janoria, K. G.; Gieser, G.; Bateman, D. A.; Przepiorka, D.; Shen, Y. L.; Shord, S. S.; Sheth, C. M.; Banerjee, A.; Liu, J.; Goldberg, K. B.; Farrell, A. T.; Blumenthal, G. M.; Pazdur, R., FDA Approval Summary: (Daunorubicin and Cytarabine) Liposome for Injection for the Treatment of Adults with High-Risk Acute Myeloid Leukemia. *Clinical Cancer Research* **2019,** *25* (9), 2685.
64. Danhier, F., To exploit the tumor microenvironment: Since the EPR effect fails in the clinic, what is the future of nanomedicine? *Journal of Controlled Release* **2016,** *244*, 108-121.
65. Matsumura, Y.; Maeda, H., A new concept for macromolecular therapeutics in cancer chemotherapy: mechanism of tumoritropic accumulation of proteins and the antitumor agent smancs. *Cancer Res* **1986,** *46* (12 Pt 1), 6387-92.
66. Hua, S.; de Matos, M. B. C.; Metselaar, J. M.; Storm, G., Current Trends and Challenges in the Clinical Translation of Nanoparticulate Nanomedicines: Pathways for Translational Development and Commercialization. *Frontiers in Pharmacology* **2018,** *9* (790).

67. Bae, Y. H.; Park, K., Targeted drug delivery to tumors: myths, reality and possibility. *J Control Release* **2011,** *153* (3), 198-205.
68. Caster, J. M.; Patel, A. N.; Zhang, T.; Wang, A., Investigational nanomedicines in 2016: a review of nanotherapeutics currently undergoing clinical trials. *Wiley Interdiscip Rev Nanomed Nanobiotechnol* **2017,** *9* (1).
69. Toffoli, G.; Cernigoi, C.; Russo, A.; Gallo, A.; Bagnoli, M.; Boiocchi, M., Overexpression of folate binding protein in ovarian cancers. *Int J Cancer* **1997,** *74* (2), 193-8.
70. Sudimack, J.; Lee, R. J., Targeted drug delivery via the folate receptor. *Adv Drug Deliv Rev* **2000,** *41* (2), 147-62.
71. Reddy, J. A.; Allagadda, V. M.; Leamon, C. P., Targeting therapeutic and imaging agents to folate receptor positive tumors. *Curr Pharm Biotechnol* **2005,** *6* (2), 131-50.
72. Reddy, J. A.; Dorton, R.; Dawson, A.; Vetzel, M.; Parker, N.; Nicoson, J. S.; Westrick, E.; Klein, P. J.; Wang, Y.; Vlahov, I. R.; Leamon, C. P., In vivo structural activity and optimization studies of folate-tubulysin conjugates. *Mol Pharm* **2009,** *6* (5), 1518-25.
73. Dohmen, C.; Fröhlich, T.; Lächelt, U.; Rohl, I.; Vornlocher, H. P.; Hadwiger, P.; Wagner, E., Defined Folate-PEG-siRNA Conjugates for Receptor-specific Gene Silencing. *Mol Ther Nucleic Acids* **2012,** *1*, e7.
74. Li, Y.; Lin, J.; Huang, Y.; Li, Y.; Yang, X.; Wu, H.; Wu, S.; Xie, L.; Dai, L.; Hou, Z., Self-Targeted, Shape-Assisted, and Controlled-Release Self-Delivery Nanodrug for Synergistic Targeting/Anticancer Effect of Cytoplasm and Nucleus of Cancer Cells. *ACS Appl Mater Interfaces* **2015,** *7* (46), 25553-9.
75. Li, Y.; Lin, J.; Wu, H.; Chang, Y.; Yuan, C.; Liu, C.; Wang, S.; Hou, Z.; Dai, L., Orthogonally functionalized nanoscale micelles for active targeted codelivery of methotrexate and mitomycin C with synergistic anticancer effect. *Mol Pharm* **2015,** *12* (3), 769-82.
76. Cui, F.; Lin, J.; Li, Y.; Li, Y.; Wu, H.; Yu, F.; Jia, M.; Yang, X.; Wu, S.; Xie, L.; Ye, S.; Luo, F.; Hou, Z., Bacillus-shape design of polymer based drug delivery systems with janus-faced function for synergistic targeted drug delivery and more effective cancer therapy. *Mol Pharm* **2015,** *12* (4), 1318-27.
77. Ryser, H. J.; Shen, W. C., Conjugation of methotrexate to poly(L-lysine) increases drug transport and overcomes drug resistance in cultured cells. *Proc Natl Acad Sci U S A* **1978,** *75* (8), 3867-70.
78. Thomas, T. P.; Huang, B.; Choi, S. K.; Silpe, J. E.; Kotlyar, A.; Desai, A. M.; Zong, H.; Gam, J.; Joice, M.; Baker, J. R., Jr., Polyvalent dendrimer-methotrexate as a folate receptor-targeted cancer therapeutic. *Mol Pharm* **2012,** *9* (9), 2669-76.
79. Lee, D. J.; Kessel, E.; Edinger, D.; He, D.; Klein, P. M.; Voith von Voithenberg, L.; Lamb, D. C.; Lächelt, U.; Lehto, T.; Wagner, E., Dual antitumoral potency of EG5 siRNA nanoplexes armed with cytotoxic bifunctional glutamyl-methotrexate targeting ligand. *Biomaterials* **2016,** *77*, 98-110.
80. Li, Z.; Zhao, R.; Wu, X.; Sun, Y.; Yao, M.; Li, J.; Xu, Y.; Gu, J., Identification and characterization of a novel peptide ligand of epidermal growth factor receptor for targeted delivery of therapeutics. *The FASEB Journal* **2005,** *19* (14), 1978-1985.
81. Zou, Y.; Xia, Y.; Meng, F.; Zhang, J.; Zhong, Z., GE11-Directed Functional Polymersomal Doxorubicin as an Advanced Alternative to Clinical Liposomal Formulation for Ovarian Cancer Treatment. *Molecular Pharmaceutics* **2018,** *15* (9), 3664-3671.

82. Müller, K.; Klein, P. M.; Heissig, P.; Roidl, A.; Wagner, E., EGF receptor targeted lipo-oligocation polyplexes for antitumoral siRNA and miRNA delivery. *Nanotechnology* **2016,** *27* (46), 464001.
83. Nascimento, A. V.; Singh, A.; Bousbaa, H.; Ferreira, D.; Sarmento, B.; Amiji, M. M., Overcoming cisplatin resistance in non-small cell lung cancer with Mad2 silencing siRNA delivered systemically using EGFR-targeted chitosan nanoparticles. *Acta Biomaterialia* **2017,** *47*, 71-80.
84. Klutz, K.; Schaffert, D.; Willhauck, M. J.; Grünwald, G. K.; Haase, R.; Wunderlich, N.; Zach, C.; Gildehaus, F. J.; Senekowitsch-Schmidtke, R.; Göke, B.; Wagner, E.; Ogris, M.; Spitzweg, C., Epidermal Growth Factor Receptor-targeted 131I-therapy of Liver Cancer Following Systemic Delivery of the Sodium Iodide Symporter Gene. *Molecular Therapy* **2011,** *19* (4), 676-685.
85. Schäfer, A.; Pahnke, A.; Schaffert, D.; van Weerden, W. M.; de Ridder, C. M. A.; Rödl, W.; Vetter, A.; Spitzweg, C.; Kraaij, R.; Wagner, E.; Ogris, M., Disconnecting the Yin and Yang Relation of Epidermal Growth Factor Receptor (EGFR)-Mediated Delivery: A Fully Synthetic, EGFR-Targeted Gene Transfer System Avoiding Receptor Activation. *Human Gene Therapy* **2011,** *22* (12), 1463-1473.
86. Grünwald, G. K.; Vetter, A.; Klutz, K.; Willhauck, M. J.; Schwenk, N.; Senekowitsch-Schmidtke, R.; Schwaiger, M.; Zach, C.; Wagner, E.; Göke, B.; Holm, P. S.; Ogris, M.; Spitzweg, C., EGFR-Targeted Adenovirus Dendrimer Coating for Improved Systemic Delivery of the Theranostic NIS Gene. *Molecular therapy. Nucleic acids* **2013,** *2* (11), e131-e131.
87. Fröhlich, T.; Edinger, D.; Klager, R.; Troiber, C.; Salcher, E.; Badgujar, N.; Martin, I.; Schaffert, D.; Cengizeroglu, A.; Hadwiger, P.; Vornlocher, H. P.; Wagner, E., Structure-activity relationships of siRNA carriers based on sequence-defined oligo (ethane amino) amides. *J Control Release* **2012,** *160* (3), 532-41.
88. Zhang, P.; Steinborn, B.; Lächelt, U.; Zahler, S.; Wagner, E., Lipo-Oligomer Nanoformulations for Targeted Intracellular Protein Delivery. *Biomacromolecules* **2017,** *18* (8), 2509-2520.
89. Schaffert, D.; Troiber, C.; Salcher, E. E.; Fröhlich, T.; Martin, I.; Badgujar, N.; Dohmen, C.; Edinger, D.; Klager, R.; Maiwald, G.; Farkasova, K.; Seeber, S.; Jahn-Hofmann, K.; Hadwiger, P.; Wagner, E., Solid-phase synthesis of sequence-defined T-, i-, and U-shape polymers for pDNA and siRNA delivery. *Angew Chem Int Ed Engl* **2011,** *50* (38), 8986-9.
90. Schaffert, D.; Badgujar, N.; Wagner, E., Novel Fmoc-polyamino acids for solid-phase synthesis of defined polyamidoamines. *Org Lett* **2011,** *13* (7), 1586-9.
91. Troiber, C.; Edinger, D.; Kos, P.; Schreiner, L.; Kläger, R.; Herrmann, A.; Wagner, E., Stabilizing effect of tyrosine trimers on pDNA and siRNA polyplexes. *Biomaterials* **2013,** *34* (5), 1624-33.
92. Lächelt, U.; Kos, P.; Mickler, F. M.; Herrmann, A.; Salcher, E. E.; Rödl, W.; Badgujar, N.; Brauchle, C.; Wagner, E., Fine-tuning of proton sponges by precise diaminoethanes and histidines in pDNA polyplexes. *Nanomedicine* **2014,** *10* (1), 35-44.
93. Vlahov, I. R.; Wang, Y.; Kleindl, P. J.; Leamon, C. P., Design and regioselective synthesis of a new generation of targeted chemotherapeutics. Part II: Folic acid conjugates of tubulysins and their hydrazides. *Bioorg Med Chem Lett* **2008,** *18* (16), 4558-61.
94. Casi, G.; Neri, D., Antibody–Drug Conjugates and Small Molecule–Drug Conjugates: Opportunities and Challenges for the Development of Selective Anticancer Cytotoxic Agents. *Journal of Medicinal Chemistry* **2015,** *58* (22), 8751-8761.

95. Vergote, I.; Leamon, C. P., Vintafolide: a novel targeted therapy for the treatment of folate receptor expressing tumors. *Ther Adv Med Oncol* **2015,** *7* (4), 206-218.
96. Armstrong, M.; Plieth, J., Immunogen fails to leap Forward. *Evaluate* **2019,** (https://www.evaluate.com/vantage/articles/news/trial-results/immunogen-fails-leap-forward).
97. Wang, P.; Kankala, R. K.; Chen, B.; Long, R.; Cai, D.; Liu, Y.; Wang, S., Poly-allylamine hydrochloride and fucoidan-based self-assembled polyelectrolyte complex nanoparticles for cancer therapeutics. *J Biomed Mater Res A* **2019,** *107* (2), 339-347.
98. Drogoz, A.; David, L.; Rochas, C.; Domard, A.; Delair, T., Polyelectrolyte complexes from polysaccharides: formation and stoichiometry monitoring. *Langmuir* **2007,** *23* (22), 10950-8.
99. Müller, K.; Kessel, E.; Klein, P. M.; Höhn, M.; Wagner, E., Post-PEGylation of siRNA Lipo-oligoamino Amide Polyplexes Using Tetra-glutamylated Folic Acid as Ligand for Receptor-Targeted Delivery. *Mol Pharm* **2016,** *13* (7), 2332-45.
100. Klein, P. M.; Reinhard, S.; Lee, D. J.; Müller, K.; Ponader, D.; Hartmann, L.; Wagner, E., Precise redox-sensitive cleavage sites for improved bioactivity of siRNA lipopolyplexes. *Nanoscale* **2016,** *8* (42), 18098-18104.
101. Gu, X.; Wei, Y.; Fan, Q.; Sun, H.; Cheng, R.; Zhong, Z.; Deng, C., cRGD-decorated biodegradable polytyrosine nanoparticles for robust encapsulation and targeted delivery of doxorubicin to colorectal cancer in vivo. *Journal of Controlled Release* **2019,** *301*, 110-118.
102. Kaiser, E.; Colescott, R. L.; Bossinger, C. D.; Cook, P. I., Color test for detection of free terminal amino groups in the solid-phase synthesis of peptides. *Anal Biochem* **1970,** *34* (2), 595-8.
103. Reinhard, S.; Zhang, W.; Wagner, E., Optimized Solid-Phase-Assisted Synthesis of Oleic Acid Containing siRNA Nanocarriers. *ChemMedChem* **2017,** *12* (17), 1464-1470.
104. Kularatne, S. A.; Venkatesh, C.; Santhapuram, H. K.; Wang, K.; Vaitilingam, B.; Henne, W. A.; Low, P. S., Synthesis and biological analysis of prostate-specific membrane antigen-targeted anticancer prodrugs. *J Med Chem* **2010,** *53* (21), 7767-77.
105. Truebenbach, I.; Kern, S.; Loy, D. M.; Höhn, M.; Gorges, J.; Kazmaier, U.; Wagner, E., Combination Chemotherapy of L1210 Tumors in Mice with Pretubulysin and Methotrexate Lipo-Oligomer Nanoparticles. *Mol Pharm* **2019,** *16* (6), 2405-2417.
106. Danhier, F., To exploit the tumor microenvironment: since the EPR effect fails in the clinic, what is the future of nanomedicine? *J Control Release* **2016**.
107. Li, J.; Wang, F.; Sun, D.; Wang, R., A review of the ligands and related targeting strategies for active targeting of paclitaxel to tumours. *J Drug Target* **2016,** *24* (7), 590-602.
108. Saito, G.; Swanson, J. A.; Lee, K. D., Drug delivery strategy utilizing conjugation via reversible disulfide linkages: role and site of cellular reducing activities. *Adv Drug Deliv Rev* **2003,** *55* (2), 199-215.
109. Schafer, F. Q.; Buettner, G. R., Redox environment of the cell as viewed through the redox state of the glutathione disulfide/glutathione couple. *Free Radic Biol Med* **2001,** *30* (11), 1191-212.
110. Endocyte, Folic Acid-Tubulysin Conjugate EC1456 In Patients With Advanced Solid Tumors. *Clinical Trial NCT01999738*.
111. Leamon, C. P.; Reddy, J. A.; Vetzel, M.; Dorton, R.; Westrick, E.; Parker, N.; Wang, Y.; Vlahov, I., Folate targeting enables durable and specific antitumor

responses from a therapeutically null tubulysin B analogue. *Cancer Res* **2008,** *68* (23), 9839-44.
112. Zuckerman, J. E.; Choi, C. H.; Han, H.; Davis, M. E., Polycation-siRNA nanoparticles can disassemble at the kidney glomerular basement membrane. *Proc Natl Acad Sci U S A* **2012,** *109* (8), 3137-42.
113. Kulkarni, S. A.; Feng, S. S., Effects of particle size and surface modification on cellular uptake and biodistribution of polymeric nanoparticles for drug delivery. *Pharm Res* **2013,** *30* (10), 2512-22.
114. Govender, T.; Stolnik, S.; Garnett, M. C.; Illum, L.; Davis, S. S., PLGA nanoparticles prepared by nanoprecipitation: drug loading and release studies of a water soluble drug. *J Control Release* **1999,** *57* (2), 171-85.
115. Owen, S. C.; Chan, D. P. Y.; Shoichet, M. S., Polymeric micelle stability. *Nano Today* **2012,** *7* (1), 53-65.
116. Chou, L. Y. T.; Ming, K.; Chan, W. C. W., Strategies for the intracellular delivery of nanoparticles. *Chemical Society Reviews* **2011,** *40* (1), 233-245.
117. Salatin, S.; Yari Khosroushahi, A., Overviews on the cellular uptake mechanism of polysaccharide colloidal nanoparticles. *J Cell Mol Med* **2017,** *21* (9), 1668-1686.
118. Blanco, E.; Shen, H.; Ferrari, M., Principles of nanoparticle design for overcoming biological barriers to drug delivery. *Nat Biotechnol* **2015,** *33* (9), 941-51.
119. Huhn, D.; Kantner, K.; Geidel, C.; Brandholt, S.; De Cock, I.; Soenen, S. J.; Rivera Gil, P.; Montenegro, J. M.; Braeckmans, K.; Mullen, K.; Nienhaus, G. U.; Klapper, M.; Parak, W. J., Polymer-coated nanoparticles interacting with proteins and cells: focusing on the sign of the net charge. *ACS Nano* **2013,** *7* (4), 3253-63.
120. Zhu, C.; Jung, S.; Luo, S.; Meng, F.; Zhu, X.; Park, T. G.; Zhong, Z., Co-delivery of siRNA and paclitaxel into cancer cells by biodegradable cationic micelles based on PDMAEMA-PCL-PDMAEMA triblock copolymers. *Biomaterials* **2010,** *31* (8), 2408-16.
121. Moscow, J. A., Methotrexate transport and resistance. *Leuk Lymphoma* **1998,** *30* (3-4), 215-24.
122. Klein, E.; Leborgne, C.; Ciobanu, M.; Klein, J.; Frisch, B.; Pons, F.; Zuber, G.; Scherman, D.; Kichler, A.; Lebeau, L., Nucleic acid transfer with hemifluorinated polycationic lipids. *Biomaterials* **2010,** *31* (17), 4781-8.
123. Creusat, G.; Rinaldi, A. S.; Weiss, E.; Elbaghdadi, R.; Remy, J. S.; Mulherkar, R.; Zuber, G., Proton sponge trick for pH-sensitive disassembly of polyethylenimine-based siRNA delivery systems. *Bioconjug Chem* **2010,** *21* (5), 994-1002.
124. Rostovtsev, V. V.; Green, L. G.; Fokin, V. V.; Sharpless, K. B., A stepwise huisgen cycloaddition process: copper(I)-catalyzed regioselective "ligation" of azides and terminal alkynes. *Angew Chem Int Ed Engl* **2002,** *41* (14), 2596-9.
125. Chang, P. V.; Prescher, J. A.; Sletten, E. M.; Baskin, J. M.; Miller, I. A.; Agard, N. J.; Lo, A.; Bertozzi, C. R., Copper-free click chemistry in living animals. *Proc Natl Acad Sci U S A* **2010,** *107* (5), 1821-6.
126. Hall, A.; Lächelt, U.; Bartek, J.; Wagner, E.; Moghimi, S. M., Polyplex Evolution: Understanding Biology, Optimizing Performance. *Mol Ther* **2017,** *25* (7), 1476-1490.
127. Morys, S.; Urnauer, S.; Spitzweg, C.; Wagner, E., EGFR Targeting and Shielding of pDNA Lipopolyplexes via Bivalent Attachment of a Sequence-Defined PEG Agent. *Macromol Biosci* **2018,** *18* (1).
128. Schmohl, K. A.; Gupta, A.; Grünwald, G. K.; Trajkovic-Arsic, M.; Klutz, K.; Braren, R.; Schwaiger, M.; Nelson, P. J.; Ogris, M.; Wagner, E.; Siveke, J. T.; Spitzweg, C., Imaging and targeted therapy of pancreatic ductal adenocarcinoma

using the theranostic sodium iodide symporter (NIS) gene. *Oncotarget* **2017,** *8* (20), 33393-33404.
129. Mickler, F. M.; Mockl, L.; Ruthardt, N.; Ogris, M.; Wagner, E.; Brauchle, C., Tuning nanoparticle uptake: live-cell imaging reveals two distinct endocytosis mechanisms mediated by natural and artificial EGFR targeting ligand. *Nano Lett* **2012,** *12* (7), 3417-23.
130. Schäfer, A.; Pahnke, A.; Schaffert, D.; van Weerden, W. M.; de Ridder, C. M.; Rodl, W.; Vetter, A.; Spitzweg, C.; Kraaij, R.; Wagner, E.; Ogris, M., Disconnecting the yin and yang relation of epidermal growth factor receptor (EGFR)-mediated delivery: a fully synthetic, EGFR-targeted gene transfer system avoiding receptor activation. *Hum Gene Ther* **2011,** *22* (12), 1463-73.
131. Sarli, V.; Giannis, A., Targeting the kinesin spindle protein: basic principles and clinical implications. *Clin Cancer Res* **2008,** *14* (23), 7583-7.
132. Domin, B. A.; Grill, S. P.; Bastow, K. F.; Cheng, Y. C., Effect of methotrexate on dihydrofolate reductase activity in methotrexate-resistant human KB cells. *Mol Pharmacol* **1982,** *21* (2), 478-82.
133. Saikawa, Y.; Knight, C. B.; Saikawa, T.; Page, S. T.; Chabner, B. A.; Elwood, P. C., Decreased expression of the human folate receptor mediates transport-defective methotrexate resistance in KB cells. *J Biol Chem* **1993,** *268* (7), 5293-301.
134. Linke, S. P.; Clarkin, K. C.; Di Leonardo, A.; Tsou, A.; Wahl, G. M., A reversible, p53-dependent G0/G1 cell cycle arrest induced by ribonucleotide depletion in the absence of detectable DNA damage. *Genes Dev* **1996,** *10* (8), 934-47.
135. Fairchild, C. R.; Maybaum, J.; Straw, J. A., Enhanced cytotoxicity with methotrexate in conjunction with hypoxanthine in L1210 cells in culture. *Cancer Chemother Pharmacol* **1988,** *22* (1), 26-32.
136. Kretzschmann, V. K.; Gellrich, D.; Ullrich, A.; Zahler, S.; Vollmar, A. M.; Kazmaier, U.; Fürst, R., Novel tubulin antagonist pretubulysin displays antivascular properties in vitro and in vivo. *Arterioscler Thromb Vasc Biol* **2014,** *34* (2), 294-303.
137. Huang, C.; Hsu, P.; Hung, Y.; Liao, Y.; Liu, C.; Hour, C.; Kao, M.; Tsay, G. J.; Hung, H.; Liu, G. Y., Ornithine decarboxylase prevents methotrexate-induced apoptosis by reducing intracellular reactive oxygen species production. *Apoptosis* **2005,** *10* (4), 895-907.
138. Otrocka, M.; Verschueren, H.; Malicka-Blaszkiewicz, M., The effect of methotrexate on actin and invasiveness of hepatoma Morris 5123 cells in culture. *Acta Biochim Pol* **2001,** *48* (4), 1051-60.
139. Mazur, A. J.; Nowak, D.; Mannherz, H. G.; Malicka-Blaszkiewicz, M., Methotrexate induces apoptosis in CaSki and NRK cells and influences the organization of their actin cytoskeleton. *Eur J Pharmacol* **2009,** *613* (1-3), 24-33.
140. Allegra, C. J.; Drake, J. C.; Jolivet, J.; Chabner, B. A., Inhibition of phosphoribosylaminoimidazolecarboxamide transformylase by methotrexate and dihydrofolic acid polyglutamates. *Proceedings of the National Academy of Sciences* **1985,** *82* (15), 4881-4885.
141. Tsuruta, S.; Ito, S.; Mikawa, H., Effects of adenosine and its analogues on actin polymerization in human polymorphonuclear leucocytes. *Clin Exp Pharmacol Physiol* **1993,** *20* (2), 89-94.
142. Liao, G.; Nagasaki, T.; Gundersen, G. G., Low concentrations of nocodazole interfere with fibroblast locomotion without significantly affecting microtubule level: implications for the role of dynamic microtubules in cell locomotion. *J Cell Sci* **1995,** *108 (Pt 11)*, 3473-83.
143. Danowski, B. A., Fibroblast contractility and actin organization are stimulated by microtubule inhibitors. *J Cell Sci* **1989,** *93 (Pt 2)*, 255-66.

144. Krendel, M.; Zenke, F. T.; Bokoch, G. M., Nucleotide exchange factor GEF-H1 mediates cross-talk between microtubules and the actin cytoskeleton. *Nature Cell Biology* **2002,** *4* (4), 294-301.
145. Kern, S., Antitumoral polymeric siRNA nanoformulation and pretubulysin-based combination therapies. *PhD thesis* **2019,** (available from https://edoc.ub.uni-muenchen.de/24033/1/Kern_Sarah.pdf).
146. Chello, P. L.; Sirotnak, F. M.; Dorick, D. M., Different effects of vincristine on methotrexate uptake by L1210 cells and mouse intestinal epithelia in vitro and in vivo. *Cancer Res* **1979,** *39* (6 Pt 1), 2106-12.
147. Trivedi, R.; Kompella, U. B., Nanomicellar formulations for sustained drug delivery: strategies and underlying principles. *Nanomedicine (Lond)* **2010,** *5* (3), 485-505.
148. Singh, R.; Lillard, J. W., Jr., Nanoparticle-based targeted drug delivery. *Exp Mol Pathol* **2009,** *86* (3), 215-23.
149. Liu, J. P.; Wang, T. T.; Wang, D. G.; Dong, A. J.; Li, Y. P.; Yu, H. J., Smart nanoparticles improve therapy for drug-resistant tumors by overcoming pathophysiological barriers. *Acta Pharmacol Sin* **2017,** *38* (1), 1-8.
150. Bazak, R.; Houri, M.; El Achy, S.; Kamel, S.; Refaat, T., Cancer active targeting by nanoparticles: a comprehensive review of literature. *J Cancer Res Clin Oncol* **2015,** *141* (5), 769-84.
151. Bertrand, N.; Wu, J.; Xu, X.; Kamaly, N.; Farokhzad, O. C., Cancer nanotechnology: the impact of passive and active targeting in the era of modern cancer biology. *Adv Drug Deliv Rev* **2014,** *66*, 2-25.
152. Beck-Broichsitter, M.; Nicolas, J.; Couvreur, P., Design attributes of long-circulating polymeric drug delivery vehicles. *European Journal of Pharmaceutics and Biopharmaceutics* **2015,** *97*, 304-317.
153. Moghimi, S. M.; Symonds, P.; Murray, J. C.; Hunter, A. C.; Debska, G.; Szewczyk, A., A two-stage poly(ethylenimine)-mediated cytotoxicity: implications for gene transfer/therapy. *Mol Ther* **2005,** *11* (6), 990-5.
154. Reinhard, S.; Wang, Y.; Dengler, S.; Wagner, E., Precise Enzymatic Cleavage Sites for Improved Bioactivity of siRNA Lipo-Polyplexes. *Bioconjug Chem* **2018,** *29* (11), 3649-3657.
155. Reinhard, S., Precise biodegradable carriers for nucleid acid delivery. *PhD thesis* **2019,** (available from https://edoc.ub.uni-muenchen.de/23652/1/Reinhard_Soeren.pdf).

8 Publications

Original articles

I. Truebenbach, J. Gorges, J. Kuhn, S. Kern, E. Baratti, U. Kazmaier, E. Wagner, U. Lächelt, *Sequence-Defined Oligoamide Drug Conjugates of Pretubulysin and Methotrexate for Folate Receptor Targeted Cancer Therapy*, Macromolecular bioscience (2017), 17(10).

B. Steinborn, **I. Truebenbach**, S. Morys, U. Lächelt, E. Wagner, W. Zhang, *Epidermal growth factor receptor targeted methotrexate and small interfering RNA co-delivery*, J Gene Med (2018), 20 (7-8), e3041.

S. Kern, **I. Truebenbach**, M. Hohn, J. Gorges, U. Kazmaier, S. Zahler, A.M. Vollmar, E. Wagner, *Combined antitumoral effects of pretubulysin and methotrexate*, Pharmacol Res Perspect (2019), 7(1), e00460.

I. Truebenbach, S. Kern, D.M. Loy, M. Hohn, J. Gorges, U. Kazmaier, E. Wagner, *Combination Chemotherapy of L1210 Tumors in Mice with Pretubulysin and Methotrexate Lipo-Oligomer Nanoparticles*, Mol Pharm (2019), 16 (6), 2405-2417.

I. Truebenbach, W. Zhang, Y. Wang, S. Kern, M. Höhn, S. Reinhard, J. Gorges, U. Kazmaier, E. Wagner, *Co-delivery of pretubulysin and siEG5 to EGFR overexpressing carcinoma cells. Int J Pharm (2019), 569, 118570.*

Meeting abstracts and poster presentations

I. Truebenbach, J. Gorges, U. Lächelt, U. Kazmaier, E. Wagner, *Establishment of drug-polymer constructs for selective tumor targeting*, International Symposium on Nanobiotechnology, Los Angeles, USA (February 2016)

I. Truebenbach, J. Gorges, U. Lächelt, U. Kazmaier, E. Wagner, *Targeted, sequence-defined polymeric carrier systems for tumor-selective drug delivery,* Nanoscale Matter – Novel Concepts and Functions, Venice, Italy (September 2016)

B. Steinborn, **I. Truebenbach**, S. Wuttke, E. Wagner, U. Lächelt, *Self-assembling methotrexate nanopharmaceuticals,* Design and Control of NanoSystems, Venice, Italy (September 2017)

I. Truebenbach, S. Kern, J. Gorges, D. Wendel, U. Kazmaier, E. Wagner, *Nanoparticulate co-delivery of antitumoral drugs pretubulysin and methotrexate for combination chemotherapy of L1210 leukemia cells,* Celebrating NanoScience, Venice, Italy (September 2018)

9 Acknowledgements

Throughout my time at the LMU I have learned a lot and I am very thankful to all the people who supported me.

First, I thank my supervisor Professor Dr. Ernst Wagner for giving me the opportunity to work on my dissertation within his research group. I am very grateful for his scientific input during the whole time. I learned a lot under his supervision.

I would like to thank our collaboration partners within the DFG FOR1406 project, Prof. Dr. Uli Kazmaier and Dr. Jan Gorges from Saarbrücken for the close cooperation, providing me with lots of PT.

I would like to thank Dr. Sarah Kern and Dr. Eva Kessel for much more than conducting animal experiments. Both became great friends throughout our time together.

Moreover, I would like to thank Dr. Wei Zhang for the good cooperation on several projects. I enjoyed working with her immensely. Special thanks for conducting many of the cell culture experiments with siRNA. Lately, Dr. Yanfang Wang took over. I appreciate her excellent work.

I would like to thank Dr. Ulrich Lächelt for helping me get started and his great scientific input, especially throughout the first two years of my PhD. Our successful cooperation led to the publication of my first paper.

Many thanks to Miriam for all her support in the cell culture, whether for the countless animal experiments or the confocal microscopy images, and to Wolfgang for the much-needed technical support and for being a great lab partner!

Furthermore, I would like to thank Dodo for a lot more than TEM measurements. I enjoyed our daily discussions, whether scientific or otherwise, immensely and will miss them (and you) very much!

I want to thank many more members of the Wagner research group enriching my time in the group. There's Jasmin, who brightened every day of my life, PhD- and otherwise. She's the best thing that happened to me in the last four years and I look forward to many more unforgettable moments. I would also like to thank my lab and office partners Philipp, Stephan, Anna-Lina, Simone, Teo and especially Sören. Within the years, we

did many fun things together, like PhD celebrations, Fasching and Christmas parties, football and basketball games, Oktoberfest, celebrations for new publications and many more occasions.

Moreover, I want to thank the members of the AK Wanner and AK OTS for welcoming me into their groups. Besides Praktikum, we spent many fun Thursday nights at the Teeküche and then at Milchbar.

I would like to thank the best sister in the world, Thekla, for listening to my many worries in the last years and always being there when I needed you. My life would be boring without you. Many thanks go to my mother. She is the best person I know, and I strive to be like her every day. There is no one who is prouder of me and no one who believes in me as she does. Your support is endless, and I am very grateful for all you do for me.

Finally, I would also like to thank Jannis for his love, patience and support. You have helped me through “the worst of times” and been there to celebrate the successes. I could not have done this without you and look forward to spending the rest of my life with you.